

DE GRUYTER

MATHEMATICS FOR RELIABILITY ENGINEERING

MODERN CONCEPTS AND APPLICATIONS

Edited by Mangey Ram and Liudong Xing

DE GRUYTER SERIES ON THE APPLICATIONS
OF MATHEMATICS IN ENGINEERING AND
INFORMATION SCIENCES

EBSCO Publishing : eBook Collection
2/14/2023 7:32 AM via
AN: 1290788 ; Mangey Ram, Liudong Xing
Engineering : Modern Concepts and Applications
Account: ns335141

@RETURN
PUBLIC STATIC STRING
FINAL STRING (EBSCOhost) - printed on
APPEARANCEARRAY
APPEARANCEARRAY
APPEARANCEARRAY
FINAL JAVA UTIL RANDOM

Mangey Ram and Liudong Xing (Eds.)
Mathematics for Reliability Engineering

De Gruyter Series on the Applications of Mathematics in Engineering and Information Sciences



Edited by
Mangey Ram

Volume 8

Mathematics for Reliability Engineering

Modern Concepts and Applications

Edited by
Mangey Ram and Liudong Xing

DE GRUYTER

Editors

Prof. Mangey Ram
Department of Mathematics, Computer Science and Engineering
Graphic Era Deemed to be University
566/6 Bell Road
248002 Clement Town, Dehradun, Uttarakhand, India
drmrswami@yahoo.com
and

Institute of Advanced Manufacturing Technologies
Peter the Great St. Petersburg Polytechnic University
195251, Saint Petersburg, Russia

Prof. Liudong Xing
Department of Electrical and Computer Engineering
University of Massachusetts
Dartmouth, MA 02747, USA
lxing@umassd.edu

ISBN 978-3-11-072556-8
e-ISBN (PDF) 978-3-11-072559-9
e-ISBN (EPUB) 978-3-11-072563-6
ISSN 2626-5427

Library of Congress Control Number: 2021940730

Bibliographic information published by the Deutsche Nationalbibliothek

The Deutsche Nationalbibliothek lists this publication in the Deutsche Nationalbibliografie;
detailed bibliographic data are available on the Internet at <http://dnb.dnb.de>.

© 2022 Walter de Gruyter GmbH, Berlin/Boston
Cover image: MF3d/E+/Getty Images
Typesetting: Integra Software Services Pvt. Ltd.
Printing and binding: CPI books GmbH, Leck

www.degruyter.com

Acknowledgment

During the preparation of this volume, the editors gratefully thank Walter de Gruyter and the editorial staff for their sufficient and competent assistance. We would also like to thank all the chapter authors and reviewers for their enthusiasm to contribute to this book series.

Mangey Ram
Graphic Era Deemed to be University, India
Peter the Great St. Petersburg Polytechnic University, Russia

Liudong Xing
University of Massachusetts, Dartmouth, USA

<https://doi.org/10.1515/9783110725599-202>

Preface

Mathematics always has great importance within the engineering sciences. Novel concepts and wide applicability of mathematics are the source of compact and concise primer in engineering. From foundation to advanced level, knowledge with applicability is required the most for all the engineering disciplines. This book comes with a primary aim to introduce readers to new mathematical concepts and applications, as well as to help them understand how those concepts are related to reliability engineering.

This book explores the valuable and deep interaction between reliability engineers and mathematicians, as well as the cross-fertilization and cooperation that arises when mathematics is applied to science and technology advancement. In this book, the following topics have been discussed:

- Residual resilience assessment in infrastructure networks: a case to IEEE14 bus test system
- Modeling of mixed cascading failures and resilience-based restoration selection
- Mathematical scheme for predicting impacts of reliability engineering on the time evolution of physical systems
- On the reliability structures with two common failure criteria and a single change point
- Invulnerability and survivability modeling and analysis of cloud storage systems
- Reliability evaluation of multistate systems with common bus performance sharing considering performance excess
- A fast universal algorithm for finding minimal cut-sets in networks with arbitrary structure
- Switching-algebraic symbolic analysis of the reliability of nonrepairable coherent multistate systems
- Complex system modeling method considering failure mechanism dependency
- Innovative interconnected nonlinear hybrid dynamic modeling for time-to-event processes
- A Bayesian design of zero-failure reliability demonstration tests for multicomponent systems

The book seeks to explore the contributions made by researchers and practitioners in the domain of reliability engineering from different stakeholder's perspectives. Additionally, it may guide practitioners in developing novel mathematical applications and original frameworks for effective implementation in reliability engineering. This book is written by a number of leading scientists, reliability engineers, and mathematicians who have been working on the front end of reliability science and

engineering. We hope that this book will make a positive and lasting contribution to the research and practice in the area of reliability engineering.

Mangey Ram

Graphic Era Deemed to be University, India

Peter the Great St. Petersburg Polytechnic University, Russia

Liudong Xing

University of Massachusetts, Dartmouth, USA

Editor's biography

Mangey Ram received the Ph.D. major in mathematics and minor in computer science from G. B. Pant University of Agriculture and Technology, Pantnagar, India. He has been a faculty member for around 12 years and has taught several core courses in pure and applied mathematics at undergraduate, postgraduate, and doctorate levels. He is currently a research professor at Graphic Era (Deemed to be University), Dehradun, India. Before joining the Graphic Era, he was a deputy manager (probationary officer) with Syndicate Bank for a short period. He is editor-in-chief of *International Journal of Mathematical, Engineering and Management Sciences* and *Journal of Reliability and Statistical Studies*, editor-in-chief of six book series with Elsevier, CRC Press – A Taylor and Frances Group, Walter De Gruyter Publisher Germany, and River Publisher; and the guest editor and member of the editorial board of various journals. He has published 250 plus research publications (journal articles/books/book chapters/conference articles) in IEEE, Taylor & Francis, Springer, Elsevier, Emerald, World Scientific, and many other national and international journals and conferences. Also, he has published more than 50 books (authored/edited) with international publishers like Elsevier, Springer Nature, CRC Press – A Taylor and Frances Group, Walter De Gruyter Publisher Germany, and River Publisher. His fields of research are reliability theory and applied mathematics. Dr. Ram is a senior member of the IEEE and a senior life member of Operational Research Society of India, Society for Reliability Engineering, Quality and Operations Management in India, and Indian Society of Industrial and Applied Mathematics. He has been a member of the organizing committee of a number of international and national conferences, seminars, and workshops. He has been conferred with “Young Scientist Award” by the Uttarakhand State Council for Science and Technology, Dehradun, in 2009. He has been awarded the “Best Faculty Award” in 2011; “Research Excellence Award” in 2015; and recently “Outstanding Researcher Award” in 2018 for his significant contribution in academics and research at Graphic Era (Deemed to be University), Dehradun, India.

Liudong Xing received her Ph.D. in electrical engineering from the University of Virginia, Charlottesville, USA. She is currently a professor in the Department of Electrical and Computer Engineering, University of Massachusetts, Dartmouth, USA. Her current research interests include reliability and resilience modeling, and analysis and optimization of complex systems and networks (e.g., Internet of Things and wireless sensor networks). Prof. Xing has received multiple teaching and scholar awards and was co-recipient of the Best (Student) Paper Award at several international conferences and journals. She has published over 230 journal articles and two books, titled *Binary Decision Diagrams and Extensions for System Reliability Analysis* and *Dynamic System Reliability: Modeling and Analysis of Dynamic and Dependent Behaviors*. She has served as an associate editor or editorial board member of several journals, including *Reliability Engineering & System Safety*, *IEEE Internet of Things Journal*, *International Journal of Systems Science*, and *International Journal of Mathematical, Engineering and Management Sciences*. She is a fellow of the International Society of Engineering Asset Management and a senior member of IEEE.

<https://doi.org/10.1515/9783110725599-204>

Contents

Acknowledgment — V

Preface — VII

Editor's biography — IX

Hongyan Dui, Xiaoqian Zheng, Han Wang, Liwei Chen

- 1 Residual resilience assessment in infrastructure networks: a case to IEEE14 bus test system — 1**

Jian Zhou, David W. Coit

- 2 Modeling of mixed cascading failures and resilience-based restoration selection — 21**

Jezdimir Knezevic

- 3 MIRCE Science: a mathematical scheme for predicting impacts of reliability engineering on the time evolution of physical systems — 47**

Ioannis S. Triantafyllou, Mangey Ram

- 4 On the reliability structures with two common failure criteria and a single change point — 65**

Qisi Liu, Liudong Xing, Guilin Zhao

- 5 Invulnerability and survivability modeling and analysis of cloud storage systems — 85**

Yuanying Chi, Guoqing Bai, Kaiye Gao, Rui Peng

- 6 Reliability evaluation of multistate systems with common bus performance sharing considering performance excess — 105**

Jacek Malinowski

- 7 A fast universal algorithm for finding minimal cut-sets in networks with arbitrary structure — 119**

Ali Muhammad Rushdi, Fares Ahmad Ghaleb

- 8 Switching-algebraic symbolic analysis of the reliability of non-repairable coherent multistate systems — 131**

Ying Chen

9 Complex system modeling method considering failure mechanism dependency — 153

Emmanuel A. Appiah, G. S. Ladde, Jay G. Ladde

10 Innovative interconnected nonlinear hybrid dynamic modeling for time-to-event processes — 175

Tao Yuan, Manish Kothawade, Yuan Chen

11 A Bayesian design of zero-failure reliability demonstration tests for multicomponent systems — 237

Index — 257

Hongyan Dui, Xiaoqian Zheng, Han Wang, Liwei Chen

1 Residual resilience assessment in infrastructure networks: a case to IEEE14 bus test system

Abstract: Taking infrastructure network as the research object, this chapter studies the recovery priority of failed components against diverse importance measures. First, resilience is defined and quantified, and then, the concept of residual resilience is explained. Based on the residual resilience, the corresponding optimization model is established. The commonly used importance measures are improved and extended to the residual resilience of infrastructure networks. The Copeland ranking method is used to comprehensively rank the importance measures to obtain the recovery order of the failed components. Finally, taking the IEEE14 bus test system as an example, the resilience is analyzed by the nodes and edges under a given failure set and full failure state. Residual resilience is studied for different importance measures to verify the feasibility of the model.

Keywords: Infrastructure network, residual resilience, importance measure, reliability

1.1 Introduction

With the development of society, infrastructure networks such as transportation networks, power grids, and water networks have become increasingly complex, and component failures caused by disaster events may cause severe damage to the infrastructure network. Therefore, how to quickly restore to a fully operational state, after a disaster, to improve the resilience of the infrastructure network has become a new research direction. This chapter studies the recovery sequence of failed components in the post-disaster infrastructure network. The purpose is to determine the recovery sequence of failed components so that the post-disaster infrastructure network can quickly restore to a stable operating state in a short time, thereby reducing economic losses.

In terms of resilience, Berle et al. [1] proposed a structured formal vulnerability assessment methodology, seeking to transfer the safety-oriented formal safety assessment framework into the domain of maritime supply chain vulnerability. Asadabadi and Miller-Hooks [2] proposed port reliability and resilience, as well as the role of ports in supporting a larger resilient maritime system. Adjete-Bahun et al. [3] proposed a

Hongyan Dui, Xiaoqian Zheng, Han Wang, Liwei Chen, School of Management Engineering, Zhengzhou University, Zhengzhou, China

<https://doi.org/10.1515/9783110725599-001>

simulation-based model for quantifying resilience in mass railway transportation systems by quantifying passenger delay and passenger load as the system's performance indicators. Cimellaro et al. [4] proposed the evaluation of disaster resilience, based on analytical functions related to the variation of functionality during a period of interest, including the losses in the disaster and the recovery path. Zhang et al. [5] explored resilience measures in network systems from different perspectives and analyze the characteristics of nodes and edges during failures, and the matrices of node resilience and edge resilience. Watson et al. [6] developed a model using the Monte Carlo simulation method, based on the vulnerability curve of transmission grid components and power station damage and restoration costs to predict the elasticity coefficient. Nguyen et al. [7] developed an optimization model to optimize the operation of the distribution system during a hurricane, while capturing the network operation constraints before and after the shutdown. Wang and Jin [8] proposed a power generation expansion model to realize the resilience of distribution power by the integration of renewable energy.

In terms of the importance measure, Li et al. [9] proposed a method for evaluating the importance of components of power systems to improve resilience in storms. Fang et al. [10] proposed the optimal repair time and resilience reduction worth to measure the criticality of the system components. Xu et al. [11] proposed a new resilience-based component importance measure for networks. Dui et al. [12] proposed an extended joint integrated importance measure to effectively guide the selection of preventive maintenance components, aiming to maximize gains of the system performance. Dui et al. [13] studied the Birnbaum importance measure, integrated importance measure, and the mean absolute deviation with respect to the changes in the optimal system structure throughout the system's lifetime. Pan et al. [14] studied the importance of system of systems from the perspective of resilience, analyzed the importance measure based on resilience, and offered suggestions for the design and optimization of the architecture. Espinoza et al. [15] proposed a new centrality evaluation to prove that the modification of selective elements in some networks can significantly improve the resilience of the whole system to seismic events. Li et al. [16] presented an evaluation method of importance measure to improve the wind resistance of power systems.

The impact of infrastructure network restoration on resilience is the focus of research. How can we repair the infrastructure network as soon as possible after it is attacked? What is the impact of repairing different nodes on infrastructure network resilience? Which component should be repaired first to have great influence on the improvement of infrastructure network resilience? Although there are many researches on the importance measure of failed components in infrastructure network, the existing classical importance measure based on the reliability concept cannot be directly applied to the post-disaster stage. In this chapter, against the background of infrastructure network resilience research, the recovery priority of failed components in the post-disaster stage is studied to provide suggestions and reference for the restoration of infrastructure network components in the

post-disaster stage of infrastructure network with the focus on infrastructure network resilience.

The rest of this chapter is organized as follows. Section 1.2 describes the residual resilience of infrastructure networks. Section 1.3 uses some importance measures to determine the best time period to recover the failed components and the Copeland method is used to sort the components. Section 1.4 takes the IEEE14 bus node standard test system as an example to analyze the residual resilience under different conditions. The conclusions of this chapter are given in Section 1.5.

1.2 Residual resilience of infrastructure networks

Disaster events may cause one or more components in the infrastructure network to fail. When multiple components fail after a disaster event, the main problem is to determine the repair sequence of the failed components. The goal is to maximize the resilience of the infrastructure network and restore it to the best possible state within a certain period of time. This chapter focuses on the impact of a single component on the residual resilience of the infrastructure network in different states. Therefore, the optimal repair sequence of the failed component set can result in the smallest residual resilience within the recovery time, thereby reducing economic losses.

This chapter divides the resilience process of infrastructure networks into five states and illustrates with examples, as shown in Figure 1.1.

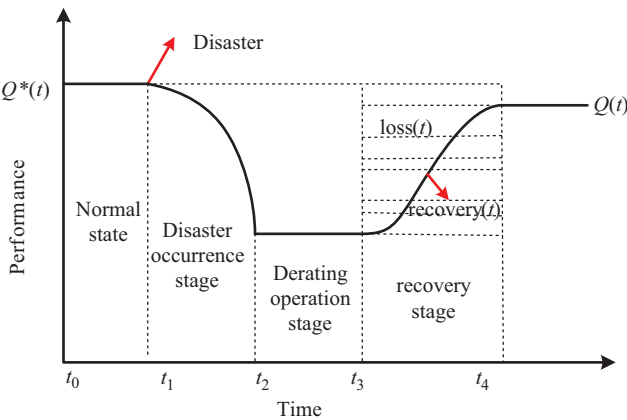


Figure 1.1: Resilience process of the infrastructure network.

- (a) Disaster prevention stage ($t_0 < t < t_1$): During this time, the infrastructure network is in normal operation. In this stage, advanced weather forecasting and decision support systems can be used to prevent and prepare for disasters.
- (b) Disaster occurrence stage ($t_1 < t < t_2$): This chapter assumes that the infrastructure network performance is in a state of nonlinear decline in this stage, and the rate of decline gradually accelerates. Disasters occur at t_1 and the infrastructure network performance is affected to a certain extent. The degree of impact depends on the severity of the disaster attack and the infrastructure network's own ability to resist.
- (c) Derating operation stage ($t_2 < t < t_3$): This chapter assumes that the infrastructure network performance is in a stable derating state in this stage. After a disaster occurs, the infrastructure network absorbs the disaster attack and operates in a derated state. Before the fault is restored, the staff can help the infrastructure network adapt to the disaster attack through a series of optimized operations according to the fault status.
- (d) The failed components recovery stage ($t_3 < t < t_4$): This chapter assumes that the infrastructure network performance gradually increases during this stage. As the recovery progresses, the increase in infrastructure network performance gradually weakens. At t_3 , the failed components start to be repaired and the infrastructure network operating state gradually recovers.
- (e) Stable operation stage ($t_4 < t$): The repair of the failed components is completed, and the infrastructure network gradually returns to its stable operation state.

The infrastructure network is defined by $G(N, L)$. N represents the set of nodes in the infrastructure network. L represents the set of edges in the infrastructure network ($L \subset \{(i, j): i, j \in N, i \neq j\}$). The set of nodes in the infrastructure network is divided into a set of supply nodes, N_S and a set of demand nodes, N_D . C_0^+ ($C_0^+ \in R^+$) is used to represent the capacity or the capacity set of the components in the infrastructure network. The capacity of edges, ij , supply node, $i \in N_S$, and demand node, $j \in N_D$ are expressed by P_{ij} , P_i^S and P_j^D , respectively. E is defined as a set of the infrastructure network components and E' is modeled as a set of failed components in the infrastructure network.

The purpose of this chapter is to determine the repair sequence of the failed component set in a given time period, with the minimum residual resilience as the objective. Therefore, a time set $t \in \{0, 1, 2, 3, \dots, T\}$ ($T \in Z^+$) composed of multiple discrete time periods is given and only one failed component is repaired in each time period. $Q_j(t)$ is modeled as the demand node j in t time period. The aim of this chapter is to maximize the flow of the demand node:

$$Q(t) = \sum_{j \in N_D} Q_j(t) \quad (1.1)$$

Residual resilience, quantified as the difference between the current resilience and the optimal resilience, is defined by

$$\frac{R(t) = \int_{t_3}^t (Q^*(t) - Q(t_3))dt - \int_{t_3}^t (Q(t) - Q(t_3))dt}{\int_{t_3}^t (Q^*(t) - Q(t_3))dt} = \frac{T^* \left(\sum_{j \in N_D} P_j^D - Q_0 \right) - \sum_{t \in T} \left[\sum_{j \in N_D} Q_j(t) - Q_0 \right]}{T^* \left(\sum_{j \in N_D} P_j^D - Q_0 \right)} \quad (1.2)$$

The value of $R(t)$ is in the range $[0, 1]$. When $Q(t) = Q(t_3)$, $R(t) = 1$, which means that the infrastructure network is still in a post-disaster state and no failed component has been successfully repaired. When $Q(t) = Q^*(t)$, $R(t) = 0$, which means it is the ideal situation for the infrastructure network to return to the target state after the disaster. $\sum_{j \in N_D} P_j(t)$ represents that the demand of all the demand nodes in N_D has been fully met, that is, $\sum_{j \in N_D} P_j(t) = Q^*(t)$. The system begins to be repaired when $t = t_3$, so $Q(t_3)$ can be represented by Q_0 .

1.3 Resilience analysis based on the importance measures

Generally speaking, importance measure is used to quantify the contribution of each component in the infrastructure network to the overall infrastructure network performance, such as reliability, risk, and availability. In this chapter, the importance measure is extended to the residual resilience for infrastructure network. The fault of the components will directly or indirectly affect the operational state of the infrastructure network. Therefore, it is necessary to determine the repair sequence of components within a certain time period to ensure that the infrastructure network status returns to normal.

The OPT importance measure is given based on the importance measure of Fang et al. [17]. The OPT importance measure of a failed component $C \in Z'$, denoted as I_C^{OPT} , is defined by

$$I_C^{OPT} = \begin{cases} I_{ij}^{OPT} = 1 + \sum_{t=1}^T (1 - \mu_{ij}(t)), & \text{if } c = ij, (i, j) \in E \\ I_i^{OPT} = 1 + \sum_{t=1}^T (1 - \mu_i(t)), & \text{if } c = i, i \in E' \end{cases} \quad (1.3)$$

where I_{ij}^{OPT} and I_i^{OPT} represent the optimal time to repair a failed edge, ij , and a failed node, i , respectively. T represents the time period necessary to restore the infrastructure network performance to the optimal state.

The OPT indicates the recovery priority of the failed components and quantifies the residual resilience of the infrastructure network once the failed components are restored. The smaller the value is, the more important is the element to the residual resilience of the infrastructure network.

Birnbaum importance measure is currently the most widely used reliability importance measure. The basic meaning of Birnbaum importance measure is the difference in the reliability of the component between the working state and the failure state. In this chapter, the Birnbaum importance measure is extended to the residual resilience study and is used to measure the influence of the component state on the residual resilience value of the infrastructure network. The Birnbaum importance measure is defined as I_C^B , which is transformed from the original to the difference between the loss value and the recovery value as follows:

$$I_C^B = R\left(T \mid \sum_{t=1}^T \mu_C(t) = 0\right) - R\left(T \mid \sum_{t=1}^T \mu_C(t) = 1\right) \quad (1.4)$$

where $R(T \mid \sum_{t=1}^T \mu_C(t) = 1)$ represents the optimal residual resilience of the infrastructure network after the failed component C recovers in the time period T . $R(T \mid \sum_{t=1}^T \mu_C(t) = 0)$ represents the optimal residual resilience value of the infrastructure network when the failed component C does not recover within the time period T . The Birnbaum importance measure is used to measure the potential impact of the state change of the failed component C on the residual resilience of the network. The greater the I_C^B , greater is the impact of the component state changes on the residual resilience of the network and higher is the recovery priority of the component.

The reliability achievement worth (RAW) is used to quantify the maximum percentage increase in infrastructure network reliability that is generated by a component. The RAW of a failed component, $C \in Z'$, is denoted as I_C^{RAW} and is defined as

$$I_C^{RAW} = \frac{R(t \mid \sum_{t=1}^t \mu_C(t) = 1)}{R(0)} \quad (1.5)$$

where the RAW importance measure corresponds to the residual resilience reduction worth. $R(0)$ represents the residual resilience of the initial state when the infrastructure network fails. $R(t \mid \sum_{t=1}^t \mu_C(t) = 1)$ represents the residual resilience of the infrastructure network in which only the failed component C recovers within the time period T . The smaller I_C^{RAW} is, greater the residual resilience of infrastructure network is affected when the failed component is restored.

The reliability reduction worth (RRW) of a failed component $C \in Z'$ is denoted as I_C^{RRW} and is defined as

$$I_C^{RRW} = \frac{R(T)}{R(T \mid \sum_{t=1}^T \mu_C(t) = 0)} \quad (1.6)$$

where the RRW corresponds to the residual resilience achievement worth. $R(T)$ is the optimal residual resilience of the infrastructure network when the unit of time is T . $R(T \mid \sum_{t=1}^T \mu_C(t) = 0)$ represents the optimal residual resilience of the infrastructure network when the failed component C needs to be recovered within the time period T .

The RRW is used to measure the potential impact on the residual resilience of the infrastructure network when the failed component fails to recover. The smaller I_C^{RRW} is, greater is the impact of the recovery of the component on the infrastructure network residual resilience.

The Fussell–Vesely importance measure is defined as the ratio of the residual resilience reduction value after the recovery of the failed component to the residual resilience that needs to be recovered. It is expressed as I_C^{FV} and is defined as follows:

$$I_C^{FV} = \frac{R(T | \sum_{t=1}^T \mu_C(t) = 0) - R(T)}{R(T | \sum_{t=1}^T \mu_C(t) = 0)} \quad (1.7)$$

where $R(T)$ represents the optimal residual resilience value of the infrastructure network when the time unit is T . $R(T | \sum_{t=1}^T \mu_C(t) = 0)$ represents the optimal residual resilience value of the infrastructure network when the failed component C has not been restored within the time period T . The importance measure is used to measure the proportion of the residual resilience reduction caused by the failed component C not recovering within the specified time. The larger the I_C^{FV} , greater is the impact on the residual resilience of the network when the failed component C has not recovered within the specified time and higher is the recovery priority of the component C .

This chapter uses Copeland method to sort the importance measures of the infrastructure network components. Copeland score is represented by the difference between the number of times that an object has defeated other objects and the number of times it has been defeated by other objects.

Let a set of component importance measures be $\{1, 2, 3, \dots, \omega\}$ and $C_{i,j}^k(i)$ be the Copeland score of component i . After comparing the k -th importance measure index for component i and component j , Copeland score is defined by

$$C_{i,j}^k(i) = \begin{cases} C_{i,j}^{k-1}(i) + 1; & v_i^k > v_j^k \\ C_{i,j}^{k-1}(i) - 1; & v_i^k < v_j^k \\ C_{i,j}^{k-1}(i); & v_i^k = v_j^k \end{cases} \quad (1.8)$$

where v_i^k and v_j^k are the k th importance measure indices of component i and component j , respectively. When v_i^k is better than v_j^k , the Copeland score of component i is increased by one and vice versa. When they are equal, the score does not change.

The total Copeland score for component i is the sum of all scores associated with the component i . It is denoted as $C_{total}(i)$ and is defined by

$$C_{total}(i) = \sum_{j \in E} C_{i,j}^\omega(i), \quad j \neq i \quad (1.9)$$

where ω is the universal set of all the important measures.

The higher the Copeland score, more important is the component to other components. The Copeland method is a very effective non-parametric ranking method, which does not need any preference information from decision makers. This method cannot guarantee that all components have different grades. When the Copeland scores of two components are equal, they have the same level of importance, which is acceptable in theory and practice. In order to calculate and minimize the residual resilience, the repaired component sequences can be obtained by combining with different importance measures.

1.4 Application in the IEEE14 bus test system

Taking the IEEE14 bus test system as an example, the recovery priority of failed components under different importance measures are calculated based on the residual resilience optimization model. The ranking analysis is carried out to prove the feasibility of the model. IEEE14 bus test system is one of the subnets of the Midwest power system in the United States, including 14 bus nodes and 20 branches. Nodes 1, 2, 3, 6, and 8 are the generator nodes as shown in Figure 1.2.

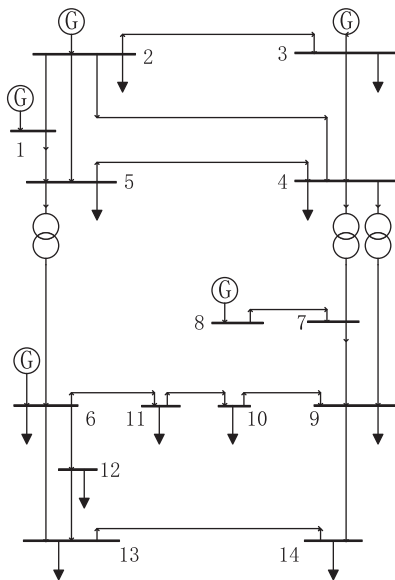


Figure 1.2: IEEE14 bus test system.

The bus nodes and branches of the test system are converted into nodes and connection edges, respectively, in the infrastructure network [18]. The nodes can be divided into three types: generator nodes, transport nodes, and load; the corresponding model

of the supply, demand, and transport nodes are S, T, and D marking respectively. The network topology is shown in Figure 1.3. The capacities of supply nodes, demand nodes, and transport nodes are 40 a.u., 25 a.u., and 100 a.u., respectively; and the capacity of the edges is 40 a.u.

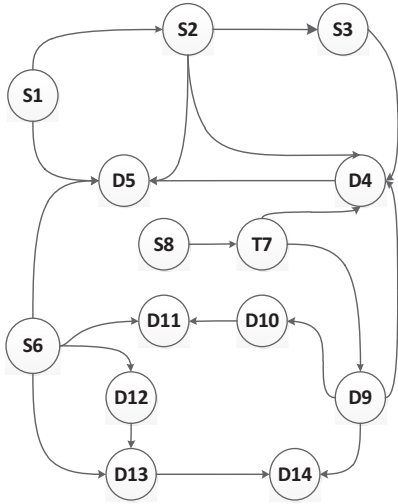


Figure 1.3: The standard network of IEEE14.

The failed nodes, E' , are assumed to be {S1, S2, S3, S6, S8, D4, D5, D9, D10, D11, D12, D13, D14, T7}. When all nodes fail, the repair of a single node cannot satisfy the requirement of the demand node. Therefore, RAW importance measure is not discussed in this part. I_i^{OPT} , I_i^B , I_i^{RRW} , I_i^{FV} of the failed nodes are as shown in Figure 1.4.

For OPT importance measure, the recovery sequence of the failed nodes is {D5, S6, D13, S2, D4, D14, T7, S8, D9, S1, D11, D10, S3, D12}. For Birnbaum importance measure, RRW importance measure, and FV importance measure, the recovery sequence is S6, {S8, D9, T7}, D5, D4, D13, and {S1, S2, S3, D10, D11, D12, D14}. According to the Copeland method, the Copeland scores of the failed nodes integrated with four importance measures are as shown in Figure 1.5. The comprehensive importance measure, in descending order, according to the Copeland scores is defined as I_i^{TOTAL} . The change of $R(t)$ is as shown in Figure 1.6.

From Figure 1.6, $R(t)$ curves of all importance measures coincide before the period 2, which is because only one failed node can be recovered in the first period and no demand node can be satisfied. For I_i^B , I_i^{RRW} , I_i^{FV} , {S6, S8, D9}, respectively were repaired in the first three periods. There was no direct relationship between the three nodes and so no flow was generated in the network. However, after the repair of node T7 in the fourth period, a bridge was built between S8 and D9, and thus $R(t)$ began to decrease. For I_i^{OPT} , $R(t)$ decreases sharply in the fourth period. The reason is that the node S2 was repaired, thereby providing traffic to the node D5

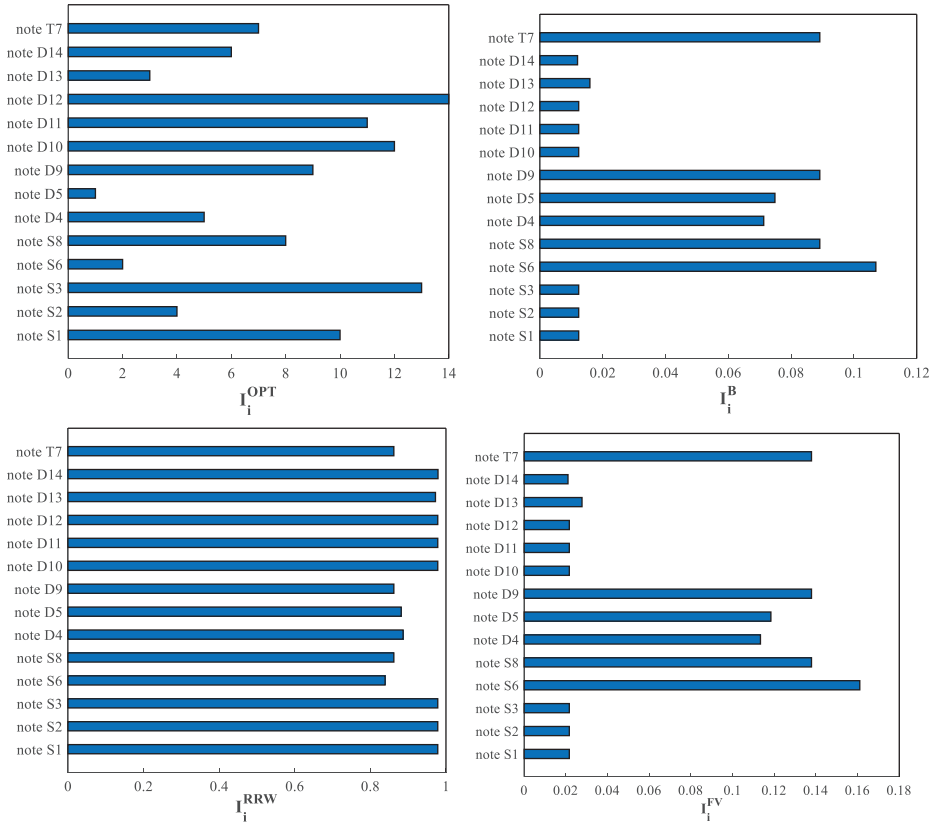


Figure 1.4: I_i^{OPT} , I_i^B , I_i^{RAW} , I_i^{FV} of all failed nodes.

in normal operation. For I_i^{TOTAL} , because of the repair of node S2, $R(t)$ decreases sharply in the eighth period.

The failed component set E' is assumed to be {linkS1S2, linkS2S3, linkS2D4, linkS1D5, linkS2D5, linkS3D4, linkD4D5, linkS8T7, linkT7D9, linkD9D10, linkS6D11, linkS6D12, linkS6D13, linkD9D14, linkD10D11, linkD12D13, linkD13D14, linkS6D5, linkT7D4, linkD9D4}. I_i^{OPT} , I_i^B , I_i^{RAW} , I_i^{RRW} , I_i^{FV} of all failed edges are as shown in Figure 1.7.

From Figure 1.7, for OPT importance measure, linkS6D12 should be repaired first, and linkD9D4 should be considered last. For RAW importance measure, the importance of the set {linkS2S3, S1D5, S2D5, S3D4, D4D4, T7D9, S6D11, D10D11} is higher, while the others are lower. For other importance measures, linkD10D11 and linkD13D14 have higher importance, while the remaining edges have lower importance.

According to the Copeland method, the Copeland scores of all failed edges integrated with the four importance measures is as shown in Figure 1.8. The change of $R(t)$ is as shown in Figure 1.9.

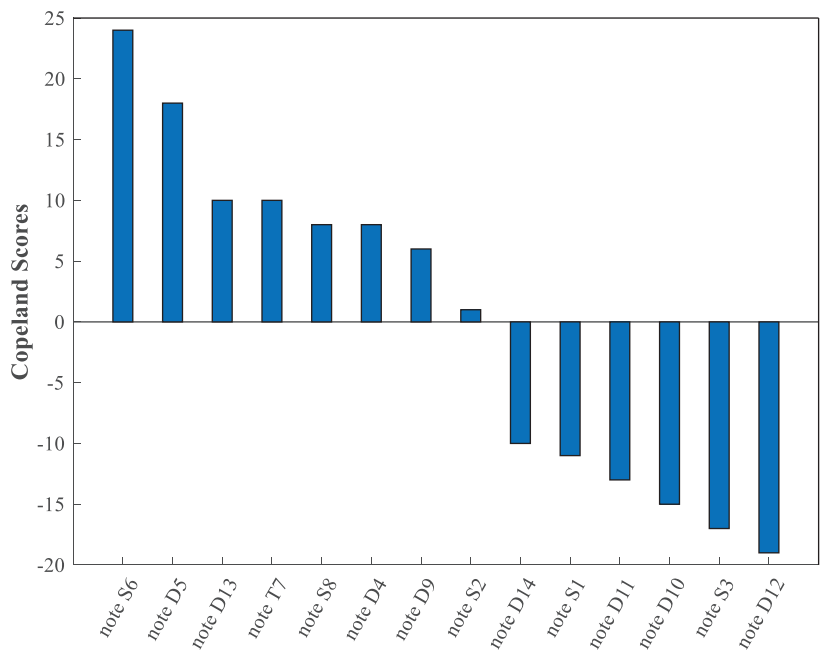


Figure 1.5: Copeland scores of all failed nodes.

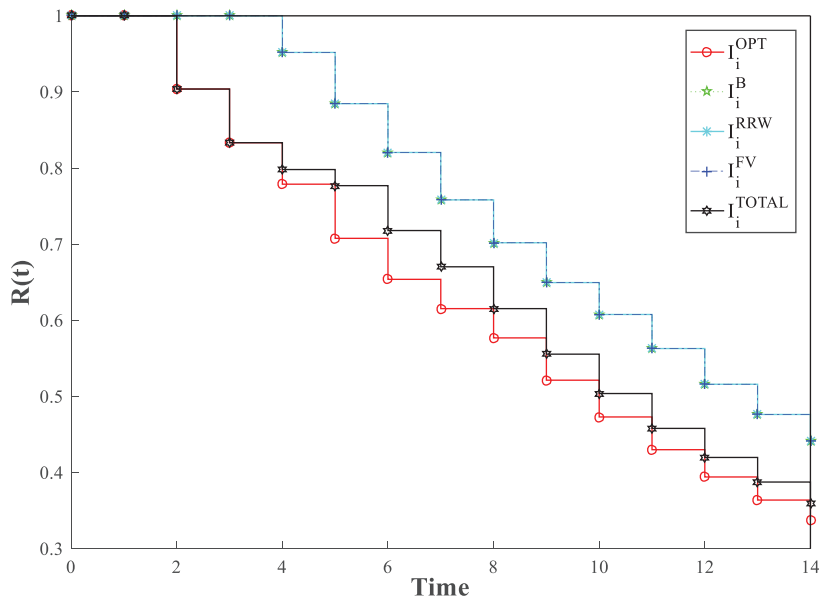


Figure 1.6: The resilience change with time.

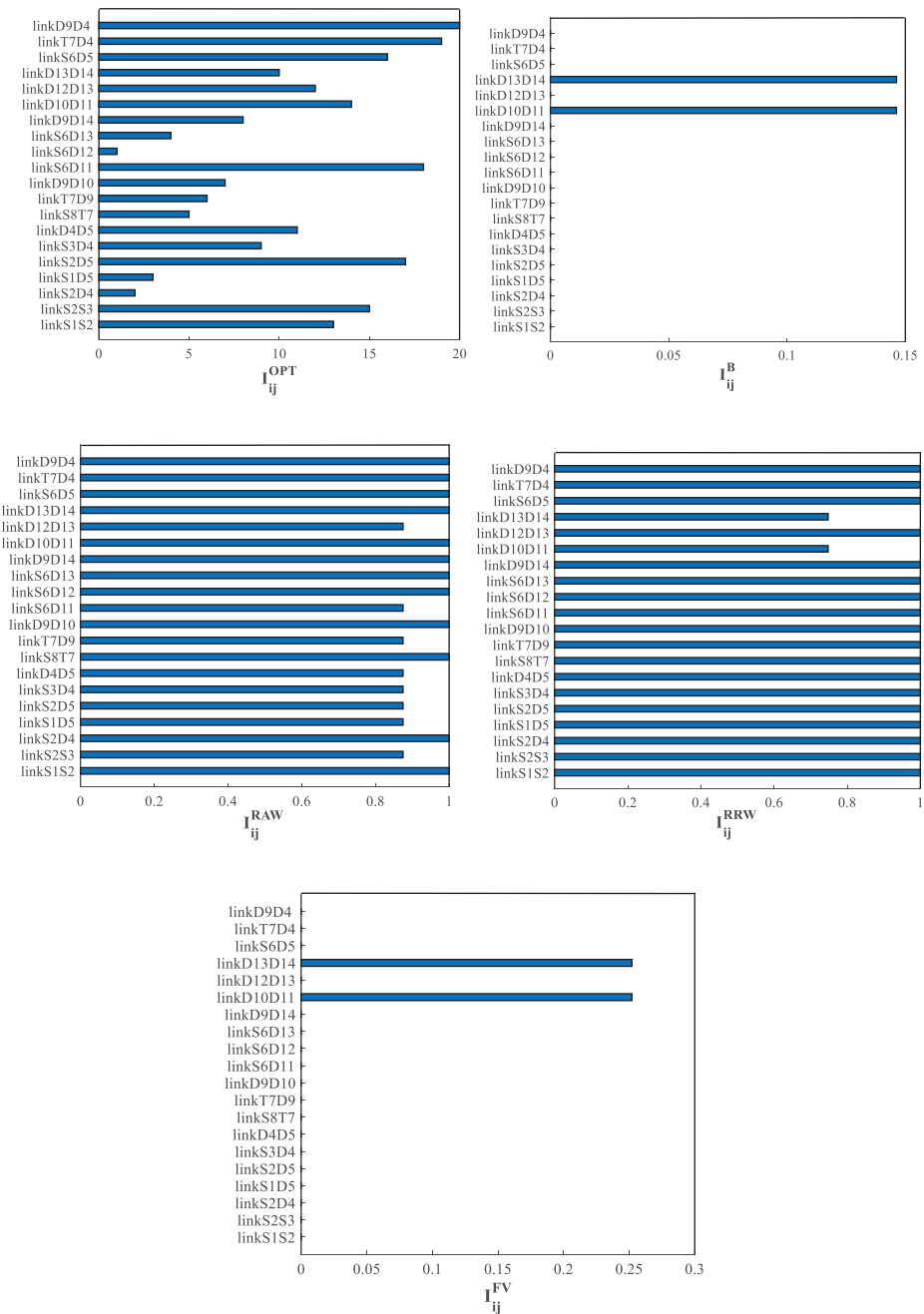


Figure 1.7: I_i^{OPT} , I_i^B , I_i^{RAW} , I_i^{RRW} , I_i^{FV} of all failed edges.

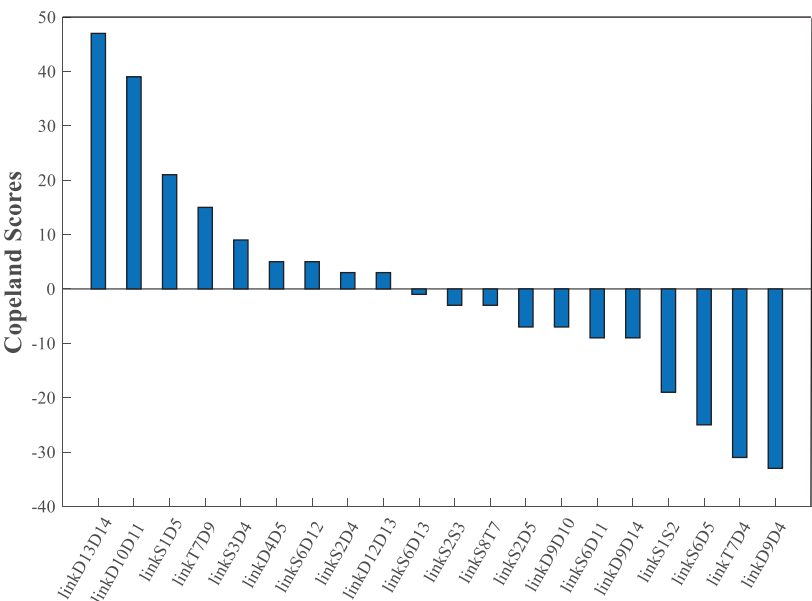


Figure 1.8: Copeland scores of all failed edges.

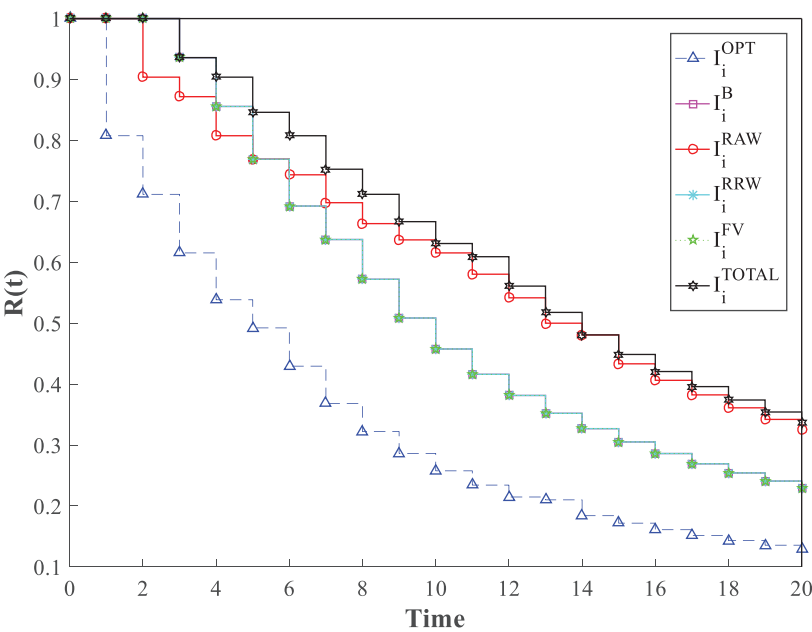


Figure 1.9: The change of $R(t)$ occurs, when all failed edges are repaired.

From Figure 1.9, $R(t)$ decreases sharply in the first four periods for the OPT importance measure. The reason is that the failed edges {Link6D12, Link2D4, Link1D5, Link6D13} are, in turn, repaired in the first four periods, which makes the supply nodes to directly meet the corresponding demand nodes. For RAW importance measure, LinkS1D5 was repaired in the second period and the demand of D5 was met; so the $R(t)$ decrease was large at this time. The $R(t)$ decreases the fastest under OPT importance measure, which is as low as 0.1288. The $R(t)$ decreases to 0.2288 for the Birnbaum importance measure, RRW importance measure, and the FV importance measure. Under RAW importance measure, $R(t)$ reaches 0.3250. $R(t)$ decreases the least to 0.3365 for TOTAL importance measure.

The failed component set E' is assumed to be {S2, S6, D4, D9, D11, T7, linkS1S2, linkS8T7, linkT7D9, linkS6D11, linkS6D12, linkS6D13, linkD12D13, linkT7D4}. I_{ij}^{OPT} of the failed components is as shown in Figure 1.10. I_i^B , I_i^{RAW} , I_i^{RRW} , I_i^{FV} of the failed components are as shown in Figure 1.11.

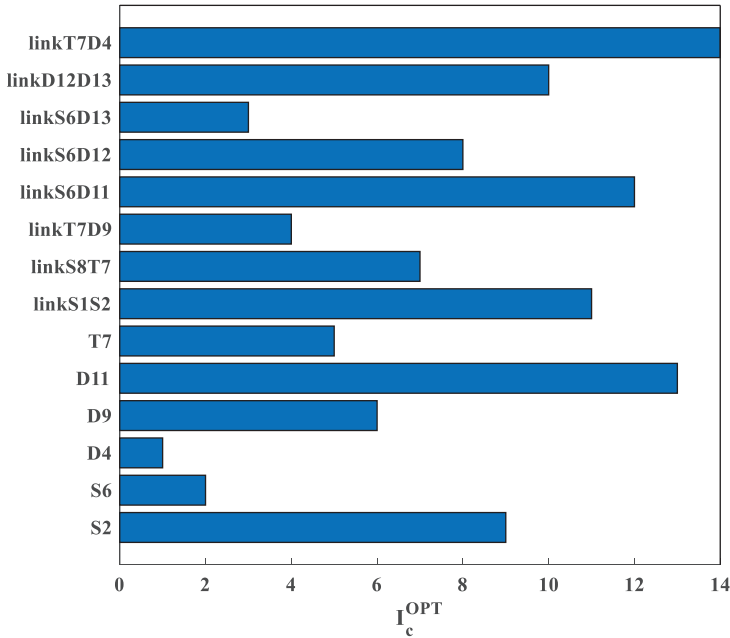


Figure 1.10: I_{ij}^{OPT} of the given failed components.

From Figure 1.11, the importance of each failed component is different for OPT importance measure and the importance of LinkT7D4 is the lowest, while that of node D4 is the highest. The recovery priority of D4 is the highest under RAW importance measure and the importance of other components is the same. For Birnbaum importance measure, RRW importance measure, and FV importance measure, S6 is more

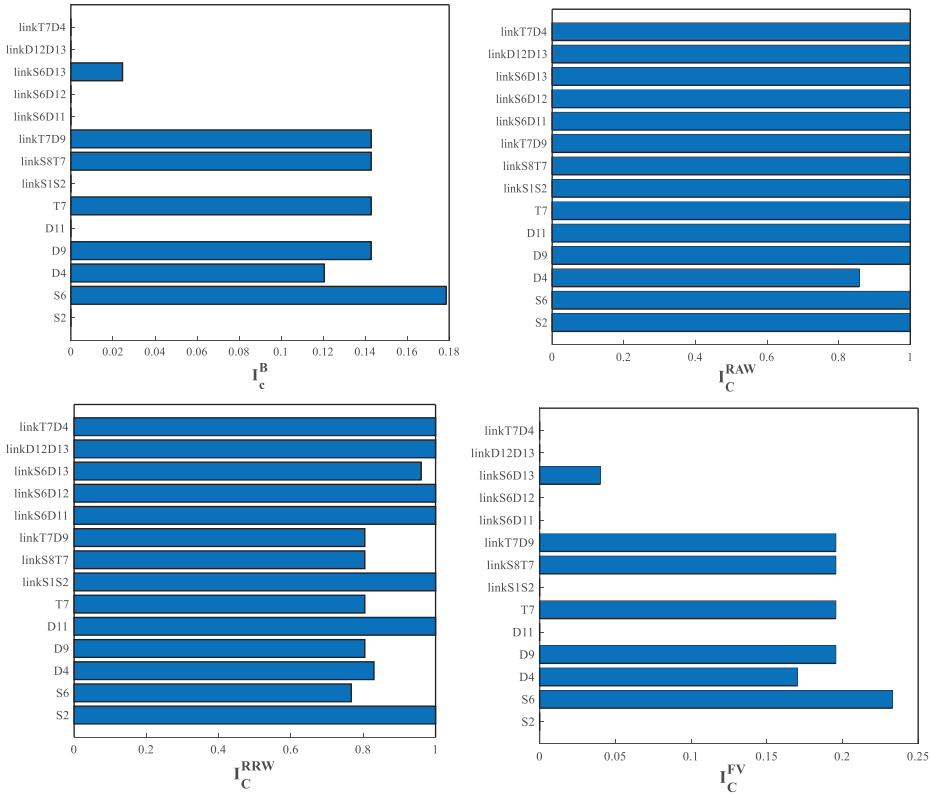


Figure 1.11: I_i^B , I_i^{RAW} , I_i^{RRW} , I_i^{FV} of the given failed components.

important for the reduction of residual resilience, followed by nodes T7, D9, Links8T7 and LinkT7D9, and the importance of other failure components is low.

Copeland method is used to calculate the scores of components and the comprehensive priority is defined by I_i^{TOTAL} . The change of $R(t)$ is as shown in Figure 1.12.

From Figure 1.12, $R(t)$ decreased significantly in the first three periods for OPT importance measure, because the repair of S6, D9 and LinkS6D13 in the first three periods directly met the requirements of node D13 and node D5. Residual resilience changes in the first and second periods for OPT importance measure and TOTAL importance measure are consistent, which is because S6 and D4 were repaired in the first two periods. The residual resilience for TOTAL importance measure in the first four periods was coincident with the Birnbaum importance measure, the RRW importance measure, and the FV importance measure. Although the repair sequence was not exactly the same, the changes in capacity were completely consistent.

For the Birnbaum importance measure, the RRW importance measure, and the FV importance measure, $R(t)$ in periods 1–3 stays at 1, because {S6, D9, T7}, respectively,

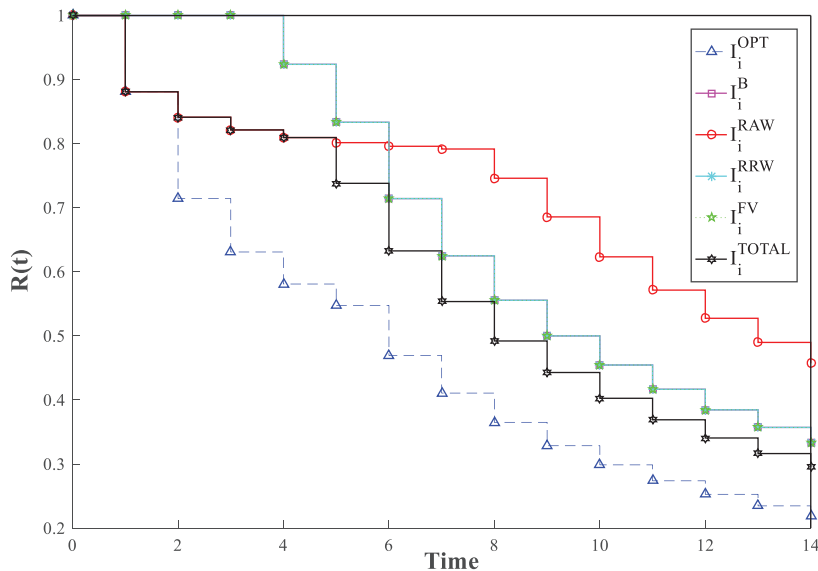


Figure 1.12: The change of $R(t)$ occurs, when the given failed components are repaired.

were repaired in periods 1–3, and the failed component was still not repaired. Therefore, the flow received by the demand node did not change.

It is assumed that all edges and nodes fail at the same time, and the optimal recovery priority of nodes and edges under the full fault set is considered. When all nodes fail, the repair of a single node cannot satisfy the requirements of the demand node. Therefore, the RAW importance measure is not discussed for the system network with full node failure state. I_i^{OPT} , I_i^B , I_i^{RRW} , I_i^{FV} of the failed components are as shown in Figure 1.13.

From Figure 1.13, for the OPT importance measure, D4 has the highest recovery priority, while LinkT7D4 has the lowest recovery priority. For Birnbaum importance measure, RRW importance measure and FV importance measure, the recovery priority of the failed component is consistent.

According to the Copeland method, the Copeland scores of the failed nodes integrated with four importance measures are as shown in Figure 1.14. The residual resilience $R(t)$ is as shown in Figure 1.15.

From Figures 1.14 and 1.15, $R(t)$ did not change in the first two periods for the OPT importance measure because nodes D4 and S3 were repaired in the first two periods. At this time, all edges in the system were not repaired until LinkS3D4 was repaired in the third period. The residual resilience changes of the TOTAL importance measure were consistent with the Birnbaum importance measure, the RRW importance measure, and the FV importance measure in the first five periods, the reason being that {S6, S8, T7, Links8T7, D4, D9} were all repaired in the first five

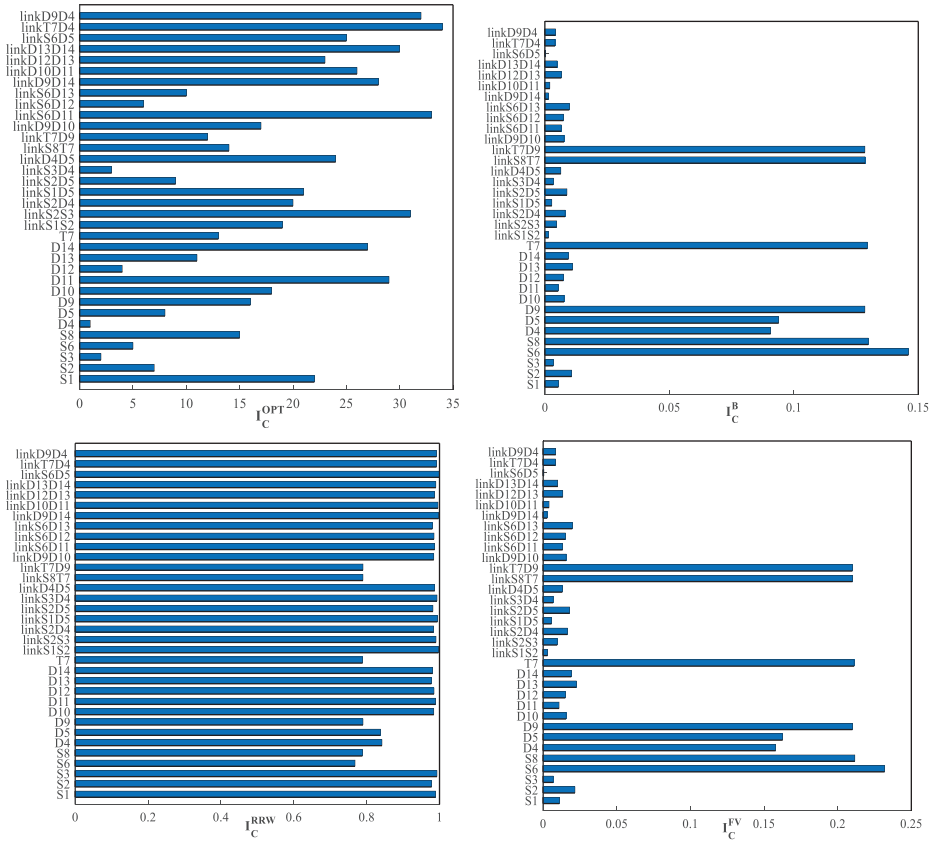


Figure 1.13: I_i^{OPT} , I_i^B , I_i^{RAW} , I_i^{FV} of all failed components.

periods, and the repair of D4 and D9 had the same influence on the running state of the network system at this time. From the sixth period, the residual resilience for the Birnbaum importance measure, the RRW importance measure, and the FV importance measure were better than the TOTAL importance measure. This is because though the bright condition repaired LinkT7D9, D9 node had been repaired for the Birnbaum importance measure, the RRW importance measure, and the FV importance measure, and the repair of LinkT7D9 directly satisfied the flow of D9 node. Starting from the 24th period, TOTAL importance measure is gradually better than the Birnbaum importance measure, the RRW importance measure, and the FV importance measure. This is because in the 24th period, LinkS3D4 was repaired under the TOTAL importance measure, which directly met the needs of D4. However, the D11 node is repaired under other important measures, which has no direct effect on the network.

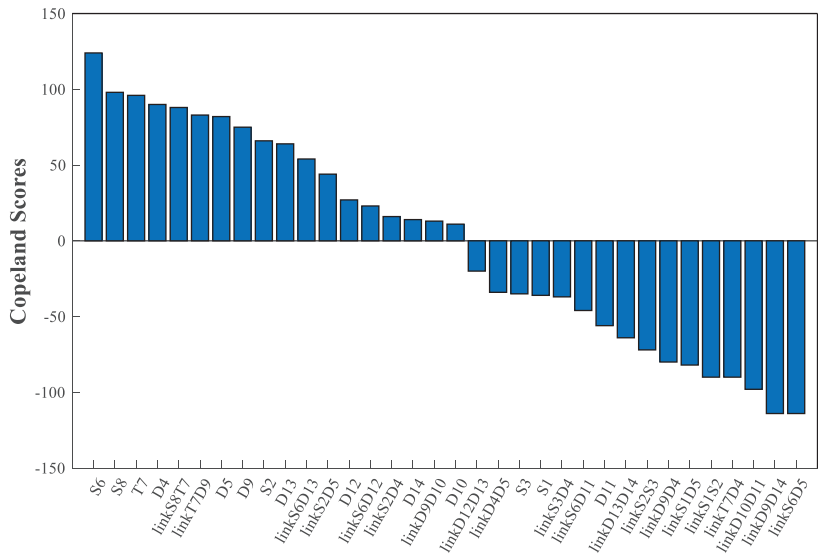


Figure 1.14: Copeland scores of all failed components.

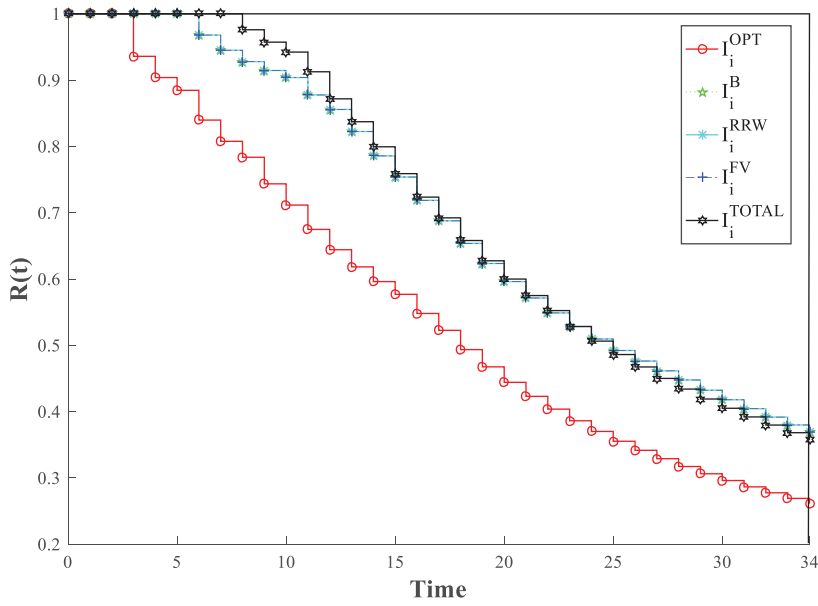


Figure 1.15: The change of $R(t)$ occurs, when all failed components are repaired.

1.5 Conclusions and future work

A residual resilience model based on the importance measure is proposed to study the recovery sequence of the failed components of the infrastructure network after a disaster. According to the different effects of the failed components on the residual resilience of the infrastructure network, after the disaster, the priority to the infrastructure network of repairing the failed component is determined. In the limited repair time, this model can help employees determine the recovery sequence of components based on different important measures and determine the best recovery sequence of failed components in the infrastructure network using the residual resilience model. This chapter provides suggestions and references for repairing failed components in the post-disaster phase of infrastructure networks.

This chapter does not specifically consider different types of disasters, which can be further studied in the future. In future, disasters can be classified and specific quantitative methods can be given according to the size of the paralyzed area under different disasters so as to make greater contributions to disaster prevention. Because different components have different repair costs, the repair sequence is also different. In future work, we will consider the recovery sequence of failed components under different cost constraints.

References

- [1] Berle, O., Asbjørnslett, B. E. & Rice, J. B. 2011. Formal vulnerability assessment of a maritime transportation system, *Reliability Engineering & System Safety*, 96(6), 696–705.
- [2] Asadabadi, A. & Miller-Hooks, E. 2020. Maritime port network resiliency and reliability through co-opetition, *Transportation Research Part E, Logistics and Transportation Review*, 137, 101916.
- [3] Adjetey-Bahun, K., Birregah, B., Châtelet, E. & Planchet, J. L. 2016. A model to quantify the resilience of mass railway transportation systems, *Reliability Engineering & System Safety*, 153, 1–14.
- [4] Cimellaro, G. P., Reinhorn, A. M. & Bruneau, M. 2010. Framework for analytical quantification of disaster resilience, *Engineering Structures*, 32(11), 3639–3649.
- [5] Zhang, C., Xu, X. & Dui, H. Y. 2020. Resilience measure of network systems by node and edge indicators, *Reliability Engineering & System Safety*, 202, 107035.
- [6] Watson, E. & Etemadi, A. 2020. Modeling electrical grid resilience under hurricane wind conditions with increased solar and wind power generation, *IEEE Transactions on Power Systems*, 35(2), 929–937.
- [7] Nguyen, H., Muhs, J. & Parvania, M. 2019. Assessing impacts of energy storage on resilience of distribution systems against hurricanes, *Journal of Modern Power Systems and Clean Energy*, 7(4), 731–740.
- [8] Wang, H. & Jin, T. 2020. Prevention and survivability for power distribution resilience: A multi-criteria renewables expansion mode, *IEEE Access*, 8, 88422–88433.

- [9] Li, G., Huang, G., Bie, Z., Lin, Y. & Huang, Y. 2019. Component importance assessment of power systems for improving resilience under wind storms, *Journal of Modern Power Systems and Clean Energy*, 7(4), 676–687.
- [10] Fang, Y., Pedroni, N. & Zio, E. 2016. Resilience-based component importance measures for critical infrastructure network systems, *IEEE Transactions on Reliability*, 65(2), 502–512.
- [11] Xu, Z. P., Ramirez-Marquez, J. E., Liu, Y. & Xiahou, T. F. 2020. A new resilience-based component importance measure for multi-state networks, *Reliability Engineering & System Safety*, 193, 106591.
- [12] Dui, H. Y., Li, S. M., Xing, L. D. & Liu, H. L. 2019. System performance-based joint importance analysis guided maintenance for repairable systems, *Reliability Engineering & System Safety*, 186, 162–175.
- [13] Dui, H. Y., Si, S. B. & Yam, R. C. M. 2018. Importance measures for optimal structure in linear consecutive-k-out-of-n systems, *Reliability Engineering & System Safety*, 169, 339–350.
- [14] Pan, X., Wang, H. X., Yang, Y. J. & Zhang, G. Z. 2019. Resilience based importance measure analysis for SoS, *Journal of Systems Engineering And Electronics*, 30(5), 920–930.
- [15] Espinoza, S., Poulos, A., Rudnick, H., De La Llera, J. C., Panteli, M. & Mancarella, P. 2020. Risk and resilience assessment with component criticality ranking of electric power systems subject to earthquakes, *Ieee Systems Journal*, 14(2), 2837–2848.
- [16] Li, G. F., Huang, G. C., Bie, Z., Lin, Y. & Huang, Y. X. 2019. Component importance assessment of power systems for improving resilience under wind storms, *Journal of Modern Power Systems and Clean Energy*, 7(4), 676–687.
- [17] Fang, Y. P., Pedroni, N. & Zio, E. 2016. Resilience-based component importance measures for critical infrastructure network systems, *IEEE Transactions on Reliability*, 65(2), 502–512.
- [18] Cai, B. P., Xie, M., Liu, Y. H., Liu, Y. L. & Feng, Q. 2018. Availability-based engineering resilience metric and its corresponding evaluation methodology, *Reliability Engineering & System Safety*, 172, 216–224.

Jian Zhou, David W. Coit

2 Modeling of mixed cascading failures and resilience-based restoration selection

Abstract: This chapter proposes a new model to describe mixed cascading failures in network systems. The new model offers advantages to analyze the combined impacts of network load dynamics and network dependency on failure propagation. Mixed cascading failures can be simulated and the influence of dependence clusters of network nodes on the robustness of network systems can be studied based on the new model. The effects of network topology on network robustness are also investigated using numerical examples. A new system resilience metric, which is time-dependent, performance-based, and normalized, is proposed. Combined with two other system performance measurements, the effects of four restoration strategies with distinct restoration priorities are analyzed based on the modified model and a typical synthetic network model. The relationship of system dependency and restoration effects regarding system resilience against cascading failures is explored. Finally, conclusion about the findings and future work directions are presented.

Keywords: Network systems, cascading failures, load dynamics, system dependency, restoration strategy, resilience

2.1 Introduction

As manmade technical systems, such as transportation systems and electricity systems, are becoming increasingly widely used, economic and social well-being are dependent on the continuous and reliable operation of these complex systems [1]. However, recent worldwide events, such as the 2003 blackout in Italy, the 2003 North American blackout and 2012 Hurricane Sandy blackout, have shown the increased vulnerability of these systems [2]. Initial component failures in these systems, even small ones, can trigger failure propagation via multiple system dependencies, which spread adverse influence on a very large scale, severely affecting the whole system performance. This domino effect of failure propagation is named cascading failures.

Jian Zhou, School of Economics and Management, Nanjing University of Science and Technology, Nanjing, China

David W. Coit, Department of Industrial and Systems Engineering, Rutgers University, New Jersey, USA

<https://doi.org/10.1515/9783110725599-002>

Cascading failures are a phenomenon of failure propagation observed in various real-life network systems, such as power grids and transportation systems. In general, a network system carries a flow of particular resource (such as electricity, gas, and data packets). Each system node individually transfers an amount of load, and in normal circumstances, this load does not exceed the capacity of that node which is limited in most of cases. Cascade failures can be briefly described as follows; when a heavily loaded network node breaks down for some reasons, the load on that node (i.e., the flow passing through it) is redistributed to other nodes in the network system. This load redistribution might cause other nodes to be overloaded, contributing to their breakdown. Even if an overloaded node does not actually fail, the pre-designed protection mechanisms may shut it down in order to prevent damage to this node [3]. As a result, the number of failed or stressed nodes continuously increases, and the failures can widely propagate. In particularly severe cases, the entire network system is influenced.

Although cascading failures occur with a low probability, a sharp degradation of system performance, even the collapse of much of the complex system, is experienced when they occur [4–7]. Some massive cascading failures have taken place in complex communication network systems, social network systems, and economic network systems [8]. Therefore, the study of this failure phenomenon is particularly significant.

Researchers have studied cascading failures in complex systems, and many models have been proposed to depict the process of cascades [9, 10]. Current cascading failures models mainly include load-capacity models [11–13], binary influence models [14], sand pile models [15, 16], optimal power algorithm (OPA) models [17, 18], and CASCADE models [19, 20]. For example, OPA models and CASCADE models focus on cascading failures in electric power systems.

Dependence relationships among network nodes, except for topological links (referring to topological connectivity), also accelerate the propagation of network failures and affect the mechanism of cascading failures [21–23]. Past incidents have demonstrated the cascading impacts posed by interdependencies, by highlighting the ways that the electricity system is dependent on other sectors, including the communications infrastructure and information systems. For instance, the 2003 Northeastern Blackout, which initially began with power lines in contact with tree branches, was magnified by a series of cascading computer failures that affected airline operations, the financial and banking sector, blood, and potable water supplies, and other critical services [24]. Hence, modeling and simulation of cascading failures considering the dependencies inside the network system becomes a vital field of research [25–29].

For engineering systems, resilience implies the ability of a system to withstand or quickly return to normal condition after the occurrence of an event that disrupts its state. It depicts the scenarios that system performance degrades due to disruptive events with uncertainty, and it reflects the capability of a system to adjust its

functionality accordingly and the recovery process. Therefore, modeling and evaluating system resilience, especially for the complex and large-scale systems, has recently raised significant interest. Many definitions of system resilience and approaches to measure it across different disciplines have been proposed. In general, system resilience is impacted by system reliability, vulnerability, and recoverability.

Unlike reliability, the idiosyncratic and low-probability nature of resilience risks makes measuring and valuating resilience challenging [30]. There has been no coordinated industry or government initiative to develop a consensus on or implement standardized resilience metrics [31]. More work is needed to incorporate existing interdependent infrastructure system models with the study of interdependent resilience [32]. Furthermore, optimize restoration of network systems regarding cascading failures for resilience enhancement is important and needs exploration.

2.2 Modeling of mixed cascading failures

In this part, a new cascading failure model has been developed to analyze the mixed system failures spreading over network systems [33]. Existing cascading failure models, which focus on network load dynamics, provide alternative methods to analyze cascading failures in network systems. However, these studies seldom consider the joint impacts of system dependencies among network nodes, which have a great impact on network system dynamic behaviors. The new model extends existing research by taking into consideration load dynamics and network dependency which forms dependence clusters in a single/isolated network system.

Dependence clusters are proposed to represent the dependence relationships of network nodes apart from the network topological connectivity. These dependence clusters include the network nodes with dependence interactions between each other that are beyond the topological connections. A typical single network containing dependence clusters is presented in Figure 2.1. The network topological structure has network nodes denoted by points. The solid lines represent the topological links in the network, while the dependent nodes are connected by dependence links represented by dashed lines. The dependence groups are circled, identifying the dependence clusters of network nodes.

A single network is defined as an unweighted, undirected, self-loop free, and single edge graph *Net*. It is represented by an adjacent matrix containing N nodes $\{v_1, v_2, \dots, v_N\}$ and M edges $\{e_1, e_2, \dots, e_M\}$. For instance, network nodes represent power stations (or sub-stations) and edges represent power transmission elements in power grids. If there is a topological link between two network nodes, the edge weight is 1 in an adjacent matrix. If there is no topological link between two nodes, the corresponding edge weight is 0. It is assumed that network load only transmits along the shortest paths between every pair of network nodes, where each path

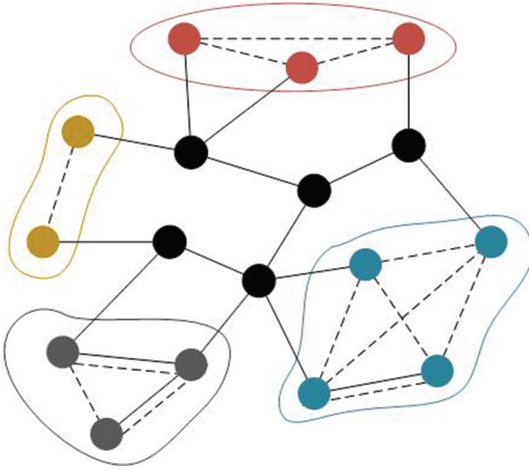


Figure 2.1: Illustration of a single network with dependence clusters of nodes [33].

consists of edges (i.e., topological links). The length of a path is calculated by summing the edge weights along the path. If there is no path between a pair of nodes, the distance between these two nodes is assumed to be infinite.

2.2.1 Main assumptions

In this section, we assume that load on node i at time t , $L_i(t)$, is defined as the “betweenness centrality” [34] of node i at time t , which can be calculated as follows:

$$L_i(t) = \sum_{s \neq i \neq l} \frac{\sigma_{sl}(i, t)}{\sigma_{sl}(t)}, \quad i, s, l \in N \quad (2.1)$$

where $\sigma_{sl}(i)$ is the number of shortest paths between nodes s and l at time t . $\sigma_{sl}(i, t)$ is the number of shortest paths between nodes s and l passing through node i at time t . s, l can be any nodes in the network system.

Other approaches to define load flow in network systems have been proposed, but the load adopted here has been widely used to depict the real flow in network systems [35–38], such as current for power grids and traffic for transportation networks. Node load is calculated based on the algorithm presented in [39]. Node capacity denotes the maximum load that a node can process without being congested. A nonlinear capacity-load model is used to define the capacity of each network node [40] as eq. (2.2):

$$C_i = \alpha \left(L_i(0) + L_i(0)^{1-\mu} \right), \quad i = 1, 2, \dots, N, \quad \alpha \geq 1, \quad 0 < \mu < 1 \quad (2.2)$$

where C_i denotes the capacity of network node i . $L_i(0)$ is the load of node i at initial time $t = 0$. α and μ denote the parameters to control network node capacity. The effects of these two parameters were discussed in the papers [12, 40], and both of them are applied to describe the nonlinear characteristic of node capacity and load.

The proposed mixed cascading failures model describes two types of network failures. First, as depicted in existing cascading failures models, dynamic network load distribution is mainly accounted for the cause of cascading failures. For this kind of failures, failed nodes and their connected links are disconnected from the network. As a result, some shortest paths between pairs of nodes in the network are changed. Network load is then redistributed along the latest shortest paths which can cause more load added to some working nodes. Once the load exceeds node capacity, these overloaded nodes are considered to be breakdown. They are removed from the network and then the compositions of some sets of shortest paths in the network are changed again. New rounds of network load redistribution along with the updated shortest paths and overload cascading failures ensued are iteratively triggered in this way. This is the load dynamics-caused failure. Second, taking into account the impacts of dependence relationships among network nodes, immediate failures of entire dependence clusters of network nodes occur if any nodes belonging to these dependence clusters break down. This is dependence-caused failure. Eq. (2.3) defines this type of failure,

$$Dep(v_i, l) = \begin{cases} 0, v_i \notin \{cluster\ l\} \\ 0, v_i \in \{cluster\ l\} \end{cases} \quad (2.3)$$

where $Dep(v_i, l)$ denotes whether network node v_i fails given dependence cluster l collapses. $Dep(v_i, l) = 1$ means that node v_i immediately fails because it belongs to cluster l , while $Dep(v_i, l) = 0$ means that node v_i does not belong to dependence cluster l and is not impacted by the collapse of cluster l . In practice, multiple dependencies are often highly complex, for example, there can be interdependencies between different dependence clusters in some systems, but it is not considered in this work. This is a reasonable assumption which is considered in many common applications [23, 28, 29].

2.2.2 Network cascading failure process

Two types of failures introduced above could iteratively occur in the network system. A network node failure caused by overload (load dynamics-caused failure) can lead to direct failures of other nodes belonging to the same dependence cluster with the overloaded nodes (dependence-caused failures). It changes network topology, and then a subsequent round of network load redistribution is triggered, which might lead to new overloaded node failures. The cascading process is briefly shown

in Figure 2.2. It should be noted that dots represent network nodes and solid lines denote topological links in Figure 2.2. Circles represent dependence clusters and dashed lines denote dependence links between dependent nodes. Once a node failure occurs, it is disconnected from the network system along with the edges/links connected to it. Since dependency among network nodes and topological connectivity links are assumed to be unrelated, node failures caused by node dependency are independent of network structure.

The main steps of the simulation of mixed cascading failures, including two iterative failure processes are depicted as follows,

- Step 1) a. Construct $Net(N, M)$, and calculate the size of the largest connected component of the network (LCC).
b. Determine dependence clusters in $Net(N, M)$.
- Step 2) Allocate capacity of each system node based on eq. (2.2).
- Step 3) a. Select failures on network nodes randomly as initial failures.
b. Remove all failed nodes and their connected edges from the network.
- Step 4) a. Determine network nodes within the dependence clusters which include initially failed nodes.
b. Remove the dependence clusters along with the edges from the network.
- Step 5) Update the shortest paths in the network based on current network structure.
- Step 6) Calculate node load at time t , $L_i(t)$, $i \in N$, after new round of load redistribution.
- Step 7) If $L_i(t) > C_i$, $i \in N$, remove the overloaded nodes and other nodes in the same dependence clusters. Then go back to Step 5. If not, go to Step 8.
- Step 8) Calculate the final size of LCC and the number of iterations of cascades, T . The simulation ends.

The metric used to evaluate the effect of mixed cascading failures on network structure is network connectivity G , which is calculated based on eq. (2.4),

$$G = \frac{N_F}{N_I} \quad (2.4)$$

where N_I is the initial size of LCC . N_F is the final size of LCC when failures stop. A larger proportion of network collapses as G decreases. T is the duration of cascading failures until it reaches the stop criteria. It is used to evaluate the speed of failure propagation.

2.2.3 Numerical examples

Network examples are performed on a general network structure, ER random network [41], which was proposed by Erdos and Renyi. It is a typical model for constructing random networks, whose load distribution and node degree distribution

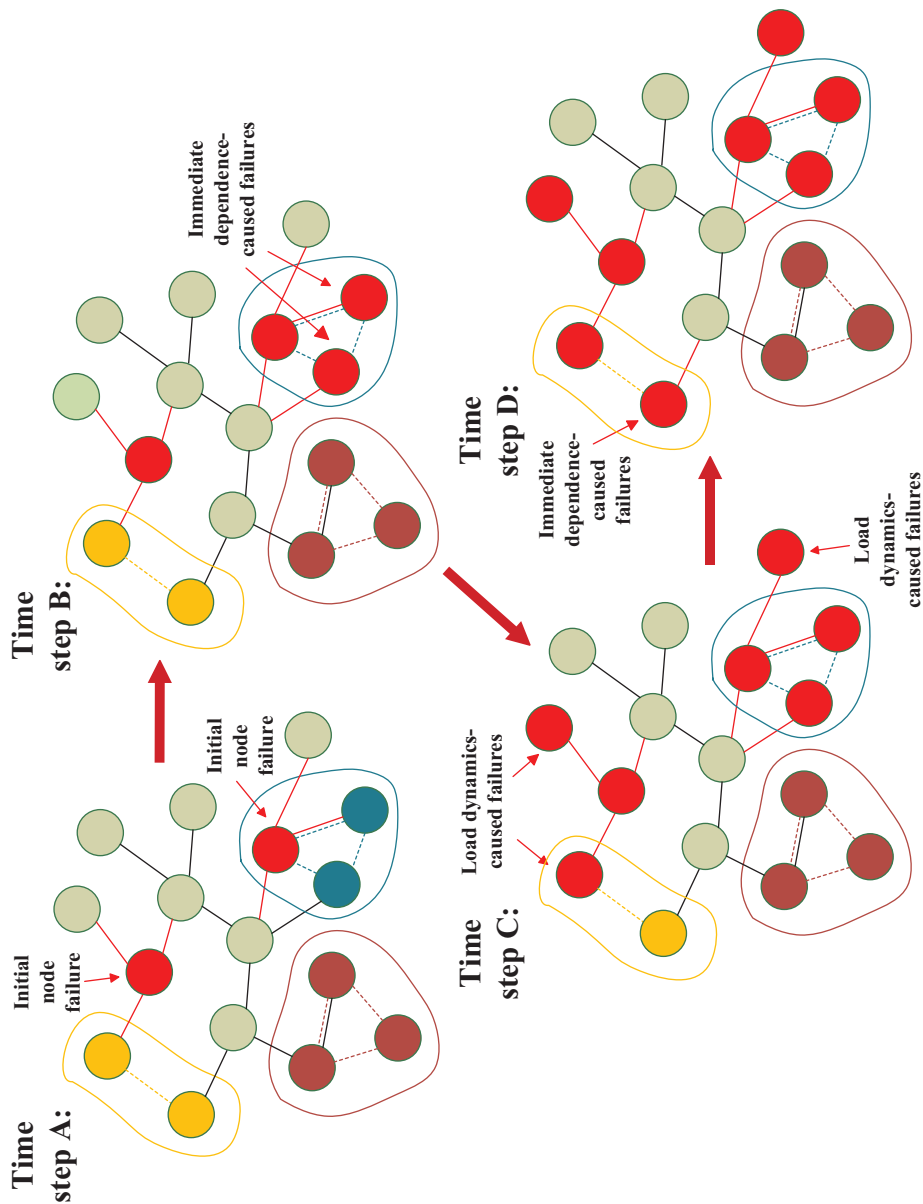


Figure 2.2: Cascading process of two types of failures in a network with dependence clusters [33].

follow Poisson distributions. Sizes of dependence clusters in a real-world network usually follow certain distributions [29]. The case that sizes of dependence clusters follow a shifted or scale adjusted Poisson distribution is studied, that is, the probability that a node belongs to a dependence cluster of size D ($D \geq 1$), $P(D)$, is given by eq. (2.5) [29],

$$P(D) = \frac{\lambda^{D-1} e^{-\lambda}}{(D-1)!}, \text{ for } D \geq 1 \quad (2.5)$$

where $\lambda = (D - \text{size}) - 1$. D -size is the mean size of dependence clusters in the network system, that is, the average number of nodes included in a dependence cluster.

The impact of the only parameter, mean size of dependence clusters D -size, on network robustness against cascading failures is explored. Figures 2.3 and 2.4 present the changing values of G and T obtained in cascading simulation using the proposed mixed cascading model. The networks in Figures 2.3 and 2.4 have $N = 1,000$ and $K = 10$. K is the average degree of network nodes. It denotes average number of topological links that a node has in the network. The parameters for C_i are $\alpha = 1.05$ and $\mu = 0.5$. $Nrem$ is the number of network nodes randomly failed at the beginning of the cascading simulation.

In Figure 2.3, every point in the curves corresponds to an average of 20 random initial failure triggers on 20 different randomly generated ER networks with the same pair of (N, K) . Note that because the curves shown in the figures are average simulation results, those curves may not be as smooth as theoretical results would suggest. The atypical behavior of some curves is attributed to the randomness associated with simulation. Figure 2.3 shows the results of parameter G versus $Nrem$, while Figure 2.4 shows the results of parameter T versus $Nrem$. Four subgraphs (a), (b), (c), (d) in the figures present the simulation results considering dependence clusters of different mean sizes, that is, D -size = 2 to 5. The plotted curves in the figures mainly present the simulation results (points) which are close to the transition point (critical point).

As illustrated in Figure 2.3, phase transition occurs as the changing trend of G versus $Nrem$. Parameter G sharply drops as $Nrem$ increases to the critical transition threshold value, $NremC$, for D -size = 3 to 5, that is, first-order phase transition occurs, and the network system breaks down directly to the totally collapsed state. $NremC$ indicates the critical number of nodes initially removed which cause collapse of the network. The network collapses when the number of initially removed nodes is larger than $NremC$, otherwise, the network does not collapse although cascading failures still can occur.

The network, which undergoes a first-order transition of cascades, indicates that the size of LCC abruptly decreases, that is, indicator G goes down discontinuously from large value (for $Nrem < NremC$) to almost zero (for $Nrem > NremC$). Such a network is obviously more vulnerable than a network that is subjected to a second-

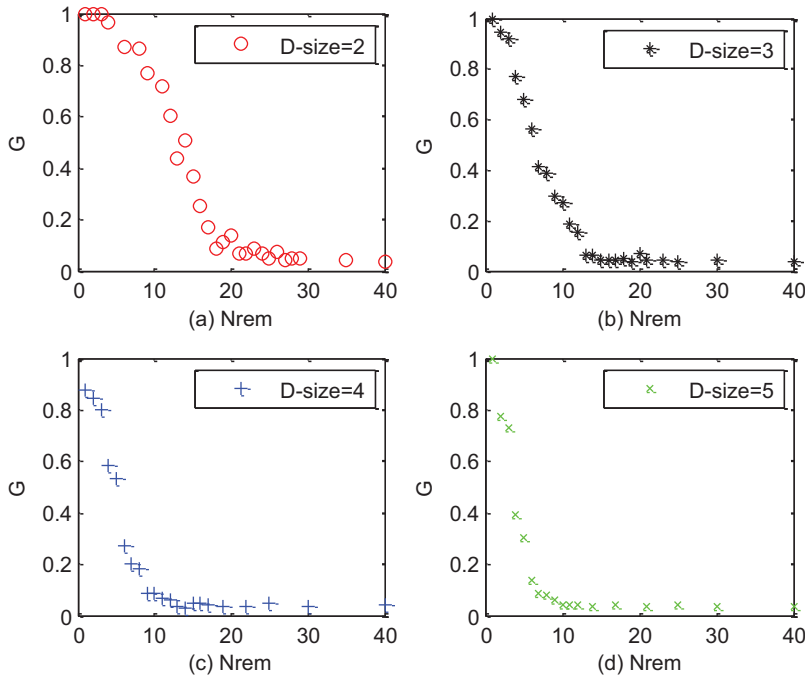


Figure 2.3: Simulation results of G for mixed cascading failures [33].

order transition of cascading failures, where G continuously decreases from a finite value to almost zero at transition point $NremC$. When the number of network nodes initially failed equals or is larger than $NremC$, cascading failures collapse the network very quickly, meaning the network is completely fragmented. Thus, $NremC$ could be used as an indicator to show the robustness of a network to cascading failures triggered by random node failures.

With $D\text{-size} = 2$ or 1 (network dependency is not considered in the cascades when $D\text{-size} = 1$), G changes continually as $Nrem$ changes, which indicates the occurrence of a second-order phase transition. In Figure 2.4, the peaks of changing trends of T also emphasize the transition points $NremC$, which are consistent with $NremC$ as shown in Figure 2.3. Moreover, as illustrated in both figures, as mean size $D\text{-size}$ increases, the value of critical transition point $NremC$ decreases. The results of transition points $NremC$ and evaluation parameter T_c in the cascading simulation in Figures 2.3 and 2.4 are presented in Table 2.1.

Based on the simulation results in Table 2.1, findings about the mixed cascading failures can be given as follows.

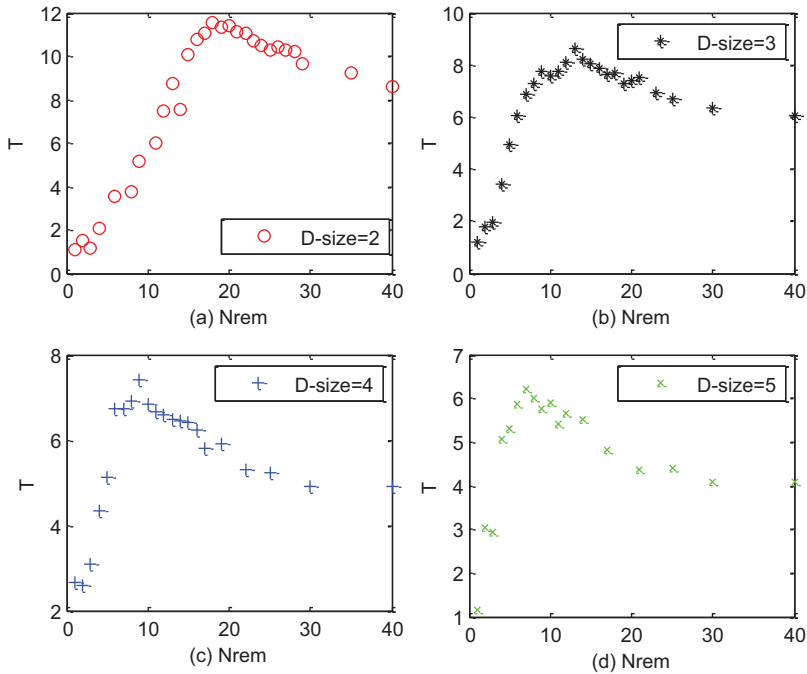


Figure 2.4: Simulation results of T for mixed cascading failures [33].

Table 2.1: T_c versus $NremC$ with different D -size under two cascading failure models [33].

D -size	Poisson distribution of dependence cluster				Without dependence clusters
	2	3	4	5	
$NremC$	18	13	9	7	46
T_c	11.57	8.6	7.4	6.2	20.75

- 1) When the sizes of dependence clusters of network nodes follow the Poisson distribution, the process of cascading failures changes from a continuous second-order phase transition to a discontinuous first-order phase transition, compared with the cascading process without considering node dependency. Based on Table 2.1, $NremC$ and T_c of the combined cascading networks (first-order phase transition) are much smaller than that of cascades without dependence clusters (second-order phase transition). This indicates that the robustness of the network when exposed to mixed cascading failures is less. Similar conclusions were observed in previous papers which focus on interdependence networks [26]. Change in the type of phase transition explains why mixed cascading failures is much more damaging.

- 2) *D-size* exerts a notable influence on the effect of dependence clusters on mixed cascading failures. As shown in the results, T_c and $NremC$ decrease if *D-size* increases. This means that the effect of dependence clusters on network robustness is higher when *D-size* increases. It indicates that for larger *D-size*, the impact of dependence clusters is more noticeable causing failure propagation. This observation is in agreement with the previous findings about the impact of parameter *D-size* in [13] which assumes all dependence clusters in the network have the same fixed sizes.
- 3) Compared with the findings in [13] with the same network, the values of T_c obtained in the new mixed cascading simulation are larger given the same values of *D-size*. This is likely because the dependence clusters considered in [26] are mean size, but they have randomly different sizes in the network for the proposed new model.

Then, the impact of the average degree of network node is presented, which is an important network topological property, denoted by K on network robustness regarding mixed cascading failures. The obtained simulation results on the ER random network ($N = 1,000$) with several values of K are illustrated in Figure 2.5.

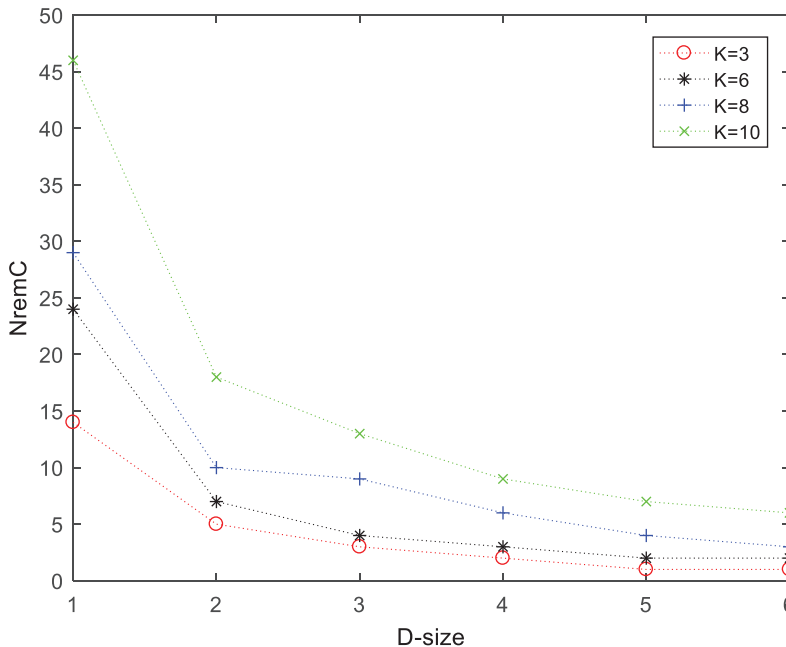


Figure 2.5: Transition points of mixed cascades under different average degree [33].

$NremC$ are plotted in Figure 2.5 as a function of D -size under different values of K . These trends of $NremC$ clearly show that D -size impacts network robustness to mixed cascading failures in ER random networks with different average degree. Small $NremC$ indicates that robustness of the network against mixed cascading failures is poor. In other words, breakdown of a few nodes can trigger the mixed cascades that collapse the entire network. It should be noted that D -size = 1 indicates a network without dependence clusters of nodes. It can be observed that values of $NremC$ for D -size = 1 differ from that under D -size ≥ 2 . The appearance of change in phase transition of cascading failures is caused by D -size. Moreover, it can be seen from Figure 2.5 that, with the same D -size, as K increases, $NremC$ also increases. The ER networks with larger average degree K are more robust to mixed cascading failures triggered by random failures of network nodes.

2.3 Resilience-based restoration selection against cascading failures

The assumption that immediate collapse of a dependence cluster occurs if any dependent nodes inside break down is made to depict the impacts of strong system dependency on failure propagation. They may not be the cases for some real-world applications since multiple dependencies can exist between network components, which result in various dependency strengths [21]. Therefore, system dependency strength regarding failure propagation is then described by the dependence cluster collapsing threshold (CCT) [42]. The application of this improved system dependency model to resilience-based system restoration against cascading failures is presented in this section. To be specific, the effects of restoration strategies on recovering network systems from cascading failures are investigated considering the impacts of multiple network system properties. Resilience loss, together with two other system performance measurements, system connectivity G and recovery time T , are used to evaluate restoration effects. Four restoration strategies with different restoration prioritizations are applied to a typical synthetic network model. The influence of system dependency on resilience-based restoration effects against cascading failures is explored.

2.3.1 System modeling and implementation process

In this section, dependency strength is introduced by dependence CCT . A dependence cluster collapses, that is, all nodes belonging to this cluster break down, once the proportion of failed nodes belonging to the dependence cluster exceeds CCT . Smaller CCT means stronger dependency strength among network nodes. It means

that failed nodes in a dependence cluster have more significant impact on the functional nodes in the same dependence cluster. The immediate collapse of a dependence cluster may result from overloaded failures once CCT is reached. In turn, dependence failures can dramatically change network topology and accelerate load dynamic-based failures. The efficiency of the shortest path regarding load transmission between nodes i and j , E_{ij} , is presented in eq. (2.6). e_k represents the edge (topological link) k , which is a part of the shortest path, between network node i and node j . The shortest path between two nodes changes if the status of any of its contained edge changes.

$$E_{ij} = \left(\sum \frac{1}{e_k} \right) \quad (2.6)$$

Network efficiency $E(Net)$ defined in eq. (2.7) is adopted as the system performance to evaluate network recovery level in terms of load transmission capability [43].

$$E(Net) = \frac{1}{N(N-1)} \sum_{i \neq j \in G_p} E_{ij} \quad (2.7)$$

Higher $E(Net)$ indicates more efficient load transmission of the network. The main steps to model mixed cascading failures and restoration implementation are as follows:

- Step 1) Total N network nodes are initially functional with allocated capacity. All dependence clusters in the network are determined.
- Step 2) Randomly select system nodes to break down due to initial interruptions.
- Step 3) Dependence clusters collapse if CCT is exceeded.
- Step 4) Network load are dynamically redistributed over the updated network structure. Overloaded nodes fail.
- Step 5) The proportion of failed nodes, R_p , is selected to start repair activities with a required repair time.
- Step 6) Go back to Step 3, until network is recovered to the predetermined level.

Network performance measurements are collected during the entire process.

2.3.2 Resilience measurement and restoration strategies

Although some resilience metrics have been proposed to measure system resilience in different areas, there are no standardized metrics for system resilience. A new resilience metric, $\mathcal{R}(t)$, which measures system resilience loss due to system failures is proposed [44]. Figure 2.6 shows the changing trend of a type of system performance, $Q(t)$, as time goes on when cascading failures occur and restoration is performed.

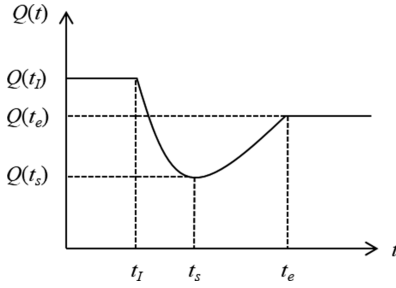


Figure 2.6: Changing trend of quality measure $Q(t)$ after failures occur and restoration implementation [44].

A disruptive event happens at time t_I . It triggers cascading failures, resulting in the decrease of system performance $Q(t)$. After conducting restoration strategies for a while, $Q(t)$ is recovered to a predetermined level at time t_e . Generally, $Q(t_I) \geq Q(t_e)$, where $Q(t_I)$ denotes the initial level of $Q(t)$ and $Q(t_e)$ denotes the recovered level of system performance. System resilience loss up to time t is measured by $\mathfrak{R}(t)$. $\mathfrak{R}(t)$ is defined as the proportion of lost system performance $Q(t)$ due to cascading failures with respect to a comparative $Q(t)$ if there is no failure up to time t . $\mathfrak{R}(t)$ is formulated in the following equation:

$$\mathfrak{R}(t) = \begin{cases} 0, & t \leq t_I \\ \frac{\int_{t_I}^t (Q(t_I) - Q(t)) dt}{Q(t_I)(t - t_I)}, & t > t_I \end{cases} \quad (2.8)$$

where $0 \leq \mathfrak{R}(t) \leq 1$, $t \in [0, t_e]$. Smaller $\mathfrak{R}(t)$ indicates less resilience loss.

The new resilience metric takes into account the time that the system stays in each stage since system resilience changes, for instance, the stage that cascading failures occur and system performance decreases. This system resilience metric is related to the measurement of a specific system performance, $Q(t)$. Because system performance can be measured from different perspectives, the considered system performance should be reflected from system resilience measurement. In the end, this resilience metric is quantitative and normalized between $[0, 1]$, which is important to make resilience of different systems comparable and make system resilience to be understandable. Thus, this metric can be applied to different types of systems for resilience analysis. In this section, the amount of network load is adopted as $Q(t)$ to calculate resilience loss $\mathfrak{R}(t)$ with respect to system load demand and supply capability.

Four different restoration strategies are adopted to recover the system when cascading failures occur. They are introduced as follows,

- (1) Random repair strategy (RR): RR is the default restoration strategy and it is applied for comparison purposes. The failed network nodes, where repair activity has not yet started, are selected to be repaired at each round of inspection based on repair proportion R_p . It denotes the proportion of failed components, whose repairing activities have not yet begun, that can start to be repaired.

- (2) High-degree first repair strategy (HDFR): HDFR is targeted for the repair order assigned according to the degree of failed nodes. Failed components, of which repairing has not yet started, are repaired in descending order of node degree, that is, network nodes with higher node degrees are repaired with higher priority.
- (3) Short-time first repair strategy (STFR): STFR involves the repair order assigned based on the required repair time of failed nodes. The restoration prioritizes the failed nodes that require shorter repair time.
- (4) High-load first repair strategy (HLFR): HLFR strategy prioritizes repair based on the amount of load carried by the failed nodes. Failed nodes where repair activity has not yet started at inspection are repaired in descending order of the amount of node load.

It requires an exact order of repair actions since more than one new node failures might exist at the inspection. Ties, which occur when new failed nodes have the same condition (i.e., the same node degree, the same required repair time or the same load), are broken by the first fail first repair policy. The repair activity of failed nodes, once started, will not stop until they are completed. For simplicity, it is assumed that the restoration resources are available to do so. As a result, the number of new repair activities of failed nodes, which get started at the inspection, is decided by the repair proportion R_p and the total number of failed nodes, whose repair activity has not started yet.

2.3.3 Numerical examples

In this section, the impacts of two network dependence characteristics (*CCT* and *D-size*) and load dynamics on restoration effects regarding system resiliency are investigated. In the numerical examples performed on ER random networks, the repair proportion R_p is set to be 0.7, that is, the proportion of failed nodes whose repair activities have not yet started can be selected to start repairing is 0.7 at inspection. The simulation process includes failure propagation and restoration implementation. For generalization, multiple simulations are conducted under the same condition to calculate the average of resilience loss and other measurements, which are collected since failures happen until network efficiency is recovered to 95% of its initial level. The required repair time of each failed node is randomly selected between 1 to 3 time units, that is, time steps in the simulation. The time from failures occur to restoring the system to the predetermined level, T , is represented by the total number of iterations of simulated failure propagation during the process. Simulation iteration represents a fixed duration of time.

Cascading failures are triggered by randomly selecting failures on network nodes. The triggering mechanism depicts random failures of system components. Different numbers of initially failed nodes (N_{rem}) are considered in this work, which

are 9, 15, 21, 27, 33, 39, 45, 51, 57, and 63. To minimize random errors, simulation results for a specific $Nrem$ correspond to the average of results over many realizations of randomly selecting nodes to fail. Numeric examples are conducted on ER network models. The ER networks used in this work contain 500 nodes and average node degree K of 11.92. Note that all the following results from ER networks are averaged over 90 realizations.

2.3.3.1 Test on random repair strategy

First, RR strategy is performed on ER networks. The numerical results of average resilience loss and G are illustrated in Figure 2.7. Scenarios for different CCT and D -size are considered, i.e., $CCT = 0.5, 0.7, 0.9$, D -size = 2, 4, 6, 8, 10, respectively.

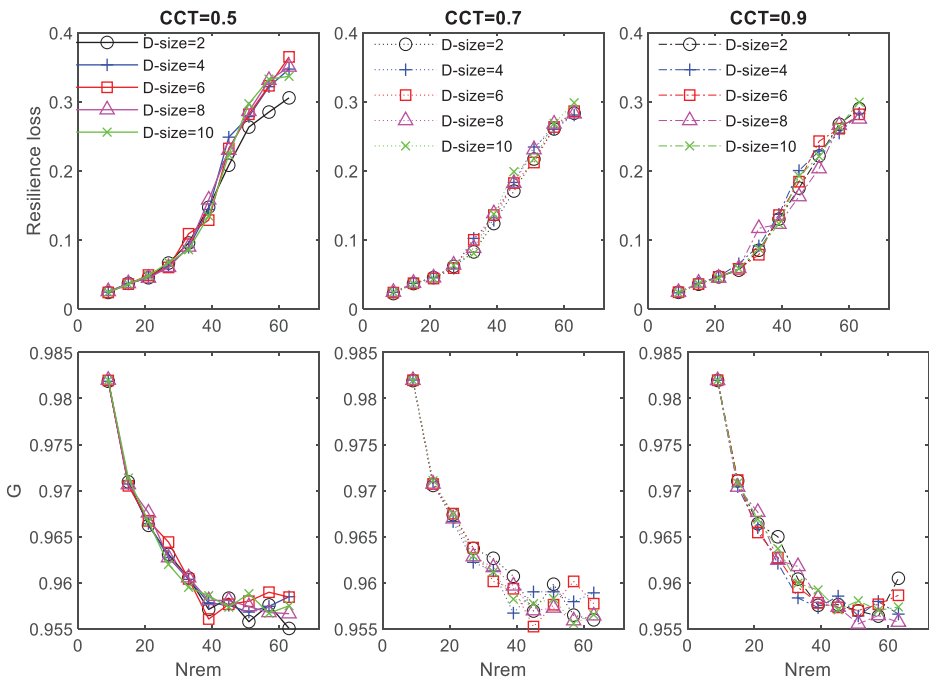


Figure 2.7: Average results of resilience loss and G as a function of $Nrem$ [44].

Resilience loss increases as $Nrem$ increases no matter the value of CCT or D -size. The incremental speed of resilience loss increases noticeably when $Nrem$ surpasses a threshold. It indicates that the effectiveness of RR strategy on reducing resilience loss decreases when $Nrem$ is large enough. G declines sharply as $Nrem$ increases initially, while the rate of decline decreases when $Nrem$ exceeds a threshold. Note that the thresholds of $Nrem$ regarding the trends of resilience loss and G are almost the

same. It means that system connectivity stays the same after network efficiency is recovered to the predetermined level, although resilience loss increases as *Nrem* increases.

Table 2.2 presents the average results of resilience loss and *T* over different *Nrem*. Based on Table 2.2, weak dependency strength corresponding to big *CCT* can reduce resilience loss. *T* decreases as *CCT* increases or *D-size* decreases. It can be an indication that stronger dependence characteristics (either stronger dependency strength or larger scale of dependence cluster) impair restoration effects against cascading failures.

Table 2.2: Average results of resilience loss and *T* for different *Nrem* [44].

Resilience loss (%)	<i>D-size</i>					Aver- age	<i>T</i>	<i>D-size</i>					Aver- age
	2	4	6	8	10			2	4	6	8	10	
<i>CCT</i> = 0.5	14.8	16.0	16.1	16.1	15.8	15.8	<i>CCT</i> = 0.5	10.4	17.2	18.4	19.6	20.1	17.1
<i>CCT</i> = 0.7	13.0	13.5	13.4	13.6	13.7	13.4	<i>CCT</i> = 0.7	7.1	7.6	7.9	7.9	7.5	7.6
<i>CCT</i> = 0.9	13.3	13.7	13.5	13.1	13.5	13.4	<i>CCT</i> = 0.9	7.6	7.5	7.6	7.1	7.8	7.5
Average	13.7	14.4	14.3	14.3	14.3	14.2	Average	8.4	10.8	11.3	11.5	11.8	10.8

2.3.3.2 Test on high-degree first repair strategy

Average results of resilience loss, *G* and *T* versus *Nrem* for the HDFR strategy are presented in Figure 2.8. According to Figure 2.8, both resilience loss and *T* increase when *Nrem* increases, while *G* decreases as *Nrem* increases. Table 2.3 shows the average results of resilience loss and *T*. It should be noted that different *D-size* does not cause a notable difference regarding three measurements under HDFR strategy, that is, there is a significant overlap between the plotted curves obtained from different *D-size*.

Similar to what was observed previously, the biggest resilience loss and the largest *T* are obtained with the smallest *CCT*. It means that weak dependency strength denoted by large *CCT* contributes to high network resilience against cascading failures.

2.3.3.3 Test on short-time first repair strategy

Average resilience loss, *G* and *T* with different number of *Nrem* under STFR strategy are presented in Figure 2.9. Different *D-size* and *CCT* are considered separately.

The results in Figure 2.9 show the remarkable impacts of *CCT*. Although the changing trends of resilience loss, *G* and *T* as *Nrem* increases are consistent with

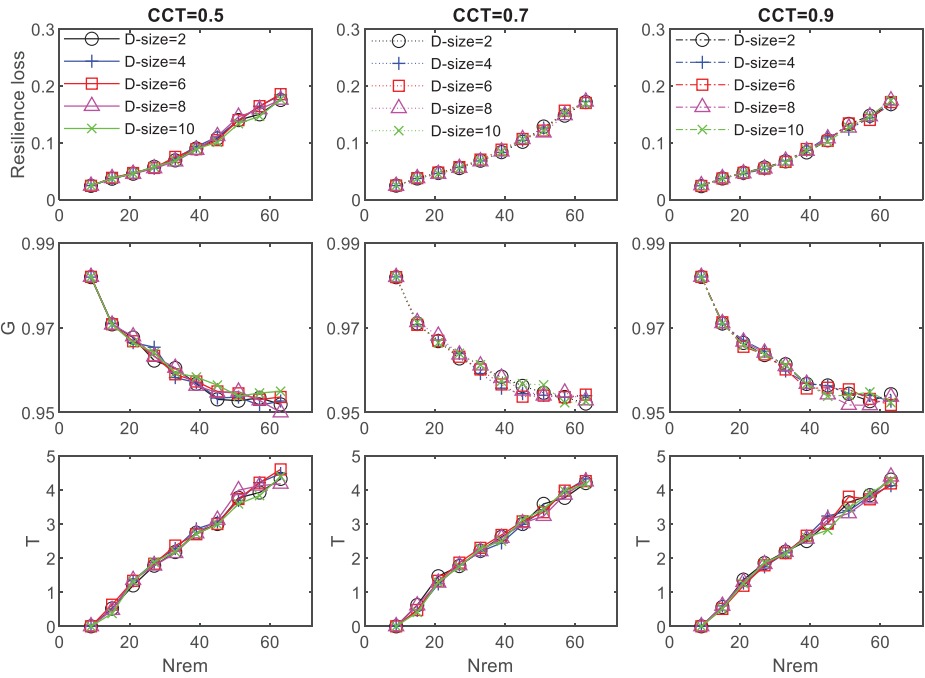


Figure 2.8: Average results of resilience loss, G and T as a function of $Nrem$ [44].

Table 2.3: Average resilience loss and T for different $Nrem$ [44].

Resilience loss (%)	<i>D-size</i>					Average T		<i>D-size</i>					Average
	2	4	6	8	10			2	4	6	8	10	
$CCT=0.5$	9.0	9.3	9.2	9.1	8.8	9.1	$CCT=0.5$	2.3	2.4	2.4	2.4	2.3	2.4
$CCT=0.7$	8.6	8.7	8.8	8.6	8.6	8.7	$CCT=0.7$	2.3	2.3	2.3	2.3	2.3	2.3
$CCT=0.9$	8.7	8.6	8.7	8.7	8.7	8.7	$CCT=0.9$	2.3	2.3	2.3	2.3	2.3	2.3
Average	8.8	8.9	8.9	8.8	8.7	8.8	Average	2.3	2.3	2.3	2.3	2.3	2.3

what was observed, it is clear that larger CCT contributes to larger resilience loss and longer T .

The results in Table 2.4 illustrate that both resilience loss and T can be reduced by increasing CCT , that is, weakening dependency strength among network nodes. Besides, resilience loss, G and T possess the similar relationship with $Nrem$ as observed above. Resilience loss and T increase as $Nrem$ increases, whereas G decreases as $Nrem$ increases.

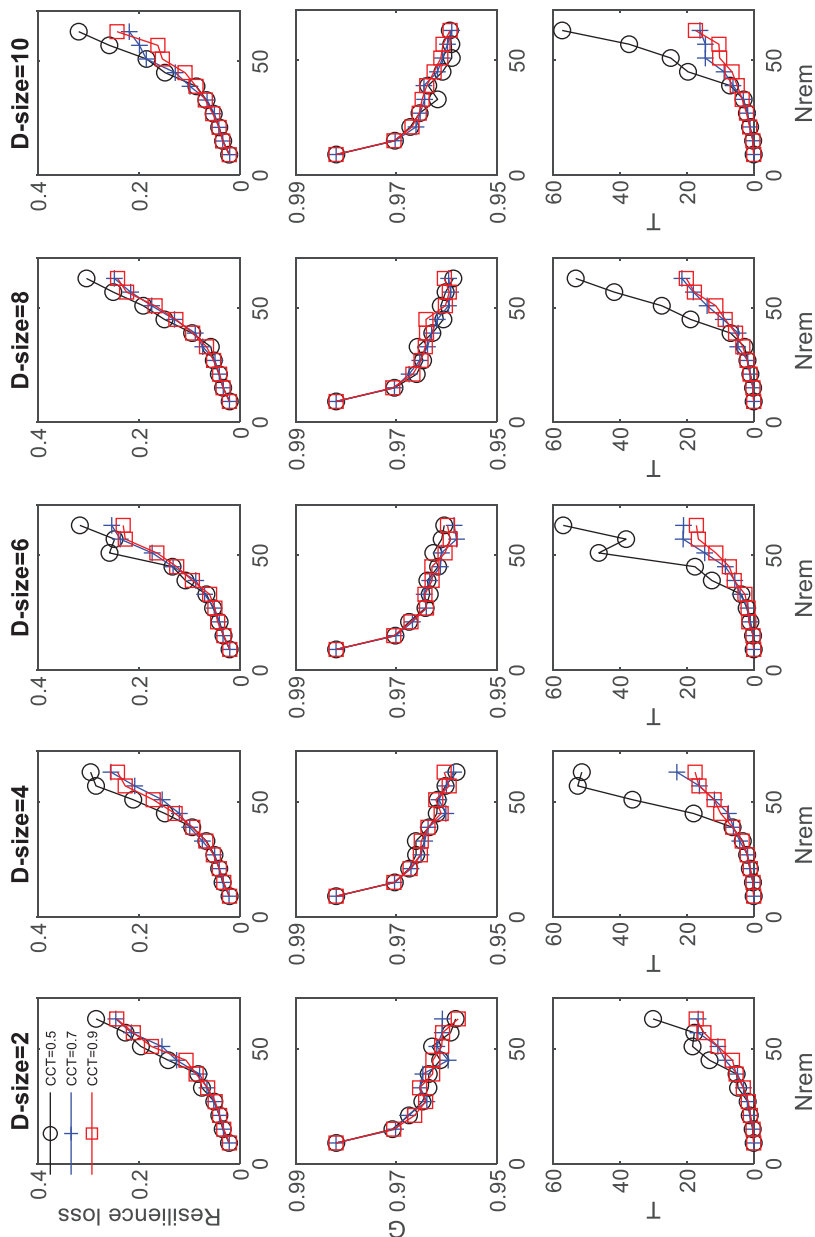


Figure 2.9: Average results of resilience loss, G and T as a function of $Nrem$. Scenarios with CCT and D -size are considered ($CCT = 0.5, 0.7, 0.9$, D -size = 2, 4, 6, 8, 10) [44].

Table 2.4: Average resilience loss and T for different $Nrem$ [44].

Resilience loss (%)	<i>D-size</i>					Aver- age	T	<i>D-size</i>					Aver- age
	2	4	6	8	10			2	4	6	8	10	
$CCT=0.5$	11.5	12.5	12.8	12.0	12.1	12.2	$CCT=0.5$	9.2	17.1	17.8	15.4	15.2	14.9
$CCT=0.7$	10.3	10.6	11.0	10.8	10.4	10.6	$CCT=0.7$	6.3	7.2	7.8	7.5	6.6	7.1
$CCT=0.9$	10.3	10.8	10.5	10.7	9.7	10.4	$CCT=0.9$	6	6.8	6.4	7	5.6	6.4
Average	10.7	11.3	11.4	11.2	10.7	11.1	Average	7.2	10.4	10.7	10.0	9.1	9.5

2.3.3.4 Test on high-load first repair strategy

Finally, HLFR strategy is applied regarding mixed cascading failures. The numerical results of average G and T under HLFR strategy are presented in Figure 2.10. The changing trends of G and T in Figure 2.10 are similar to what was previously presented in Figure 2.9 G decreases while T increases as $Nrem$ increases. We can also observe the thresholds regarding the changing rate of G and T once $Nrem$ exceeds.

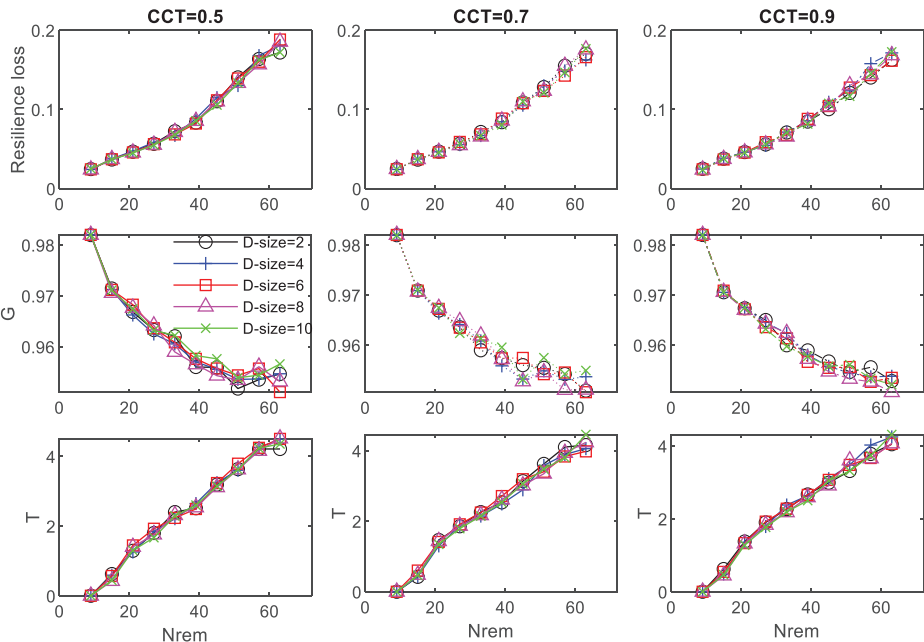


Figure 2.10: Average results of G and T as a function of $Nrem$ under different CCT and $D-size$ [44].

According to Table 2.5, average resilience loss continues to decrease when CCT increases, that is, weaken dependency strength can help to reduce system load loss caused by cascading failures. It is consistent with the results obtained in above cases.

Table 2.5: Average of resilience loss and T for different $Nrem$ [44].

Resilience loss (%)	D-size					Average T		D-size					Average	
	2	4	6	8	10			2	4	6	8	10		
$CCT = 0.5$	9.1	9.2	9.1	9.0	8.9	9.1	$CCT = 0.5$	2.4	2.4	2.4	2.4	2.4	2.4	
$CCT = 0.7$	8.8	8.6	8.6	8.8	8.7	8.7	$CCT = 0.7$	2.4	2.3	2.3	2.3	2.3	2.3	
$CCT = 0.9$	8.4	8.8	8.6	8.6	8.6	8.6	$CCT = 0.9$	2.3	2.3	2.3	2.3	2.3	2.3	
Average	8.8	8.9	8.8	8.8	8.7	8.8	Average	2.4	2.3	2.3	2.3	2.3	2.3	

Figure 2.11 presents average resilience loss, G and T for different D -size (D -size = 2, 4, 6, 8, 10) under four restoration strategies. The biggest resilience loss is incurred by RR strategy, while the smallest resilience loss and the shortest T are achieved by conducting HDFR strategy or HLFR strategy. The largest G is achieved by adopting STFR strategy, whereas the corresponding T and resilience loss is less desirable compared with that under HDFR strategy or HLFR strategy. In addition, resilience loss and T under RR strategy or STFR strategy are the most undesirable when $CCT = 0.5$. It indicates that the restoration effects of these two strategies are weakened by strong dependency strength. It should be mentioned again that the restoration process is stopped when network efficiency is recovered to 95% of its initial value.

2.4 Conclusion

In this chapter, we investigated the mixed cascading failures considering the combined impacts of network load dynamics and network dependency. The new model provides advantages to properly simulate the cascades aggregated by the important two factors. Statistical distribution is applied to model dependence clusters of network nodes to describe network dependency. The results show that the robustness of network system with dependent nodes under mixed cascading failures becomes poor. Network deteriorates rapidly in a form of a first-order phase transition with a critical number of nodes initially breakdown. A larger average node degree contributes to stronger network robustness which is helpful to maintain network connectivity when cascading failures occur. While a larger mean size of dependence clusters could cause more harm.

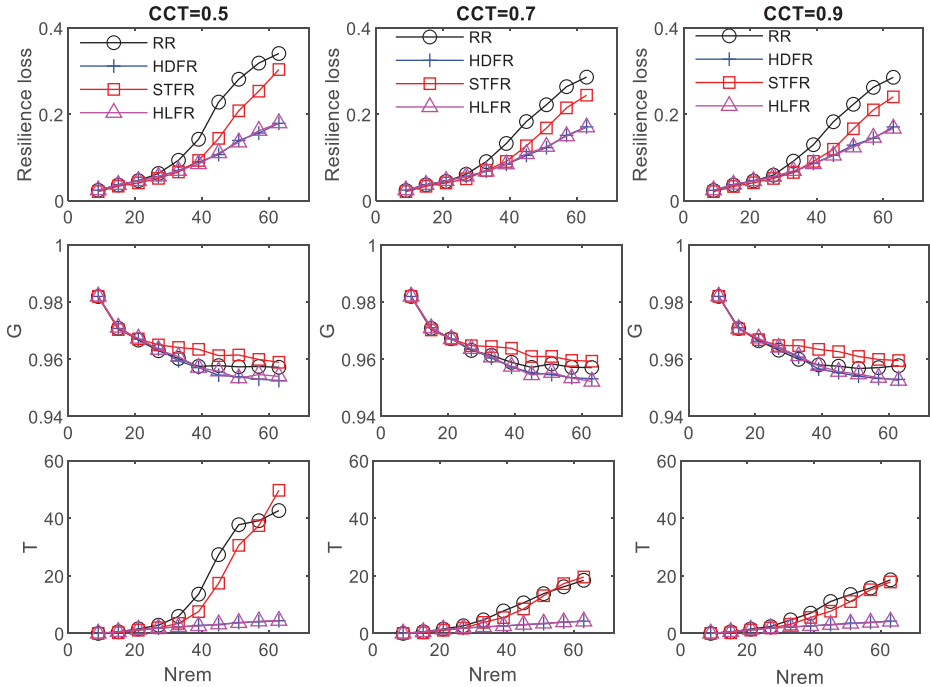


Figure 2.11: Average resilience loss, G and T over D -size versus $Nrem$ for three CCT under four restoration strategies [44].

Furthermore, the impacts of system dependency and their interactions with the effectiveness of resilience-based restoration strategies are explored. Network resilience loss metric is proposed and applied to perform a comprehensive evaluation. Based on the results, strong dependency strength impairs system resilience by aggravating the influence of failed components. While the mean size of dependence clusters, indicating dependence scale, does not show a monotonic impact on restoration effects. Restoration prioritization strategy should be selected according to the specific preference.

The proposed model for mixed cascading failures can be used as a basis for analyzing cascading failures and their impacts on network performance. It helps to understand failure propagation in network systems and evaluate network robustness. The results provide insights for integrating restoration effects with system dependency impacts to select restoration strategy for mitigating the influence of cascading failures.

In future studies, system failures originating from network links, which exists in some real-world systems, can be analyzed. The study of mixed cascading failures triggered by extreme events, such as intentional attacks and extreme weather, is another direction. Budget constraints for resilience-based restoration optimization can also be incorporated for future research.

References

- [1] Zio, E. & Piccinelli, R. 2010. Randomized flow model and centrality measure for electrical power transmission network analysis, *Reliability Engineering and System Safety*, 95(4), 379–385.
- [2] Hines, P., Apt, J. & Talukdar, S., Trends in the history of large blackouts in the United States, *Power and Energy Society General Meeting-Conversion and Delivery of Electrical Energy in the 21st Century*, IEEE, 2008, pp. 1–8.
- [3] Rosato, V., Issacharoff, L., Tiriticco, F., Meloni, S., Porcellinis, S. & Setola, R. 2008. Modelling interdependent infrastructures using interacting dynamical models, *International Journal of Critical Infrastructures*, 4(1–2), 63–79.
- [4] Romero, J. J. 2012. Blackouts illuminate India's power problems, *IEEE Spectrum*, 49(10), 11–12.
- [5] Sachtjen, M. L., Carreras, B. A. & Lynch, V. E. 2000. Disturbances in a power transmission system, *Physical Review E*, 61(5), 4877–4882.
- [6] Dobson, I., Carreras, B. A., Lynch, V. E. & Newman, D. E. 2007. Complex systems analysis of series of blackouts: Cascading failure, critical points, and self-organization, *Chaos*, 17(2), 13.
- [7] Andersson, G., Donalek, P., Farmer, R., Hatziargyriou, N., Kamwa, I., Kundur, P., Martins, N., Paserba, J., Pourbeik, P., Sanchez-Gasca, J., Schulz, R., Stankovic, A., Taylor, C. & Vittal, V. 2005. Causes of the 2003 major grid blackouts in North America and Europe, and recommended means to improve system dynamic performance, *IEEE Transactions on Power Systems*, 20(4), 1922–1928.
- [8] Dorogovtsev, S. N. & Mendes, J. F. 2002. Evolution of networks, *Advances in physics*, 51(4), 1079–1187.
- [9] Motter, A. E. & Lai, Y.-C. 2002. Cascade-based attacks on complex networks, *Physical Review E*, 66(6), 065102.
- [10] Crucitti, P., Latora, V. & Marchiori, M. 2004. Model for cascading failures in complex networks, *Physical Review E*, 69(4), 045104.
- [11] Li, X.-y., Wang, H.-l. Urban public transport network study of cascading failure, *Machinery & Electronics* (2010) S1.
- [12] Zhou, J., Huang, N., Wang, X. & Zhao, F., An improved model for cascading failures in complex networks, 2012 IEEE 2nd International Conference on Cloud Computing and Intelligence Systems, 2012, pp. 721–725.
- [13] Zhou, J., Huang, N., Sun, X., Wang, K. & Yang, H., A new model of network cascading failures with dependent nodes, *Reliability and Maintainability Symposium (RAMS)*, 2015 Annual, IEEE, 2015, pp. 1–6.
- [14] Watts, D. J. 2002. A simple model of global cascades on random networks, *Proceedings of the National Academy of Sciences*, 99(9), 5766–5771.
- [15] Hong, S., Lv, C., Zhao, T., Wang, B., Wang, J. & Zhu, J. 2016. Cascading failure analysis and restoration strategy in an interdependent network, *Journal of Physics A: Mathematical and Theoretical*, 49(19), 195101.
- [16] Lee, K. M., Goh, K. I. & Kim, I. M. 2012. Sandpiles on Multiplex Networks, *Journal of the Korean Physical Society*, 60(4), 641–647.
- [17] Dobson, I., Chen, J., Thorp, J., Carreras, B. A. & Newman, D. E., Examining criticality of blackouts in power system models with cascading events, *System Sciences*, 2002. HICSS. Proceedings of the 35th Annual Hawaii International Conference on, IEEE, 2002, p. 10 pp.
- [18] Dobson, I., Carreras, B. A., Lynch, V. E., Nkei, B. & Newman, D. E. 2005. Estimating failure propagation in models of cascading blackouts, *Probability in the Engineering and Informational Sciences*, 19(4), 475–488.

- [19] Kim, J. & Dobson, I. 2010. Approximating a loading-dependent cascading failure model with a branching process, *IEEE Transactions on Reliability*, 59(4), 691–699.
- [20] Dobson, I., Carreras, B. A. & Newman, D. E. 2005. A loading-dependent model of probabilistic cascading failure, *Probability in the Engineering and Informational Sciences*, 19(1), 15–32.
- [21] Parshani, R., Buldyrev, S. V. & Havlin, S. 2010. Interdependent Networks: Reducing the Coupling Strength Leads to a Change from a First to Second Order Percolation Transition, *Physical Review Letters*, 105(4), 048701.
- [22] Vespignani, A. 2010. Complex networks: The fragility of interdependency, *Nature*, 464(7291), 984–985.
- [23] Bai, Y. N., Huang, N., Wang, L. & Wu, Z. X. 2016. Robustness and Vulnerability of Networks with Dynamical Dependency Groups, *Scientific reports*, 6, 9.
- [24] G.o.t.U.S.a. Canada, Joint United States-Canada Electric Grid Security and Resilience Strategy, (2016).
- [25] Radicchi, F. 2015. Percolation in real interdependent networks, *Nature physics*, 11(7), 597–602.
- [26] Buldyrev, S. V., Parshani, R., Paul, G., Stanley, H. E. & Havlin, S. 2010. Catastrophic cascade of failures in interdependent networks, *Nature*, 464(7291), 1025–1028.
- [27] Baxter, G. J., Dorogovtsev, S. N., Goltsev, A. V. & Mendes, J. F. F. 2012. Avalanche Collapse of Interdependent Networks, *Physical Review Letters*, 109(24), 248701.
- [28] Parshani, R., Buldyrev, S. V. & Havlin, S. 2011. Critical effect of dependency groups on the function of networks, *Proceedings of the National Academy of Sciences of the United States of America*, 108(3), 1007–1010.
- [29] Bashan, A., Parshani, R. & Havlin, S. 2011. Percolation in networks composed of connectivity and dependency links, *Physical Review E*, 83(5), 8.
- [30] Kintner-Meyer, M. C. W., Homer, J. S., Balducci, P. J. & Weimar, M. R. Valuation of Electric Power System Services and Technologies, Pacific Northwest National Lab. (PNNL), Richland, WA (United States), 2017.
- [31] t.Q.E.R.Q.T. Force, Quadrennial Energy Review Second Installment: Transforming The Nation's Electricity System, Quadrennial Energy Review (QER), 2017.
- [32] Hosseini, S., Barker, K. & Ramirez-Marquez, J. E. 2016. A review of definitions and measures of system resilience, *Reliability Engineering and System Safety*, 145, 47–61.
- [33] Zhou, J., Huang, N., Coit, D. W. & Felder, F. A. 2018. Combined effects of load dynamics and dependence clusters on cascading failures in network systems, *Reliability Engineering and System Safety*, 170, 116–126.
- [34] Goh, K. I., Kahng, B. & Kim, D. 2001. Universal behavior of load distribution in scale-free networks, *Physical Review Letters*, 87(27), 4.
- [35] Hong, S., Zhang, X. J., Zhu, J. X., Zhao, T. D. & Wang, B. Q. 2016. Suppressing failure cascades in interconnected networks: Considering capacity allocation pattern and load redistribution, *Modern Physics Letters B*, 30(5), 16.
- [36] Li, S. D., Li, L. X., Yang, Y. X. & Luo, Q. 2012. Revealing the process of edge-based-attack cascading failures, *Nonlinear Dynamics*, 69(3), 837–845.
- [37] Kinney, R., Crucitti, P., Albert, R. & Latora, V. 2005. Modeling cascading failures in the North American power grid, *European Physical Journal B*, 46(1), 101–107.
- [38] Ren, H. P., Song, J. H., Yang, R., Baptista, M. S. & Grebogi, C. 2016. Cascade failure analysis of power grid using new load distribution law and node removal rule, *Physica a-Statistical Mechanics and Its Applications*, 442, 239–251.
- [39] Zhou, T., Liu, J. G. & Wang, B. H. 2006. Notes on the algorithm for calculating betweenness, *Chinese Physics Letters*, 23(8), 2327–2329.

- [40] Zhou, J., Huang, N., Sun, X. L., Xing, L. D. & Zhang, S. 2015. Network Resource Reallocation Strategy Based on An Improved Capacity-Load Model, *Eksplotacja Niezawodnosc*, 17(4), 487–495.
- [41] Erdos, P. & Rényi, A. 1961. On the evolution of random graphs, *Bulletin of the International Institute Statistics*, 38(4), 343–347.
- [42] Bai, Y., Huang, N., Wang, L. & Wu, Z. 2016. Robustness and vulnerability of networks with dynamical dependency groups, *Scientific reports*, 6, 37749.
- [43] Latora, V. & Marchiori, M. 2001. Efficient behavior of small-world networks, *Physical Review Letters*, 87(19), 198701.
- [44] Zhou, J., Coit, D. W., Felder, F. A. & Wang, D. 2021. Resiliency-based restoration optimization for dependent network systems against cascading failures, *Reliability Engineering and System Safety*, 207, 107383.

Jezdimir Knezevic

3 MIRCE Science: a mathematical scheme for predicting impacts of reliability engineering on the time evolution of physical systems

Abstract: The main objective of this chapter is to introduce the reliability engineering community to the innovative mathematical scheme contained in MIRCE Science for describing and predicting the time evolution of physical systems. Thus, the impact of reliability engineering decisions on complex interactions between failure events and maintenance actions that drive the behavior of physical systems can be quantified and modified at the design stage, rather than implementing expensive and time-consuming modifications driven by in-service statistics.

The concept of the MIRCE Functionability Equation developed by [1] is introduced in this chapter as a new analytical prerequisite for the prediction of expected work done by functionable systems. Hence, it becomes possible to perform quantitative trade-off between feasible reliability and maintenance options to select the compromising solution that would yield the greatest benefit measured through the work done.

To illustrate the advantages of applying MIRCE Science to the reliability engineering decision-making process a numerical example is provided, where the trade-off between reliability improvements by increasing the expected time to failure by 50% or decreasing maintenance time by 50% is addressed. The challenges related to the applicability of MIRCE Science to reliability engineering are also discussed in the chapter.

Keywords: MIRCE Science, MIRCE Functionability Equation, reliability engineering predictions, maintenance engineering predictions, predictions of the expected work, normalization of system engineering design

Dedication: The body of knowledge presented in this chapter resulted from the research performed by the author after hearing the following statement by Jack Hessburg, the Chief Mechanic of the Boeing New Airplanes [1990–1999], “I as a designer have to fill my customer in as well, I have to decide where I’m going to put economic redundancy into my design, because it costs money. If you have the full answer to that, would you please see me after this meeting! There’s a Nobel Prize in it. We have really not developed the discipline where we know how to normalise that, yet.” [1]

Jezdimir Knezevic, MIRCE Academy, Woodbury Park, Exeter, UK

<https://doi.org/10.1515/9783110725599-003>

3.1 Introduction

The philosophy of MIRCE Science is based on the premise that the purpose of the existence of any functionable system is to do a work. The work is considered to be done when the expected measurable function is performed through time. The best way to achieve that is to increase the revenue generating work done by a functionable system, while reducing the resources consumed for it. One way toward that target is to improve the reliability of consisting parts by using appropriate engineering and production methods. Another way is to reduce maintenance time by applying appropriate condition monitoring and management technologies. Although there are infinite number of combinations between the amount of improvements in reliability and reduction in maintenance time, it is safe to conclude that the work done is driven by their combined impact. Their impact on the amount of work done by a functionable system during its operational life could quantify through the following two approaches:

- Measuring it during the operation process
- Predicting it during the planning process

Measuring the work done is a rather straightforward process where the operational hours are counted together with resources consumed.¹ However, possessing the data regarding the past performance of functionable systems does not have any impact on the past revenue, reputation, loyalty, and other measures of a functionable system's effectiveness. On the other hand, the ability to predict the future performance, at the planning stage, gives an opportunity for any changes necessary to create functionable systems with desirable performance to be made, within the given budget. In return it will generate the expected return on their investment (e.g., profit, reputation, loyalty, public benefit, and similar). However, to achieve that, it is necessary to have a mathematical model² that would facilitate that, as mathematics is the only body of knowledge that enables quantitative predictions to be made in all natural sciences, from quantum mechanics (the motions of subatomic particles) to astrophysics (the motion of spacecraft).

Although, reliability and maintenance are well-recognized disciplines in their own rights, best to the author's knowledge there is no body of knowledge for predicting their combined impact on the work done and resources consumed, in a quantitative and comparative manner.

¹ Boeing 747, registration number N747PA, which belonged to Pan Am airways, have delivered the work of 80,000 flying hours and received 806,000 maintenance man-hours, during the 22 years of in-service life

² Newton, Maxwell, Lagrange, Boltzmann and other well know and applied equations for predicting the physical behaviour of natural world.

The main objective of this chapter is to introduce reliability and maintenance engineers to MIRCE Science, a body of knowledge that enables quantitative prediction of the complex interactions between reliability and maintenance on the work done and resources required [1]. Hence, by making use of the MIRCE Functionability Equation it is possible to perform quantitative trade-off between feasible reliability and maintenance options to select the compromising solution that would yield greater productivity measured through the work done.

3.2 Brief overview of MIRCE Science

According to MIRCE Science, at any instant of calendar time, a given functionable system could be in one of the following two macrostates [1]:

- Positive Functionability State (PFS), a generic name for a state in which a functionable system is able to deliver the expected measurable function(s).
- Negative Functionability State (NFS), a generic name for a state in which a functionable system is unable to deliver the expected measurable function(s), resulting from any reason whatsoever.

However, components within a system could be in many microstates. For example:

- A component can be in a passive state, that is, it is operational (not failed) but not actually working either because it was set to be a backup for another component or because of other reasons. In the case of the engine failure a gearbox and many other parts will become passive.
- A component can fail but this failure is undetected. This can be the state of the fire extinguisher in a corridor. Such a state differs from the common failed state because restoration will not take place until the failure is detected.
- A component may be operational under a high load. This means that it may have different stresses, probably narrower, than in normal operation.
- A component may fail and the failure detected but some resources needed for its repair, such as spare parts or a crane needed to lift it, which are not available. Again this is a different state because the commencing of repair depends on the state of other resources, not on detection.

The number of microstates in which components could find themselves states is basically unlimited and truly depends on the engineering grasp of the operating conditions of the component. According to [2], the possible states of a component/system can be determined in accordance with the following two criteria:

- A different state will be determined if the operation of the component or the system alters under this state.

- A new state will be defined if the future behavior of the component or the system will be altered.

It is necessary to stress that in some cases the physical properties of a component could determine its state, rather than the function it performs. For example, suppose that a door is colored in bright yellow paint. Potentially the paint may deteriorate until the door becomes black. Are these two separate states: “Yellow” and “Black”? This is on the top of other states “Door does not open,” “Door does not close,” “Door makes noises when moved.” The answer depends on the operating conditions. For example, if the door is used at night with no lights around then there is a chance that users carrying equipment would bump into the door, thinking it is open, and consequently damages the equipment. Thus, as the color of the door may affect the future operation of the whole system, not the operation of the door itself, then the color should be identified as a state.

In MIRCE Science work done by a functionable system is uniquely defined by the trajectory generated by its motion through MIRCE Space.³ That motion is driven by functionability actions, which are classified as:

- Positive Functionability Action (PFA) is a generic name for any natural process or human activity that compels a system to move to a PFS. Typical examples are: servicing, lubrication, visual inspection, repair, replacement, final repair, examination, partial restoration, inspection, storage, modification, transportation, sparing, cannibalization, refurbishment, health monitoring, restoration, packaging, diagnostics, and similar.
- Negative Functionability Action (NFA) is a generic name for any natural process or human activity that compels a system to move to a NFS. Typical examples are: thermal ageing, actinic degradation, acid reaction, bird strike, warping, abrasive wear, suncups formation on the blue ice runway, fatigue, pitting, thermal buckling, photo-oxidation, production errors, strong wind, maintenance error, hail damage, lightening strike, COVID-19, quality problems, hard landing, and sand storm.

The time evolution of a functionable system through MIRCE Space is physically manifested through the occurrences of functionability events, which are classified as:

- Positive Functionability Event (PFE), a generic name for any physically observable occurrence in the calendar time that signifies the transition of a functionable system from a NFS to a PFS.

³ MIRCE Space is a conceptual 3-dimensional space containing infinite set of possible discrete functionability states that a functionable system could be found in, at any instant of the calendar time, and corresponding probabilities [1].

- Negative Functionability Event (NFE), a generic name for any physically observable occurrence in the calendar time that signifies the transition of a functionable system from a PFS to a NFS.

Consequently, the concept of the time evolution in MIRCE Science is conceptualized as the motion of a functionable system through functionality states, resulting from any functionability actions whatsoever and the actions required to generate any functionability motion.

3.3 Mathematical principles of MIRCE Science

The ability to “normalize” all competing options of a functionable system enables comparisons to be made between them and finally select the best one, in accordance with a given criterion. Hence, MIRCE Science is a body of knowledge that enables quantitative assessment of the impact of the multidimensional interactions between:

- consisting components (mechanical, electrical, electronics, and so forth);
- system architecture (active and passive redundancies);
- natural environment (temperature, wind, humidity, fog, and many others);
- human rules regarding:
 - operation process (levels of stress, frequencies of use and similar),
 - maintenance policies: preventive, condition based, opportunistic, and so on,
 - support strategies: in-house support, outsource, combined.

According to the MIRCE Science philosophia⁴ positive work is done when a functionable system is delivering a functionality performance, which means that it must be in positive a functionability state. Thus, work done in proportion to the cumulative time that a system spends in PFS during a stated period of calendar time T .

According to Knezevic [1], the expected positive work to be done by a functionable system during a given interval of calendar time T , $PWF_s(T)$, measured in calendar hours, Hr, can be calculated by making use of the following equation:

$$PWF_s(T) = \int_0^T y_s(t) dt \quad [HR] \quad (3.1)$$

where $y_s(t)$ is MIRCE Functionability Equation⁵ [3], which quantifies the probability of the event *{system is being in a PFS at instant of calendar time t }*, thus:

⁴ https://www.academia.edu/8357448/Mirce_Functionability_Equation

⁵ MIRCE Akademy, Woodbury Park, Exeter, UK

$$y_s(t) = P\{PFS_s(t)\} = \sum_{i=1}^{\infty} y_s^i(t) = \sum_{i=1}^{\infty} [O_s^{i-1}(t) - F_s^i(t)], \quad t > 0 \quad (3.2)$$

where $O_s^{i-1}(t) = P(TPE_s^{i-1} \leq t)$ and $F_s^i(t) = P(TNE_s^i \leq t)$. It is necessary to point out that $O_{s,0}(0) = 1$, in accordance with the first axiom of MIRCE Science [1].

The infinite sum of positive and negative functions represents a mathematical scheme that in MIRCE Science defines the sequential occurrences of the functionability events in the direction of the calendar time, for each feasible variation of the functionable system considered. In the language of mathematics these are systems of the convolution integrals. Thus, the sequential positive functionability functions, $O_s^i(t)$, which defines the probability that the $O_s^i(t)$ in the life of a functionable system, will take place before or at the instant of calendar time t , is defined by the following convolution integrals [1]:

$$\begin{aligned} O_s^i(t) &= P(TPE_s^i \leq t) \\ &= P(TNE_s^i + TPE_{s,i} \leq t) \\ &= P(TNE_s^i \leq x \cap TPE_{s,i} \leq t - x) \\ &= P(TNE_s^i \leq x) \times P(TPE_{s,i} \leq t - x) \\ &= \int_0^t F_s^i(x) o_{s,i}(t-x) dx = \int_0^t F_s^i(x) dO_{s,i}(t-x), \quad i=1, 2, \dots, \infty, \quad t \geq 0 \end{aligned} \quad (3.3)$$

In order for the i th sequential PFE^i to take place before, or at the instant of calendar time t , it is necessary that the previous functionability event, which in this case is NFE^i , take place sometime before time t , denoted by x in the above expression. Then, the sequential PFE_i has to take place during the remaining interval of calendar time, which in this case is denoted with $t - x$.

The process of defining the negative sequential distribution Function, $F_s^i(t)$, which defines the probability that the i th sequential NFE_s of a functionable system will take place before or at an instant of calendar time t , follows the same mathematical principle. Thus, the sequential negative functionability functions are fully defined in the following way

$$\begin{aligned} F_s^i(t) &= P(TNE_s^i \leq t) \\ &= P(TPE_s^{i-1} + TNE_{s,i} \leq t) \\ &= P(TPE_s^{i-1} \leq x \cap TNE_{s,i} \leq t - x) \\ &= P(TPE_s^{i-1} \leq x) \times P(TNE_{s,i} \leq t - x) \\ &= \int_0^t O_s^{i-1}(x) f_{s,i}(t-x) dx = \int_0^t O_s^{i-1}(x) dF_{s,i}(t-x), \quad i=1, 2, \dots, \infty, \quad t \geq 0 \end{aligned} \quad (3.4)$$

This multidimensional set of convolution integrals defines the motion of a functionable system through MIRCE Space, depicting and passing through each sequential functionability state in the direction of calendar time, generating a trajectory unique to each functionable system [6]. Thus, the same set of generic equations, when applied to different operational and maintenance policies generate different trajectories of the motion through MIRCE Space, which means different functionability performance, namely different work done and different resources consumed. Hence, [1] has created a generic platform on which each feasible plan for the operation and maintenance policies and strategies would generate its own future “trajectory” for a system under consideration.

3.4 Application of MIRCE Science to reliability engineering

To illustrate the applicability of MIRCE Science to the reliability engineering design process the quantitative assessment of the combined impact of reliability and maintenance on the performance of a functionable system, a hypothetical example will be used.

The simplest possible functionable system consists of one component that exists in two functionable states, namely PFS and NFS. Even further, a single positive or negative action causes the occurrences of positive and negative events at which the functionable system changes its functionable states.



Figure 3.1: Reliability block diagram for a hypothetical system whose failure will occur if a component A fails.

It is necessary to stress that this example is chosen, not because the real functionable systems consist of a single component, but because it is extremely useful for the understanding of the mathematical scheme that defines the motion of a functionable system through MIRCE Space. This knowledge, in turn, quantifies its expected functionability performance, namely the expected work done and corresponding resources consumed.

To demonstrate the applicability of MIRCE Science mathematical scheme to the quantitative assessment of the combined impact of reliability engineering and maintenance management decisions on the performance of a functionable system the following three options of the future system are addressed:

Option 1: Basic reliability engineering design: The functionable system under consideration is expected to experience an occurrence of an NFE during a continuous operation with the expected value of $E[TNE_S] = 1,080$ Hr. What is the amount of

a positive work expected to be delivered during a calendar year of continuous operation, without performing any maintenance action?

Option 2: Adding maintenance actions: What would be the additional work done if the system is designed in the way that maintenance actions could be performed after occurrences of failures? Assume that the design-in maintenance action that returns a functionable system to PFS has the expected value of $E[TPE_S] = 168$ Hr.

Option 3: Lifelong engineering interactions: Assuming that options 1 and 2 are not satisfying system engineering requirements, an additional amount of money has been allocated to the project. Contributing engineering departments have been asked to make the proposal for the increase of the expected work done, for a given extra budget. The following two proposals were made:

- **Option 3.1:** The reliability engineering department submitted a proposal in which they were stating that by investing the additional funds allocated into a new technology in the manufacturing process it is possible to extend the basic design expected life of a component A by 50%.
- **Option 3.2:** The maintenance engineering department submitted a proposal in which they were stating that by investing the additional funds allocated into new testing and diagnostic equipment it is possible to reduce the duration of a maintenance task defined for a component A in option 2 by 50%.

Which option should be adopted and why?

Undoubtedly, the ability to accurately predict the answer to the above questions, at the early stages of the design of a functionable system, is invaluable for decision-makers. The engineering solutions and management methods applied in the design office govern the operational effectiveness of future systems, which should be optimized within the given budget, to generate the maximum return on investment like: profit, reputation, loyalty, and public benefit.

3.5 MIRCE Science based mathematical analysis of design options

Option 1

Based on the information available the only possible conclusion regarding the probability distribution of the TNE of a component A is that it is fully defined by the exponential distribution, which is uniquely defined by the expected value, which in this case is equal to scale parameter $A_N = E[TNE_S] = 1,080$ Hr. The expected positive functionability work from this design option could be determined by obtaining the numerical solution to eq. (3.1).

A generic expression for an exponentially distributed cumulative distribution function of a random variable TNE_i is $F_{S,i}(t) = P(NFE_{S,i} \leq t) = 1 - e[-(t/A_N)]$, $i = 1, \infty$. Based on the data available, the probability of the first NFE of a system, $O_s^i(t)$, taking place before of at a given instant of time t is

$$\begin{aligned} F_S^1(t) &= P(TPE_{S,0} + NFE_{S,1} \leq t) \\ &= \int_0^t O_{S,0}(x) dF_{S,1}(t-x) = F_{S,1}(t) \\ &= 1 - e[-(t/1080)], \quad 0 \leq t \leq \infty \end{aligned}$$

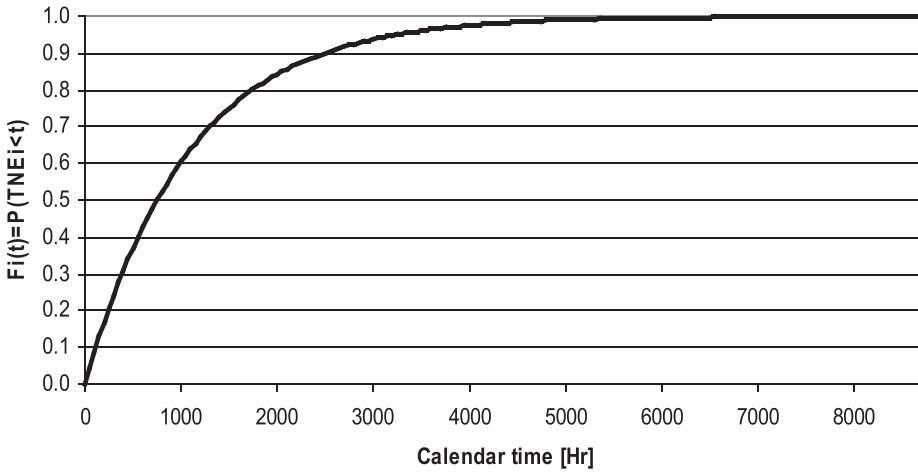


Figure 3.2: Cumulative distribution function of the time to the first negative functionability event (NFE) of a system considered, $F_{S,1}(t) = F_S^1(t)$.

In this specific case, where it is decided that not to take any action after the occurrence of the first NFE, MIRCE Functionability Equation, shown in Figure 3.3, is defined as

$$y(t) = \sum_{i=1}^1 [O_s^{i-1}(t) - F_S^i(t)] = O_S^0(t) - F_S^1(t) = 1 - F_S^1(t) = e[-(t/1,080)]$$

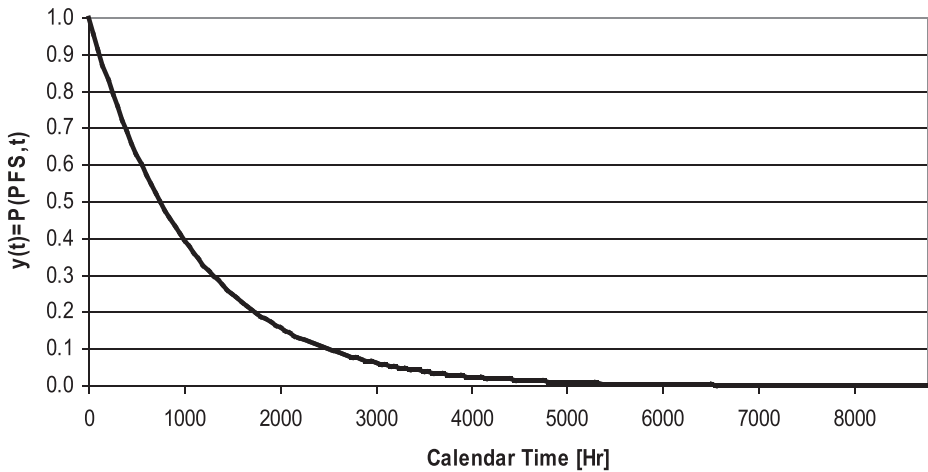


Figure 3.3: MIRCE Functionability Equation for the design option 1.

Finally, it is possible to derive the expression for the expected work done, by solving the following integral expression: $PFW(T) = \int_0^T [e(-t/A_N)]dt$. This integral could be solved by the substitution method, as shown below:

$$u = -\left(\frac{1}{A_N}\right)t \rightarrow du = -\left(\frac{1}{A_N}\right)dt \rightarrow dt = -\frac{1}{\left(\frac{1}{A_N}\right)}du = -(A_N)du$$

$$\text{for } t=0 \rightarrow u=0 \quad t=T \rightarrow u = -\left(\frac{T}{A_N}\right)$$

$$PFW(T) = \int_0^{-\left(\frac{T}{A_N}\right)} [e^u](-A_N)du$$

$$= -A_N \int_0^{-\left(\frac{T}{A_N}\right)} [e^u]du = -A_N[e^u]_0^{-\left(\frac{T}{A_N}\right)}$$

$$= -A_N e^{-\left(\frac{T}{A_N}\right)} + [A_N e^{-0}]$$

$$= A_N \left[1 - e^{-\left(\frac{T}{A_N}\right)} \right]$$

For the planned continuous operation of the functionable system during a calendar year, $T = 24 \times 365 = 8,760$ Hr. Hence, the amount of expected positive functionability work to be done by the design option considered is:

$$PFW(8760) = 1080 \times [1 - e(-(8760/1080))] = 1079.68 \text{ Hr}$$

In summary, a functionable system defined with the available data is expected to deliver 1,079.68 h of work during the available 8,760 calendar hours, as shown in Figure 3.4.

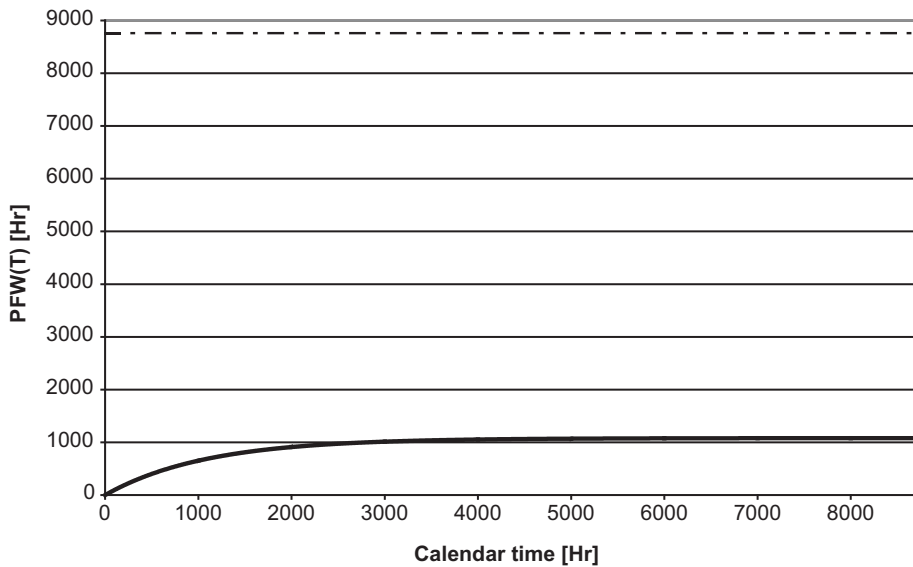


Figure 3.4: Expected work done by option 1 of the system considered (bold black line) during the annual calendar hours available (broken line).

Option 2

Following the logic used in the analysis of option 1, in this particular example, the exponential theoretical distribution with the expected value of $E[TPE_S] = A_P = 168$ Hr is used to describe the motion of a system through PFS. Thus, according to the data available, the cumulative distribution function for the time of occurrence of i_{th} PFE is defined as $O_{S,i}(t) = 1 - \exp(-t/A_P)$, $i = 1, \infty$. Thus, the MIRCE Functionability Equation (eq. (3.2)) becomes fully defined by the set of convolution integrals which are of the form of the Gamma probability distribution, as the convoluting functions are

defined by the identical exponentially distributed random variables, $TNE_{S,i}$ and $TPE_{S,i}$ in the following way:

$$O_s^i(t) = P(TPE_s^i \leq t) = \int_0^t \left[\frac{(1/A_P)(t/A_P)^{i-1} e^{-(t/A_P)}}{(i-1)!} \right] dt, i = 1, 2, \infty, t \geq 0$$

$$F_s^i(t) = P(TNE_s^i \leq t) = \int_0^t \left[\frac{(1/A_N)(t/A_N)^{i-1} e^{-(t/A_N)}}{(i-1)!} \right] dt, i = 1, 2, \infty, t \geq 0$$

Dubi [5], has proven that a generic expression for the MIRCE Functionability Equation (eq. (3.2)) for equally exponentially distributed time to negative and PFEs, as defined above, is equal to

$$y_S(t) = \left[\frac{A_N}{A_P + A_N} + \frac{A_P}{A_P + A_N} e^{-\left(\frac{A_P + A_N}{A_P A_N}\right)t} \right] \quad (3.5)$$

By substituting the values for A_N and A_P in eq. (3.5) the trajectory of the system being in PFS and doing the expected work through evolutionary time is obtained and for the example used is plotted in Figure 3.5.

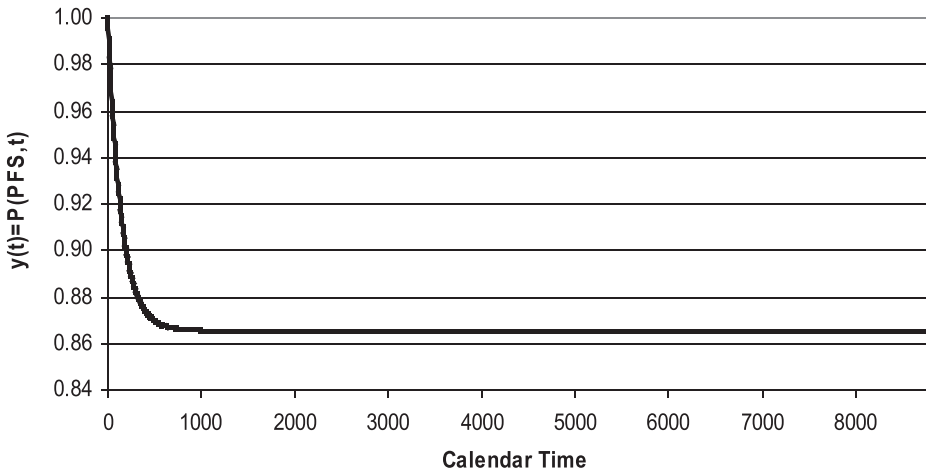


Figure 3.5: The probability of a system being in PFS during a calendar year of operation.

The amount of the expected positive work to be done by the system defined by option 2 could be calculated by substituting the function $y(t)$ into eq. (3.1), thus:

$$PFW(T) = \int_0^T y(t) dt = \int_0^T \left[\frac{A_N}{A_P + A_N} + \frac{A_P}{A_P + A_N} e^{-\left(\frac{A_P + A_N}{A_P A_N}\right)t} \right] dt$$

The analytical solution to the above integral could be obtained by making use of the following substitution, thus:

Finally,

$$\begin{aligned}
 PFW(T) &= \int_0^{-\left(\frac{A_P+A_N}{A_P A_N}\right)T} \left[\frac{A_N}{A_P+A_N} + \frac{A_P}{A_P+A_N} e^u \right] \left(-\frac{A_P A_N}{A_P+A_N} \right) du \\
 &= -\frac{A_N A_P}{A_P+A_N} \int_0^{-\left(\frac{A_P+A_N}{A_P A_N}\right)T} \left[\frac{A_N}{A_P+A_N} + \frac{A_P}{A_P+A_N} e^u \right] du \quad (3.6) \\
 &= -\frac{A_N A_P}{A_P+A_N} \left[-\frac{T}{A_P} - \frac{A_P}{A_P+A_N} \left(1 - e^{-\left(\frac{A_P+A_N}{A_P A_N}\right)T} \right) \right]
 \end{aligned}$$

After substituting the values for the parameters in the above expression, the expected positive functionality work will be 7,600.34 Hr, as shown in Figure 3.6.

Thus, by designing a system in the way that it is possible to return it in PFS after the occurrence of NFE by performing specific maintenance activities, the expected work done by a system will increase by 6,520.66 Hr, in respect to the expected work done by option 1.

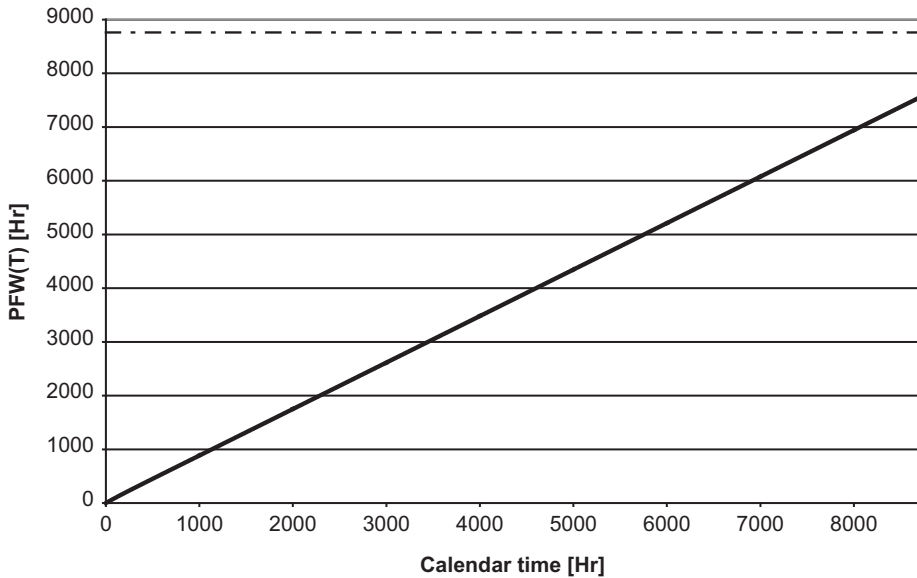


Figure 3.6: Expected work done by option 2 of the system considered (bold black line) during the annual calendar hours available (broken line).

Option 3

The quantitative impact on the future work done by a system considered resulting from the recommendation made by the reliability engineering and maintenance engineering departments could be obtained by applying the MIRCE Science mathematical scheme presented in this chapter.

- **Option 3.1:** By implementing proposed changes in design, originated by the reliability engineering team, the expected time to the occurrence of NFE, will increase from 1,080 to 1,620 Hr, while maintaining the same probability distribution for $TPE_{S,i}$, thus:

$$\begin{aligned}
 PFW(8760) &= -\frac{A_N A_P}{A_P + A_N} \left[-\frac{T}{A_P} - \frac{A_P}{A_P + A_N} \left(1 - e^{-\left(\frac{A_N + A_P}{A_P \times A_N}\right) T} \right) \right] \\
 &= -\frac{1620 \times 168}{1620 + 168} \left[-\frac{8760}{168} - \frac{168}{1620 + 168} \left(1 - e^{-\left(\frac{1620 + 168}{1620 \times 168}\right) 8760} \right) \right] \\
 &= 7951.21 \text{ Hr}
 \end{aligned}$$

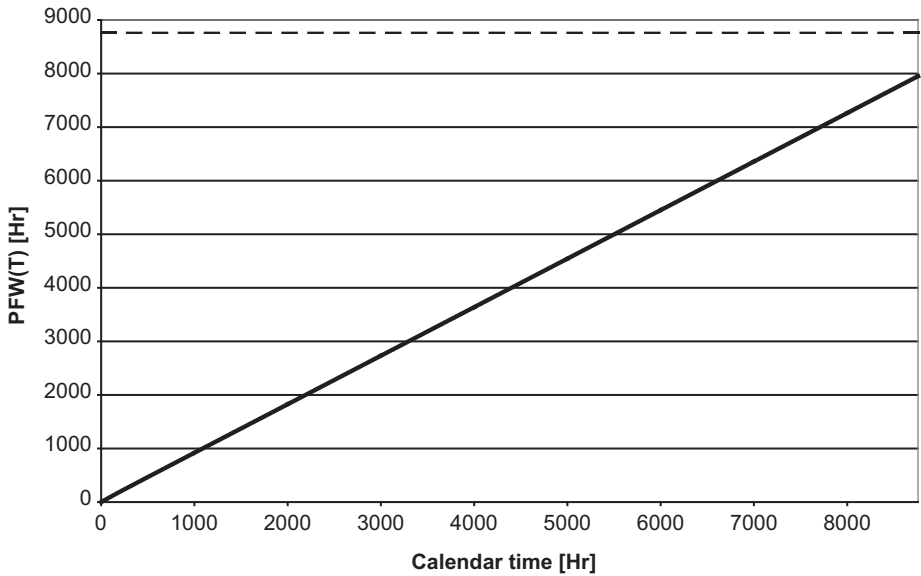


Figure 3.7: Expected work done by option 3.1 of the system considered (bold black line) during the annual calendar hours available (broken line).

- **Option 3.2:** As a result of improved testing and diagnostics equipment, proposed by the maintenance engineering department the expected time in NFS will be reduced to $A_P = 84$ Hr, while maintaining the same probability distribution for $TNE_{S,i}$, hence:

$$\begin{aligned}
 PFW(8,760) &= -\frac{A_N A_P}{A_P + A_N} \left[-\frac{T}{A_P} - \frac{A_P}{A_P + A_N} \left(1 - e^{-\left(\frac{A_N + A_P}{A_P \times A_N} \right) T} \right) \right] \\
 &= -\frac{1,080 \times 84}{1,080 + 84} \left[-\frac{8,760}{84} - \frac{84}{1,080 + 84} \left(1 - e^{-\left(\frac{1,080 + 84}{1,080 \times 84} \right) 8,760} \right) \right] \\
 &= 8,133.46 \text{ Hr}
 \end{aligned}$$

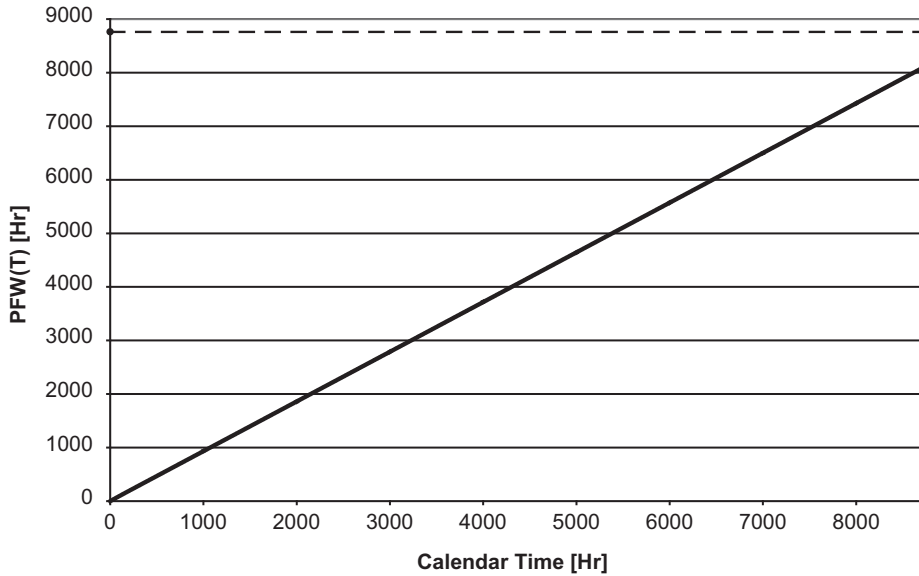


Figure 3.8: Expected work done by option 3.2 of the system considered (bold black line) during the annual calendar hours available (broken line).

Based on the predicted expected work done by the system under consideration, by applying the MIRCE Science equations the final solution to be recommended for the adoption for the future system is option 3.2. This feasible design solution provides additional work of 351 Hr in respect to option 3.1 (improved reliability) and 533 Hr with respect to option 2.

The impact of all feasible solutions presented above on revenue, cost, and profit could be easily predicted by making use of the MIRCE Profitability Equation presented in [4].

3.6 MIRCE Science based physical analysis of design options

The mathematical analysis of the four feasible design options, considered in this chapter, has shown that is expected that option 3.2 will provided the highest amount of work during the year of operation, with the same monetary value of resources investment in design as the other three. This conclusion was made by quantitatively evaluating the MIRCE Functionability Equation for each design option using the available input data.

From a mathematical point of view the obtained results are correct as none of the mathematical equations violate any mathematical laws. However, as these are engineering design options, it is the duty of design engineers and reliability analysts to select the input data into mathematical predictions. This is primarily related to the selection of mathematical models that define physical mechanisms that generate the motion of functionable systems through functionability states, as the MIRCE Functionability Equation is presented in a generic form, suitable for any application. However, the specific probability functions have to be selected by the designers of specific systems.

In the above example, exponential probability distributions are selected for random variables, TNEi and TPEi, purely for the ease of the calculation of corresponding convolution integrals (eqs. (3.3) and (3.4)).

From a reliability point of view the mathematical assumption made had the following physical consequences, thus component A cannot:

- experience any manufacturing, transportation and installation actions that would generate a NFE;
- experience any time or usage related degradation mechanisms like corrosion, fatigue, thermal deformation, creep, wear, and similar;
- experience any maintenance or storage induced action that would generate a NFE;
- be exposed to seasonal, operational, or geographical variability.

From a maintenance point of view the mathematical assumption made had the following physical consequences, no maintenance action applied to the component A can have a fix duration of time required for its successful completion like:

- 24 h for a paint to dry,
- 12 h for a physical/chemical analysis used as a part of the troubleshooting process,
- 7 days contractual provisioning of spare parts.

The above statements of reliability and maintenance are a physical reality known and experienced by engineers, managers, technicians and others involved with the

operation process of functionable systems. Based on the above analysis of the observable physical reality excluded by mathematical assumptions of exponentially distributed times of the evolution of functionability of a system through MIRCE Space, [1] presented in the numerical example used in this paper, the following two points must be made:

1. Equations (3.1) and (3.2) are generic expressions applicable to any functionable system, operating in any natural environment, exposed to any human imposed rules. In order to be utilized during the design process it is necessary that reliability and maintenance professionals involved to identify mathematical laws that adequately described the physical reality of their systems and then seek a method for evaluation of convolution integrals defined by eqs. (3.3) and (3.4).
2. Equations (3.5) and (3.6) provide accurate predictions of the expected work to be done during the in-service lives of functionable systems given that operational and maintenance limitations, some of which are listed above, and many others, are not applicable to their systems, otherwise the predictions would be incorrect.

3.7 A few words more about quantitative evaluation of MIRCE Functionability Equation and work done

The numerical example used in this chapter is related to a system that consists of a single component, where both positive and NFAs are mathematically represented by corresponding exponential probability distributions, for a very simple reason. This combination is the only case for which an explicit closed mathematical solution exists.

In view of the fact that realistic systems involve more than a single component with more than one functionability event generating mechanisms the possibility of finding an analytical solution for multidimensional convolution integrals defined by eqs. (3.3) and (3.4) are seldom possible due to the inability of mathematics to deal with the large number of convolution functions and their interactions. These types of problems are not specifically related to MIRCE Science, they are common to all scientific disciplines of this nature, as it is a known mathematical fact that the integral equations do not have analytical solutions [5].

The most suitable way forward for any real functionable systems, of any complexity of operational reality, is to apply the Monte Carlo method as the only viable approach with which solutions for the MIRCE Functionability Equation and thereby for the system performance may be obtained. It is applicable to systems with multiple interacting components, with aging mechanisms and any operation, maintenance and support rules. Thus, the Monte Carlo method provides the performance function of a system for any given scenario and with any form of resources, but it is beyond the scope of this chapter.

3.8 Conclusions

The main objective of this chapter was to introduce the reliability engineering community to the innovative mathematical scheme contained in MIRCE Science for describing and predicting the time evolution of physical systems. Thus, the impact of reliability engineering decisions on complex interactions between failure events and maintenance actions that drive the behavior of physical systems can be quantified and modified at the design stage, rather than implementing expensive and time-consuming modifications driven by in-service statistics.

The concept of the MIRCE Functionability Equation developed by Knezevic [1] is introduced in this chapter as an analytical prerequisite for the prediction of expected work done by functionable systems. Hence, it becomes possible to perform quantitative trade-off between feasible reliability and maintenance options to select the compromising solution that would yield greatest benefit measured through the work done.

To illustrate the advantages of applying MIRCE Science to reliability engineering decision-making process a numerical example is provided, where the trade-off between reliability improvements by increasing the expected time to failure by 50% or decreasing maintenance time by 50% is addressed.

The challenges related to the applicability of MIRCE Science to reliability engineering, mainly driven by the mathematical inability to analytically deal with multi-dimensional convolution integrals, are highlighted in the chapter and the use of the Monte Carlo method is recommended.

References

- [1] Knezevic, J. The Origin of MIRCE Science, MIRCE Science, Exeter, UK, 2017 ISBN 978-1-904848-06-6, 2017, 232.
- [2] Dubi, A. 2003. System Engineering g Science, Analytical Principles and Monte Carlo Methods, MIRCE Science, Exeter, UK, 2003, 164.
- [3] Knezevic, J. 2014. MIRCE Functionability Equation, International Journal of Engineering Research and Applications, 4(8), (Version 7), August 2014 93–100. ISSN: 2248–9622 (open access publication).
- [4] Knezevic, J. 2016. MIRCE Profitability Equation, Journal of Mechanical Engineering, pages 115–122. 13(2), April-June 2016, University of Zenica, Faculty of Mechanical Engineering, Zenica, Bosnia and Herzegovina, ISSN 1512–5173.
- [5] Dubi, A. 2000. Monte Carlo Applications in Systems Engineering, John Wiley & Sons, Chichester, UK, 2000, 268.
- [6] Varde, P.V., Prakash, R.V., Joshi, N.S. Risk Based Technologies, MIRCE Science Based Operational Risk Assessment, Springer Nature Singapore Pte. Ltd., Singapore, 2019, 223–258.

Ioannis S. Triantafyllou, Mangey Ram

4 On the reliability structures with two common failure criteria and a single change point

Abstract: In this chapter, we study consecutive-type systems with two common failure criteria and a single change point. The aforementioned reliability structures consist of n independent components, of which the first n_1 units are identically distributed with common reliability p_1 , while the remaining ones share a different functioning probability p_2 . The general setup of the proposed structures is presented in detail, while explicit expressions for the reliability and mean time to failure of the aforementioned models are provided. An extensive numerical experimentation is accomplished for investigating the behavior of the underlying structures with a single change point for different values of the design parameters.

Keywords: Consecutive-type systems, two common failure criteria, change point, mean time to failure, reliability function

4.1 Introduction

In the field of reliability engineering, an enthralling issue calls for suitable structural designs, which are strongly connected to real-life problems or existing contrivances. A specific group of reliability models, which seems to reel in the scientists during the last decades, is the family of consecutive-type structures. Given the abundance of their practical implementations in engineering and statistical modelling, the so-called consecutive-type systems comprise an engrossing scope of practical interest and research activity.

The general framework of constructing a consecutive-type structure relies on n linearly or circularly arranged units. The resulting structure stops its operation, whenever a pre-specified stopping rule (or even more) is satisfied. A great variety of such systems has been already introduced in the literature. For example, a consecutive- k -out-of- n : F structure consists of n linearly ordered components and fails if and only if at least k consecutive components fail [7., 27, 28] or [13]. Additionally,

Ioannis S. Triantafyllou, Department of Computer Science and Biomedical Informatics, University of Thessaly, Lamia, Greece, e-mail: itriantafyllou@uth.gr

Mangey Ram, Department of Mathematics, Computer Science and Engineering, Graphic Era Deemed to be University, Dehradun, Uttarakhand, India, e-mail: mangeyram@gmail.com; Institute of Advanced Manufacturing Technologies, Peter the Great St. Petersburg Polytechnic University, 195251, Saint Petersburg, Russia

<https://doi.org/10.1515/9783110725599-004>

the so-called r -within-consecutive- k -out-of- n : F structure, which was established by [20], fails if and only if there exist k consecutive components which include among them, at least r failed units [11, 16, 17, 22, 29]. A quite different modification of the common consecutive- k -out-of- n : F system is known as the m -consecutive- k -out-of- n : F system; it consists of n linearly ordered components such that the system fails if and only if there are at least m nonoverlapping runs of k consecutive failed units [9, 11, 15]. For some recent contributions on the field of consecutive-type structures, interested readers are referred to refs. [6, 12, 25].

On the other hand, some applications are related to two different criteria and several reliability structures have been established and studied in the literature. For instance, the (n, f, k) structure proposed by Chang et al. [1] fails if, and only if, there exist at least f failed units or at least k consecutive failed units. Several reliability characteristics of the so-called $[n, f, k]$ systems are studied in detail by Triantafyllou [26] and Zuo et al. [30]. Among others, the $\langle n, f, k \rangle$ structure (see, e.g. [5, 23]) and the constrained $[k, d]$ -out-of- n : F system [10, 24] are well-known consecutive-type reliability systems with two failure criteria. For a precise overview on the consecutive-type systems, we refer to the detailed reviews offered by Zao et al. [3] and Triantafyllou [21] and the well-documented monographs provided by Chang et al. [2] and Kuo and Zuo [14]. A detailed presentation of several reliability advances in various fields of engineering and physical sciences is also offered by Ram [19].

Throughout the lines of the present chapter, we study reliability structures with a single change point, for example, we focus on systems with two common failure criteria and two different types of units. More specifically, the (n, f, k) structure with a single change point is introduced. The general setup of the proposed reliability system is presented in Section 4.2, while explicit expressions for some reliability characteristics of it are provided in Section 4.3. A detailed numerical experimentation given in Section 4.4 offers some evidence for the performance of the (n, f, k) structure with a single change point. Finally, Section 4.5 summarizes the contribution of this chapter, while some practical concluding remarks are also highlighted.

4.2 The general setup of (n, f, k) structures with a single change point

Let us first consider an (n, f, k) system consisting of n independent and linearly ordered units. As already mentioned, the particular structure fails if and only if there exist at least f failed components or at least k consecutive failed components. We next assume that the first n_1 components of the (n, f, k) system share a common reliability p_1 (components of Type A, hereafter), while the remaining ones, namely the rest $n_2 = n - n_1$ units have a common reliability p_2 (components of Type B, hereafter), where $p_2 \neq p_1$. The location of the $(n_1 + 1)$ th unit could be thought as a change point

of the system and consequently the structure described above, is called $[n, f, k]$ system with a single change point. It is straightforward that in case of $p_2 = p_1 = p$, the aforementioned structure reduces to the traditional $[n, f, k]$ system introduced by Ram [1]. It is worth mentioning that reliability structures with one or more change points have been already introduced in the literature [8, 18].

Figure 4.1 represents the proposed $(n, f, k]$ system with a single change point.

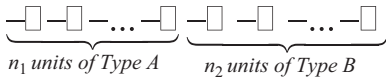


Figure 4.1: The $(n, f, k]$ system with a single change point.

The components of type A are represented by the symbol W and share the same reliability p_1 , while the rest units of type B appear as d and have reliability p_2 . The resulting structure fails whenever at least f components fail or at least k consecutive units stop their operation. Note that the abovementioned failure criteria could be reached by the aid of components either exclusively of the same type or even of both types. For example, let us next consider the $(n, f, k]$ system with a single change point by defining the design parameters as follows:

$$n = 10, n_1 = 5, n_2 = 5, f = 3, k = 2, p_1 = 0.8, p_2 = 0.9.$$

In other words, the aforementioned model contains 10 *i.i.d.* units, which are linearly ordered (see Figure 4.2). The first five units share a common reliability $p_1 = 0.8$, while the remaining five ones have a common reliability $p_2 = 0.9$. The resulting $(10, 3, 2)$ system with a change point fails if and only if at least three units fail or at least two consecutive components stop their operation.

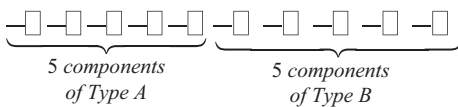


Figure 4.2: The $(10, 3, 2)$ system with a single change point.

Whenever a group of at least three (not necessarily consecutive) components fail or at least two consecutive units fail, the $(10, 3, 2)$ structure with a single change point stops its operation. It is noticeable that the abovementioned triad of failed units or the couple of consecutive failed units could include either units of type A or units of type B. For instance, if the last component of the first five ones and the first of the last five units of the system fail, then the $(10, 3, 2)$ structure with a single change point stops its operation.

4.3 Reliability characteristics of (n, f, k) structures with a single change point

In this section, we investigate the behavior of the (n, f, k) structures with a single change point. A closed expression for computing the bulk of path sets of the system containing i units of type A and j units of type B is provided, while the reliability function and the MTTF of the structures are also investigated.

Generally speaking, the (n, f, k) system with a single change point could be handled from two different points of view. The differentiation between these two scenarios depends exclusively on the status of the first component of the group of components of type B. More specifically, based on the first scenario (*Scenario 1*, hereafter) the first component of type B, for example, the first d which appears in the structure line, is supposed to be in functioning state. We next denote by 0 and 1 the failure and functioning state of each component respectively. Consequently, a common sequence of n binary elements (under *Scenario 1*), containing i working units of type A (w.c.A) and j working units of type B (w.c.B) is represented as

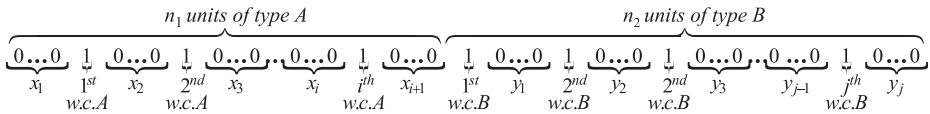


Figure 4.3: The (n, f, k) system with a single change point under *Scenario 1*.

Note that x_r , $r = 2, 3, \dots, i$ denotes the total number of 0s, which are located between two successive 1s throughout the components of type A. At the same time, x_1 corresponds to the components' failures of type A occurred before the appearance of the first working component of this type. In other words, the variable x_r , $r = 2, 3, \dots, i$ expresses the length of run of 0s in each urn between successive 1s throughout the first n_1 components, while x_1 indicates the length of the first run of 0s. It is straightforward that x_r , $r = 2, 3, \dots, i$ obey the following restrictions

$$0 \leq x_r \leq n_1, r = 1, 2, \dots, i \text{ and } \sum_{r=1}^i x_r = n_1 - i. \quad (4.1)$$

Following a parallel argumentation, we denote by y_s , $s = 1, 2, \dots, j$ the amount of 0s between successive 1s throughout the components of type B. In other words, the variable y_s , $s = 1, 2, \dots, j$ corresponds to the length of run of 0s in each urn between successive 1s throughout the n_2 components of type B. It is straightforward that the following conditions ensue

$$0 \leq y_s \leq n_2, s = 1, 2, \dots, j \text{ and } \sum_{s=1}^j y_s = n_2 - j. \quad (4.2)$$

On the other hand, the second scenario (*Scenario 2*, hereafter) requires that the first component of type *B* located in the structure line is supposed to be in failure state. Therefore, a binary sequence of n elements (under *Scenario 2*), containing i working units of type *A* (w.c.A) and j working units of type *B* (w.c.B) is represented in the Figure 4.4.

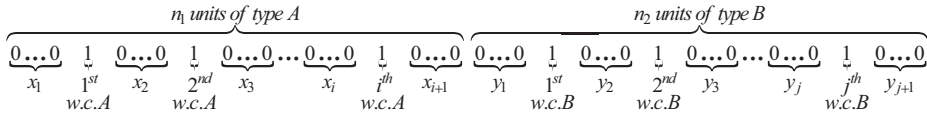


Figure 4.4: The (n, f, k) system with a single change point under *Scenario 2*.

Note that once again, x_r , $r = 1, 2, \dots, i, i + 1$ and y_s , $s = 1, 2, \dots, j, j + 1$ are connected to the length of runs of 0s in the respective urn. Clearly, the aforementioned quantities obey the following set of restrictions (under *Scenario 2*)

$$0 \leq x_r \leq n_1, r = 1, 2, \dots, i, i + 1, \sum_{r=1}^{i+1} x_r = n_1 - i - 1$$

and

$$0 \leq y_s \leq n_2, s = 1, 2, \dots, j, j + 1, \sum_{s=1}^{j+1} y_s = n_2 - j - 1. \quad (4.3)$$

In order to study further the performance of the (n, f, k) system with a single change point, it is crucial to determine the bulk of path sets containing i units of type *A* and j units of type *B* for the proposed structure $(r_{n_1, n_2, f, k}(i, j))$, hereafter). By denoting as $r_{n_1, n_2, f, k}(i, j, 1)$ ($r_{n_1, n_2, f, k}(i, j, 0)$), the number of path sets of the (n, f, k) structure with a single change point under *Scenario 1* (*Scenario 2*), we readily obtain that

$$r_{n_1, n_2, f, k}(i, j) = r_{n_1, n_2, f, k}(i, j, 1) + r_{n_1, n_2, f, k}(i, j, 0). \quad (4.4)$$

Let us first consider the *Scenario 1*, assuming that the (n, f, k) system with a single change point follows the scheme appeared in Figure 4.3. In other words, we suppose that the first unit of type *B* operates. The number of binary sequences of the components of type *A* and *B* (under *Scenario 1*) which assure the operation of the resulting structure equals to the amount of integer solutions of the next linear system

$$x_1 + x_2 + \dots + x_{i+1} = n_1 - i \quad (4.5)$$

such that

$$0 \leq x_\lambda \leq k - 1, \text{ for } \lambda = 1, 2, \dots, i + 1$$

and

$$y_1 + y_2 + \cdots + y_j = n_2 - j \quad (4.6)$$

such that

$$0 \leq y_\theta \leq k-1, \text{ for } \theta = 1, 2, \dots, j,$$

while $i + j \geq n - f + 1$.

The number of integer solutions of the linear eqs. (4.5) and (4.6) is given by ([4] p. 138)

$$Q = \binom{n_1}{i} + \sum_{r=1}^{i+1} (-1)^r \sum \binom{n_1 - r(k-1) - r}{i} \quad (4.7)$$

and

$$V = \binom{n_2}{j-1} + \sum_{r=1}^j (-1)^r \sum \binom{n_2 - r(k-1) - r - 1}{j-1} \quad (4.8)$$

respectively. Denoting by $[a]$ the integer part of a real number a , it is evident that in case of $i > [(n_1 - i)/k] - 1$ the outer sum of eq. (4.7) becomes zero. Actually, the same conclusion could be drawn for the outer sum of eq. (4.8) if $j > [(n_2 - j)/k]$. Additionally, note that in the inner sum appeared in formulae (4.7) and (4.8), the summation is extended over all r -combinations of the available indices. Consequently, the number of integer solutions of the linear eqs. (4.5) and (4.6) could be viewed as

$$Q = \sum_{r=0}^{\min(i+1, [(n_1-i)/k])} (-1)^r \binom{i+1}{r} \binom{n_1 - rk}{i} \quad (4.9)$$

and

$$V = \sum_{r=0}^{\min(j, [(n_2-j)/k])} (-1)^r \binom{j}{r} \binom{n_2 - rk - 1}{j-1}. \quad (4.10)$$

Based on the above formulae, the number of path sets of the (n, f, k) system with a single change point under *Scenario 1* is expressed as

$$r_{n_1, n_2, f, k}(i, j, 1) = Q \cdot V$$

or equivalently

$$r_{n_1, n_2, f, k}(i, j, 1) = \sum_{r=0}^{\min(i+1, [(n_1-i)/k])} (-1)^r \binom{i+1}{r} \binom{n_1 - rk}{i} \cdot \sum_{r=0}^{\min(j, [(n_2-j)/k])} (-1)^r \binom{j}{r} \binom{n_2 - rk - 1}{j-1}. \quad (4.11)$$

Employing analogous arguments as those mentioned previously, we shall next deal with the so-called *Scenario 2*. We now assume that the (n, f, k) system with a single change point follows the scheme appeared in Figure 4.4. In other words, we suppose that the first component of type *B* has failed. The amount of binary sequences of the components of type *A* and *B* (under *Scenario 2*) which ensure the operation of the resulting structure equals to the amount of integer solutions of the next linear system

$$x_1 + x_2 + \cdots + x_i = n_1 - i - x_{i+1} \quad (4.12)$$

such that

$$0 \leq x_\lambda \leq k-1, \text{ for } \lambda = 1, 2, \dots, i$$

and

$$y_2 + y_3 + \cdots + y_{j+1} = n_2 - j - y_1 \quad (4.13)$$

such that

$$0 \leq y_\theta \leq k-1, \text{ for } \theta = 2, 3, \dots, j,$$

while $i + j \geq n - f + 1$, $x_{i+1} + y_1 \leq k-1$, $x_{i+1} \geq 0$, $y_1 > 0$.

The amount of integer solutions of eqs. (4.12) and (4.13) is given by ([4] p. 138)

$$W = \sum_{r=0}^i (-1)^r \binom{i}{r} \binom{n_1 - x_{i+1} - rk - 1}{i-1} \quad (4.14)$$

and

$$Z = \sum_{r=0}^j (-1)^r \binom{j}{r} \binom{n_2 - y_1 - rk - 1}{j-1} \quad (4.15)$$

respectively, for all x_{i+1}, y_1 such that $x_{i+1} + y_1 \leq k-1$. It is evident that in case of $i > [(n_1 - i - x_{i+1})/k]$, the outer sum of eq. (4.14) becomes zero. Actually, the same conclusion could be drawn for the outer sum of eq. (4.15) if $j > [(n_2 - j - y_1)/k]$. Additionally, note that in the inner sum appeared in formulae (4.14) and (4.15), the summation is extended over all r -combinations of the available indices. Consequently, the number of integer solutions of the linear eqs. (4.12) and (4.13) could be rewritten as

$$W = \sum_{r=0}^{\min(i, [(n_1 - i - x_{i+1})/k])} (-1)^r \binom{i}{r} \binom{n_1 - x_{i+1} - rk - 1}{i-1} \quad (4.16)$$

and

$$Z = \sum_{r=0}^{\min(j, [(n_2 - j - y_1)/k])} (-1)^r \binom{j}{r} \binom{n_2 - y_1 - rk - 1}{j-1} \quad (4.17)$$

for all x_{i+1}, y_1 such that $x_{i+1} + y_1 \leq k-1$. Due to the above formulae, the amount of path sets of the (n, f, k) structure with a single change point under *Scenario 2* is given as

$$r_{n_1, n_2, f, k}(i, j, 0) = \sum_{x_{i+1} + y_1 \leq k-1} W \cdot Z$$

or equivalently

$$\begin{aligned} r_{n_1, n_2, f, k}(i, j, 0) = & \sum_{x=0}^{k-2} \sum_{y=1}^{k-x-1} \sum_{r=0}^{\min(i, [(n_1-i-x_{i+1})/k])} (-1)^r \binom{i}{r} \binom{n_1-x_{i+1}-rk-1}{i-1} \\ & \times \sum_{r=0}^{\min(j, [(n_2-j-y_1)/k])} (-1)^r \binom{j}{r} \binom{n_2-y_1-rk-1}{j-1}. \end{aligned} \quad (4.18)$$

It is now straightforward that combining formulae (4.4), (4.11), and (4.18), the number of path sets of the $[n, f, k]$ system with a single change point is readily determined.

Note that a parallel argumentation, as the one applied previously, has been implemented by Eryilmaz [8] for a different reliability structure, which is known as consecutive- k -out-of- n . Generally speaking, having at hand the amount of path sets of the model including i units of type A and j units of type B , we could readily derive closed formulae for computing the reliability function and the mean time to failure (MTTF) of the $(n, f, k]$ system with a single change point. In order to obtain the desired expressions, we need to clear up whether the amount of units of each type is pre-specified or it is randomly determined. Under the assumption that the amount of units of each type is fixed, for example, the design parameters n_1, n_2 are preordained, the reliability function of the $(n, f, k]$ model with a single change point is given as

$$R_{n_1, n_2, f, k}(p_1, p_2) = \sum_{i=0}^{n_1} \sum_{j=\min(n-f+1-i, n_2)}^{n_2} r_{n_1, n_2, f, k}(i, j) p_1^i (1-p_1)^{n_1-i} p_2^j (1-p_2)^{n_2-j}, \quad (4.19)$$

where $r_{n_1, n_2, f, k}(i, j)$ represents the bulk of path sets of the structure containing i units of type A and j units of type B . In such a framework, the (n, f, k) systems with a single change point dispose a fixed number of components of each type and their MTTF can be represented as ($i+j \geq n-f+1$)

$$\text{MTTF}_{n_1, n_2, f, k}(F_1, F_2) = \sum_{i=0}^{n_1} \sum_{j=\min(n-f+1-i, n_2)}^{n_2} r_{n_1, n_2, f, k}(i, j) \int_0^\infty \bar{F}_1^i(t) F_1^{n_1-i}(t) \bar{F}_2^j(t) F_2^{n_2-j}(t) dt, \quad (4.20)$$

where $\bar{F}_1(t) = 1 - F_1(t)$ and $\bar{F}_2(t) = 1 - F_2(t)$ correspond to the reliability (survival) function of units of type A and type B correspondingly.

On the other hand, if the amount of units of each type is random, it is evident that the reliability function of the (n, f, k) structure with a single change point could be determined by implementing suitable conditioning arguments. More specifically, we first introduce the random variable N_1 , which expresses the number of units of type A ($0 \leq N_1 \leq n$). Denoting by $f(n_1) = P(N_1 = n_1)$ the probability mass function of N_1 , we express the reliability of the (n, f, k) system with a single change point, given that the amount of units of each type is now random, as

$$R_{n,f,k}(p_1, p_2) = \sum_{n_1=0}^n R_{n_1, n-n_1, f, k}(p_1, p_2) f(n_1). \quad (4.21)$$

Moreover, the MTTF of the (n, f, k) structure with a single change point consisting of random number of units of each type, can be readily viewed as

$$\text{MTTF}_{n,f,k}(F_1, F_2) = \sum_{n_1=0}^n \text{MTTF}_{n_1, n-n_1, f, k}(F_1, F_2) f(n_1). \quad (4.22)$$

4.4 Numerical results

In this section, we accomplish a numerical experimentation to evaluate the performance of the (n, f, k) structure with a single change point. The computations are carried out via the theoretical results discussed in Section 4.3. We first illustrate the reliability function of the aforementioned structure under several designs, namely for different values of the design parameters n , n_1 , n_2 , f , k , p_1 , and p_2 .

Table 4.1: Reliability of the (n, f, k) system with a single change point for fixed n_1, n_2 .

n	(f, k)	(n_1, n_2)	(p_1, p_2)	$R_{n1, n2, f, k}(p_1, p_2)$
7	(3,2)	(5,2)	(0.93,0.95)	0.973968
			(0.91,0.95)	0.960409
		(4,3)	(0.93,0.95)	0.976352
			(0.91,0.95)	0.965918
	(3,4)	(3,4)	(0.93,0.95)	0.978725
			(0.91,0.95)	0.971369
		(2,5)	(0.93,0.95)	0.981090
			(0.91,0.95)	0.976805

Table 4.1 (continued)

n	(f, k)	(n_1, n_2)	(p_1, p_2)	$R_{n1, n2, f, k}(p_1, p_2)$
8	(4,2)	(5,2)	(0.93,0.95)	0.975921
			(0.91,0.95)	0.963563
		(4,3)	(0.93,0.95)	0.978092
			(0.91,0.95)	0.968520
		(3,4)	(0.93,0.95)	0.980267
			(0.91,0.95)	0.973494
		(2,5)	(0.93,0.95)	0.982444
			(0.91,0.95)	0.978478
	(3,2)	(6,2)	(0.93,0.95)	0.967599
			(0.91,0.95)	0.950047
		(5,3)	(0.93,0.95)	0.970129
			(0.91,0.95)	0.955955
		(4,4)	(0.93,0.95)	0.972633
			(0.91,0.95)	0.961743
		(3,5)	(0.93,0.95)	0.975115
			(0.91,0.95)	0.967441
		(2,6)	(0.93,0.95)	0.977580
			(0.91,0.95)	0.973085
	(4,2)	(6,2)	(0.93,0.95)	0.971381
			(0.91,0.95)	0.956251
		(5,3)	(0.93,0.95)	0.973549
			(0.91,0.95)	0.961191
		(4,4)	(0.93,0.95)	0.975720
			(0.91,0.95)	0.966149
		(3,5)	(0.93,0.95)	0.977895
			(0.91,0.95)	0.971123
		(2,6)	(0.93,0.95)	0.980072
			(0.91,0.95)	0.976109

Table 4.1 (continued)

n	(f, k)	(n_1, n_2)	(p_1, p_2)	$R_{n1, n2, f, k}(p_1, p_2)$
9	(3,2)	(7,2)	(0.93,0.95)	0.960426
			(0.91,0.95)	0.938332
		(6,3)	(0.93,0.95)	0.963136
			(0.91,0.95)	0.944724
		(5,4)	(0.93,0.95)	0.965809
			(0.91,0.95)	0.950954
		(4,5)	(0.93,0.95)	0.968449
			(0.91,0.95)	0.957041
		(3,6)	(0.93,0.95)	0.971058
			(0.91,0.95)	0.963012
		(2,7)	(0.93,0.95)	0.973641
			(0.91,0.95)	0.968898
	(4,2)	(7,2)	(0.93,0.95)	0.966789
			(0.91,0.95)	0.948846
		(6,3)	(0.93,0.95)	0.968961
			(0.91,0.95)	0.953792
		(5,4)	(0.93,0.95)	0.971135
			(0.91,0.95)	0.958751
		(4,5)	(0.93,0.95)	0.973311
			(0.91,0.95)	0.963722
		(3,6)	(0.93,0.95)	0.975489
			(0.91,0.95)	0.968707
		(2,7)	(0.93,0.95)	0.977670
			(0.91,0.95)	0.973701
10	(3,2)	(7,3)	(0.93,0.95)	0.955291
			(0.91,0.95)	0.932106
		(6,4)	(0.93,0.95)	0.958160
			(0.91,0.95)	0.938840
		(5,5)	(0.93,0.95)	0.960987

Table 4.1 (continued)

n	(f, k)	(n_1, n_2)	(p_1, p_2)	$R_{n1, n2, f, k}(p_1, p_2)$
			(0.91, 0.95)	0.945400
		(4, 6)	(0.93, 0.95)	0.963774
			(0.91, 0.95)	0.951801
		(3, 7)	(0.93, 0.95)	0.966524
			(0.91, 0.95)	0.958066
	(4, 2)	(7, 3)	(0.93, 0.95)	0.964289
			(0.91, 0.95)	0.946244
		(6, 4)	(0.93, 0.95)	0.966474
			(0.91, 0.95)	0.951230
		(5, 5)	(0.93, 0.95)	0.968659
			(0.91, 0.95)	0.956221
		(4, 6)	(0.93, 0.95)	0.970846
			(0.91, 0.95)	0.961219
		(3, 7)	(0.93, 0.95)	0.973033
			(0.91, 0.95)	0.966225

Based on Table 4.1, one may readily observe the following concluding remarks:

- The reliability of the (n, f, k) structure with a single change point increases as the probability p_1 increases.
- The reliability of the (n, f, k) structure with a single change point grows as the probability p_2 grows.
- The reliability of the (n, f, k) structure with a single change point grows as the parameter f grows.
- The reliability of the (n, f, k) structure with a single change point grows as the parameter n decreases.

Note that the practical guidelines mentioned above hold true under the assumption that the remaining design parameters remain unchangeable.

We next carry out a numerical experimentation with respect to the MTTF of the (n, f, k) structure with a single change point. Based on eq. (4.20), we perform several numerical computations for revealing the behavior of MTTF of the resulting reliability structure. In order to make the integral expression more convenient, we next consider that the components of both types provide proportional hazard rates (*Model I*,

hereafter). In other words, denoting by H the baseline distribution for all components with corresponding hazard rate $\lambda(t)$, then the reliability function of components of type A and type B is given as

$$\bar{F}_1(t) = \bar{H}^{\delta_1}(t) \text{ and } \bar{F}_2(t) = \bar{H}^{\delta_2}(t)$$

respectively, where $\delta_1, \delta_2 > 0$, $t \geq 0$. Moreover, it is straightforward that the hazard rates of the components of type A and type B are expressed as $\delta_1 \cdot \lambda(t)$ and $\delta_2 \cdot \lambda(t)$ correspondingly. Recalling eq. (4.20), the MTTF of the (n, f, k) structure with a single change point under *Model I* is rewritten as

$$\begin{aligned} & \text{MTTF}_{n_1, n_2, f, k}(F_1, F_2) \\ &= \sum_{i=0}^{n_1} \sum_{j=\min(n-f+1-i, n_2)}^{n_2} r_{n_1, n_2, f, k}(i, j) \int_0^\infty \bar{H}^{\delta_1 i}(t) (1 - \bar{H}^{\delta_1}(t))^{n_1-i} \bar{H}^{\delta_2 j}(t) (1 - \bar{H}^{\delta_2}(t))^{n_2-j} dt. \end{aligned}$$

We next apply the well-known binomial theorem and the MTTF of the underlying structure can now be expressed as

$$\begin{aligned} & \text{MTTF}_{n_1, n_2, f, k}(F_1, F_2) \\ &= \sum_{i=0}^{n_1} \sum_{j=\min(n-f+1-i, n_2)}^{n_2} r_{n_1, n_2, f, k}(i, j) \sum_{\mu=0}^{n_1-i} \sum_{\nu=0}^{n_2-j} (-1)^{\mu+\nu} \binom{n_1-i}{\mu} \binom{n_2-j}{\nu} \\ & \quad \int_0^\infty (\bar{H}(t))^{\delta_1(\mu+i) + \delta_2(\nu+j)} dt. \end{aligned} \quad (4.23)$$

Once the distribution function H is specified, the MTTF of the (n, f, k) structure with a single change point is readily determined by the aid of (4.23). For instance, let us next consider the exponential distribution with parameter θ , for example, the baseline distribution function is given as $\bar{H}(t) = e^{-\theta t}$, $\theta > 0$, $t \geq 0$. Consequently, the MTTF of the resulting structure can be computed by the aid of the following formula

$$\begin{aligned} & \text{MTTF}_{n_1, n_2, f, k}(F_1, F_2) \\ &= \sum_{i=0}^{n_1} \sum_{j=\min(n-f+1-i, n_2)}^{n_2} \sum_{\mu=0}^{n_1-i} \sum_{\nu=0}^{n_2-j} (-1)^{\mu+\nu} \frac{r_{n_1, n_2, f, k}(i, j)}{\theta(\delta_1(\mu+i) + \delta_2(\nu+j))} \binom{n_1-i}{\mu} \binom{n_2-j}{\nu}. \end{aligned} \quad (4.24)$$

Based on eq. (4.24), we next compute the MTTF of the (n, f, k) structure with a single change point under *Model I* with exponential baseline distribution. Table 4.2 presents the corresponding numerical results for several designs.

Table 4.2: Mean time to failure of the (n, f, k) system with a single change point for fixed n_1, n_2 .

n	(n_1, n_2)	(f, k)	$(\delta_1, \delta_2, \theta)$	MTTF
10	(5,5)	(4,3)	(0.3, 0.1, 0.2)	12.1866
		(6,3)		17.3064
		(6,2)		9.90844
		(4,3)	(0.3, 0.1, 0.5)	4.87464
		(6,3)		6.92256
		(6,2)		3.96377
	(6,4)	(4,3)	(0.3, 0.1, 0.2)	10.9963
		(6,3)		15.6038
		(6,2)		8.98593
		(4,3)	(0.3, 0.1, 0.5)	4.39852
		(6,3)		6.24151
		(6,2)		3.59437
	(7,3)	(4,3)	(0.3, 0.1, 0.2)	10.0007
		(6,3)		14.2945
		(6,2)		8.26426
		(4,3)	(0.3, 0.1, 0.5)	4.00027
		(6,3)		5.71780
		(6,2)		3.30570
20	(10,10)	(8,6)	(0.1, 0.2, 0.1)	33.8475
		(10,6)		45.7564
		(10,4)		40.7474
		(8,6)	(0.1, 0.2, 0.3)	11.2825
		(10,6)		15.2521
		(10,4)		13.5825
	(12,8)	(8,6)	(0.1, 0.2, 0.1)	36.3496
		(10,6)		49.1463
		(10,4)		43.7658
		(8,6)	(0.1, 0.2, 0.3)	12.1165

Table 4.2 (continued)

<i>n</i>	(n_1, n_2)	(f, k)	$(\delta_1, \delta_2, \theta)$	MTTF
		(10,6)		16.3821
		(10,4)		14.5886
	(14,6)	(8,6)	(0.1, 0.2, 0.1)	39.1498
		(10,6)		52.9792
		(10,4)		47.3841
		(8,6)	(0.1, 0.2, 0.3)	13.0499
		(10,6)		17.6597
		(10,4)		15.7947

The baseline distribution is assumed to be the exponential with parameter θ .

It is of some practical interest to construct several figures in order to shed light on the behavior of the reliability function of the (n, f, k) system with a single change point. Each figure depicts reliability values of the underlying structure versus two different design parameters under the assumption that the remaining ones are pre-specified. Figures 4.5 and 4.6 illustrate the reliability function of the $(10, 3, 2)$ system with a single change point for several probability values p_1 and p_2 .

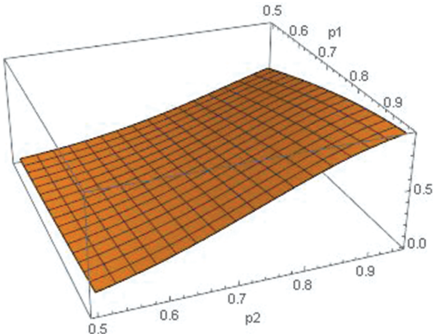


Figure 4.5: Reliability of the (n, f, k) system with a single point versus p_1, p_2 ($n_1 = 3, n_2 = 7, f = 3, k = 2$).

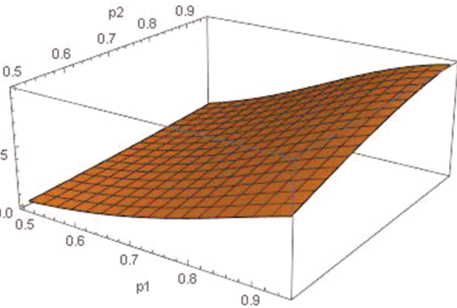


Figure 4.6: Reliability of the (n, f, k) system with a single change point versus p_1, p_2 ($n_1 = 7, n_2 = 3, f = 3, k = 2$).

Based on Figures 4.5 and 4.6, one may readily conclude the following:

- The reliability of the (10, 3, 2) system with a single change point increases with respect of p_1 .
- The reliability of the (10, 3, 2) system with a single change point increases with respect of p_2 .

It is of some interest to focus on the impact of the design parameters n_1 and n_2 on the global performance of the (n, f, k) system with a single change point. Since parameters n_1 and n_2 correspond to the amount of units of type *A* and *B* respectively, it is crucial to set up an optimal framework with respect to the number of units of each type which is involved to the resulting structure.

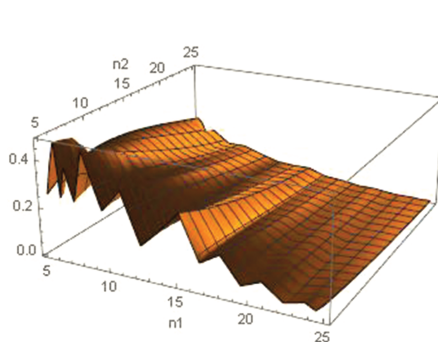


Figure 4.7: Reliability of the (n, f, k) system with a single point versus n_1, n_2 ($p_1 = 0.8$, $p_2 = 0.9$, $f = 3$, $k = 2$).

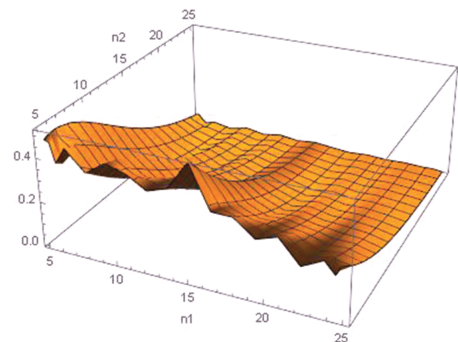


Figure 4.8: Reliability of the (n, f, k) system with a single change point versus n_1, n_2 ($p_1 = 0.9$, $p_2 = 0.8$, $f = 3$, $k = 2$).

For pre-specified f , k , p_1 , and p_2 , Figures 4.7 and 4.8 reveal that the (n, f, k) system with a single change point maximizes its attribution for moderate values of design parameters n_1 and n_2 . At the same time, based on Figures 4.7 and 4.8, one may easily observe that large values of parameters n_1 and n_2 lead to deterioration of the performance of the structure.

The following figures depict the impact of design parameters f and k on the reliability values of the (n, f, k) system with a single change point. According to Figures 4.9 and 4.10, we conclude that as the parameter f increases, the reliability of the resulting structure increases too. Additionally, the same remark could be confirmed for the influence of parameter k on the behavior of the (n, f, k) system with a single change point.

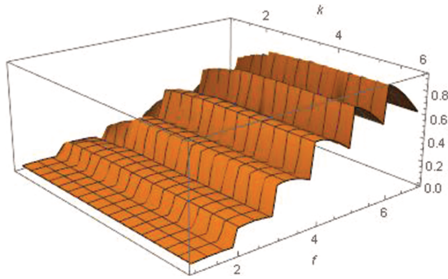


Figure 4.9: Reliability of the (n, f, k) system with a single point versus f, k ($p_1 = 0.8$, $p_2 = 0.9$, $n_1 = 10$, $n_2 = 10$).

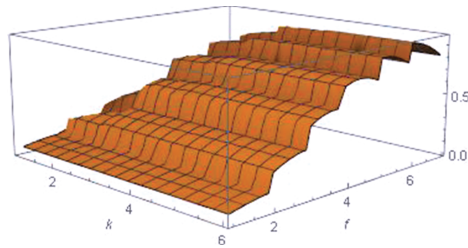


Figure 4.10: Reliability of the (n, f, k) system with a single point versus f, k ($p_1 = 0.9$, $p_2 = 0.8$, $n_1 = 10$, $n_2 = 8$).

4.5 Discussion

In this chapter, the (n, f, k) system with a single change point is introduced. Some reliability characteristics of the proposed structure are studied, and the corresponding closed formulae are also delivered. The performance of the (n, f, k) system with a single change point is evaluated by the aid of its reliability function and MTTF. Based on the practical guidelines and remarks, which have been pointed out in Section 4.4, one may choose the appropriate set of design parameters in order to optimize the performance of the resulting (n, f, k) system with a single change point. A parallel reliability study of well-known structures with a single change point seems to be an intriguing issue for further investigation.

References

- [1] Chang, J.G., Cui, L., Hwang, F.K. 1999. Reliabilities for systems, *Statistics & Probability Letters*, 43(3), 237–242.
- [2] Chang, J.G., Cui, L., Hwang, F.K. 2000. *Reliabilities of consecutive-k systems*, Kluwer Academic Publishers, The Netherlands.
- [3] Chao, M.T., Fu, J.C., Koutras, M.V. 1995. Survey of reliability studies of consecutive-k-out-of-n: F & related systems, *IEEE Transactions on Reliability*, 44(1), 120–127.
- [4] Charalambides, C. 2002. *Enumerative Combinatorics*, Chapman & Hall/CRC, Boca Raton, U.S.A.
- [5] Cui, L., Kuo, W., Li, J., Xie, M. 2006. On the dual reliability systems of and, *Statistics & Probability Letters*, 76(11), 1081–1088.
- [6] Dafnis, S.D., Makri, F.S., Philippou, A.N. 2019. The reliability of a generalized consecutive system, *Applied Mathematics and Computation*, 359, 186–193.
- [7] Derman, C., Lieberman, G.J., Ross, S.M. 1982. On the consecutive-k-out-of-n: F system, *IEEE Transactions on Reliability*, 31(1), 57–63.

- [8] Eryilmaz, S. 2016. Consecutive k -out-of- n : lines with a change point, *Proc. IMechE Part O: Journal of Risk and Reliability*, 230(6), 545–550.
- [9] Eryilmaz, S., Koutras, M.V., Triantafyllou, I.S. 2011. Signature based analysis of m -consecutive k -out-of- n : F systems with exchangeable components, *Naval Research Logistics*, 58(4), 344–354.
- [10] Eryilmaz, S., Zuo, M.J. 2010. Constrained (k,d) -out-of- n systems, *International Journal of Systems Science*, 41(3), 679–685.
- [11] Griffith, W.S. 1986. On consecutive- k -out-of- n : failure systems and their generalizations, In Basu, A.P., ed *Reliability and Quality Control*, Elsevier, Amsterdam, 157–165.
- [12] Kumar, A., Ram, M. 2019. Signature of linear consecutive k -out-of- n systems, In Ram, M., Dohi, T., eds *Systems Engineering: Reliability Analysis using k -out-of- n structures*, CRC Press: Taylor & Francis Group, 207–216.
- [13] Kumar, A., Singh, S.B., Ram, M. 2019. Reliability appraisal for consecutive- k -out-of- n : F system of non-identical components with intuitionistic fuzzy set, *International Journal of Operation Research*, 36, 362–374.
- [14] Kuo, W., Zuo, M.J. 2003. *Optimal Reliability Modeling: Principles and Applications*, John Wiley & Sons, N.J.
- [15] Makri, F.S., Philippou, A.N. 1996. Exact reliability formulas for linear and circular m -consecutive- k -out-of- n : F systems, *Microelectronics Reliability*, 36, 657–660.
- [16] Makri, F.S., Psillakis, Z.M. 1996a. Bounds for reliability of k -within two dimensional consecutive- r -out-of- n : failure systems, *Microelectronics Reliability*, 36, 341–345.
- [17] Makri, F.S., Psillakis, Z.M. 1996b. On consecutive k -out-of- r -from- n : F systems: A simulation approach, *International Journal of Modelling and Simulation*, 16, 15–20.
- [18] Peng, R., Xiao, H. 2018. Reliability of Linear Consecutive k -out-of- n systems with two change points, *IEEE Transactions on Reliability*, 67(3), 1019–1029.
- [19] Ram, M. 2013. On system reliability approaches: a brief survey, *International Journal of System Assurance Engineering and Management*, 4(2), 101–117.
- [20] Tong, Y.L. 1985. A rearrangement inequality for the longest run, with an application to network reliability, *Journal of Applied Probability*, 22, 386–393.
- [21] Triantafyllou, I.S. 2015. Consecutive-type reliability systems: an overview and some applications, *Journal of Quality and Reliability Engineering*, 2015, Article ID 212303, 20 pages.
- [22] Triantafyllou, I.S. 2020a. Signature-based reliability study of r -within-consecutive- k -out-of- n : F systems, In *Safety and Reliability Modeling and Its Applications*, (Eds. H. Pham & M. Ram), Elsevier, *accepted for publication*.
- [23] Triantafyllou, I.S. 2020b. Reliability study of $\langle n, f, 2 \rangle$ systems: a generating function approach, *International Journal of Mathematical, Engineering and Management Sciences*, *accepted for publication*.
- [24] Triantafyllou, I.S. 2020c. On the lifetime and signature of the constrained (k,d) out-of- n : F reliability systems, *International Journal of Mathematical, Engineering and Management Sciences*, *accepted for publication*.
- [25] Triantafyllou, I.S. 2020d. On consecutive k_1 and k_2 -out-of- n : F reliability systems, *Mathematics*, 8, 630.
- [26] Triantafyllou, I.S., Koutras, M.V. 2014. Reliability properties of systems, *IEEE Transactions on Reliability*, 63(1), 357–366.
- [27] Triantafyllou, I.S., Koutras, M.V. 2008a. On the signature of coherent systems and applications for consecutive- k -out-of- n : F systems, In Bedford, T., Quigley, J., Walls, L., Alkali, B., Daneshkhan, A., Hardman, G., eds *Advances in Mathematical Modeling for Reliability*, IOS Press, Amsterdam, 119–128.

- [28] Triantafyllou, I.S., Koutras, M.V. 2008b. On the signature of coherent systems and applications, *Probability in the Engineering and Informational Science*, 22(1), 19–35.
- [29] Triantafyllou, I.S., Koutras, M.V. 2011. Signature and *IFR* preservation of 2-within-consecutive k -out-of- $n:F$ systems, *IEEE Transactions on Reliability*, 60(1), 315–322.
- [30] Zuo, M.J., Lin, D., Wu, Y. 2000. Reliability evaluation of combined k -out-of- $n:F$, consecutive- k -out-of- $n:F$ and linear connected- (r,s) -out-of- $(m,n):F$ system structures, *IEEE Transactions on Reliability*, 49, 99–104.

Qisi Liu, Liudong Xing, Guilin Zhao

5 Invulnerability and survivability modeling and analysis of cloud storage systems

Abstract: In this chapter, we present mathematical modeling and analysis of invulnerability and survivability for cloud storage systems, in particular, the cloud-RAID (redundant array of independent disks) storage system. The invulnerability corresponds to the system's capability of operating correctly while being immune to cyberattacks. The survivability corresponds to the system's capability of operating correctly despite the occurrence of malicious cyberattacks and physical disk failures. The semi-Markov process (SMP) is applied to model and analyze invulnerability and survivability at the disk level. Multivalued decision diagrams and combinatorics are applied to assess these performance metrics at the cloud storage system level. The presented methodology is flexible in handling diverse distribution types of state transition time. Influences of different model parameters on the disk-level and system-level performance are demonstrated through an in-depth case study on a cloud-RAID-5 system.

Keywords: Cloud storage, combinatorics, cyberattack, disk fault, invulnerability, multivalued decision diagram, semi-Markov process, survivability

5.1 Introduction

Individual disks are subject to incidental failures due to factors such as defects and aging/wear-out, posing reliability risks to the cloud storage system. The cloud storage system, and in general, the modern technological systems are also vulnerable to cyberattacks [1–6]. As a specific example, denial-of-service (DoS) attacks can be launched using sound waves (without using any internet connection), which may outage the service and even cause permanent damages or pose life-threatening dangers to hardware components like medical devices [7]. This chapter presents the mathematical modeling and analysis of invulnerability and survivability for cloud storage systems, in particular, the cloud-RAID (redundant array of independent disks) storage system considering effects of both disk physical failures and malicious cyberattacks. The invulnerability refers to the system's capability of operating correctly while being immune to malicious attacks. The survivability refers to the system's capability of performing the intended function despite the occurrence of malicious cyberattacks or accidental physical failures [8].

Qisi Liu, Liudong Xing, Guilin Zhao, Department of Electrical and Computer Engineering, University of Massachusetts, Dartmouth, USA

<https://doi.org/10.1515/9783110725599-005>

Considerable research efforts have been dedicated to the quantitative reliability modeling and evaluation of cloud storage systems. These works were mainly concerned with the behavior of cloud storage systems in the presence of random physical failures, without considering the effects of cyberattacks. For example, Iliadis et al. studied the reliability of geo-replicated cloud storage systems, taking into account different bandwidths within a site and between sites [9]. Liu and Xing modeled the reliability of a cloud-RAID-6 storage system, using a hybrid analytical method [10]. Mandava and Xing investigated the reliability modeling and optimization for cloud-RAID storage systems, subject to fault-level coverage [11] and element-level coverage [12]. Nachiappan et al. examined two types of data reliability techniques (replication and erasure coding) for cloud storage systems in the big data application [13]. Zhang et al. proposed a Markov decision-process modeling framework to analyze the reliability of cloud storage systems [14].

A limited body of research has also been dedicated to the quantitative security modeling and analysis, considering effects from cyberattacks. For example, Xing and Levitin suggested a probabilistic modeling method to evaluate data security and reliability for a cloud system using the data partition policy against co-resident attacks [15]. In [16], Levitin et al. extended the method of [15] for cloud systems, using a combined data partition and replication policy. Liu et al. analyzed the security risk occurrence probability for a system, subject to cyberattacks with multiple sequence-dependent hazardous actions [17]. Liu and Xing proposed a continuous-time Markov chain-based approach to assess the invulnerability and survivability of cloud-RAID systems considering both cyberattacks and physical failures [18]. However, the method of [18] is only limited to the exponential state transition time distribution, that is, the state transition time occupies the memoryless property. In other words, the storage disks do not age with time, which is often not true in practice.

In this chapter, a semi-Markov process (SMP)-based approach is presented to model and evaluate the performance of each disk in the form of different state probabilities, invulnerability, and survivability. The SMP-based approach is applicable to any type of state transition time distribution. Based on the disk-level performance analysis, multivalued decision diagrams (MDD) and combinatorics-based methods are presented to assess the invulnerability and survivability of the entire cloud-RAID storage system. Influences of several parameters modeling the attack, failure, and recovery behaviors of disks on the disk and system performance are also examined.

The rest of this chapter has the following structure: Section 5.2 describes an example of the cloud-RAID-5 system, which is used to demonstrate the methodology and parameter effects in the subsequent sections. Section 5.3 presents the SMP-based approach for the disk-level performance analysis. Section 5.4 presents the MDD and combinatorics-based methods for the system-level performance analysis. Section 5.5 investigates impacts of several model parameters on the disk state probabilities and the entire system performance. Section 5.6 concludes this chapter and points out a few future research directions.

5.2 Example cloud-RAID-5

A cloud-RAID-5 storage system containing four storage disks [18] is used as an example to illustrate the presented invulnerability and survivability analysis method. Figure 5.1 shows the general structure of this example system that uses the distributed single parity code to achieve disk fault tolerance (in the case of one disk malfunctioning or being attacked, the entire system can continue to function).

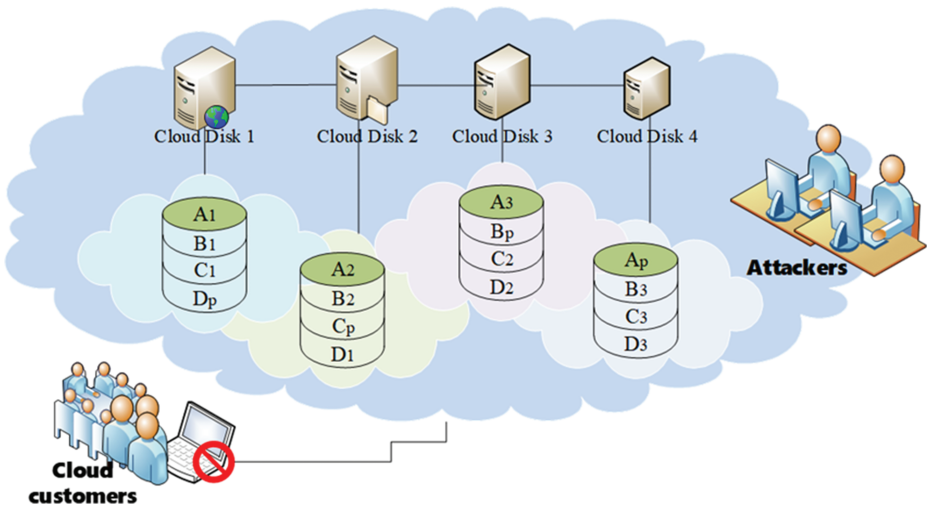


Figure 5.1: An example cloud-RAID-5 system.

Specifically, data are decomposed into blocks or stripes (A1, A2, A3, etc.) and are distributed to four disks in the array. Different disks may come from different providers or cloud data centers. The parity block (Ap, Bp, Cp, Dp) of corresponding data blocks on the same row is stored across the four disks. In the event of one disk having the service outage, the stripes stored in the affected disk can be restored using the remaining data stripes and the parity stripe, for example, via performing the exclusive OR operation when the even parity is adopted.

5.3 Disk-level modeling and analysis

5.3.1 The SMP modeling

Figure 5.2 illustrates the state transition diagram in the SMP solution method. A disk may assume four different states during its lifetime: good state 0, degradation state 1, vulnerable state 2, and complete failure state 3.

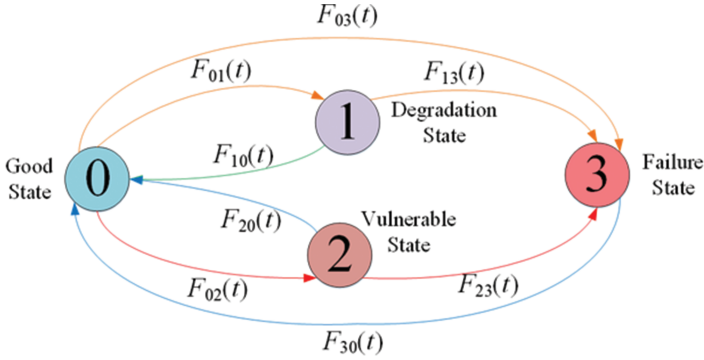


Figure 5.2: SMP model of a single disk.

Initially, the disk is in the good state 0, where both reliability and security attributes hold, and data can be accessed correctly. From state 0, the disk can transit to state 1 due to a media or recoverable error; or to state 3 due to unrecoverable hardware failure or some security threats (e.g., data deletion/tempering through insecure APIs). Under state 1, the disk can go back to state 0 if the media error can be restored by the self-recovery mechanism of the disk; or the disk transits to state 3 if the restoration effort fails and the data get lost permanently. From state 0, the disk may also transit to the vulnerable state 2 due to cyberattacks like distributed denial-of-service (DDoS) attacks or events (like the Black Friday virtual shopping) that cause explosive visits to servers. Under state 2, the disk still works but with some latency. From state 2, the disk may transit back to state 0 by performing certain timely contingency strategies; or transit to state 3 if no timely remedial actions are taken (i.e., being defenseless) or the DDoS attack size increases. In the case of the disk in state 3 being caused by DDoS attacks, the disk failure/inaccessibility may be fully restored, bringing the disk back to state 0 via, for example, getting adequate spare bandwidth for volumetric attacks, utilizing some attack mitigation service, or implementing some incident response plan [19].

All the state transition times are characterized by general cumulative distribution functions (CDF), for example, $F_{ij}(t)$ for the transition time from state i to state j ($i, j = 0, 1, 2, 3$). In the subsequent illustrative analysis, the Weibull distribution is chosen due to its wide application in reliability engineering and its flexibility in representing diverse failure rate behaviors [20, 21]. The Weibull distribution has the CDF of $F_{ij}(t, \alpha_{ij}, \beta_{ij}) = 1 - \exp\left(- (t/\alpha_{ij})^{\beta_{ij}}\right)$, where $(\alpha_{ij}, \beta_{ij})$ are scale and shape parameters, respectively. In the case of $\beta_{ij} = 1$, it becomes the exponential distribution; in the case of $\beta_{ij} = 2$, it becomes the Rayleigh distribution.

5.3.2 The SMP steady-state analysis

The steady-state analysis of an SMP model can be conducted in four stages [17, 22, 23]:

Stage 1: Define the one-step transition probability matrix $\mathbf{K}(t)$ (also known as the kernel matrix) of the SMP's embedded Markov chain (EMC) [23]. Each element in the matrix $k_{ij}(t)$ represents the probability that the disk just entered state i , the next transition takes place in time t , and the subsequent state is state j . All the elements on the same row of $\mathbf{K}(t)$ always sum to 1. In eq. (5.1) we illustrate the matrix $\mathbf{K}(t)$ for the SMP model of Figure 5.2, where the non-zero elements are defined in eqs. (5.2)–(5.9). The integrals involved in eqs. (5.2)–(5.9) are evaluated using Wolfram Mathematics and MATLAB in this work.

$$\mathbf{K}(t) = \begin{bmatrix} 0 & k_{01} & k_{02} & k_{03} \\ k_{10} & 0 & 0 & k_{13} \\ k_{20} & 0 & 0 & k_{23} \\ k_{30} & 0 & 0 & 0 \end{bmatrix} \quad (5.1)$$

$$k_{30}(t) = F_{30}(t) = 1 - e^{-\left(\frac{t}{a_{30}}\right)^{\beta_{30}}} \quad (5.2)$$

$$k_{10}(t) = \int_0^t \bar{F}_{13}(x) dF_{10}(x) = \frac{\beta_{10}}{\alpha_{10}^{\beta_{10}}} \int_0^t x^{\beta_{10}-1} e^{-\left[\left(\frac{x}{a_{10}}\right)^{\beta_{10}} + \left(\frac{x}{a_{13}}\right)^{\beta_{13}}\right]} dx \quad (5.3)$$

$$k_{13}(t) = \int_0^t \bar{F}_{10}(x) dF_{13}(x) = \frac{\beta_{13}}{\alpha_{13}^{\beta_{13}}} \int_0^t x^{\beta_{13}-1} e^{-\left[\left(\frac{x}{a_{10}}\right)^{\beta_{10}} + \left(\frac{x}{a_{13}}\right)^{\beta_{13}}\right]} dx \quad (5.4)$$

$$k_{20}(t) = \int_0^t \bar{F}_{23}(x) dF_{20}(x) = \frac{\beta_{20}}{\alpha_{20}^{\beta_{20}}} \int_0^t x^{\beta_{20}-1} e^{-\left[\left(\frac{x}{a_{20}}\right)^{\beta_{20}} + \left(\frac{x}{a_{23}}\right)^{\beta_{23}}\right]} dx \quad (5.5)$$

$$k_{23}(t) = \int_0^t \bar{F}_{20}(x) dF_{23}(x) = \frac{\beta_{23}}{\alpha_{23}^{\beta_{23}}} \int_0^t x^{\beta_{23}-1} e^{-\left[\left(\frac{x}{a_{20}}\right)^{\beta_{20}} + \left(\frac{x}{a_{23}}\right)^{\beta_{23}}\right]} dx \quad (5.6)$$

$$k_{01}(t) = \int_0^t \bar{F}_{02}(x) \bar{F}_{03}(x) dF_{01}(x) = \frac{\beta_{01}}{\alpha_{01}^{\beta_{01}}} \int_0^t x^{\beta_{01}-1} e^{-\left[\left(\frac{x}{a_{01}}\right)^{\beta_{01}} + \left(\frac{x}{a_{02}}\right)^{\beta_{02}} + \left(\frac{x}{a_{03}}\right)^{\beta_{03}}\right]} dx \quad (5.7)$$

$$k_{02}(t) = \int_0^t \bar{F}_{01}(x) \bar{F}_{03}(x) dF_{02}(x) = \frac{\beta_{02}}{\alpha_{02}^{\beta_{02}}} \int_0^t x^{\beta_{02}-1} e^{-\left[\left(\frac{x}{a_{01}}\right)^{\beta_{01}} + \left(\frac{x}{a_{02}}\right)^{\beta_{02}} + \left(\frac{x}{a_{03}}\right)^{\beta_{03}}\right]} dx \quad (5.8)$$

$$k_{03}(t) = \int_0^t \bar{F}_{01}(x) \bar{F}_{02}(x) dF_{03}(x) = \frac{\beta_{03}}{\alpha_{03}^{\beta_{03}}} \int_0^t x^{\beta_{03}-1} e^{-\left[\left(\frac{x}{\alpha_{01}}\right)^{\beta_{01}} + \left(\frac{x}{\alpha_{02}}\right)^{\beta_{02}} + \left(\frac{x}{\alpha_{03}}\right)^{\beta_{03}}\right]} dx \quad (5.9)$$

This work focuses only on the SMP steady-state analysis, where the kernel matrix is evaluated as $\mathbf{K}(\infty)$, as shown in the following equation:

$$\mathbf{K}(\infty) = \begin{bmatrix} 0 & k_{01}(\infty) & k_{02}(\infty) & k_{03}(\infty) \\ k_{10}(\infty) & 0 & 0 & k_{13}(\infty) \\ k_{20}(\infty) & 0 & 0 & k_{23}(\infty) \\ k_{30}(\infty) & 0 & 0 & 0 \end{bmatrix} \quad (5.10)$$

Stage 2: Solve the steady-state equations of the EMC, that is, $\mathbf{v} = \mathbf{v} \cdot \mathbf{K}(\infty)$ and $\mathbf{v} \cdot \mathbf{e}^T = 1$, with the steady-state probability vector $\mathbf{v} = [v_0 \ v_1 \ v_2 \ v_3]$ and $\mathbf{e} = [1 \ 1 \ 1 \ 1]$ to obtain the steady-state probabilities v_i . Wolfram Mathematica is applied in this work to obtain values of v_i ($i = 0, 1, 2, 3$).

Stage 3: Evaluate the sojourn time T_i in each system state i ($i = 0, 1, 2, 3$). For the SMP model of Figure 5.2, the sojourn time T_i can be evaluated using eqs. (5.11)–(5.14) [23]:

$$T_0 = \int_0^\infty \bar{F}_{01} \bar{F}_{02} \bar{F}_{03} dt = \int_0^\infty e^{-\left[\left(\frac{x}{\alpha_{01}}\right)^{\beta_{01}} + \left(\frac{x}{\alpha_{02}}\right)^{\beta_{02}} + \left(\frac{x}{\alpha_{03}}\right)^{\beta_{03}}\right]} dt \quad (5.11)$$

$$T_1 = \int_0^\infty \bar{F}_{10} \bar{F}_{13} dt = \int_0^\infty e^{-\left[\left(\frac{x}{\alpha_{10}}\right)^{\beta_{10}} + \left(\frac{x}{\alpha_{13}}\right)^{\beta_{13}}\right]} dt \quad (5.12)$$

$$T_2 = \int_0^\infty \bar{F}_{20} \bar{F}_{23} dt = \int_0^\infty e^{-\left[\left(\frac{x}{\alpha_{20}}\right)^{\beta_{20}} + \left(\frac{x}{\alpha_{23}}\right)^{\beta_{23}}\right]} dt \quad (5.13)$$

$$T_3 = \int_0^\infty \bar{F}_{30}(t) dt \quad (5.14)$$

Stage 4: Evaluate the steady-state probability P_i ($i = 0, 1, 2, 3$) of the SMP model using the following equation [23]:

$$P_i = \frac{v_i T_i}{\sum_{j \in \{0, 1, 2, 3\}} v_j T_j} \quad (5.15)$$

where the steady-state probability v_i in the EMC is obtained in stage 2 and the sojourn time T_j at state j is obtained in stage 3.

With the steady-state probabilities P_i ($i = 0, 1, 2, 3$) for the SMP model, the disk survivability is evaluated as $S = 1 - P_3 = P_0 + P_1 + P_2$; the disk invulnerability is evaluated as $I = 1 - P_2 - P_3 = P_0 + P_1$.

5.4 Cloud-RAID system-level modeling and analysis

The cloud-RAID storage system is a multistate system, where each disk is a multistate component with four states, as defined in Section 5.3.1. We analyze the system-level survivability and invulnerability of the cloud-RAID system with heterogeneous and homogeneous disks in this section.

5.4.1 Heterogeneous disks

The MDD model [24, 25] is applied to evaluate the system-level survivability and invulnerability of the cloud-RAID system with heterogeneous disks.

Figure 5.3 illustrates an MDD node modeling a disk, w ($w = 1, 2, 3, 4$), where each edge models a different state of the disk (edge j models state j). Each edge j is associated with the occurrence probability of the corresponding state, denoted by P_{wj} ($j=0, 1, 2, 3$).

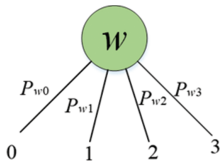


Figure 5.3: An MDD non-sink node modeling disk w .

The entire cloud-RAID-5 can be in one of the following four states: good (state 0), degraded (state 1), vulnerable (state 2), and failed (state 3). Specifically, the system occupies the failed state when at least two out of the four disks are failed (i.e., in disk state 3). Thus, under state 3, the entire system is essentially a 2-out-of-4: F system and can be modeled using the MDD in the lattice structure of Figure 5.4.

In Figure 5.4, sink nodes “1” and “0” model the system being in or not in the failed state, respectively. Based on the MDD model, $P_{\text{sys}=3}(t)$ (the system failed state probability) can be evaluated by adding probabilities of all paths from root node 1 to sink node “1”, as follows:

$$P_{\text{sys}=3}(t) = P_{13}P_{23} + (1 - P_{13})P_{23}P_{33} + (1 - P_{13})(1 - P_{23})P_{33}P_{43} + P_{13}(1 - P_{23})P_{33} \\ + (1 - P_{13})P_{23}(1 - P_{33})P_{43} + P_{13}(1 - P_{23})(1 - P_{33})P_{43} \quad (5.16)$$

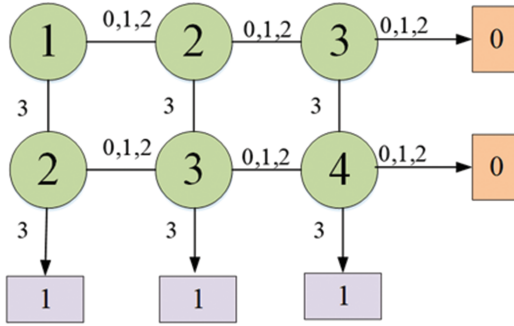


Figure 5.4: MDD for the failed state of the cloud-RAID-5.

where P_{wj} is the probability of disk w occupying state j ($w = 1, 2, 3, 4$, and $j = 0, 1, 2, 3$).

As another example, consider the good state of the cloud-RAID-5 system. The system occupies the good state 0 when at least three out of the four disks are good (i.e., in disk state 0). Thus, under state 0, the entire system is essentially a 3-out-of-4: G system and can be modeled using the MDD in the lattice structure of Figure 5.5.

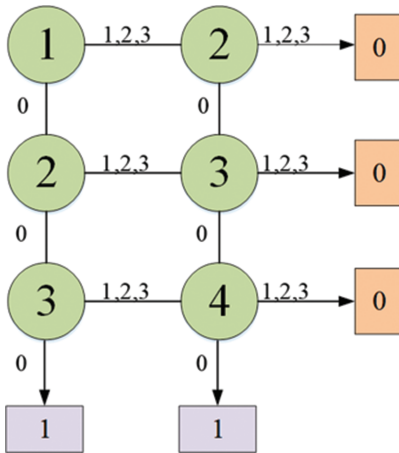


Figure 5.5: MDD for the good state of the cloud-RAID-5.

Based on the MDD model in Figure 5.5, $P_{\text{sys}=0}(t)$ (the system good state probability) can be evaluated by adding probabilities of all paths from root node 1 to sink node “1”, as follows:

$$P_{\text{sys}=0}(t) = P_{10} P_{20} P_{30} + P_{10} P_{20} (1 - P_{30}) P_{40} + P_{10} (1 - P_{20}) P_{30} P_{40} + (1 - P_{10}) P_{20} P_{30} P_{40} \quad (5.17)$$

5.4.2 Homogeneous disks

For homogeneous cloud-RAID-5, all the disks in the array have the same state probabilities, that is, $P_{wj} = P_j$. In this case, combinatorics can be applied to evaluate the different system state probabilities. Specifically, based on the state definitions in Section 5.4.1, the system's failed state and good state probabilities can be evaluated using eqs. (5.18) and (5.19), respectively:

$$P_{sys=3}(t) = C_4^2(P_3)^2(1-P_3)^2 + C_4^3(P_3)^3(1-P_3) + C_4^4(P_3)^4 \quad (5.18)$$

$$P_{sys=0} = C_4^3(P_0)^3(1-P_0) + C_4^4(P_0)^4 \quad (5.19)$$

The entire cloud-RAID-5 is vulnerable (in state 2) when at least two out of the four disks are vulnerable (i.e., in disk state 2) and no two disks are failed (i.e., in disk state 3) at the same time. Specific combinations under state 2 include (1) two disks are vulnerable (state 2) and the other two disks are good (state 0) or degraded (state 1); (2) two disks are vulnerable, one disk is failed (state 3), and one disk is either good or degraded; (3) three disks are vulnerable and the remaining one disk is good, or degraded, or failed; (4) all the four disks are vulnerable (in state 2). The evaluation expression for the system vulnerable state probability based on combinatorics is given as follows:

$$P_{sys=2} = C_4^2(P_2)^2(P_0 + P_1)^2 + C_4^2C_4^1(P_2)^2P_3(P_0 + P_1) + C_4^3(P_2)^3(1-P_2) + C_4^4(P_2)^4 \quad (5.20)$$

Any state other than the good (state 0), vulnerable (state 2) and failed (state 3) states is regarded as the degraded state (state 1). Thus, the system degraded state probability can be simply derived as follows:

$$P_{sys=1} = [1 - P_{sys=0} - P_{sys=2} - P_{sys=3}] \quad (5.21)$$

5.4.3 Survivability and invulnerability analysis

With the system state probabilities evaluated using either MDDs or combinatorics (particularly eqs. (5.18)–(5.21)), the survivability and invulnerability of the cloud-RAID-5 system can be obtained as in eqs. (5.22) and (5.23), respectively:

$$S_{sys} = [P_{sys=0} + P_{sys=1} + P_{sys=2}] = [1 - P_{sys=3}] \quad (5.22)$$

$$I_{sys} = [P_{sys=0} + P_{sys=1}] = [1 - P_{sys=2} - P_{sys=3}] \quad (5.23)$$

5.5 Analysis results

In this section, we examine effects of different state transition time distribution parameters on the disk performance and, further, on the entire system performance. Specifically, we study effects of the Weibull distribution parameters (α or β) of transitions F_{02} , F_{23} , and F_{30} on the disk steady-state probabilities, as well as on the entire system survivability and invulnerability. Different parameter values of F_{02} reflect different DDoS attack behaviors that may rely on factors like different habits of hackers or different targeted countries [26]. Parameters of F_{23} reflect different behaviors of failing to defend the disk against the DDoS attacks. Parameters of F_{30} model the disk recovery capability.

Based on statistics and survey reports from refs. [26–28], Table 5.1 presents baseline values of model parameters for the study.

Table 5.1: Default values of parameters, unless otherwise specified.

CDF	Distribution	Parameter values
F_{01}	Exponential	$\alpha_{01} = 9.25, \beta_{01} = 1$
F_{02}	Rayleigh	$\alpha_{02} = 0.28, \beta_{02} = 2$
F_{03}	Exponential	$\alpha_{03} = 6.94, \beta_{03} = 1$
F_{10}	Weibull	$\alpha_{10} = 0.69, \beta_{10} = 0.9$
F_{13}	Rayleigh	$\alpha_{13} = 4.629, \beta_{13} = 2$
F_{20}	Weibull	$\alpha_{20} = 0.86, \beta_{20} = 0.74$
F_{23}	Weibull	$\alpha_{23} = 0.37, \beta_{23} = 1.5$
F_{30}	Exponential	$\alpha_{30} = 0.24, \beta_{30} = 1$

5.5.1 Effects of scale parameter α

Figures 5.6, 5.8, and 5.10 summarize the steady-state probabilities of different disk states under changing values of scale parameters, α_{02} , α_{23} , and α_{30} , respectively. Figures 5.7, 5.9, and 5.11 summarize the entire system survivability and invulnerability under changing values of these scale parameters.

As observed from Figure 5.6, when α_{02} (modeling transition time from the good state to the vulnerable state due to DDoS attacks) changes from 0.28 to 10 h, the disk good state probability (P_0) has an increasing trend. This is intuitive, since the increasing α_{02} corresponds to weaker DDoS attack strength. Correspondingly, the disk survivability ($S = 1 - P_3$) also increases with α_{02} . Consequently, the entire system survivability $S_{\text{sys}-02}$ and invulnerability $I_{\text{sys}-02}$ increase quickly as α_{02} increases, as shown in Figure 5.7.

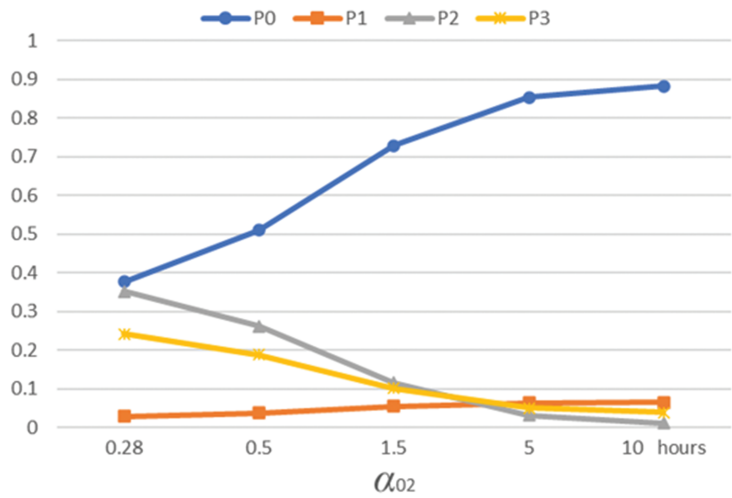


Figure 5.6: Steady-state probabilities of each disk state with changing α_{02} .

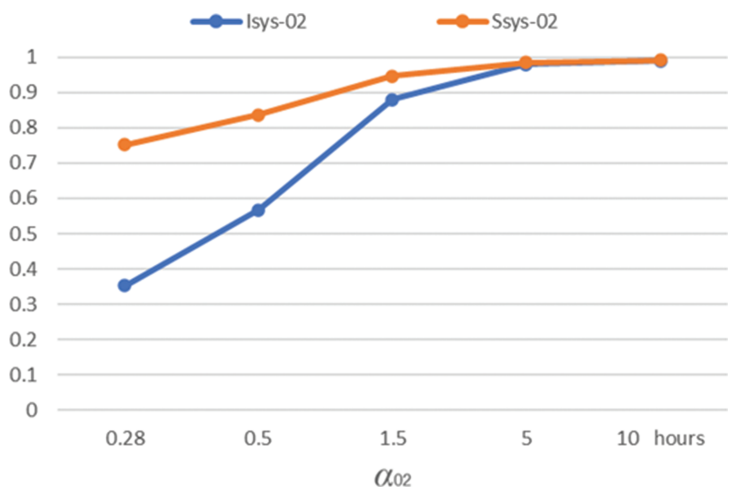


Figure 5.7: System survivability and invulnerability with changing α_{02} .

As observed from Figure 5.8, when α_{23} (modeling transition time from the vulnerable state to the failed state) changes from 0.37 to 10 h, the disk vulnerability state probability (P_2) increases while the disk failure state probability (P_3) decreases since it takes a longer time for the disk to leave state 2. Thus, the disk survivability ($S = 1 - P_3$) increases with α_{23} . Consequently, the entire system survivability $S_{\text{sys}-23}$ shows an increasing trend. However, the system invulnerability $I_{\text{sys}-23} = 1 - P_{\text{sys}=2} - P_{\text{sys}=3}$ shows a decreasing trend, as increasing α_{23} increases the disk vulnerable state probability P_2 more significantly as shown in Figure 5.9.

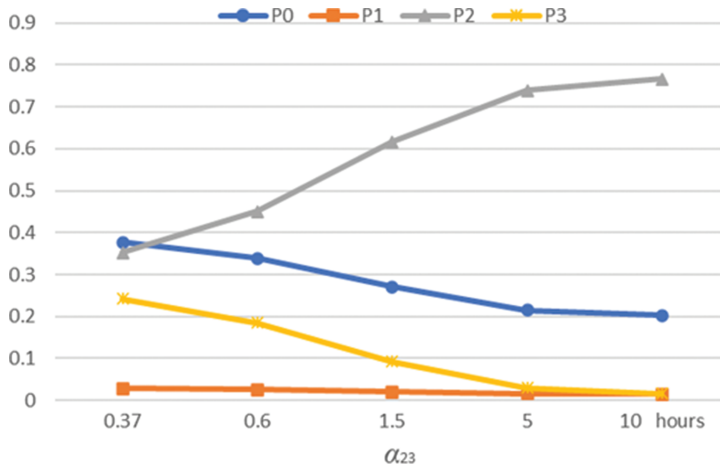


Figure 5.8: Steady-state probabilities of each disk state with changing α_{23} .

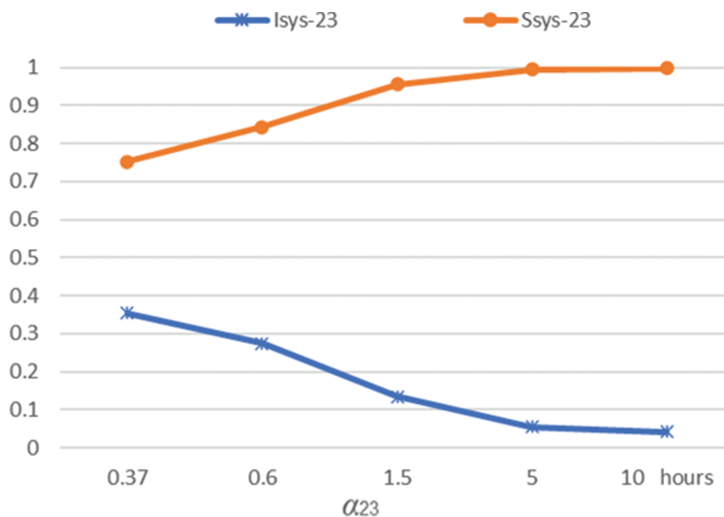


Figure 5.9: System survivability and invulnerability with changing α_{23} .

As observed from Figure 5.10, when α_{30} (modeling transition time from the failed state to the good state) changes from 0.37 to 10 h, the disk failed state probability (P_3) increases quickly while the disk good state probability (P_0) decreases since it takes a longer time for the disk to leave state 3. Thus, the disk survivability ($S = 1 - P_3$) decreases quickly with α_{30} . Consequently, the entire system survivability S_{sys-30} and invulnerability I_{sys-30} both decrease significantly as α_{30} increases, as shown in Figure 5.11.

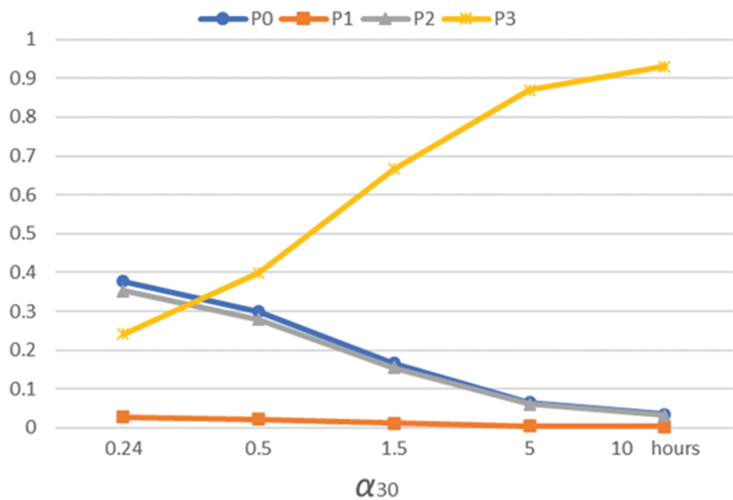


Figure 5.10: Steady-state probabilities of each disk state with changing α_{30} .

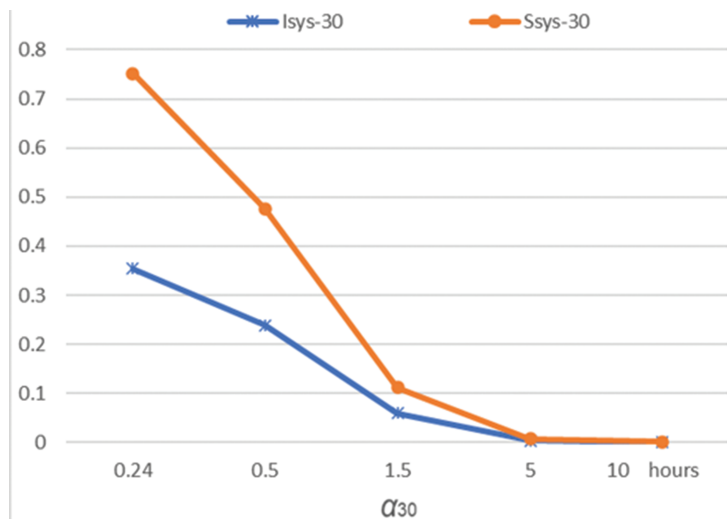


Figure 5.11: System survivability and invulnerability with changing α_{30} .

5.5.2 Effects of shape parameter β

Different values of the shape parameter β model different failure rate behaviors [20, 21]. Specifically, when $\beta = 1$, a constant failure rate is modeled; when $\beta < 1$, a decreasing failure rate is modeled; when $\beta > 1$, an increasing failure rate is modeled. In this study,

values of (0.1, 0.5, 1, 1.5, and 2) are chosen to investigate the impact of the shape parameter.

Figures 5.12, 5.14, and 5.16 summarize the steady-state probabilities of different disk states under changing values of shape parameters β_{02} , β_{23} , and β_{30} , respectively. Figures 5.13, 5.15, and 5.17 summarize the entire system survivability and invulnerability under changing values of these shape parameters.

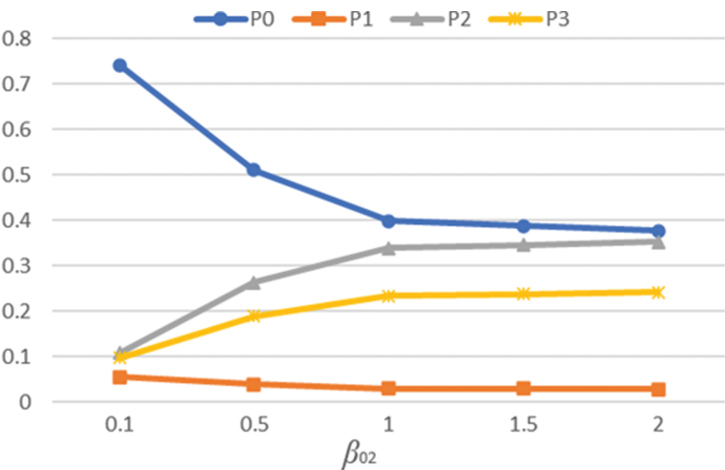


Figure 5.12: Steady-state probabilities of each disk state with changing β_{02} .

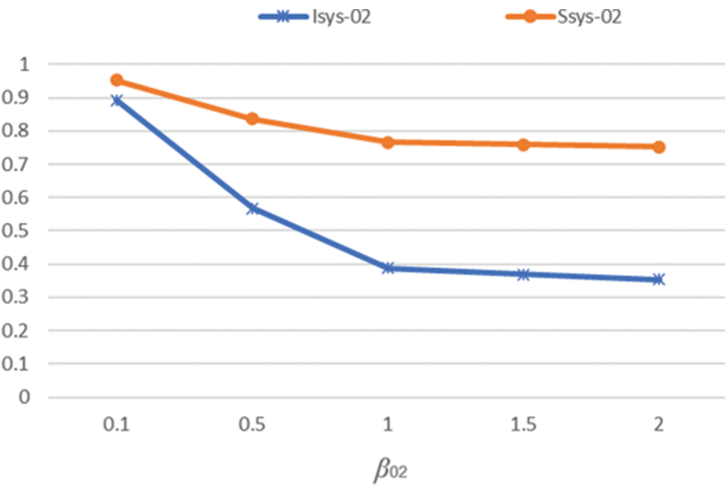


Figure 5.13: System survivability and invulnerability with changing β_{02} .

As observed from Figure 5.12, when β_{02} varies from 0.1 to 2, the good-state probability P_0 drops quickly from 0.75 to 0.377, while the state 2 probability increases (further, the probability of its subsequent state 3 also increases), since the rate of leaving state 0 is increasing. Consequently, both system invulnerability I_{sys-02} and survivability S_{sys-02} show a decreasing trend, as shown in Figure 5.13.

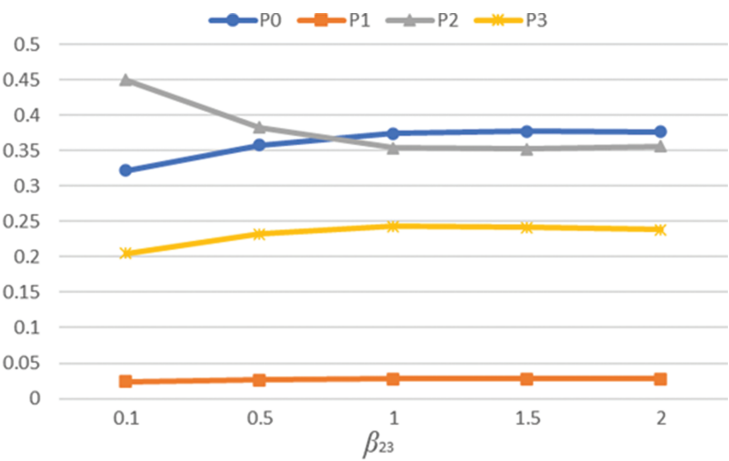


Figure 5.14: Steady-state probabilities of each disk state with changing β_{23} .

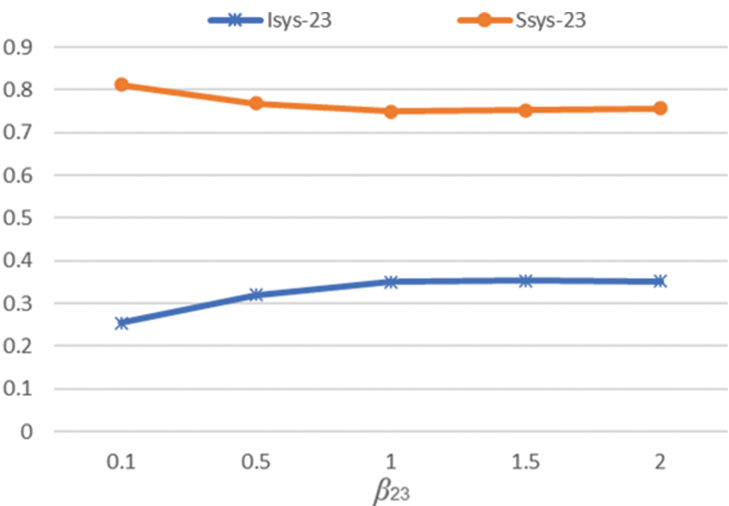


Figure 5.15: System survivability and invulnerability with changing β_{23} .

Figure 5.14 plots the disk steady-state probabilities when β_{23} varies. As β_{23} varies from 0.1 to 2, the vulnerable state probability P_2 decreases while the state 3 probability increases since the rate of leaving state 2 is increasing. Consequently, as observed from Figure 5.15, the system survivability $S_{\text{sys}-23}$ decreases slightly while the system invulnerability $I_{\text{sys}-23}$ shows an increasing trend due to the interaction between P_2 and P_3 .

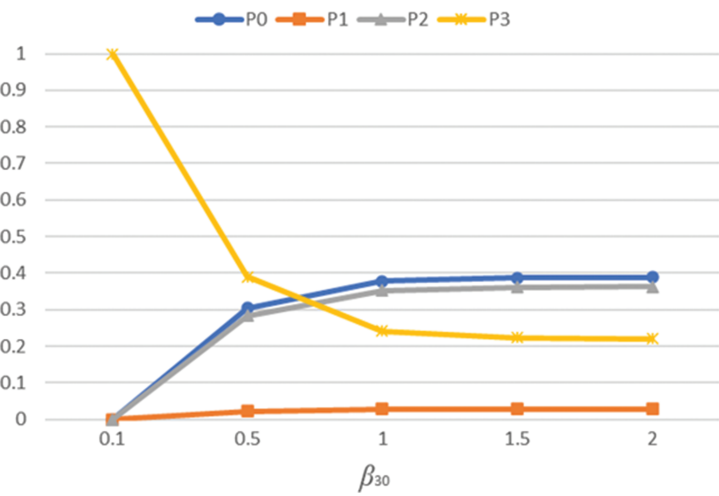


Figure 5.16: Steady-state probabilities of each disk state with changing β_{30} .

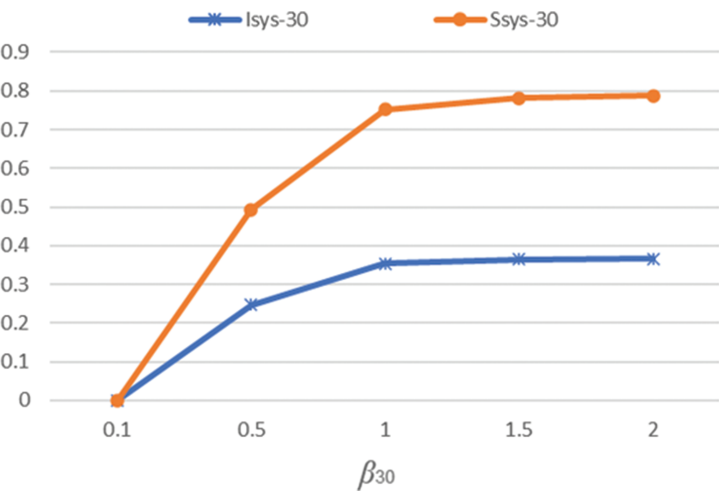


Figure 5.17: System survivability and invulnerability with changing β_{30} .

Figure 5.16 illustrates each disk's steady-state probabilities when β_{30} varies. As β_{30} varies from 0.1 to 2, the failed state probability P_3 decreases significantly while the state 0 probability increases since the rate of leaving state 3 is increasing. Thus, the disk survivability ($S = 1 - P_3$) increases quickly with β_{30} . Consequently, as shown in Figure 5.17, the system survivability $S_{\text{sys}-30}$ and invulnerability $I_{\text{sys}-30}$ both increase quickly.

5.6 Conclusion and future work

In this chapter, the survivability and invulnerability at both the disk level and the cloud-RAID system level are modeled and evaluated. The proposed methodology encompasses an SMP-based method for the disk steady-state probability analysis, and an MDD-based method (for heterogeneous disks) as well as a combinatorics-based method (for homogeneous disks) for the system-level state probability analysis. The methodology is not limited by the distribution type of the state transition time. Impacts of several model parameters (representing the attack, defense, and recovery capability of the disk) are investigated in detail using numerical results from analyzing a cloud-RAID-5 system. The proposed methodology can be applied in the solution to the disk allocation problem, which determines the combination of cloud disks (from different vendors) that maximizes the cloud-RAID system survivability or invulnerability.

The proposed methodology is applicable to only the steady-state or asymptotic state probability analysis. In the future, we are interested in extending the methodology to the time-dependent state probability evaluation. We are also interested in considering the sequential attack events modeled in [17] for the survivability and invulnerability analysis of cloud storage systems.

References

- [1] Chou, T. S. 2013. Security threats on cloud computing vulnerabilities, *International Journal of Computer Science & Information Technology*, 5(3), 79–88. <https://doi.org/10.5121/ijcsit.2013.5306>.
- [2] Escudero, C., Sicard, F. & Zamai, E. Process-Aware Model based IDSs for Industrial Control Systems Cybersecurity: Approaches, Limits and Further Research. 2018 IEEE 23rd International Conference on Emerging Technologies and Factory Automation (ETFA). Turin, Italy, 2018. DOI: <https://doi.org/10.1109/ETFA.2018.8502585>.
- [3] George, G. & Thampi, S. M. A graph-based decision support model for vulnerability analysis in IoT networks. *International Symposium on Security in Computing and Communication*. Springer, Singapore, 2018.

- [4] Xing, L. 2020. Reliability in Internet of Things: current status and future perspectives, *IEEE Internet of Things Journal*, 7(8), 6704–6721. <https://doi.org/10.1109/JIOT.2020.2993216>.
- [5] Xing, L. 2021. Cascading failures in Internet of Things: review and perspectives on reliability and resilience, *IEEE Internet of Things Journal*, 8(1), 44–64. 10.1109/JIOT.2020.3018687.
- [6] Xing, L., Levitin, G. & Xiang, Y. 2019. Defending N-version Programming Service Components against Co-resident Attacks in IoT Cloud Systems, *IEEE Transactions on Services Computing*, <https://doi.org/10.1109/TSC.2019.2904958>.
- [7] Shahrad, M., Mosenia, A., Song, L., Chiang, M., Wentzlaff, D. & Mittal, P. Acoustic denial of service attacks on hard disk drives. 2018 Workshop on Attacks and Solutions in Hardware Security. Toronto, Canada 2018. DOI: <https://doi.org/10.1145/3266444.3266448>.
- [8] Fung, C., Chen, Y. L., Wang, X., Lee, J., Tarquini, R., Anderson, M. & Linger, R. Survivability analysis of distributed systems using attack tree methodology. 2005 IEEE Military Communications Conference. Atlantic City, NJ, USA 2005. DOI: <https://doi.org/10.1109/MILCOM.2005.1605745>.
- [9] Iliadis, I., Sotnikov, D., Ta-Shma, P. & Venkatesan, V. Reliability of geo-replicated cloud storage systems. 2014 IEEE 20th Pacific Rim International Symposium on Dependable Computing. Singapore, Singapore, 2014. DOI: <https://doi.org/10.1109/PRDC.2014.30>.
- [10] Liu, Q. & Xing, L. 2015. Reliability modeling of cloud-RAID-6 storage system, *International Journal of Future Computer and Communication*, 4(6), 415–420. <https://doi.org/10.18178/ijfcc.2015.4.6.428>.
- [11] Mandava, L. & Xing, L. 2019. Balancing reliability and cost in cloud-RAID systems with fault-level coverage, *Int J Math Eng Manag Sci*, 4(5), 1068–1080. <https://doi.org/10.33889/IJMEMS.2019.4.5-085>.
- [12] Mandava, L. & Xing, L. 2020. Optimizing Imperfect Coverage Cloud-RAID Systems Considering Reliability and Cost, *International Journal of Reliability, Quality and Safety Engineering*, 27(2), 2040001. <https://doi.org/10.1142/S021853932040001X>.
- [13] Nachiappan, R., Javadi, B., Calheiros, R. N. & Matawie, K. M. 2017. Cloud storage reliability for big data applications: A state of the art survey, *Journal of Network and Computer Applications*, 97, 35–47, <https://doi.org/10.1016/j.jnca.2017.08.011>.
- [14] Zhang, R., Lin, C., Meng, K. & Zhu, L. A modeling reliability analysis technique for cloud storage system. 2013 The 15th IEEE International Conference on Communication Technology. Guilin, China 2013. DOI: <https://doi.org/10.1109/ICCT.2013.6820346>.
- [15] Xing, L. & Levitin, G. 2017. Balancing theft and corruption threats by data partition in cloud system with independent server protection, *Reliability Engineering & System Safety*, 167, 248–254, <https://doi.org/10.1016/j.ress.2017.06.006>.
- [16] Levitin, G., Xing, L. & Dai, Y. 2018. Co-residence based data vulnerability vs. security in cloud computing system with random server assignment, *European Journal of Operational Research*, 267(2), 676–686. <https://doi.org/10.1016/j.ejor.2017.11.064>.
- [17] Liu, Q., Xing, L. & Zhou, C. 2019. Probabilistic modeling and analysis of sequential cyber-attacks, *Engineering Reports*, 1(4), e12065. <https://doi.org/10.1002/eng2.12065>.
- [18] Liu, Q. & Xing, L. 2021. Survivability and Vulnerability Analysis of Cloud RAID Systems under Disk Faults and Attacks, *International Journal of Mathematical, Engineering and Management Sciences*, 6(1), 15–29. <https://doi.org/10.33889/IJMEMS.2021.6.1.003>.
- [19] Mirkovic, J. & Reiher, P. 2004. A taxonomy of DDoS attack and DDoS defense mechanisms, *ACM SIGCOMM Computer Communication Review*, 34(2), 39–53. <https://doi.org/10.1145/997150.997156>.
- [20] Dohi, T., Goševa-Popstojanova, K. & Trivedi, K. 2001. Estimating software rejuvenation schedules in high-assurance systems, *The Computer Journal*, 44(6), 473–485. <https://doi.org/10.1093/comjnl/44.6.473>.

- [21] Trivedi, K. S. Probability and statistics with reliability, queuing, and computer science applications, 2nd ed, NY, USA, John Wiley & Sons Press, 2016, <https://doi.org/10.1002/9781119285441>.
- [22] Kharoufeh, J. P., Solo, C. J. & Ulukus, M. Y. 2010. Semi-Markov models for degradation-based reliability, IIE Transactions, 42(8), 599–612. <https://doi.org/10.1080/07408170903394371>.
- [23] Kumar, G., Jain, V. & Gandhi, O. P. 2013. Availability analysis of repairable mechanical systems using analytical semi-Markov approach, Quality Engineering, 25(2), 97–107. <https://doi.org/10.1080/08982112.2012.751606>.
- [24] Xing, L. & Amari, S. V. Binary decision diagrams and extensions for system reliability analysis, Wiley-Scrivener, Beverly, Massachusetts, USA, John Wiley & Sons Press, 2015, <https://doi.org/10.1002/9781119178026>.
- [25] Xing, L. & Dai, Y. 2009. A new decision-diagram-based method for efficient analysis on multistate systems, IEEE Transactions on Dependable and Secure Computing, 6(3), 161–174. <https://doi.org/10.1109/TDSC.2007.70244>.
- [26] Avital, N., Zawoznik, A., Azaria, J. & Lambert, K. 2019 Global DDoS Threat Landscape Report. Imperva Research Labs. (Accessed in January 2021, at <https://www.imperva.com/blog/2019-global-ddos-threat-landscape-report/>.)
- [27] Check Point. Security report 2020. Check Point Software Technologies Ltd, 2020. (Accessed in January 2021, at <https://www.bristol.de/wp-content/uploads/2020/03/2020-security-report.pdf>.)
- [28] Hummel, R. Netscout threat intelligence report on Netscout System INC, 2019. (Accessed in January 2021, at https://www.netscout.com/sites/default/files/2020-02/SECR_001_EN-2001_Web.pdf.)

Yuanying Chi, Guoqing Bai, Kaiye Gao, Rui Peng

6 Reliability evaluation of multistate systems with common bus performance sharing considering performance excess

Abstract: In a multistate system (MSS) with common bus performance sharing, the residual performance of any subunit can be shared to other subunits with insufficient performance by the common bus with stochastic sharing capacity. This study extends the reliability evaluation model by considering both the minimum and maximum requirements of elements, which should not only meet the random minimum requirements of each single element but also require that there should be no excess performance. The reliability of the MSS is estimated by using the universal generating function technique. Numerical example is presented to illustrate the procedures.

Keywords: Performance excess, multistate system, probability mass function, common bus

6.1 Introduction

A system is usually composed of some components with different functions. Under certain environmental conditions, these components work with different functional intensities to accomplish the expected tasks of the system. This functional intensity is called system performance. A system with multiple functional states is called as a multistate system (MSS) [1, 2]. In order to meet the common needs of the whole system, it was proposed that the performance of MSS can be shared by the common bus system, where a multistate unit (MSU) with finite performance intensity transmits performance through the sharing mechanism [3]. In the systems of practice such as heating, integrated circuit, power grid, and communication and production systems, the demand and the corresponding performance of each component are

Acknowledgments: The work was partly supported by the National Natural Science Foundation of China (no. 91646201), the National Key R&D Program of China (no. 2017YFC0803300), and the National Social Science Foundation of China (no. 19ZDA081).

Yuanying Chi, Rui Peng, School of Economics and Management, Beijing University of Technology, Beijing, China

Guoqing Bai, School of Economics and Management, Beijing University of Technology, Beijing, China, e-mail: BAIGQ@emails.bjut.edu.cn

Kaiye Gao, School of Economics and Management, Beijing Information Science and Technology University; Academy of Mathematics and System Science, Chinese Academy of Sciences

<https://doi.org/10.1515/9783110725599-006>

stochastic [4–8]. If the performance of a unit is surplus after meeting its own demand, then the common bus can transmit the excess performance to other units that cannot meet their demand by their own performances to improve the reliability of the system [9–11]. The stochastic capacity of the transmission system decides its performance that can be transmitted.

In the reliability assessment of traditional MSS in which performance can be shared by the common bus system, reliability of MSS is expressed as the probability of meeting the requirements of all components [4, 12–14]. For example, Peng et al. [15] investigated the reliability of a system with a performance group of limited size. Based on Peng et al. [15], Qiu and Ming [16] extended the MSS reliability evaluation model from the aspect of system transmission loss. On the basis of predecessors, Wu et al. [17] considered the sharing model of maximum redistribution and enriched the sharing model of MSS. Some studies further applied MSS reliability analysis and modeling into practice. For example, Xiao and Cao [22] considered the power sharing between different regions and modeled the reliability of the grid. A general grid reliability evaluation algorithm was proposed to optimize the optimal performance redundancy of the grid. The voltage reliability of integrated circuits was analyzed by Jiao et al. [23], according to the finite element method.

However, no previous reliability study considered the performance excess. In the practice application of MSS with performance sharing mechanism, the system or component may collapse due to the excess performance [18–21, 24]. For example, in integrated circuits, excessive voltages of electronic components will damage the components and further affect the reliability of integrated circuit; in heating systems, overheat will damage the components and may further lead to the breakdown of the whole system as well as the external cost of environmental pollution. The similar phenomenon occurs in some systems in electric power industry such as the renewable energy power generation system that is connected to multiple regions. In such systems, power generation and demand in each region are varied, so that when excess power is generated and cannot be absorbed in time, either the equipment in this system or supplied by this system will be damaged due to excessive voltage, or there will be high-energy storage cost to prevent this damage. Thus, ignoring performance excess can lead to overestimation of the reliability for systems with performance sharing mechanism.

To address the effect of performance excess in MSS reliability analysis, this chapter extends the MSS reliability model considering common bus performance sharing mechanism. In the extended model, not only the system reliability needs to meet the random minimum demand of a single element but also that the entire system or components cannot have excess performance. The minimum and maximum demands of elements are considered in this model at the same time, which prevents not only the failure of the system due to unsatisfied demands but also the system from collapsing due to excessive performance.

There are two innovative contributions of this research: First, MSS with common bus performance sharing is studied under the consideration of both the minimum and maximum requirements of elements, which should not only meet the random minimum requirements of each single element but also require that there should be no excess performance. Second, the reliability of the MSS is assessed by the universal generating function (UGF) technology, and the MSS reliability evaluation model with universal bus performance sharing is extended.

The remaining contents of this study are arranged as follows: Section 6.2 proposes an MSS model considering performance excess whose performance can be shared by the common bus system. Section 6.3 describes the reliability assessment procedures of the MSS based on UGF operator. Section 6.4 illustrates the proposed model with numerical examples analysis. Section 6.5 concludes this work.

6.2 The model of an MSS with common bus performance sharing considering performance excess

The symbols used in this chapter are shown in Tables 6.1 and 6.2.

Table 6.1: Acronym.

UGF	Universal generating function
MSU	Multistate unit
MSS	Multistate system
pmf	Probability mass function

Table 6.2: Notation.

N	Number of MSUs
Ω	Set of MSUs
G_i	Stochastic performance of MSU i
WV_i	Stochastic demand for MSU i
W_i	Stochastic demand lower bound for MSU i
V_i	Stochastic demand upper bound for MSU i
C	Stochastic transfer capability for common bus performance sharing system

Table 6.2 (continued)

D_i	Stochastic performance defect for MSU <i>i</i>
S_i	Stochastic residual performance for MSU <i>i</i>
S	The remaining overall performance of MSS in the absence of performance sharing
D	The insufficient overall performance of MSS in the absence of performance sharing
T	A stochastic number of reallocation performance
R	The probability that a common bus system has neither surplus nor deficit is also called the reliability of the system: $R = \Pr\{D = 0 \cap S = 0\}$
$u_i(z)$	The pmf of MSU <i>i</i> 's stochastic performance is expressed by using UGF
$\omega_i(z)$	The pmf of stochastic demand for MSU <i>i</i> is expressed by using UGF
$\Delta_i(z)$	The pmf of performance insufficiency and performance surplus for MSU <i>i</i> is expressed by using UGF
$U_\Omega(z)$	The pmf of performance insufficiency and performance surplus for subset Ω of MSUs is expressed by using UGF
$\hat{U}_A(z)$	The pmf of excess performance is expressed by using UGF after the performance of MSS fully shared
$\tilde{U}_A(z)$	The pmf of insufficient performance is expressed by using UGF after the performance of MSS fully shared
$E[e]$	Expectancy of event e
\mathbf{g}_i	A collection of possible performance values for G_i
g_{ih}	h th performance value for G_i
p_{ih}	The probability of $G_i = g_{ih}$
\mathbf{w}_i	A collection of possible demand values for WV_i
$[w_{ik}, v_{ik}]$	k th demand value for WV_i
q_{ik}	The probability of $WV_i = [w_{ih}, v_{ih}]$
\mathbf{c}	A collection of possible capacity values for C
c_l	l th capacity value for C
β_l	The probability of $C = c_l$
\otimes_φ	The integrated operator expressed by using UGF
Pe_D	Penalty deficiency
$\beta_l \text{Pe}_S$	Excess penalty

The system considered consists of N MSUs. Each unit i has a stochastic discrete performance G_i and the corresponding probability. Every MSU has to satisfy its stochastic demand threshold WV_i that contains a lower bound W_i and an upper bound V_i , that is, $WV_i = [W_i, V_i]$; there is a probability of WV_i being a preset value. The common bus system connects all MSUs in series. MSUs with sufficient performance can redistribute the surplus performance to other MSUs with insufficient performance through the system. The system has a stochastic transmission capacity C and corresponding probability. Through a performance redistribution (transport) system, MSUs with insufficient performance can obtain the surplus performance of other MSUs. After performance sharing redistribution, the system fails if any one or more of the following three events occur: (1) the system has excess performance; (2) at least one requirement of individual performance is not satisfied. An illustration for the system is shown in Figure 6.1.

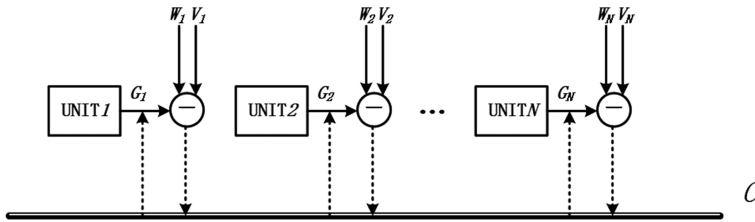


Figure 6.1: An illustrative system considering performance excess.

In order to facilitate the modeling process, we firstly assume that there is no performance sharing in the MSS, and then estimate the performance deficit and surplus of MSS without performance sharing transmission. In this case, the total system performance surplus over the demand lower bound can be calculated as the larger one between zero and the performance of the MSS subtracting the lower bound of the demand, which is

$$S_W = \sum_{i=1}^N S_i = \sum_{i=1}^N \max(G_i - W_i, 0), \quad (6.1)$$

and the total deficiency of the system performance over the demand lower bound can be calculated as the larger one between the demand lower bound subtracting the total system performance and zero, which is

$$D_W = \sum_{i=1}^N D_i = \sum_{i=1}^N \max(W_i - G_i, 0). \quad (6.2)$$

Similarly, the total residual of the MSS performance over demand upper bound is

$$S_V = \sum_{i=1}^N S_i = \sum_{i=1}^N \max(G_i - V_i, 0), \quad (6.3)$$

and the total deficiency of the MSS performance over demand upper bound is

$$D_V = \sum_{i=1}^N D_i = \sum_{i=1}^N \max(V_i - G_i, 0). \quad (6.4)$$

Then under the common bus system of performance transmission, the performance that will be shared to replenish those components with performances lower than demand lower bound is

$$T_W = \min(S_W, D_W, C) = \min\left(\sum_{i=1}^N \max(G_i - W_i, 0), \sum_{i=1}^N \max(W_i - G_i, 0), C\right). \quad (6.5)$$

Similarly, the performance that can be drawn from components with performance bigger than demand upper bound is

$$T_V = \min(S_V, D_V, C) = \min\left(\sum_{i=1}^N \max(G_i - V_i, 0), \sum_{i=1}^N \max(V_i - G_i, 0), C\right). \quad (6.6)$$

Note that S and D are random variables statistically dependent on each other, but independent from C .

From eq. (6.5), the system performance deficiency comparing with demand lower bound after sharing is

$$\begin{aligned} \tilde{D} &= D_W - T_W = D - \min(S_W, D_W, C) = \max(0, D_W - \min(S_W, C)) \\ &= \max\left(0, \sum_{i=1}^N \max(W_i - G_i, 0) - \min\left(\sum_{i=1}^N \max(G_i - W_i, 0), C\right)\right). \end{aligned} \quad (6.7)$$

Similarly, the system performance surplus comparing with demand upper bounds after sharing is

$$\begin{aligned} \hat{S} &= S_V - T_V = S_V - \min(S_V, D_V, C) = \max(0, D_V - \min(S_V, D)) \\ &= \max\left(0, \sum_{i=1}^N \max(W_i - G_i, 0) - \min\left(\sum_{i=1}^N \max(G_i - W_i, 0), C\right)\right). \end{aligned} \quad (6.8)$$

Finally, the reliability of the MSS will be estimated as the probability of neither performance deficiency nor performance excess, that is

$$\begin{aligned}
R &= \Pr\{\tilde{D}=0 \cap \hat{S}=0\} \\
&= \Pr\left\{ \max\left(0, \sum_{i=1}^N \max(W_i - G_i, 0) - \min\left(\sum_{i=1}^N \max(G_i - W_i, 0), C\right)\right) = 0 \right. \\
&\quad \left. \cap \max\left(0, \sum_{i=1}^N \max(W_i - G_i, 0) - \min\left(\sum_{i=1}^N \max(G_i - W_i, 0), C\right)\right) = 0 \right\}. \quad (6.9)
\end{aligned}$$

6.3 Reliability of the MSS based on UGF

6.3.1 UGF operator

Universal general generating function represents the probability distribution of stochastic variable Y_i , whose polynomial form is expressed as

$$u_i(z) = \sum_{h=1}^{k_i} \alpha_{i,h} z^{y_{i,h}}. \quad (6.10)$$

The number of possible values of the variable Y_i is k_i , and probability that Y_i occupies $y_{i,h}$ is $\alpha_{i,h}$, where $0 < h < k_i$, that is, $\alpha_{i,h} = \Pr\{Y_i = y_{i,h}\}$.

To acquire the probability of n independent stochastic variables $\varphi(Y_1, \dots, Y_n)$ by using UGF, a combination operator is used as shown in the following equation:

$$\begin{aligned}
U(z) &= \bigotimes_{\varphi} (u_1(z), u_2(z), \dots, u_n(z)) \\
&= \bigotimes_{\varphi} \left(\sum_{h_1=1}^{k_1} \alpha_{1,h_1} z^{y_{1,h_1}}, \dots, \sum_{h_n=1}^{k_n} \alpha_{n,h_n} z^{y_{n,h_n}} \right) \\
&= \sum_{h_1=1}^{k_1} \sum_{h_2=1}^{k_2} \dots \sum_{h_n=1}^{k_n} \prod_{j=1}^n \alpha_j h_j z^{\varphi(y_{1,h_1} \dots y_{n,h_n})}, \quad (6.11)
\end{aligned}$$

where multiplicity $U(z)$ means the whole probable contradictory composes, realized by combining the probability of each combination with the function value of this combination (Y_1, \dots, Y_n) .

6.3.2 Reliability evaluation procedures

It is assumed that the stochastic realization of G_i occupies value from the set $\mathbf{g}_i = \{g_{i,1}, g_{i,2}, \dots, g_{i,H_i}\}$, and the stochastic demand $WV_i = [W_i V_i]$ occupies value from the set $\mathbf{wv}_i = [w_i, v_i] = \{[w_{i,1}, v_{i,1}], [w_{i,2}, v_{i,2}], \dots, [w_{i,K_i}, v_{i,K_i}]\}$. Then, using UGF technique, we can have the following equations.

The pmf of G_i is represented as

$$u_i(z) = \sum_{h=1}^{H_i} p_{i,h} z^{g_{i,h}}, \quad (6.12)$$

where $p_{i,h} = \Pr\{G_i = g_{i,h}\}$.

And the pmf of $WV_i = [W_i V_i]$ is represented as

$$\omega_i(z) = \sum_{k=1}^{K_i} q_{i,k} z^{[w_{i,k}, v_{i,k}]}, \quad (6.13)$$

where $q_{i,k} = \Pr\{WV_i = [W_i, V_i] = [w_{i,k}, v_{i,k}]\}$.

The stochastic transmission capacity C occupies value from the set $c = \{c_1, c_2, \dots, c_L\}$, which is represented as

$$\eta(z) = \sum_{l=1}^L \beta_l z^{c_l}, \quad (6.14)$$

where $\beta_l = \Pr\{C = c_l\}$.

In this model, each combination of states and demands of entire MSUs produces the outcome of deficient performance D and residual performance S , respectively. A new UGF operator must be adopted to calculate the probability of the dependent variables S and D . This UGF operator can correspond to the probability of MSUs' state combination to the situation of surplus S and deficiency D . First, the UGF operator corresponding to the probability of S_i and D_i for each MSU needs to be obtained, and on this basis, the new UGF operator can be obtained. Equations (6.12) and (6.13) have obtained the UGF operators of G_i and WV_i , respectively. The UGF operator of S_i and D_i can be obtained by using the following combination operator \otimes :

$$\begin{aligned} \Delta_i(z) &= u_i(z) \otimes \omega_i(z) \\ &= \sum_{h=1}^{H_i} \sum_{k=1}^{K_i} p_{i,h} q_{i,k} z^{\min(0, g_{i,h} - w_{i,k}), \min(0, w_{i,k} - g_{i,h}); \min(0, g_{i,h} - v_{i,k}), \min(0, v_{i,k} - g_{i,h})} \\ &= \sum_{m=1}^{M_j} \pi_{i,m} z^{s_{i,m_{lb}}, d_{i,m_{lb}}; s_{i,m_{ub}}, d_{i,m_{ub}}}. \end{aligned} \quad (6.15)$$

The probability distribution of composite events can be represented by the following UGF operator: $\pi_{i,m} = \Pr\{S_i = s_{i,m} \cap D_i = d_{i,m}\}$. Let

$$U_{\Omega}(z) = \sum_{f=1}^{F\Omega} \pi_{\Omega,f} z^{s_{\Omega,f_{lb}}, d_{\Omega,f_{lb}}; s_{\Omega,f_{ub}}, d_{\Omega,f_{ub}}} \quad (6.16)$$

represent the probability of insufficient performance and surplus performance under a combination of units in the set Ω . To obtain the probability distribution of insufficient performance and surplus performance under the unit combinations in the set $\Omega \cup i$, the operators will be applied as follows:

$$\begin{aligned}
 U_{\Omega \cup i}(z) &= U_{\Omega}(z) \otimes_{+} \Delta_i(z) \\
 &= \left(\sum_{f=1}^{F_{\Omega}} \pi_{\Omega,f} z^{s_{\Omega,f_{lb}}, d_{\Omega,f_{lb}}, s_{\Omega,f_{ub}}, d_{\Omega,f_{ub}}} \right) \otimes_{+} \left(\sum_{m=1}^{M_i} \pi_{i,m} z^{s_{i,m_{lb}}, d_{i,m_{lb}}, s_{i,m_{ub}}, d_{i,m_{ub}}} \right) \\
 &= \sum_{f=1}^{F_{\Omega}} \sum_{m=1}^{M_i} \pi_{\Omega,f} \pi_{i,m} z^{s_{\Omega,f_{lb}} + s_{i,m_{lb}}, d_{\Omega,f_{lb}} + d_{i,m_{lb}}, s_{\Omega,f_{ub}} + s_{i,m_{ub}}, d_{\Omega,f_{ub}} + d_{i,m_{ub}}} \\
 &= \sum_{f=1}^{F_{\Omega \cup i}} \pi_{\Omega \cup i,f} z^{s_{\Omega \cup i,f_{lb}}, d_{\Omega \cup i,f_{lb}}, s_{\Omega \cup i,f_{ub}}, d_{\Omega \cup i,f_{ub}}}.
 \end{aligned} \tag{6.17}$$

Thus, a recursive procedure is obtained and the probability of system performance deficiency and excess can be expressed by the UGF operator, as follows:

- (a) Assign $U_{\Omega}(z) = U_{\emptyset}(z) = z^{0,0,0,0}$.
- (b) For $i = 1, 2, \dots, N$, again acquire $U_{\Omega \cup i}(z) = U_{\Omega}(z) \otimes_{+} \Delta_i(z)$ and appoint $\Omega = \Omega \cup i$.

According to this procedure, the UGF operator for the probability of system performance deficiency and excess can be expressed as follows:

$$U_A(z) = \sum_{f=1}^{F_A} \pi_{A,f} z^{s_{A,f_{lb}}, d_{A,f_{lb}}, s_{A,f_{ub}}, d_{A,f_{ub}}}. \tag{6.18}$$

Then, given $\eta(z)$ as the probability distribution of transmission capacity C , we can obtain the final system $\tilde{U}_A(z)$ by expressing the probability distribution of performance excess and performance deficiency after performance sharing, which is consistent with eq. (6.4). The form of the corresponding combination operator is

$$\begin{aligned}
 \tilde{U}_A(z) &= U_A(z) \otimes_{\varphi} \eta(z) = \left(\sum_{f=1}^{F_A} \pi_{A,f} z^{s_{A,f_{lb}}, d_{A,f_{lb}}, s_{A,f_{ub}}, d_{A,f_{ub}}} \right) \otimes_{\varphi} \left(\sum_{l=1}^L \beta_l z^{c_l} \right) \\
 &= \sum_{f=1}^{F_A} \sum_{l=1}^L \pi_{A,f} \beta_l z^{\max(0, d_{A,f_{lb}} - \min(s_{A,f_{lb}}, c_l)); \max(0, s_{A,f_{ub}} - \min(d_{A,f_{ub}}, c_l))} \\
 &= \sum_{f=1}^{\tilde{F}} \tilde{q}_f z^{\tilde{d}_f; \tilde{s}_f}.
 \end{aligned} \tag{6.19}$$

The reliability of MSS is the probability of $\tilde{d}_f = 0 \cap \tilde{s}_f = 0$ (the probability that both performance excess and performance deficiency are zero), namely, the coefficient \tilde{q}_f of $\tilde{q}_f z^{0;0}$ in the UGF formula (6.19).

6.4 Numerical examples

Consider a heating system that consists of two independent MSUs. The stochastic performance of the first unit is $\mathbf{g}_1 = \{4, 6, 0\}$, $p_1 = \{0.6, 0.2, 0.2\}$; and the stochastic performance of the second unit is $\mathbf{g}_2 = \{2, 0\}$, $p_2 = \{0.9, 0.1\}$. The stochastic demand of the first unit is $\mathbf{wv}_1 = \{[4, 5], [2, 3]\}$, $q_1 = \{0.3, 0.7\}$, while the stochastic demand for the second unit is $\mathbf{wv}_2 = \{[2, 3], [0, 1]\}$, $q_2 = \{0.4, 0.6\}$. The heating transmission capacity is $\mathbf{c} = \{4, 1, 0\}$, $\beta = \{0.8, 0.1, 0.1\}$. The pmf values are shown in Tables 6.3–6.5.

Table 6.3: The pmf values of performances for units 1 and 2.

i	1		2	
	$p_{i,h}$	$g_{i,h}$	$p_{i,h}$	$g_{i,h}$
1	0.6	4	0.9	2
2	0.2	6	0.1	0
3	0.2	0	–	–

Table 6.4: The pmf values of demands for locations 1 and 2.

i	1		2	
	$q_{i,k}$	$wv_{i,h}$	$q_{i,k}$	$wv_{i,h}$
1	0.3	[4,5]	0.4	[2,3]
2	0.7	[2,3]	0.6	[0,1]

Table 6.5: The pmf values of the capacity for the performance sharing system.

1		2		3	
β_l	c_l	β_l	c_l	β_l	c_l
0.8	4	0.1	1	0.1	0

UGF operator corresponding to unit 1 is

$$u_1(z) = 0.6z^6 + 0.2z^4 + 0.2z^0, \quad \omega_1(z) = 0.3z^{[4,5]} + 0.7z^{[2,3]}.$$

UGF operator corresponding to unit 2 is

$$u_2(z) = 0.9z^2 + 0.1z^0, \quad \omega_2(z) = 0.4z^{[2,3]} + 0.6z^{[0,1]}.$$

UGF operator corresponding to the capacity for the performance sharing system is

$$\eta(z) = (0.8z^4 + 0.1z^1 + 0.1z^0).$$

For $u_1(z)$ and $\omega_1(z)$, the combination operator $\underset{\Leftrightarrow}{\otimes}$ is used to acquire the pmf of S_1 and D_1 through the UGF:

$$\begin{aligned} \Delta_1(z) &= u_1(z) \underset{\Leftrightarrow}{\otimes} \omega_1(z) \\ &= (0.6z^6 + 0.2z^4 + 0.2z^0) \underset{\Leftrightarrow}{\otimes} (0.3z^{[4,5]} + 0.7z^{[2,3]}) \\ &= 0.18z^{2,0;1,0} + 0.42z^{4,0;3,0} + 0.06z^{0,0;0,1} + 0.14z^{2,0;1,0} + 0.06z^{0,4;0,5} + 0.14z^{0,2;0,3} \\ &= 0.42z^{4,0;3,0} + 0.32z^{2,0;1,0} + 0.06z^{0,0;0,1} + 0.14z^{0,2;0,3} + 0.06z^{0,4;0,5}. \end{aligned}$$

For $u_2(z)$ and $\omega_2(z)$, the combination operator $\underset{\Leftrightarrow}{\otimes}$ is used to obtain the pmf of D_2 and S_2 expressed by the UGF:

$$\begin{aligned} \Delta_2(z) &= u_2(z) \underset{\Leftrightarrow}{\otimes} \omega_2(z) \\ &= (0.9z^2 + 0.1z^0) \underset{\Leftrightarrow}{\otimes} (0.4z^{[2,3]} + 0.6z^{[0,1]}) \\ &= 0.36z^{0,0;0,1} + 0.54z^{2,0;1,0} + 0.04z^{0,2;0,3} + 0.06z^{0,0;0,1} \\ &= 0.54z^{2,0;1,0} + 0.42z^{0,0;0,1} + 0.04z^{0,2;0,3}. \end{aligned}$$

the pmf of D and S expressed by the UGF is acquired through the following recursive process:

$$\begin{aligned} U_{\{1\}}(z) &= U_{\emptyset}(z) \underset{+}{\otimes} \Delta_1(z) = \Delta_1(z) \\ &= 0.42z^{4,0;3,0} + 0.32z^{2,0;1,0} + 0.06z^{0,0;0,1} + 0.14z^{0,2;0,3} + 0.06z^{0,4;0,5}, \end{aligned}$$

$$\begin{aligned}
U_A(z) &= U_{\{1,2\}}(z) = U_{\{1\}}(z) \underset{+}{\otimes} \Delta_2(z) \\
&= (0.42z^{4,0;3,0} + 0.32z^{2,0;1,0} + 0.06z^{0,0;0,1} + 0.14z^{0,2;0,3} + 0.06z^{0,4;0,5}) \\
&\quad \underset{+}{\otimes} (0.54z^{2,0;1,0} + 0.42z^{0,0;0,1} + 0.04z^{0,2;0,3}) \\
&= 10^{-2} \left[\begin{aligned} &22.68z^{6,0;4,0} + 17.28z^{4,0;2,0} + 3.24z^{2,0;1,1} + 7.56z^{2,2;1,3} + 3.24z^{2,4;1,5} + 17.64z^{4,0;3,1} \\ &+ 13.44z^{2,0;1,1} + 2.52z^{0,0;0,2} + 5.88z^{0,2;0,4} + 2.52z^{0,4;0,6} + 1.68z^{4,2;3,3} + 1.28z^{2,2;1,3} \\ &+ 0.24z^{0,2;0,4} + 0.56z^{0,4;0,6} + 0.24z^{0,6;0,8} \end{aligned} \right] \\
&= 10^{-2} \left[\begin{aligned} &16.68z^{2,0;1,1} + 17.28z^{4,0;2,0} + 17.64z^{4,0;3,1} + 22.68z^{6,0;4,0} + 8.84z^{2,2;1,3} + 3.24z^{2,4;1,5} \\ &+ 1.68z^{4,2;3,3} + 2.52z^{0,0;0,2} + 6.12z^{0,2;0,4} + 3.08z^{0,4;0,6} + 0.24z^{0,6;0,8} \end{aligned} \right].
\end{aligned}$$

Then the combined operator $\underset{\varphi}{\otimes}$ is used for $U_A(z)$ and $\eta(z)$ to obtain system UGF after performance sharing, as shown below:

$$\begin{aligned}
\tilde{U}_A(z) &= U_A(z) \underset{\varphi}{\otimes} \eta(z) \\
&= 10^{-2} \left[\begin{aligned} &16.68z^{2,0;1,1} + 17.28z^{4,0;2,0} + 17.64z^{4,0;3,1} + 22.68z^{6,0;4,0} + 8.84z^{2,2;1,3} + 3.24z^{2,4;1,5} \\ &+ 1.68z^{4,2;3,3} + 2.52z^{0,0;0,2} + 6.12z^{0,2;0,4} + 3.08z^{0,4;0,6} + 0.24z^{0,6;0,8} \end{aligned} \right] \underset{\varphi}{\otimes} \\
&\quad (0.8z^4 + 0.1z^1 + 0.1z^0) \\
&= 10^{-2} \left[\begin{aligned} &13.344z^{0;0} + 1.668z^{0;0} + 1.668z^{0;1} + 13.824z^{0;2} + 1.728z^{0;2} + 1.728z^{0;2} \\ &+ 14.112z^{0;2} + 1.764z^{0;2} + 1.764z^{0;3} + 18.144z^{0;4} + 2.268z^{0;4} + 2.268z^{0;4} \\ &+ 7.072z^{0;0} + 0.884z^{1;0} + 0.884z^{2;1} + 2.592z^{2;0} + 0.324z^{3;0} + 0.324z^{4;1} \\ &+ 1.344z^{0;0} + 0.168z^{1;2} + 0.168z^{2;3} + 2.016z^{0;0} + 0.252z^{0;0} + 0.252z^{0;0} \\ &+ 4.896z^{2;0} + 0.612z^{2;0} + 0.612z^{2;0} + 2.464z^{4;0} + 0.308z^{4;0} + 0.308z^{4;0} \\ &+ 0.192z^{6;0} + 0.024z^{6;0} + 0.024z^{6;0} \end{aligned} \right] \\
&= 10^{-2} \left[\begin{aligned} &(13.344 + 1.668 + 7.072 + 1.344 + 2.016 + 0.252 + 0.252)z^{0;0} + 1.668z^{0;1} \\ &+ (13.824 + 1.728 + 1.728 + 14.112 + 1.764)z^{0;2} + 1.764z^{0;3} + (18.144 + 2.268 + 2.268)z^{0;4} \\ &+ 0.884z^{1;0} + 0.168z^{1;2} + (2.592 + 4.896 + 0.612 + 0.612)z^{2;0} + 0.884z^{2;1} + 0.168z^{2;3} \\ &+ (2.464 + 0.308 + 0.308)z^{4;0} + (0.192 + 0.024 + 0.024)z^{6;0} \end{aligned} \right] \\
&= 0.25948z^{0;0} + 0.01668z^{0;1} + 0.33156z^{0;2} + 0.01764z^{0;3} + 0.2268z^{0;4} + 0.00884z^{1;0} + 0.00168z^{1;2} \\
&\quad + 0.08712z^{2;0} + 0.00884z^{2;1} + 0.00168z^{2;3} + 0.0308z^{4;0} + 0.0024z^{6;0}.
\end{aligned}$$

The coefficient of $z^{0;0}$ indicates that the MSS has no deficiency and no excess after sharing. The coefficient in the term $z^{0;0}$ represented that the probability is 0.25948, which implies that the system reliability $R = 0.25948$.

6.5 Conclusion and future work

In this chapter, the reliability of MSS with common bus performance sharing is generalized to consider both performance deficiency and performance excess. A reliability and expected loss assessment algorithm for the MSS is proposed based on the UGF technology. Finally, a numerical experiment is shown to elucidate the procedure. The research on location optimization of MSUs to improve system reliability will be continued in the future.

References

- [1] Lisnianski, A. & Levitin, G. (2003). Multi-state system reliability, assessment, optimization and applications. World Scientific. p. 207–237. Assessment Optimization & Applications. <https://www.scopus.com/record/display.uri?eid=2-s2.0-41449093062&origin=inward>
- [2] Misra, K. B. 2008. Handbook of performability engineering. Springer-Verlag London Limited, International Journal of Performability Engineering, <https://www.scopus.com/record/display.uri?eid=2-s2.0-41449093062&origin=inward>.
- [3] Levitin, G. 2011, Reliability of multi-state systems with common bus performance sharing, IIE Transactions, 43(7), 518–524. <http://dx.doi.org/10.1080/0740817X.2010.523770>.
- [4] Yu, H., Yang, J. & Mo, H. 2014. Reliability analysis of repairable multi-state system with common bus performance sharing, Reliability Engineering & System Safety, 132, 90–96, <http://dx.doi.org/10.1016/j.res.2014.07.017>.
- [5] Yu, H., Yang, J., Lin, J. & Zhao, Y. 2017, Reliability evaluation of non-repairable phased-mission common bus systems with common cause failures, Computers & Industrial Engineering, 111(9), 445–457. <http://dx.doi.org/10.1016/j.cie.2017.08.002>.
- [6] Zhao, X., Congshan, W., Wang, S. & Wang, X. 2018, Reliability analysis of multi-state k-out-of-n: G system with common bus performance sharing, Computers & Industrial Engineering, 124(10), 359–369. <https://doi.org/10.1016/j.cie.2018.07.034>.
- [7] Levitin, G., Xing, L. et al., 2019. Dynamic availability and performance deficiency of common bus systems with imperfectly repairable components, Reliability Engineering & System Safety, 189, 58–66. <https://doi.org/10.1016/j.res.2019.04.007>.
- [8] Yi, K., Xiao, H., Kou, G. & Peng, R. 2019, Trade-off between maintenance and protection for multi-state performance sharing systems with transmission loss, Computers & Industrial Engineering, 136(10), 305–315. <https://doi.org/10.1016/j.cie.2019.07.030>.
- [9] Zhai, Q., Ye, Z., Peng, R. & Wang, W. 2017, Defense and attack of performance-sharing common bus systems, European Journal of Operational Research, 256(3), 962–975. <http://dx.doi.org/10.1016/j.ejor.2016.06.059>.
- [10] Cheng, C., Yang, J. et al., 2020. Reliability assessment of multi-state phased mission systems with common bus performance sharing considering transmission loss and performance storage, Reliability Engineering & System Safety, 199, 106917. <https://doi.org/10.1016/j.res.2020.106917>.
- [11] Su, P., Wang, G. et al., 2020. Reliability evaluation of a k-out-of-n(G)-subsystem based multi-state system with common bus performance sharing, Reliability Engineering & System Safety, 198, 106884. <https://doi.org/10.1016/j.res.2020.106884>.

- [12] Xiao, H. & Peng, R. 2014. Optimal allocation and maintenance of multi-state elements in series-parallel systems with common bus performance sharing, *Computers & Industrial Engineering*, 72, 143–151, <http://dx.doi.org/10.1080/0740817X.2010.523770>.
- [13] Xiao, H., Shi, D., Ding, Y. & Peng, R. 2016. Optimal loading and protection of multi-state systems considering performance sharing mechanism, *Reliability Engineering & System Safety*, 149, 88–95, <https://doi.org/10.1016/j.res.2015.12.001>.
- [14] Peng, R., Liu, H. & Xie, M. 2016, A study of reliability of multi-state systems with two performance sharing groups, *Quality & Reliability Engineering International*, 32(7), 2623–2632. <https://doi.org/10.1002/qre.1963>.
- [15] Peng, R., Xiao, H. & Liu, H. 2017. Reliability of multi-state systems with a performance sharing group of limited size, *Reliability Engineering & System Safety*, 166, 164–170, <https://doi.org/10.1016/j.res.2016.09.008>.
- [16] Qiu, S. & Ming, H. X. G. 2019, Reliability evaluation of multi-state series-parallel systems with common bus performance sharing considering transmission loss, *Reliability Engineering & System Safety*, 189(9), 406–415. <https://doi.org/10.1016/j.res.2019.04.029>.
- [17] Wu, D., Chi, Y. et al. , 2019. Reliability of capacitated systems with performance sharing mechanism, *Reliability Engineering & System Safety*, 189, 335–344. <https://doi.org/10.1016/j.res.2019.05.007>.
- [18] Wu, R. & Sansavini, G. 2020. Integrating reliability and resilience to support the transition from passive distribution grids to islanding microgrids, *Applied Energy*, 272, 115254, <https://doi.org/10.1016/j.apenergy.2020.115254>.
- [19] Xiao, H., Zhang, Y. et al., 2020. Optimal design of a linear sliding window system with consideration of performance sharing, *Reliability Engineering & System Safety*, 198, 106900. <https://doi.org/10.1016/j.res.2020.106900>.
- [20] Ahmadi, S. E., Rezaei, N. et al., 2020. Energy management system of networked microgrids through optimal reliability-oriented day-ahead self-healing scheduling, *Sustainable Energy, Grids and Networks*, 23, 100387. <https://doi.org/10.1016/j.segan.2020.100387>.
- [21] Li, D., Li, Z. et al., 2020. An implementation of hot-swap circuit with high reliability, *Microelectronics Journal*, 100, 104777. <https://doi.org/10.1016/j.mejo.2020.104777>.
- [22] Xiao, H. & Cao, M. 2020. Balancing the demand and supply of a power grid system via reliability modeling and maintenance optimization, *Energy*, 210, 118470, <https://doi.org/10.1016/j.energy.2020.118470>.
- [23] Jiao, J., De, X. et al. , 2019. Integrated circuit failure analysis and reliability prediction based on physics of failure, *Engineering Failure Analysis*, 104, 714–726. <https://doi.org/10.1016/j.engfailanal.2019.05.021>.
- [24] K., G. and Y. X., et al. (2019). Economic Design of a Linear Consecutively Connected System Considering Cost and Signal Loss. *IEEE Transactions on Systems, Man, and Cybernetics: Systems*: 1–13. doi: 10.1109/TSMC.2019.2946195.

Jacek Malinowski

7 A fast universal algorithm for finding minimal cut-sets in networks with arbitrary structure

Abstract: This contribution presents a newly developed fast algorithm enumerating all minimal cut-sets that separate two distinguished nodes in a graph-modeled network in which both links and nodes are failure-prone. Prior to running the algorithm, the tree of acyclic paths connecting the given pair of nodes has to be constructed (this is not a drawback because many existing algorithms for cut-sets enumeration use this tree in order to eliminate “stub” edges or subgraphs through which no acyclic path passes). Subsequently, the algorithm scans the acyclic paths tree in a bottom-up manner generating successive cut-sets and verifying if they are non-redundant, that is, do not include previously generated cut-sets. Owing to the original verification method, redundant cut-sets are eliminated without being compared to previously found nonredundant ones. Another strong point of the algorithm is that it only operates on the tree of acyclic paths, that is, no other analysis of a network’s topology is performed. It can be applied to networks with both directed and undirected links, and the cut-sets can be composed of both links and nodes. Many algorithms for finding minimal cut-sets assume that all the links are either directed or undirected and/or the nodes are perfectly reliable, which is quite restricting from the practical point of view. The presented algorithm is free from these limitations. Also, the unique cut-sets generation technique makes it significantly faster than many known methods, as confirmed by theoretical analysis and experiments carried out on example networks.

Keywords: Graph-structured network, acyclic path, minimal cut-set, structure function, nonredundant product, cut-sets enumeration

7.1 Introduction

This work presents a recently developed fast algorithm that enumerates all minimal s - t cut-sets that separate the source node from the sink node in a graph-structured network with directed and undirected links. An s - t cut-set is such a set of network elements that there is no connection from the source to the sink node if all elements of this set are removed or failed. A cut-set is minimal if no its subset is a cut-set. Unlike most known algorithms for that purpose that analyze the network structure itself, the

Jacek Malinowski, Systems Research Institute, Polish Academy of Sciences,
e-mail: jacek.malinowski@ibspan.waw.pl

<https://doi.org/10.1515/9783110725599-007>

one presented herein scans the tree of acyclic paths connecting the source with the sink node, and finds successive minimal cut-sets in the process. Thus, for its operation, the algorithm needs the acyclic paths tree of a network under consideration. This tree is easily constructed using the breadth-first search or depth-first search procedure. It should be noted that this is not an excessive requirement, because many existing methods for minimal cut-sets enumeration start from finding the acyclic paths in order to detect and delete “stub” edges or subgraphs through which no acyclic path passes. Let us note that, in reliability terms, the acyclic paths connecting two nodes of a network are the minimal path-sets of the system that are operable if there is a connection from the source to the sink node. Also, a minimal cut-set only contains elements of minimal path-sets (for that matter, it must contain at least one element of each minimal path-set), hence a network element not belonging to any minimal path-set does not belong to any minimal cut-set, either. Such an element is sometimes called irrelevant, while a relevant element is one that belongs to at least one minimal path-set.

The general idea of the algorithm is to scan the acyclic paths tree from bottom to top, generate new cut-sets by appropriately combining the previously found minimal cut-sets, and check if the newly generated cut-sets are minimal. The efficiency of the algorithm is due to the fact that it only generates a small number of non-minimal cut-sets, and the minimality check involves a fairly small number of comparisons with already found minimal cut-sets. Apart from being highly efficient, the algorithm is also universal in the sense that it assumes that both links and nodes can be elements of path-sets or cut-sets, which, in reliability terms, means that both links and nodes can fail. This is important for two reasons. First, most algorithms for minimal cut-sets enumeration do not take node failures into account (cf. [1–3, 7, 10, 11, 14]), hence the one presented here is one of those filling the gap. Second, in real networks, node failures are often more harmful than link failures (e.g., router or switch failures in computer networks); therefore, they should be reckoned with when network reliability analysis is carried out. Still, algorithms for identifying cut-sets composed of nodes or including them can be found, for example, in [5, 8, 10]. Last but not the least, the algorithm can be applied to networks with both directed and undirected links. This feature further adds to its universality, especially in view of the fact that most known methods for minimal cut-sets enumeration are designed for networks with undirected links. However, there exist methods focused on networks with directed links alone, such as those presented in [7].

7.2 Notation, definitions, and preliminaries

If not explicitly stated, for explanations to some definitions refer to Figure 7.2.

n – the number of relevant components in the network

e_i – the i th relevant component, $i=1, \dots, n$; for convenience, we will equate the components with their indices, that is, we will refer to e_i as “the component i ”

y_i – the Boolean variable representing the state of e_i ; $y_i=1$ if e_i is failed, $y_i=0$ if e_i is operable

σ, τ – the source and the terminal node

$\Phi(y_1, \dots, y_n)$ – the network's structure function, that is, a Boolean function expressing the state of connection between σ and τ ; $\Phi=0$ if there exists a path from σ to τ composed of operable elements, $\Phi=1$ if such a path does not exist

$T_{\sigma,\tau}$ – the tree of acyclic paths from σ to τ

t – a node in $T_{\sigma,\tau}$

t_1, \dots, t_m – the multi-child nodes of $T_{\sigma,\tau}$ ordered so that t_1 is the root node and the multi-child nodes located directly below t_k have consecutive indices

k^* – the largest k such that there is a multi-child node below t_k ; $k^*=3$ in Figure 7.2

$c(k)$ – the number of child nodes of t_k , for example, $c(2)=2$

$\lambda(k)$ – the number of leaf nodes below t_k , for example, $\lambda(2)=3$

$S(k,j)$ – the j th section outgoing from a multi-child node t_k , that is, the set of elements between t_k (excluded) and the nearest multi-child (included) or leaf (excluded) node located below t_k ; sections outgoing from the same node are numbered from left to right, for example, $S(2,1)=\{3,C,6,D,8\}$ and $S(2,2)=\{5,E\}$ are the first and the second section outgoing from t_2

$u(k,j)$ – a number defined as follows: $u(k,j)=h$ if the lowest element in $S(k,j)$ is the multi-child node t_h , otherwise $u(k,j)=0$ (the lowest element in $S(k,j)$ is a link to a leaf node), for example, $u(2,1)=0$ and $u(2,2)=4$

$\Psi_{k,j}$ – a Boolean sum associated with $S(k,j)$, defined as follows:

$$\Psi_{k,j} = \left(\bigvee_{i \in S(k,j)} y_i \right) \vee \Phi_{u(k,j)} \quad (7.1)$$

where $j=1, \dots, c(k)$ and $\Phi_{u(k,j)} = 0$ if $u(k,j)=0$

Φ_k – the Boolean expression obtained by multiplying $\Psi_{k,1}, \dots, \Psi_{k,c(k)}$, that is,

$$\Phi_k = \bigwedge_{j=1}^{c(k)} \Psi_{k,j} \quad (7.2)$$

π, ρ – Boolean products of variables from the set $\{y_1, \dots, y_n\}$

\subseteq, \subset – weak and strong inclusion relations between π and ρ ; $\pi \subseteq \rho$ if ρ has all the variables of π , or $\pi \subset \rho$ if $\pi \subseteq \rho$ and $\pi \neq \rho$

$E(\pi)$ – the set of elements corresponding to the variables of product π , for example, $E(\pi)=\{1,2,4\}$ if $\pi=y_1y_2y_4$

$\varphi(E)$ – the product corresponding to the set of elements E , for example, $\varphi(E)=y_1y_2y_4$ if $E=\{1,2,4\}$

In the paper, we will frequently use the terms “redundant” and “nonredundant” in reference to the products composing a Boolean sum. Let Φ be a sum of different Boolean products and let ρ be a component of Φ . If Φ contains another component π such that $\pi \subset \rho$, then ρ will be called redundant in Φ , that is, $\Phi = \Phi - \rho$, where $\Phi - \rho$ denotes Φ without the component ρ . If no such component π exists then ρ will be

called nonredundant in Φ . Clearly, $\Phi = \Phi^*$, where Φ^* is obtained by deleting all redundant products from Φ .

Let us note that the definitions of $\Psi_{k,j}$ and Φ_k are recursive, that is, Φ_k is computed using $\Phi_{u(k,j)}$ for $j=1, \dots, c(k)$. Clearly, if $k \geq k^*$, then $u(k,j)=0$ for $j=1, \dots, c(k)$, which provides the initial values for the recursive computations. Also note that the definitions of y_i and Φ are “failure oriented,” since 1 is the value assigned to a failed component or network, while it is more common to associate 0 with a failed object. However, these definitions allow simply expressing Φ in terms of minimal cut-sets. It is a well-known fact in reliability theory (see [3]) that:

$$\Phi(y_1, \dots, y_n) = \bigvee_{j=1, \dots, v} \bigwedge_{i \in C_j} y_i \quad (7.3)$$

where v is the number of all minimal cut-sets of a coherent system (see [3] for definition), and C_j denotes the j th minimal cut-set. It is easy to check that networks considered in this paper are coherent systems, if relevant components alone are taken into account. In consequence, representing Φ as the Boolean sum of minimal products of the variables y_1, \dots, y_n is equivalent to finding the minimal cut-sets of the analyzed system. These cut-sets are simply the sets of indices of the variables comprising individual products.

In order to better explain the definitions of $S(k,j)$, $u(k,j)$, $\Psi_{k,j}$, Φ_k , and the algorithm for the minimal cut-sets enumeration presented in the next section, we will use a small exemplary network whose structure and tree of acyclic paths from source node A to terminal node F are presented in Figures 7.1 and 7.2. The multi-child nodes $t_1, t_2, t_3, t_4, t_5, t_6$ are distinguished with circles. The last fragment of the only acyclic path not ending in F (i.e., ABEDC) is deleted from the tree.

Let us consider the node t_3 . In Figure 7.2, we see that $c(3)=2$, $S(3,1)=\{3,B,5,E\}$, $S(3,2)=\{6,D\}$, $u(3,1)=5$, $u(3,2)=6$, $\Psi_{5,1}=y_3 \vee y_B \vee y_5 \vee y_E \vee \Phi_5$, $\Psi_{3,2}=y_6 \vee y_D \vee \Phi_6$, and $\Phi_3=\Psi_{3,1} \wedge \Psi_{3,2}$. Further, for $k=5$ we have: $c(5)=2$, $S(5,1)=\{7,D,8\}$, $S(5,2)=\{9\}$, $u(5,1)=0$, $u(5,2)=0$, $\Psi_{5,1}=y_7 \vee y_D \vee y_8$, $\Psi_{5,2}=y_9$, and $\Phi_5=\Psi_{5,1} \wedge \Psi_{5,2}$. The analogous equalities hold for $k=6$.

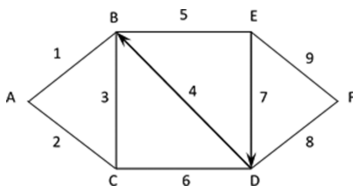


Figure 7.1: The structure of an example network with directed and undirected links.

In order to avoid unnecessary expansion of the acyclic paths tree, which could result in a significant increase in computing time, our considerations will be limited only to networks without one-element cut-sets. Networks with one-element cut-sets can be regarded as series systems composed of modules, where each module is a

7.3 Computing Φ_k as a sum of non-redundant products

As follows from (7.1) and (7.2), Φ_k is obtained by multiplying $c(k)$ Boolean sums, where each sum is composed of a number of single variables and $\Phi_{u(k,j)}$. If $k > k^*$ then Φ_k is obtained by multiplying $c(k)$ sums of single variables, hence is Φ_k a sum of products. For example, $\Phi_4 = (y_7 \vee y_D \vee y_8)y_9 = y_7y_9 \vee y_Dy_9 \vee y_8y_9$. Thus, by induction, Φ_k is also a sum of products for k decreasing from k^* to 1. The products in Φ_k correspond to cut-sets in $T_{\sigma,\tau}$ separating t_k (and all nodes above t_k) from the leaf nodes located below t_k . Indeed, the variables of each product in Φ_k correspond to a set obtained by selecting one element from each path connecting t_k with a leaf node. If the variables of at least one product in Φ_k are all ones, then each path from t_k to a leaf node contains a failed element, which means that t_k is separated from the leaf nodes located below t_k .

We will now show that the non-redundant products composing Φ_1 , which can be obtained recursively by computing Φ_k for k decreasing from m to 1, correspond to minimal cut-sets separating each path in G from σ to τ . First, we prove the following auxiliary lemma:

Lemma 7.1: *If Γ is a cut-set in $T_{\sigma,\tau}$ that separates t_k from the leaf nodes located below t_k , then Φ_k contains a product π , such that $E(\pi) \subseteq \Gamma$.*

Proof. By assumption, Γ contains one or more elements of each path from t_k to a leaf node. Let Γ' be obtained by selecting one component of Γ from each such path. Clearly, $\Gamma' \subset \Gamma$. The definition of Φ_k yields that the product $\pi = \varphi(\Gamma')$ is a component of Φ_k . The proof is completed by noting that $E(\pi) = \Gamma' \subset \Gamma$.

Using the above lemma, we will prove the following theorem:

Theorem 7.1: *Γ is a minimal cut-set in $T_{\sigma,\tau}$ separating t_k from the leaf nodes located below t_k if and only if $\varphi(\Gamma)$ is a nonredundant product in Φ_k .*

Proof. For brevity, we will write “cut-set” instead of “cut-set separating t_k from” The following implications hold:

Γ is a minimal cut-set $\Rightarrow \Gamma$ is a cut-set $\Rightarrow \Phi_k$ contains a product π such that $E(\pi) \subseteq \Gamma \Rightarrow E(\pi)$ is a cut-set and $E(\pi) = \Gamma$

The second of the above implications is a consequence of Lemma 1. The third one is true, because Γ , being minimal, cannot include a cut-set other than itself. Note that $\pi = \varphi(\Gamma)$. Further, we have the following implications:

$$\pi' \subset \pi \Rightarrow E(\pi') \subset E(\pi) = \Gamma \Rightarrow \pi' \text{ is not a product in } \Phi_k$$

The last statement holds, as otherwise, $E(\pi')$ would be a cut-set and a proper subset of Γ , which is impossible due to minimality of Γ . In view of the above implications, $\pi = \varphi(\Gamma)$ is a nonredundant product in Φ_k , which ends the first part of the proof.

For the proof of the second part, let us assume that $\varphi(\Gamma)$ is a nonredundant product in Φ_k . It follows that Γ is a cut-set. Suppose that Γ is not minimal and Γ' is a minimal cut-set such that $\Gamma' \subset \Gamma$. As follows from the just proved first part of the lemma, $\varphi(\Gamma')$ is a (nonredundant) product in Φ_k . Obviously, $\varphi(\Gamma') \subset \varphi(\Gamma)$, hence $\varphi(\Gamma)$ is redundant in Φ_k . This contradicts the initial assumption; hence Γ is a minimal cut-set. The whole proof is thus completed.

Corollary: *It follows immediately that the nonredundant products composing Φ_1 are in one-to-one correspondence with the minimal cut-sets separating each path in G from σ to τ .*

For further considerations, we will need the following additional notation:

$\Pi_{k,h}$ – the h th acyclic path from t_k to a leaf-node, $1 \leq h \leq \lambda(k)$

$\beta_{k,h}(\Gamma)$ – the lowest element of Γ in $\Pi_{k,h}$, $1 \leq h \leq \lambda(k)$

H – a subset of $\{1, \dots, \lambda(k)\}$

$d(j)$ – the number of paths from t_k to leaf nodes, passing through the j th child node of t_k , $1 \leq j \leq c(k)$; note that $d(1) + \dots + d(c(k)) = \lambda(k)$

We will also need the following lemma:

Lemma 7.2: *Γ is a minimal cut-set intersecting each path $\Pi_{k,h}$, $h \in H$, if and only if the following two conditions hold:*

1) $\Gamma \cap \Pi_{k,h} \neq \emptyset$ for each $\Pi_{k,h}$, $h \in H$

2) for each $e \in \Gamma$, there exists $h \in H$ such that $\Gamma \cap \Pi_{k,h} = \{e\}$

Proof. The first condition yields that Γ is a cut-set intersecting each path $\Pi_{k,h}$, $h \in H$. The second one states that for each $e \in \Gamma$, we can find $h \in H$ such that $[\Gamma \setminus \{e\}] \cap \Pi_{k,h} = \emptyset$, that is, $\Gamma \setminus \{e\}$ has no common elements with $\Pi_{k,h}$. This means that every proper subset of Γ does not intersect at least one path $\Pi_{k,h}$, $h \in H$, therefore Γ is a minimal cut-set.

The next theorem provides a quick way to check if $\pi_1 \wedge \pi_2$ is redundant in $\Psi_{k,1} \wedge \dots \wedge \Psi_{k,j} \wedge \Psi_{k,j+1}$, where π_1 and π_2 are nonredundant products in $\Psi_{k,1} \wedge \dots \wedge \Psi_{k,j}$ and $\Psi_{k,j+1}$ respectively. It will be used in the algorithm computing Φ_k according to formula (7.2).

Theorem 7.2: *Let Γ be a cut-set intersecting each path $\Pi_{k,h}$, $h \in H$, and let $\Gamma' = \bigcup_{h \in H} \{\beta_{k,h}(\Gamma)\}$. Further, let Γ'' be obtained from Γ' by removing each element e such that every $\Pi_{k,h}$, $h \in H$, that contains e also contains another element of Γ' . Then Γ'' is a minimal cut-set.*

Proof. Γ' is a cut-set because, as follows from its definition, Γ' contains (at least) one element of each path $\Pi_{k,h}$, $h \in H$. Let us note that a path from t_k to a leaf node may contain multiple elements of Γ' . For example, if $k=2$ and $\Gamma=\{5,6,7,8\}$, then $\Gamma'=\{6,7,8\}$ and $\Pi_{2,3}$ contains all elements of Γ' . Clearly, if $\Gamma' \subset \Gamma$, then Γ is not minimal. Furthermore, if $e \in \Gamma'$ and each path containing e contains another element of Γ' , then $\Gamma' \setminus \{e\}$ is still a cut-set, because it contains (at least) one element of every path $\Pi_{k,h}$, $h \in H$. Removing all such elements of Γ' , we obtain Γ'' that satisfies both conditions of Lemma 7.2. Thus, Γ'' is a minimal cut-set.

Corollary: Let π_1 and π_2 be nonredundant products in $\Psi_{k,1} \wedge \dots \wedge \Psi_{k,j}$ and $\Psi_{k,j+1}$ respectively, $1 \leq j \leq c(k)-1$. Let also $H = \{1, \dots, d(1) + \dots + d(j+1)\}$. If $\Gamma = E(\pi_1 \wedge \pi_2)$ is a proper superset of $\Gamma' = \bigcup_{h \in H} \{\beta_{k,h}(\Gamma)\}$ then Γ is not a minimal cut-set intersecting each path Π_h , $h \in H$, that is, $\pi_1 \wedge \pi_2$ is redundant in $\Psi_{k,1} \wedge \dots \wedge \Psi_{k,j} \wedge \Psi_{k,j+1}$. Moreover, Γ'' (obtained from Γ' , as per Theorem 7.2) is a minimal cut-set, hence, if $\Gamma = \Gamma''$ then $\pi_1 \wedge \pi_2$ is a non-redundant product.

For clarity, let us illustrate the above redundancy condition. Let $k=3$, $j=1$, $\pi_1=y_5$, $\pi_2=y_4y_8$. We have: $c(3)=2$, $d(1)=2$, $d(2)=2$, $H=\{1, \dots, 4\}$, $\pi_1 \wedge \pi_2 = y_5y_4y_8$, $\beta_{3,1}(\pi_1 \wedge \pi_2) = 8$, $\beta_{3,2}(\pi_1 \wedge \pi_2) = 5$, $\beta_{3,3}(\pi_1 \wedge \pi_2) = 5$, $\beta_{3,4}(\pi_1 \wedge \pi_2) = 8$. Since $\Gamma = E(\pi_1 \wedge \pi_2) = \{4,5,8\}$ and $\Gamma' = \bigcup_{h \in H} \beta_{3,h}(\pi_1 \wedge \pi_2) = \{5,8\}$, the product $y_5y_4y_8$ is redundant in $\Psi_{3,1} \wedge \Psi_{3,2}$ which is equal to Φ_3 .

It should be noted that if Γ' is a proper subset of Γ (as in the above example), then it is not necessary to find Γ'' in order to check whether Γ is (or is not) a minimal cut-set. However, if $\Gamma'=\Gamma$, we need Γ'' to ascertain if Γ is minimal. The analysis of several simple networks showed that Γ' is a minimal cut-set provided $\Gamma = E(\pi_1 \wedge \pi_2)$ (H and Γ are not chosen arbitrarily). However, it remains an open problem whether this is true, in general. Clearly, the check if Γ is minimal (i.e., $\phi(\Gamma)$ is nonredundant) would be quicker, if it were not necessary to compute Γ'' in the case when $\Gamma'=\Gamma$.

We end this section with a theorem that allows quick elimination of a significant number of redundant products, without the need to check them for redundancy, as in Theorem 7.2.

Theorem 7.3: Let π and π_1 be nonredundant in $\Psi_{k,1} \wedge \dots \wedge \Psi_{k,j}$ and let ρ and ρ_1 be non-redundant in $\Psi_{k,j+1}$, where $\pi \neq \pi_1$, $\rho \neq \rho_1$, $1 \leq j \leq c(k)-1$. If $\pi=\rho$ then π is nonredundant, while $\pi_1\rho$ and $\pi\rho_1$ are redundant in $\Psi_{k,1} \wedge \dots \wedge \Psi_{k,j} \wedge \Psi_{k,j+1}$. Further, if either $\pi \subset \rho$ or $\rho \subset \pi$, then either ρ or π is nonredundant, while either $\pi_1\rho$ or $\pi\rho_1$ is redundant in $\Psi_{k,1} \wedge \dots \wedge \Psi_{k,j} \wedge \Psi_{k,j+1}$.

Proof. Theorem 7.3 follows immediately from the fact that $\pi_1\rho \leq \rho = \pi\rho$ if $\pi \subseteq \rho$ and $\pi\rho_1 \leq \pi = \pi\rho$ if $\rho \subseteq \pi$.

7.4 The cut-set enumeration algorithm

The following algorithm, constructed on the basis of Theorems 7.2 and 7.3, computes Φ_1 as a Boolean sum of non-redundant products.

Algorithm 7.1

```

For  $k=m$  down to  $k=1$  do
  For  $j=1$  to  $c(k) - 1$  do {
    Assign 0 to  $\Psi_{k,1} \wedge \dots \wedge \Psi_{k,j+1}$ ;
    If  $\pi=\rho$  for  $\pi$  in  $\Psi_{k,1} \wedge \dots \wedge \Psi_{k,j}$  and  $\rho$  in  $\Psi_{k,j+1}$ , remove  $\pi$  and  $\rho$  from the respective sums
    and add  $\pi$  to  $\Psi_{k,1} \wedge \dots \wedge \Psi_{k,j+1}$ ;
    If  $\pi \subset \rho$  or  $\rho \subset \pi$  for  $\pi$  in  $\Psi_{k,1} \wedge \dots \wedge \Psi_{k,j}$  and  $\rho$  in  $\Psi_{k,j+1}$ , move  $\rho$  or  $\pi$  from the respective
    sum to  $\Psi_{k,1} \wedge \dots \wedge \Psi_{k,j+1}$ ;
    For each  $\pi$  in  $\Psi_{k,1} \wedge \dots \wedge \Psi_{k,j}$  and  $\rho$  in  $\Psi_{k,j+1}$ , check if  $\pi\rho$  satisfies the nonredundancy
    condition from Corollary to Theorem 7.2 and, if so, add  $\pi\rho$  to  $\Psi_{k,1} \wedge \dots \wedge \Psi_{k,j+1}$ ;
  }
  Assign  $\Psi_{k,1} \wedge \dots \wedge \Psi_{k,c(k)}$  to  $\Phi_k$ 
}

```

As follows from Theorem 7.1, the Boolean sum, Φ_1 computed in the last cycle of the external for-loop is composed of nonredundant products corresponding to the minimal cut-sets separating t_l from all the leaf nodes located below t_l . This means that $\Phi=\Phi_1$, and the components of Φ correspond to the minimal cut-sets separating σ from τ in the considered network.

7.5 An illustrative example

Algorithm 7.1 will now be applied to the network in Figure 7.1, whose tree of acyclic paths is shown in Figure 7.2. In order to avoid complex expressions, it will be assumed that either all the nodes or all the links are failure-free, that is, the cut-sets only consist of either links or nodes, respectively. In the first case (failure-free nodes), it holds that $y_A = \dots = y_F = 0$, and the following results are obtained:

$$\Phi_6 = \Psi_{6,1} \Psi_{6,2} = (y_4 \vee y_5 \vee y_9) y_8 = y_4 y_8 \vee y_5 y_8 \vee y_9 y_8$$

$$\Phi_5 = \Psi_{5,1} \Psi_{5,2} = \Phi_4 = \Psi_{4,1} \Psi_{4,2} = (y_7 \vee y_8) y_9 = y_7 y_9 \vee y_8 y_9$$

$$\Phi_3 = \Psi_{3,1} \Psi_{3,2} = (y_3 \vee y_5 \vee \Phi_5) (y_6 \vee \Phi_6)$$

$$\begin{aligned}
&= (y_3 \vee y_5 \vee y_7 y_9 \vee y_8 y_9)(y_6 \vee y_4 y_8 \vee y_5 y_8 \vee y_9 y_8) \\
&= y_5 y_8 \vee y_8 y_9 \vee (y_3 \vee y_5 \vee y_7 y_9)(y_6 \vee y_4 y_8) \\
&= y_5 y_8 \vee y_8 y_9 \vee y_3 y_6 \vee y_3 y_4 y_8 \vee y_5 y_6 \vee y_5 y_4 y_8 \# \vee y_7 y_9 y_6 \vee y_7 y_9 y_4 y_8 \# \\
&= y_5 y_8 \vee y_8 y_9 \vee y_3 y_6 \vee y_3 y_4 y_8 \vee y_5 y_6 \vee y_7 y_9 y_6 \\
\Phi_2 &= \Psi_{2,1} \Psi_{2,2} = (y_3 \vee y_6 \vee y_8)(y_5 \vee \Phi_4) \\
&= (y_3 \vee y_6 \vee y_8)(y_5 \vee y_7 y_9 \vee y_8 y_9) \\
&= y_8 y_9 \vee (y_3 \vee y_6 \vee y_8)(y_5 \vee y_7 y_9) \\
&= y_8 y_9 \vee y_3 y_5 \vee y_3 y_7 y_9 \vee y_6 y_5 \vee y_6 y_7 y_9 \vee y_8 y_5 \vee y_8 y_7 y_9 \# \\
&= y_8 y_9 \vee y_3 y_5 \vee y_3 y_7 y_9 \vee y_6 y_5 \vee y_6 y_7 y_9 \vee y_8 y_5 \\
\Phi_1 &= \Psi_{1,1} \Psi_{1,2} = (y_1 \vee \Phi_2)(y_2 \vee \Phi_3) \\
&= y_8 y_9 \vee y_5 y_8 \vee y_6 y_7 y_9 \vee y_5 y_6 \vee (y_1 \vee y_3 y_5 \vee y_3 y_7 y_9)(y_2 \vee y_3 y_6 \vee y_3 y_4 y_8) \\
&= y_8 y_9 \vee y_5 y_8 \vee y_6 y_7 y_9 \vee y_5 y_6 \vee y_1 y_2 \vee y_1 y_3 y_6 \vee y_1 y_3 y_4 y_8 \vee y_3 y_5 y_2 \vee y_3 y_5 y_6 \# \\
&\quad \vee y_3 y_5 y_4 y_8 \# \vee y_3 y_7 y_9 y_2 \vee y_3 y_7 y_9 y_6 \# \vee y_3 y_7 y_9 y_4 y_8 \# \\
&= y_8 y_9 \vee y_5 y_8 \vee y_6 y_7 y_9 \vee y_5 y_6 \vee y_1 y_2 \vee y_1 y_3 y_6 \vee y_1 y_3 y_4 y_8 \vee y_3 y_5 y_2 \vee y_3 y_7 y_9 y_2
\end{aligned}$$

The products marked with hashes are redundant and have to be deleted. Consequently, if the nodes are failure-free, the network in Figure 7.1 has the following minimal cut-sets: {8,9}, {5,8}, {6,7,9}, {5,6}, {1,2}, {1,3,6}, {1,3,4,8}, {2,3,5}, {2,3,7,9}.

In the second case (failure free links), we have $y_1 = \dots = y_9 = 0$, and the algorithm produces the following results:

$$\begin{aligned}
\Phi_6 &= (y_4 \vee y_B \vee y_5 \vee y_E \vee y_9)y_8 = (y_E \vee y_B)0 = 0 \\
\Phi_5 &= \Phi_4 = (y_7 \vee y_D \vee y_9)y_9 = (y_D)0 = 0 \\
\Phi_3 &= (y_3 \vee y_B \vee y_5 \vee y_E \vee \Phi_5)(y_6 \vee y_D \vee \Phi_6) = (y_B \vee y_E)y_D = y_B y_D \vee y_E y_D \\
\Phi_2 &= (y_3 \vee y_C \vee y_6 \vee y_D \vee y_8)(y_5 \vee y_E \vee \Phi_4) = (y_C \vee y_D)y_E = y_C y_E \vee y_D y_E \\
\Phi_1 &= (y_1 \vee y_B \vee \Phi_2)(y_2 \vee y_C \vee \Phi_3) = (y_B \vee y_C y_E \vee y_D y_E)(y_C \vee y_B y_D \vee y_E y_D) = \\
&= y_B y_D \vee y_C y_E \vee y_D y_E \vee y_B y_C
\end{aligned}$$

Consequently, if the links are failure-free, the network in Figure 7.1 has the following minimal cut-sets: {B,D}, {C,E}, {D,E}, {B,C}. Obviously, the considered network also has one-element minimal cut-sets {A} and {E}, not enumerated by the algorithm.

If both link and node failures were taken into account, the algorithm would proceed in the same way as presented above; however, the computations would be more complex. Nevertheless, the reader is encouraged to attempt them.

7.6 Conclusions and further research

Using the network presented in Figure 7.1, Algorithm 7.1 was compared to other methods for generating minimal cut-sets, published in the relevant literature, for example, Abel and Bicker [1], Arunkumar and Lee [2], or Beichelt [3], as well as those published more recently, for example, Ross [8, 9], Yeh [14]. In all those tests, Algorithm 7.1 proved to be no less efficient than its counterparts. Besides, Algorithm 7.1 can be applied, without adjustments, to directed, partly directed, or undirected graphs. Moreover, it can generate cut-sets including both nodes and links, while many existing methods are limited to cut-sets composed of links alone. Thus, they do not take node failures into account, which is unacceptable from the practical point of view. Admittedly, the tree of loop-free paths has to be constructed before Algorithm 7.1 is put to operation, but these paths have to be known, in order to eliminate “stub” subgraphs through which no loop-free path passes and whose components are irrelevant for the functioning of a network. Often, the construction of the acyclic paths tree is necessary when both minimal path-sets and minimal cut-sets are to be found, if a more detailed reliability analysis of a network has to be carried out.

As far as future development of the presented method is concerned, its applicability should be extended to networks with weighted elements, so that the cut-sets can be generated according to non-decreasing weights, as in Yeh [12]. Such ordering of minimal cut-sets is required by algorithms for finding the so-called d -cut-sets limiting the maximum throughput in flow networks. One should also try to modify Algorithm 7.1 so that it only finds minimal cut-sets with a limited number of elements, which is desirable for practical reasons. Further, it seems worthwhile to adapt Algorithm 7.1 to special types of networks, such as electrical grids considered in Che [4], or k -out-of- n networks, where a node requires a given number of inputs so that it can generate an output, analyzed in Yeh [13]. Last but not the least, the author will endeavor to prove the hypothesis formulated at the end of Section 7.3, allowing the acceleration of non-redundancy checks of products obtained in the course of Algorithm 7.1.

References

- [1] Abel, U. & Bicker, R. 1982. Determination of All Minimal Cut-Sets between a Vertex Pair in an Undirected Graph, *IEEE Transactions on Reliability*, R-31, 167–171.
- [2] Arunkumar, S. & Lee, S. H. 1979. Enumeration of all minimal cut-sets for a node pair in a graph, *IEEE Transactions on Reliability*, R-28, 51–55.
- [3] Beichelt, F. 1988. *Zuverlässigkeit strukturierter Systeme*, VEB Verlag Technik, Berlin.
- [4] Che, Y. et al. , 2017. A Hierarchical Approach for Fast Calculating Minimal Cut Sets of a Microgrid”, *Mathematical Problems in Engineering*, <https://doi.org/10.1155/2017/5154740>.

- [5] Kurita, K. & Kobayashi, Y. (2020) Efficient Enumerations for Minimal Multicuts and Multiway Cuts, 45th International Symposium on Mathematical Foundations of Computer Science (MFCS 2020), Article No. 60, 60:1–60:14.
- [6] Malinowski, J. 2010. A new efficient algorithm for generating all minimal tie-sets connecting selected nodes in a mesh-structured network, *IEEE Transactions on Reliability*, 59, 203–211.
- [7] Mishra, R. et al., 2016. Enumeration of minimal cut-sets for directed networks with comparative reliability study for paths or cuts, *Quality and Reliability Engineering International*, 32(2), 555–565.
- [8] Prasad, V. C. et al., 1992. Generation of vertex and edge cut sets, *Microelectronics Reliability*, 32, 1291–1301.
- [9] Ross, S. 2010. *Introduction to probability models* – 10th edition, Elsevier.
- [10] Singh, B. 1994. Enumeration of node cut sets for an s-t network, *Microelectronics Reliability*, 34, 559–561.
- [11] Tsukiyama, S. et al., 1980. An algorithm to enumerate all cut sets of a graph in linear time per cut set, *Journal of the Association for Computing Machinery*, 27(4), 619–632.
- [12] Yeh, L.-P. et al., 2010. Efficient Algorithms for the Problems of Enumerating Cuts by Non-decreasing Weights, *Algorithmica*, 56, 297–312.
- [13] Yeh, W.-C. 2006. A new algorithm for generating minimal cut sets in k-out-of-n networks, *Reliability Engineering and System Safety*, 99, 36–43.
- [14] Yeh, W.-C. 2006. A simple algorithm to search for all MCs in networks, *European Journal of Operational Research*, 174, 1694–1705.

Ali Muhammad Rushdi, Fares Ahmad Ghaleb

8 Switching-algebraic symbolic analysis of the reliability of non-repairable coherent multistate systems

Abstract: This chapter presents a switching-algebraic analysis of non-repairable coherent multistate systems (MSSs) with independent non-identical multistate components. We adapt various switching-algebraic binary concepts and tools such as probability-ready expressions (PREs), Boolean quotients, the Boole–Shannon expansion, and the Karnaugh map to the multistate case. This chapter analyzes a multistate reliability system without explicit utilization of the algebraic techniques of multiple-valued logic or those of multivalued discrete-function theory. The analysis required is achieved via the evaluation of each of the multiple non-zero levels of the system output as a binary or propositional function of the system multivalued inputs. The formula of each of these levels is then written as a PRE, thereby allowing its immediate conversion, on a one-to-one basis, into a probability value. The symbolic reliability analysis of two small coherent MSSs is completed successfully herein, yielding results that have been checked symbolically, and can also be shown to agree numerically with those obtained earlier. The algebraic techniques used are supplemented by illustrative visualization via multivalued Karnaugh maps. Emphasis is placed on the generalization of concepts of coherent binary systems to those of coherent multistate ones, rather than innovating new unfamiliar stand-alone concepts for these latter systems.

Keywords: System reliability, probability-ready expression, multistate system, multiple-valued logic, minimal upper vector, maximal lower vector

8.1 Introduction

There are many standard research techniques for the reliability analysis of multistate systems (MSSs) [1], most of which rely on the utilization of discrete non-binary functions [2–4] or multiple-valued logic [5–24]. The main theme of this chapter is that instead of tightening or narrowing the paradigms of discrete functions or multivalued logic to fit the multistate reliability problem, one could generalize or enlarge the switching-algebraic reliability analysis to suit the multistate case. The starting point in our scheme pertains to reliability per se, and hence the adaptation to the

Ali Muhammad Rushdi, Fares Ahmad Ghaleb, Department of Electrical and Computer Engineering, Faculty of Engineering, King Abdulaziz University, P. O. Box 80200, Jeddah, 21589, Kingdom of Saudi Arabia

<https://doi.org/10.1515/9783110725599-008>

multistate case is straightforward. By contrast, the starting point in the standard analysis does not relate directly to reliability, or even to probability, and has to augment its course of action with some probability techniques, which might be lacking in efficiency.

This chapter extends algebraic techniques and tools of switching algebra or binary logic to ones of multiple-valued logic, so as to evaluate each of the multiple non-zero levels of the system output as an individual binary or propositional function of the system multivalued inputs. The formula of each of these levels is then written as a probability-ready expression (PRE), thereby allowing its immediate conversion, on a one-to-one basis, into a probability or expected value. The proposed analysis will be seen to be particularly simple when the MSS is binary-imaged, that is, when its success at each specific level is dependent only on component successes at the same level [24–31]. However, the proposed analysis is still valid (albeit with increasing complexity) for systems that are not binary-imaged. This chapter strives to provide a pedagogically oriented treatment that establishes a clear and insightful interrelationship between binary modeling and MSS modeling by stressing that multivalued concepts are natural and simple extensions of two-valued ones. Visual insight secured through the use of Karnaugh maps aids in the comprehension of coherent-system concepts, whether they are binary and multi-state. A notable achievement for the multistate case is the clarification of the subtle relation between a minimal upper vector (MUV) at a certain level and a prime implicant of success (minimal path) at that level, or the dual relation between a maximal lower vector (MLV) at a certain level and a prime implicant of failure (minimal cutset) at that level. Many authors [1, 26] consider that the MUVs and MLVs play the role of (or are synonymous to) minimal paths and minimal cutsets, respectively. However, a minimal path constitutes all the upper vectors extending (inclusively) from a particular MUV to the all-highest vector, while a minimal cutset comprises all the lower vectors extending (inclusively) from the all-0 vector to a particular MLV.

The organization of the remainder of this chapter is as follows. Section 8.2 presents important assumptions, notation and nomenclature. Section 8.3 introduces the concept of Boolean quotient in a multivalued context. Section 8.4 extends the concept of a PRE from the binary to the multistate case. Section 8.5 provides a quick review of the concept of the Boole–Shannon expansion, again with an emphasis on its interpretation in a multivalued sense. In Sections 8.6 and 8.7, the chapter presents its main contribution through the multivalued analysis of two specific (albeit standard) MSSs. Section 8.6 deals with a non-homogeneous two-component system that is not binary-imaged, while Section 8.7 handles a homogenous binary-imaged three-component system. Section 8.8 concludes the chapter.

8.2 Assumptions, notation, and nomenclature

8.2.1 Assumptions

- The model considered is one of a MSS with multistate components, specified by the structure or success function $S(X)$ [1]

$$S: \{0, 1, \dots, m_1\} \times \{0, 1, \dots, m_2\} \times \dots \times \{0, 1, \dots, m_n\} \rightarrow \{0, 1, \dots, M\}. \quad (8.1)$$

- The system is generally non-homogeneous, that is, the number of system states $(M+1)$ and the numbers of component states (m_1+1) , (m_2+1) , \dots , (m_n+1) might differ. When these numbers have a common value the system reduces to a homogeneous one.
- The system is a non-repairable one with statistically independent non-identical (heterogeneous) components.
- The system is a coherent one enjoying the properties of causality, monotonicity, and component relevancy [21, 22, 28–31].
- The system is not necessarily binary-imaged or dominant [27].

8.2.2 Notation

Symbol	Description
--------	-------------

X_k	A multivalued input variable representing component k ($1 \leq k \leq n$), where $X_k \in \{0, 1, \dots, m_k\}$, and $m_k \geq 1$ is the highest value of X_k .
-------	--

$X_k\{j\}$	A binary variable representing instant j of X_k
------------	---

$$X_k\{j\} = \{X_k = j\},$$

that is, $X_k\{j\} = 1$ if $X_k = j$ and $X_k\{j\} = 0$ if $X_k \neq j$. The instances $X_k\{j\}$ for $\{0 \leq j \leq m_k\}$ form an orthonormal set, namely, for $\{1 \leq k \leq n\}$

$$\bigvee_{j=0}^{m_k} X_k\{j\} = 1, \quad (8.2a)$$

$$X_k(j_1) X_k(j_2) = 0 \quad \text{for } j_1 \neq j_2. \quad (8.2b)$$

Orthonormality is very useful in constructing inverses or complements. The complement of the union of certain instances is the union of the complementary instances. In particular, the complement of $X_k\{\geq j\} = X_k\{j, j+1, \dots, m_k\}$ is given by $X_k\{< j\} = X_k\{0, 1, \dots, j-1\}$.

(continued)

Symbol Description

$X_k\{\geq j\}$ An upper value of $X_k\{0 \leq j \leq m_k\}$:

$$X_k\{\geq j\} = X_k\{j, j+1, \dots, m_k\} = \bigvee_{i=j}^{m_k} X_k\{i\} = X_k\{j\} \vee X_k\{j+1\} \vee \dots \vee X_k\{m_k\}. \quad (8.3)$$

The value $X_k\{\geq 0\}$ is identically equal to 1. The set $X_k\{\geq j\}$ for $\{1 \leq j \leq m_k\}$ is neither independent nor disjoint. It is difficult to manipulate, but it is convenient for translating a verbal or map description of a coherent component into a mathematical form when viewing component success at level j . The complement of $X_k\{\geq j\}$ is

$$X_k\{< j\} = X\{0, 1, \dots, j-1\} = X_k\{0\} \vee X_k\{1\} \vee \dots \vee X_k\{j-1\} = X_k\{k \leq (j-1)\}. \quad (8.4)$$

A lower value of $X_k\{0 \leq j \leq m_k\}$:

$$X_k\{\leq j\} = X_k\{0, 1, \dots, j\} = \bigvee_{i=0}^j X_k\{i\} = X_k\{0\} \vee X_k\{1\} \vee \dots \vee X_k\{j-1\} \vee X_k\{j\}. \quad (8.5)$$

The value $X_k\{\leq m_k\}$ is identically 1. The set $X_k\{\leq j\}$ for $\{0 \leq j \leq (m_k - 1)\}$ is neither independent nor disjoint, and hence it is not convenient for mathematical manipulation though it is suitable for expressing component failure at level $(j+1)$. Instances, upper values, and lower values are related by

$$\begin{aligned} X_k\{j\} &= X_k\{\geq j\} X_k\{< (j+1)\} = X_k\{\geq j\} \bar{X}_k\{\geq (j+1)\} \\ &= X_k\{\leq j\} X_k\{> (j-1)\} = X_k\{\leq j\} \bar{X}_k\{\leq (j-1)\}. \end{aligned} \quad (8.6)$$

S A multivalued output variable representing the system, where

$$S \in \{0, 1, \dots, M\}, \quad (8.7)$$

and $M \geq 1$ is the highest value attained by the system. The system is called homogeneous if $M = m_1 = m_2 = \dots = m_n$. The function $S(X)$ is usually called the system success or the structure function. It is conveniently represented by a multivalued Karnaugh map (MVKM) [18, 19, 21, 22, 28–31]. Its complement $\bar{S}(X)$ is called the system failure, and is also a multivalued variable of $(M+1)$ values. The sum $S(X)$ is identically equal to M .

$S\{j\}$ A binary variable representing instant j of S

$$S\{j\} = \{S(X) = j\}, \quad (8.8)$$

that is, $S\{j\} = 1$ if $S(X) = j$, and $S\{j\} = 0$ if $S(X) \neq j$. The instances $S\{j\}$ for $\{0 \leq j \leq M\}$ form an orthonormal set, that is

$$\bigvee_{j=0}^M S\{j\} = 1, \quad (8.9)$$

$$S\{j_1\} S\{j_2\} = 0 \quad \text{for } j_1 \neq j_2, \quad (8.10)$$

which means that one, and only one, of the $(M+1)$ instances of S has the value 1, while the other instances are all 0's.

$S\{\geq j\}$ An upper value of S

$$S\{\geq j\} = S\{j, j+1, \dots, M\} = \bigvee_{i=j}^M S\{i\}. \quad (8.11)$$

(continued)

Symbol Description

 $S\{\leq j\}$ A lower value of S

$$S\{\leq j\} = S\{0, 1, \dots, j\} = \bigvee_{i=0}^j S\{i\}. \quad (8.12)$$

Instances, upper values, and lower values of S are related by

$$S\{j\} = S\{\geq j\} \quad S\{< (j+1)\} = S\{\geq j\} \quad \bar{S}\{\geq (j+1)\} = S\{\leq j\} \quad S\{> (j-1)\}. \quad (8.13)$$

8.2.3 Nomenclature**8.2.3.1 A vector X**

- A specific value of the input arguments $X = [X_1 \ X_2 \ \dots \ X_n]^T$ of the multivalued structure function S ;
- A particular cell of the MVKM of S or the binary Karnaugh map of any of its instances $S\{j\}$, upper values $S\{\geq j\}$, or lower values $S\{\leq j\}$.

8.2.3.2 An upper vector for level $j > 0$

- A particular value of X such that $S(X) \geq j$, $\{j = 1, 2, \dots, M\}$;
- A true vector for $S\{\geq j\}$, that is, a vector such that $S\{\geq j\} = 1$, $\{j = 1, 2, \dots, M\}$;
- A map cell for system success at level j , $\{j = 1, 2, \dots, M\}$.

8.2.3.3 A minimal upper vector at level $j > 0$, denoted θ_{ji}

An upper vector X for level j such that $S(Y) < j$, $\{j = 1, 2, \dots, M\}$ for any vector $Y < X$. Such a vector is a member of the set of MUVs at level $j > 0$, denoted by $\theta(j)$.

8.2.3.4 An upper prime implicant at level $j > 0$, denoted P_{ji}

- The set of upper vectors X for level j $\{1 \leq j \leq M\}$ such that

$$\theta_{ji} \leq X \leq U.$$

- The loop P_{ji} in the $S\{\geq j\}$ map whose cells are not lower than θ_{ji} ;

$$P_{ji} = \bigwedge_{k=1}^n X_k \{ \geq \theta_{ji}(k) \}, \quad (8.14)$$

$$S\{ \geq j \} = \bigvee_i P_{ji}. \quad (8.15)$$

8.2.3.5 The all-highest vector U

$$U = [m_1 \quad m_2 \quad \dots \quad m_n]^T$$

The vector where each input argument attains its highest value

This vector belongs to each of the upper prime implicants at all levels, that is, to P_{ji} for all i and all $j > 0$. Due to causality, the structure function must attain its maximum when $X = U$, that is, $S(U) = M$.

8.2.3.6 A lower vector for level $j < M$

- A particular value of X such that $S(X) \leq j$, $\{j = 0, 1, \dots, (M-1)\}$;
- A true vector for system failure $S\{ \leq j \}$, that is, a vector such that $S\{ \leq j \} = 1$, $\{j = 0, 1, \dots, (M-1)\}$;
- A false vector for $S\{ > j \} = S\{ \geq (j+1) \}$, $j = 0, 1, \dots, (M-1)$;
- A map cell for system failure at level j $\{j = 1, 2, \dots, M\}$.

8.2.3.7 A maximal lower vector at level $j < M$, denoted σ_{ji}

A lower vector X for level j such that $S\{Y\} > j$, $\{j = 1, 2, \dots, M\}$ for any vector $Y > X$. Such a vector is a member of the set of MLVs at level $j < M$, denoted by $\sigma(j)$.

8.2.3.8 A lower prime implicant at level $j < M$, denoted Q_{ji}

- The set of lower vectors X for level j $\{0 \leq j \leq (M-1)\}$ such that

$$L \leq X \leq \sigma_{ji}.$$

- The loop in the $S\{ \leq j \}$ map whose cells are not higher than σ_{ji} ;

$$Q_{ji} = \bigwedge_{k=1}^n X_k \{ \leq \sigma_{ji}(k) \},$$

$$S\{ \leq j \} = \bigvee_i Q_{ji}. \quad (8.17)$$

8.2.3.9 The all-lowest vector L

The vector where each input argument attains its lowest value

$$L = [0 \quad 0 \quad \dots \quad 0]^T. \quad (8.18)$$

This vector belongs to all lower prime implicants at all levels, that is, to Q_{ji} for all i and all $j \in \{1, \dots, M\}$. Due to causality, the structure function attains its minimum when $X = L$, that is, $S(L) = 0$.

8.2.3.10 The expected value of a certain instance $S\{j\}$

The expected value of a certain instance $S\{j\}$ of S , $\{j = 0, 1, \dots, M\}$

$$E\{S\{j\}\} = E\{S\{\geq j\}\} - E\{S\{\geq (j+1)\}\} = E\{S\{\leq j\}\} - E\{S\{\leq (j-1)\}\}, \quad (8.19a)$$

where

$$E\{S\{\geq (M+1)\}\} = 0, \quad (8.19b)$$

$$E\{S\{\leq (-1)\}\} = 0, \quad (8.19c)$$

$$E\{S\{\geq 0\}\} = 1, \quad (8.19d)$$

$$E\{S\{\leq M\}\} = 1. \quad (8.19e)$$

The availability of two formulas for $E\{S\{j\}\}$ allows us to select the formula that is better in some sense (easier to derive, more compact to express, etc.). Otherwise, we might evaluate both formulas and check that they agree. Both sets of formulas $\{(8.19a), (8.19b), (8.19d)\}$ and formulas $\{(8.19a), (8.19c), (8.19e)\}$ confirm the arithmetic normality property

$$\sum_{j=0}^M E\{S\{j\}\} = 1. \quad (8.20)$$

8.2.3.11 The probability transform

The expectation $E\{.. \}$ of any logic expression (binary or multivalued) might be obtained through a probability-transform operation [32, 33]. An expression for $E\{S\}$ is a multi-affine function in its arguments (an algebraic function depicting a straight line relation in each of the arguments), and this expression has the same “truth table” as that of the logic function S [33]. Despite the different mathematical natures of S and $E\{S\}$, they are both of a multi-affine structure, and they have “truth tables” of exactly the same entries.

8.2.3.12 Multistate interpretation of binary systems

For a binary system ($M = 1$), there is a single level other than level 0, namely level 1. In this case, success at level 1 is $S\{\geq 1\} = S\{1\}$, while failure at level 1 is $S\{< 1\} = S\{0\}$. In the binary case, there is no need to refer to level 1 since it is the only non-zero level and is implicitly understood by default, and we simply refer to system success and system failure \bar{S} instead of $S\{1\}$ and $S\{0\}$.

8.3 Boolean quotients

The concept of a Boolean quotient is an important switching-algebraic concept that can be conveniently viewed in a multivalued context [29]. Given a two-valued Boolean function (a switching function) f and a term t , the Boolean quotient of f with respect to t , denoted by (f/t) , is defined to be the function formed from f by imposing the constraint $\{t = 1\}$ explicitly [33, 34], namely

$$f/t = [f]_{t=1}. \quad (8.21)$$

In the multivalued context, the term t is a product (ANDing) of literals. Each of the multivalued variables is either absent or present in the form of a particular literal, which might be a single instance or the ORing of several instances. A fundamental property of the Boolean quotient states that a term ANDed with a function is equal to the term ANDed with the Boolean quotient of the function with respect to the term, namely

$$t \wedge f = t \wedge (f/t). \quad (8.22)$$

If the term t is a factor of the function f (i.e., $f = t \wedge g$, $t \wedge f = f$), then (8.22) takes the simpler form

$$f = t \wedge (f/t). \quad (8.23)$$

We denote a Boolean quotient by an inclined slash (f/t) . However, it is possible to denote it by a vertical bar $(f|t)$ to stress the equivalent meaning (borrowed from conditional probability) of f conditioned by t or given t [29].

8.4 Probability-ready expressions

The concept of a PRE is well known in the two-valued logical domain [33], and it is still valid for the multivalued logical domain [28–31]. A PRE is a random expression that can be directly transformed, on a one-to-one basis, to its statistical expectation (its probability of being equal to 1) by replacing all logic variables by their statistical

expectations, and also replacing logical multiplication and addition (ANDing and ORing) by their arithmetic counterparts. A logic expression is a PRE if

- a) all *O*Red products (terms formed by ANDing) are *disjoint* (*mutually exclusive*), and
- b) all *AN*Ded sums (alterms formed via ORing) are *statistically independent*.

Condition (a) is satisfied if for every pair of *O*Red terms, there is at least a single opposition, that is, there is at least one variable that appears with a certain set of instances in one term and appears with a complementary set of instances in the other. Condition (b) is satisfied if for every pair of *AN*Ded alterms (sums of disjunctions of literals), one alterm involves variables describing a certain set of components, while the other alterm depends on variables describing a set of different components (under the assumption of independence of components). While there are many methods to introduce characteristic (a) of orthogonality (disjointness) into a Boolean expression [29–33], there is no way to induce characteristic (b) of statistical independence. The best that one can do is to observe statistical independence when it exists, and then be careful not to destroy or spoil it, but instead try to take advantage of it. Since we have the freedom of handling a problem from a success or a failure perspective, a choice should be made as to which of the two perspectives can more readily produce a more-compact PRE form. It is better to look at success for a system of no or poor redundancy (a series or almost-series system), and to view failure for a system of full or significant redundancy (a parallel or almost-parallel system) [33].

The introduction of orthogonality might be achieved as follows. We now assume that neither of the two terms A and in the sum $(A \vee B)$ subsumes the other ($A \vee B \neq A$ and $A \vee B \neq B$) and the two terms are not disjoint ($A \wedge B \neq 0$). We further assume that the literals Y_k ($1 \leq k \leq e$) belong to A but do not belong to B . Then, we write $(A \vee B)$ as [30]

$$A \vee B = A \vee B (\bar{Y}_1 \vee Y_1 \bar{Y}_2 \vee Y_1 Y_2 \bar{Y}_3 \vee \cdots \vee Y_1 Y_2 \cdots Y_{e-1} \bar{Y}_e). \quad (8.24)$$

Each literal Y_k in (8.24) stands for a disjunction of certain instances of some variable $X_{i(k)}$ and hence \bar{Y}_k is a disjunction of the complementary instances of the same variable. As a result of (8.24), the first term A remains intact, while the second term B is replaced by e terms which are each disjoint with A and are also disjoint among themselves. This means that one has a choice of either disjointing B with A in $A \vee B$, or disjointing A with B in $B \vee A$. The usual (greedy) practice that is likely to yield good results is to order the terms in a given disjunction so that those with fewer literals appear earlier.

8.5 The Boole–Shannon expansion

The most effective way for converting a Boolean formula into a PRE form is the Boole–Shannon expansion, which takes the following form in the two-valued case [28–31, 33, 35]

$$f(X) = (\bar{X}_i \wedge f(X|0_i)) \vee (X_i \wedge f(X|1_i)). \quad (8.25)$$

This Boole–Shannon expansion expresses a (two-valued) Boolean function $f(X)$ in terms of its two subfunctions $f(X|0_i)$ and $f(X|1_i)$. These subfunctions are equal to the Boolean quotients $f(X)/\bar{X}_i$ and $f(X)/X_i$, and hence are obtained by restricting X_i in the expression of $f(X)$ to 0 and 1, respectively. If $f(X)$ is a function of n variables, the two subfunctions $f(X|0_i)$ and $f(X|1_i)$ are functions of most $(n-1)$ variables. A multivalued extension of (8.25) is

$$\begin{aligned} S(X) &= X_i\{0\} \wedge (S(X)/X_i\{0\}) \vee X_i\{1\} \wedge (S(X)/X_i\{1\}) \vee X_i\{2\} \\ &\quad \wedge (S(X)/X_i\{2\}) \vee \cdots \vee X_i\{m_i\} \wedge (S(X)/X_i\{m_i\}). \quad (8.26) \\ &\quad \wedge (S(X)/X_i\{2\}) \vee \cdots \vee X_i\{m_i\} \wedge (S(X)/X_i\{m_i\}). \end{aligned}$$

A formal proof of (8.31) is achieved by “perfect induction” [30]. The expansion (8.26) might be viewed as a justification of the construction of the MVKM used herein. This expansion transforms directly, on a one-to-one basis, to the probability domain as

$$\begin{aligned} E\{S(X)\} &= E\{X_i\{0\}\} * E\{S(X)/X_i\{0\}\} \\ &\quad + E\{X_i\{1\}\} * E\{S(X)/X_i\{1\}\} + E\{X_i\{2\}\} \\ &\quad * E\{S(X)/X_i\{2\}\} + \cdots + E\{X_i\{m_i\}\} * E\{S(X)/X_i\{m_i\}\}. \quad (8.27) \end{aligned}$$

Equation (8.27) might be viewed as a restatement of the total probability theorem, provided we interpret the expectation of a Boolean quotient as a conditional probability [33, 36]. It is the basis of multivalued decision diagrams, that are optimally employed for the reliability analysis of MSSs [30], and that constitute the multivalued counterpart of the binary decision diagrams [35].

8.6 A non-homogeneous non-binary-imaged two-variable example

This example is taken from one of the best available textbooks on multistate reliability [1], wherein the example is solved via techniques borrowed from the theory of discrete functions [2]. The solution given by Lisnianski and Levitin [1] handles discrete functions reasonably, but then seeks probability expressions through

effectively using the inclusion–exclusion (IE) principle, which is notorious for its poor computational complexity and its production of prohibitively long reliability expressions that result in exaggerated round-off errors [37, 38]. The solution presented herein avoids the IE shortcomings through the derivation of a PRE while still in the Boolean domain. Not only is the solution procedure much simpler and more intuitive than any standard solution, such as the one given by Lisnianski and Levitin [1], but the final expressions obtained are much more compact as well. Though the current system lacks a binary image, most of its analysis herein deals solely with binary entities such as $S\{\geq j\}$, $S\{\leq j\}$, and $S\{j\}$. The ultimate goal of the analysis is to obtain $E\{S\{j\}\}$ for $j = 0, 1, \dots, M$, which might be conveniently obtained through the analysis of $S\{\leq j\}$. It is only toward the end of this section that we deal explicitly with the multivalued S rather than with its binary instances.

The system considered in this example is a non-homogeneous one specified by the function table of its structure or success function $S(X)$

$$S: \{0, 1, 2, 3, 4\} \times \{0, 1, 2, 3\} \rightarrow \{0, 1, 2, 3\}. \quad (8.28)$$

This function table is shown in Figure 8.1, and is conveniently identified to be in the form of a MVKM. All entries of this map are explicitly given, but this is a superfluous representation of this coherent structure function, since it suffices to specify either (a)

X_1	0	1	2	3	4	
	0	0	1	1	2	0
	0	0	1	2	2	1
	0	2	2	2	2	2
	1	2	2	3	3	3
						X_2

$S(X_1, X_2)$

Figure 8.1: Multivalued Karnaugh map (MVKM) representing the structure function of the coherent multistate system of Section 8.6. The function is completely specified by either (a) the cells with blue bold entries (called minimal upper vectors) or (b) the cells with red bold entries (called maximal lower vectors). Note that the cell (0, 3) belongs to both sets in (a) and (b), and hence it is distinguished in violet (i.e., a mixture of blue and red).

the bold entries in the cells with blue color (the MUVs), or (b) the bold entries in the cells with red color (MLVs), where the cell (0, 3) belongs to both sets in (a) and (b).

The following set of equations is a complete non-binary-image characterization of the system under study. They are obtained from Figures 8.2(a), 8.3(a), and 8.4(a), respectively, and they give each binary function $S\{\geq j\}$ (for $j = 3, 2$, and 1), as a function of X in general (and not necessarily in terms of $X\{\geq j\}$ (for $j = 3, 2$, and 1) alone). Here, $S\{\geq j\}$ depicts system success at level j (upper states) in a minimal sum-of-products form

$$S\{\geq 3\} = X_1\{\geq 3\} X_2\{\geq 3\}, \quad (8.29a)$$

$$S\{\geq 2\} = X_1\{\geq 1\} X_2\{\geq 2\} \vee X_1\{\geq 3\} X_2\{\geq 1\} \vee X_1\{\geq 4\} X_2\{\geq 0\}, \quad (8.29b)$$

$$S\{\geq 1\} = X_1\{\geq 2\} \vee X_2\{\geq 3\} \vee X_1\{\geq 1\} X_2\{\geq 2\}. \quad (8.29c)$$

The MUVs at levels $j \{j=3, 2, \text{ and } 1\}$ can be observed (as minimal cells of upper loops) from Figures 8.2(a), 8.3(a), and 8.4(a), respectively, or deduced, through immediate inspection, from eqs. (8.29) as $\theta(3) = \{(3, 3)\}$, $\theta(2) = \{(1, 2), (3, 1), (4, 0)\}$, $\theta(1) = \{(2, 0), (0, 3), (1, 2)\}$. We reiterate that there exists a subtle difference between an MUV at a certain level and a corresponding prime implicant of success (minimal path) at that level, despite the existence of a one-to-one relation between them. In fact, a minimal path constitutes all the upper vectors extending (inclusively) from a particular MUV to the all-highest vector.

Similarly, the following set of eqs. (8.30) is another complete non-binary-image characterization of the system under study. They are obtained either from Figures 8.2(b), 8.3(b), and 8.4(b), respectively, or by complementation and application of De Morgan's rules to the former eq. (8.29). The new equations give each binary function $S\{\leq (j-1)\}$ (for $j=3, 2, \text{ and } 1$), as a function of X in general (and not necessarily in terms of $X\{\leq (j-1)\}$ (for $j=3, 2, \text{ and } 1$ alone) Here, $S\{< j\} = S\{\leq (j-1)\}$ depicts system failure at level j (lower states), again in a minimal sum-of-products form:

$$S\{< 3\} = S\{\leq 2\} = X_1\{\leq 2\} \vee X_2\{\leq 2\}, \quad (8.30a)$$

$$S\{< 2\} = S\{\leq 1\} = X_1\{\leq 0\} \vee X_1\{\leq 2\} X_2\{\leq 1\} \vee X_1\{\leq 3\} X_2\{\leq 0\}, \quad (8.30b)$$

$$S\{< 1\} = S\{\leq 0\} = X_1\{\leq 0\} X_2\{\leq 2\} \vee X_1\{\leq 1\} X_2\{\leq 1\}. \quad (8.30c)$$

The MLVs at level $j \{j=2, 1, \text{ and } 0\}$ can be observed (as maximal cells of lower loops) from Figures 8.2(b), 8.3(b), and 8.4(b), respectively, or deduced, through immediate inspection, from eq. (8.30) as $\sigma(2) = \{(2, 3), (4, 2)\}$, $\sigma(1) = \{(0, 3), (2, 1), (3, 0)\}$, $\sigma(0) = \{(0, 2), (1, 1)\}$. We observe that there exists also a minor difference between a MLV at a certain level and a corresponding prime implicant of failure (minimal cutset) at that level, despite the fact that each of them uniquely specifies the other. In fact, a minimal cutset constitutes all the lower vectors extending (inclusively) from the all-0 vector to the corresponding MLV. The fact that this system is non-binary-imaged is reflected in that the set $\sigma(j)$ contains members with elements other than j and the maximal elements $m_1 = 4$ and $m_2 = 3$.

Now, we replace the success expressions by PREs by using the algebraic procedure in Section 8.4, or by replacing the loops in Figures 8.2(a), 8.3(a), and 8.4(a), respectively, with non-overlapping loops. These PREs can be readily converted (on a one-to-one basis) into expected values by replacing the logical ORing and ANDing by arithmetic counterparts of addition and multiplication and replacing component instances by their expected values (see Table 8.1)

X_1	0	1	2	3	4	
						0
						1
						2
				1	1	3
						X_2

$$\{a\} S\{\geq 3\} = S\{3\} = X_1\{\geq 3\}X_2\{\geq 3\}$$

X_1	0	1	2	3	4	
	1	1	1	1	1	0
	1	1	1	1	1	1
	1	1	1	1	1	2
	1	1	1			3
						X_2

$$\{b\} S\{< 3\} = S\{0,1,2\} = S\{0\} \vee S\{1\} \vee S\{2\} = S\{\leq 2\} = X_1\{\leq 2\} \vee X_2\{\leq 2\}$$

Figure 8.2: Conventional Karnaugh maps (CKMs) for (a) success at level 3, and (b) failure at level 3 for the system of Section 8.6. Cells of bold entries denote the minimal upper vector at level 3: $\theta(3) = \{(3, 3)\}$ and the maximal lower vectors at level 2: $\sigma(2) = \{(2, 3), (4, 2)\}$.

X_1	0	1	2	3	4	
					1	0
				1	1	1
		1	1	1	1	2
		1	1	1	1	3
						X_1

$$\{a\} S\{\geq 2\} = S\{2\} \vee S\{3\} = X_1\{\geq 1\}X_2\{\geq 2\} \vee X_1\{\geq 3\}X_2\{\geq 1\} \vee X\{\geq 4\}X\{\geq 0\}$$

X_1	0	1	2	3	4	
	1	1	1	1		0
	1	1	1			1
	1					2
	1					3
						X_2

$$\{b\} S\{< 2\} = S\{\leq 1\} = S\{0,1\} = S\{0\} \vee S\{1\} = X\{\leq 0\} \vee X_1\{\leq 2\}X_2\{\leq 1\} \vee X_1\{\leq 3\}X_2\{\leq 0\}$$

Figure 8.3: Conventional Karnaugh maps (CKMs) for (a) success at level 2, and (b) failure at level 2. Cells of bold entries in (a) denote the minimal upper vectors at level 2: $\theta(2) = \{(1, 2), (3, 1), (4, 0)\}$, and those in (b) depict the maximal lower vectors at level 1: $\sigma(1) = \{(0, 3), (2, 1), (3, 0)\}$.

$$S_{\text{PRE}}\{\geq 3\} = X_1\{\geq 3\} X_2\{\geq 3\}, \quad (8.31a)$$

$$\begin{aligned} S_{\text{PRE}}\{\geq 2\} &= X_1\{\geq 4\} \vee X_1\{< 4\}(X_1\{\geq 1\}X_2\{\geq 2\} \vee (X_1\{< 1\} \\ &\vee X_1\{\geq 1\}X_2\{< 2\})X_1\{\geq 3\} X_2\{\geq 1\}) = X_1\{4\} \vee X_1\{1, 2, 3\} X_2\{\geq 2\} \vee X_1\{3\} X_2\{1\}, \end{aligned} \quad (8.31b)$$

$$\begin{aligned} S_{\text{PRE}}\{\geq 1\} &= X_1\{\geq 2\} \vee X_1\{< 2\}(X_2\{\geq 3\} \vee X_2\{< 3\}X_1\{\geq 1\}X_2\{\geq 2\}) \\ &= X_1\{\geq 2\} \vee X_1\{< 2\}X_2\{\geq 3\} \vee X_1\{1\}X_2\{2\}. \end{aligned} \quad (8.31c)$$

Next, we replace the failure expressions by PREs by using the algebraic procedure in Section 8.4, or by replacing the loops in Figures 8.2(b), 8.3(b), and 8.4(b), respectively, with non-overlapping loops. Again, these PREs can be readily converted (on a one-to-one basis) into expected values by replacing the logical ORing and ANDing by arithmetic counterparts of addition and multiplication and replacing component instances by their expected values (see Table 8.1)

$$S_{\text{PRE}}\{\leq 2\} = X_1\{\leq 2\} \vee X_1\{> 2\} X_2\{\leq 2\}, \quad (8.32a)$$

$$\begin{aligned} S_{\text{PRE}}\{\leq 1\} &= X_1\{0\} \vee X_1\{> 0\}(X_1\{\leq 2\}X_2\{\leq 1\} \vee (X_1\{> 2\} \\ &\quad \vee X_1\{\leq 2\}X_2\{> 1\})X_1\{\leq 3\}X_2\{\leq 0\}) \\ &= X_1\{0\} \vee X_1\{1, 2\}X_2\{\leq 1\} \vee X_1\{3\}X_2\{0\}, \end{aligned} \quad (8.32b)$$

$$\begin{aligned} S_{\text{PRE}}\{\leq 0\} &= X_1\{\leq 1\}X_2\{\leq 1\} \vee (X_1\{> 1\} \vee X_1\{\leq 1\}X_2\{> 1\}) \\ &\quad X_1\{\leq 0\}X_2\{\leq 2\} = X_1\{\leq 1\}X_2\{\leq 1\} \vee X_1\{0\}X_2\{2\}. \end{aligned} \quad (8.32c)$$

As stated earlier, the PRE expressions (8.31) and (8.32) can be directly converted to their expected values by replacing the AND and OR operators with the multiplication and addition operators and replacing variable instances by their expectations, namely

$$E\{X_i\{j\}\} = p_{ij}, \quad (8.33)$$

$$E\{X_i\{\geq j\}\} = p_{ij} + p_{i(j+1)} + \cdots + p_{im_i} = 1 - (p_{i0} + p_{i1} + \cdots + p_{i(j-1)}), \quad (8.34)$$

$$E\{X_i\{\leq j\}\} = p_{i0} + p_{i1} + \cdots + p_{ij} = 1 - (p_{i(j+1)} + p_{i(j+2)} + \cdots + p_{im_i}). \quad (8.35)$$

We obtain expectations $E\{S\{j\}\}$ for $j = 0, 1, \dots, M$, of various instances of the multivalued system success S , by taking differences via (8.19) of appropriate expectations of the forms of $E\{S\{\geq j\}\}$ and $E\{S\{\leq j\}\}$. Table 8.1 demonstrates the two possible alternatives for achieving this purpose. Of course, the more compact alternative is preferable.

To close this section, we note that we have so far used binary representations only to deal with the discrete multivalued function $S(X)$. According to discrete-function theory [1, 2, 30], this function should be expressed in a minimal sum-of-products form as

$$S = 0 \ S\{\geq 0\} \vee 1 \ S\{\geq 1\} \vee 2 \ S\{\geq 2\} \vee 3 \ S\{\geq 3\}, \quad (8.36)$$

where $(A \vee B)$ denotes the maximum value of A and B , and the binary expressions $S\{\geq 1\}$, $S\{\geq 2\}$, and $S\{\geq 3\}$ are given by their minimal sum-of-products forms in (8.29).

X_1	0	1	2	3	4	
			1	1	1	0
			1	1	1	1
		1	1	1	1	2
1	1	1	1	1	1	3
						X_2

$$\begin{aligned}\{a\} S \{ \geq 1 \} &= S \{ 1, 2, 3 \} = S \{ 1 \} \vee S \{ 2 \} \vee S \{ 3 \} \\ &= X_1 \{ \geq 2 \} \vee X_2 \{ \geq 3 \} \vee X_1 \{ \geq 1 \} X_2 \{ \geq 2 \}\end{aligned}$$

X_1	0	1	2	3	4	
	1	1				0
	1	1				1
	1					2
						3
						X_2

$$\{b\} S \{ < 1 \} = S \{ \leq 0 \} = X_1 \{ \leq 0 \} X_2 \{ \leq 2 \} \vee X_1 \{ \leq 1 \} X_2 \{ \leq 1 \}.$$

Figure 8.4: Conventional Karnaugh maps (CKMs) for (a) success at level 1, and (b) failure at level 1. Cells of bold entries denote the minimal upper vectors at level 1: $\theta(1) = \{(2, 0), (0, 3), (1, 2)\}$ and the maximal lower vectors at level 0: $\sigma(0) = \{(0, 2), (1, 1)\}$. The vector $(1, 2)$ is a minimal upper vector for both levels 1 and 2.

The overall minimality in (8.36) relies in the inclusion relations among these expressions

$$S \{ \geq 1 \} \geq S \{ \geq 2 \} \geq S \{ \geq 3 \}. \quad (8.37)$$

Despite the convenience of minimality offered by (8.36), it is not adequate for producing an expectation, since it has non-disjoint terms. A simpler and more convenient expression for $S(X)$ is the pseudo-Boolean expression [35, 39, 40]

$$S = 1 S \{ 1 \} + 2 S \{ 2 \} + 3 S \{ 3 \}, \quad (8.38)$$

which has the corresponding expected value (thanks to the fact that expectation of an arithmetic sum is the arithmetic sum of expectations)

$$E\{S\} = 1 E\{S \{ 1 \}\} + 2 E\{S \{ 2 \}\} + 3 E\{S \{ 3 \}\}. \quad (8.39)$$

The expected value of S lies in the interval $[0, M] = [0, 3]$, and is a weighted sum of the expectations of its instances, which, in turn, are expressed as in Table 8.1.

MUV (2, 2, 0). For this binary-imaged system, elements of $\theta(j)$ are vectors of 0 or 1 components only. Equation (8.40) might be rewritten with the symbols $\{<3\}$, $\{<2\}$, and $\{<1\}$ replaced by $\{\leq 2\}$, $\{\leq 1\}$, and $\{\leq 0\}$, namely

$$S\{\leq 2\} = X_1\{\leq 2\} \vee X_2\{\leq 2\} \vee X_3\{\leq 2\}, \quad (8.42a)$$

$$S\{\leq 1\} = X_1\{\leq 1\}X_2\{\leq 1\} \vee X_1\{\leq 1\}X_3\{\leq 1\} \vee X_2\{\leq 1\}X_3\{\leq 1\}, \quad (8.42b)$$

$$S\{\leq 0\} = X_1\{\leq 0\}X_2\{\leq 0\}X_3\{\leq 0\}. \quad (8.43a)$$

Now, eq. (8.42) (with the \leq notation) tells us that the MLVs are $\sigma(2) = \{(2, 3, 3), (3, 2, 3), (3, 3, 2)\}$, $\sigma(1) = \{(1, 1, 3), (1, 3, 1), (3, 1, 1)\}$, $\sigma(0) = \{(0, 0, 0)\}$. By contrast to the case of the MUVs in which an absent variable X_i stands for $X_i\{\geq 0\}$ and is expressed by 0 in the MUV, the present case of MLUs has an absent variable X_i standing for $X_i\{\leq 3\}$ and being expressed by 3 in the MLU. For this binary-imaged system, elements of $\sigma(j)$ are vectors of j or 3 components only. Figure 8.5 displays a MVKM representing the structure function of the present coherent multistate system. The function is completely specified by either (a) the cells with bold blue entries, which are the MUVs, or (b) the cells with bold red entries, which are the MUVs. Figure 8.6 displays three conventional Karnaugh maps (CKMs) for the binary successes at levels 3, 2, and 1, respectively, while Figure 8.7 shows CKMs for the binary failures at levels 1, 2, and 3, respectively. Equations (8.40) can be converted to PREs via the procedure in Section 8.4

$$S_{\text{PRE}}\{\geq 3\} = X_1\{\geq 3\}X_2\{\geq 3\}X_3\{\geq 3\}, \quad (8.43a)$$

$$S_{\text{PRE}}\{\geq 2\} = X_1\{\geq 2\}X_2\{\geq 2\} \vee X_1\{\geq 2\}X_2\{<2\}X_3\{\geq 2\} \vee X_1\{<2\}X_2\{\geq 2\}X_3\{\geq 2\}, \quad (8.43b)$$

$$S_{\text{PRE}}\{\geq 1\} = X_1\{\geq 1\} \vee X_1\{<1\}(X_2\{\geq 1\} \vee X_2\{<1\}X_3\{\geq 1\}). \quad (8.43c)$$

Likewise, eq. (8.42) can be converted to PREs via the procedure in Section 8.4

$$S_{\text{PRE}}\{\leq 2\} = X_1\{\leq 2\} \vee X_1\{>2\}(X_2\{\leq 2\} \vee X_2\{>2\}X_3\{\leq 2\}), \quad (8.44a)$$

$$S_{\text{PRE}}\{\leq 1\} = X_1\{\leq 1\}X_2\{\leq 1\} \vee X_1\{\leq 1\}X_2\{>1\}X_3\{\leq 1\} \vee X_1\{>1\}X_2\{\leq 1\}X_3\{\leq 1\}, \quad (8.44b)$$

$$S_{\text{PRE}}\{\leq 0\} = X_1\{\leq 0\}X_2\{\leq 0\}X_3\{\leq 0\}. \quad (8.44c)$$

8.8 Conclusions

This chapter utilizes algebraic and map tools for the reliability characterization and analysis of general multistate non-repairable coherent systems, with independent non-identical components. The chapter presents switching-algebraic expressions of

both system success and system failure at each non-zero level. These expressions are given as minimal sum-of-products formulas or as PREs. The chapter also utilizes a convenient map representation via the MVKM for the system structure function S , or via M maps of binary entries and multivalued inputs representing the success/failure at every non-zero level of the system. Further system characterizations are also given in terms of MUVs or MUVs. Great emphasis is placed on making a minimal departure from binary concepts and techniques, while taking care to clarify novel issues that emerged due to generalizations introduced by the multistate model.

A forthcoming sequel of the present work aims to adapt Boolean-based multistate techniques from main-stream reliability theory so as to handle a classical problem of ecology, namely that of survivability (of a species), defined here as the probability of successful migration of a certain organism escaping from critical source habitat patches and seeking refuge in specific destination habitat patches via heterogeneous deletable ecological corridors, possibly with uninhabitable stepping stones en route [41, 42]. This problem might be reformulated in celebrated ecology contexts other than that of migration, including those of: (a) dynamics of metapopulations, colonization, or invasion; (b) gene flow; (c) spread of infectious diseases, epidemics, or pandemics; and (d) energy transfer within food webs [43]. Binary solutions for this problem are already available [41–43], but a more powerful multistate model for it is being sought.

References

- [1] Lisnianski, A. & Levitin, G. 2003. *Multi-state System Reliability: Assessment, Optimization and Applications*, World scientific Publishing Company, DOI: 10.1142/5221.
- [2] Davio, M., Thayse, A. & Deschamps, J. P. *Discrete and Switching Functions*, McGraw-Hill, 1978.
- [3] Clarke, E. M., Fujita, M. & Zhao, X. Multi-terminal binary decision diagrams and hybrid decision diagrams, In: Sasao, T. & Fujita, M., Editors *Representations of Discrete Functions*, Springer, Boston, MA, 1996, 93–108.
- [4] Allen, C. M. & Givone, D. D. 1968. A minimization technique for multiple-valued logic systems, *IEEE Transactions on Computers*, C-17(2), 182–184. 10.1109/TC.1968.227407.
- [5] Rescher, N. *Many-Valued Logic*, McGraw Hill Book Co, New York, 1969.
- [6] Rine, D. C., Editors, *Computer Science and Multiple-Valued Logic Theory and Applications*, North Holland Publishing Company, 1977.
- [7] Vranesic, Z. G. 1977. Multiple-valued logic: An introduction and overview, *IEEE Transactions on Computers*, C-26(12), 1181–1182. 10.1109/TC.1977.1674778.
- [8] Tapia, M. A., Guima, T. A. & Katbab, A. 1991. Calculus for a multivalued-logic algebraic system, *Applied Mathematics and Computation*, 42(3), 255–285.
- [9] Urquhart, A. Basic Many-Valued Logic, In: Gabbay, D. M. & Guenther, F., Editors, *Handbook of Philosophical Logic*, Springer, Dordrecht, 2001, 249–295, DOI: 10.1093/logcom/exaa036.
- [10] Miller, D. M. & Thornton, M. A. *Multiple Valued Logic: Concepts and Representations*, San Rafael, CA, Morgan & Claypool Publishers, 2008, 10.2200/S00065ED1V01Y200709DCS012.
- [11] Shrestha, A., Xing, L. & Dai, Y. 2009. Decision diagram based methods and complexity analysis for multi-state systems, *IEEE Transactions on Reliability*, 59(1), 145–161.

- [12] Stanković, R. S., Astola, J. T. & Moraga, C. 2012. Representation of multiple-valued logic functions, *Synthesis Lectures on Digital Circuits and Systems*, 7(2), 1–168. 10.2200/S00420ED1V01Y201205DCS037.
- [13] Zaitseva, E. & Levashenko, V. 2013. Multiple-valued logic mathematical approaches for multi-state system reliability analysis, *Journal of Applied Logic*, 11(3), 350–362.
- [14] Ram, M. 2013. On system reliability approaches: a brief survey, *International Journal of System Assurance Engineering and Management*, 4(2), 101–117.
- [15] Davis, P. C., Thornton, M. A. & Manikas, T. W. Reliability block diagram extensions for non-parametric probabilistic analysis. In 2016 Annual IEEE Systems Conference (SysCon) 2016 (pp. 1–6), DOI: 10.1109/SYSCON.2016.7490656.
- [16] Meenakshi, S. S. B. 2017. Reliability analysis of multi-state complex system having two multi-state subsystems under uncertainty, *Journal of Reliability and Statistical Studies*, 10(1), 161–177.
- [17] Lisnianski, A., Frenkel, I. & Karagrigoriou, A., Editors, *Recent Advances in Multi-State Systems Reliability: Theory and Applications*, Springer, 2017.
- [18] Rushdi, A. M. 2018. Utilization of Karnaugh maps in multi-value qualitative comparative analysis, *International Journal of Mathematical, Engineering and Management Sciences*, 3(1), 28–46.
- [19] Rushdi, R. A. & Rushdi, A. M. 2018. Karnaugh-map utility in medical studies: The case of Fetal Malnutrition, *International Journal of Mathematical, Engineering and Management Sciences*, 3(3), 220–244.
- [20] Meenkashi, K., Singh, S. B. & Kumar, A. 2019. Reliability analysis of multi-state complex system with multi-state weighted subsystems, *International Journal of Quality & Reliability Management*, 36(4), 552–568.
- [21] Rushdi, A. M. & Al-Amoudi, M. A. 2019. Reliability analysis of a multi-state system using multi-valued logic, *IOSR Journal of Electronics and Communication Engineering (IOSR-JECE)*, 14(1), 1–10.
- [22] Rushdi, A. M. & Alsayegh, A. B. 2019. Reliability analysis of a commodity-supply multi-state system using the map method, *Journal of Advances in Mathematics and Computer Science*, 31(2), 1–17. 10.9734/jamcs/2019/v31i230107.
- [23] Pascual-Ortigosa, P., Sáenz-de-cabezón, E. & Wynn, H. P. 2019. Algebraic algorithms for the reliability analysis of multi-state k-out-of-n systems, *ACM Communications in Computer Algebra*, 53(3), 146–149.
- [24] Rushdi, A. M., AlHuthali, S. A., AlZahrani, N. A. & Alsayegh, A. B. 2020. Reliability Analysis of Binary-Imaged Generalized Multi-State k-out-of-n Systems, *International Journal of Computer Science and Network Security (IJCSNS)*, 20(9), 251–264. 10.22937/IJCSNS.2020.20.09.30.
- [25] Wood, A. P. 1985. Multistate block diagrams and fault trees, *IEEE Transactions on Reliability*, 34(3), 236–240. 10.1109/TR.1985.5222131.
- [26] Janan, X. 1985. On multistate system analysis, *IEEE Transactions on Reliability*, 34(4), 329–337. 10.1109/TR.1985.5222178.
- [27] Huang, J. & Zuo, M. J. 2004. Dominant multi-state systems, *IEEE Transactions on Reliability*, 53(3), 362–368. DOI: 10.1109/TR.2004.833311.
- [28] Rushdi, A. M. & Al-Amoudi, M. A. 2018. Switching-algebraic analysis of multi-state system reliability, *Journal of Engineering Research and Reports*, 3(3), 1–22. 10.9734/jerr/2018/v3i316877.
- [29] Rushdi, A. M. 2019. Utilization of symmetric switching functions in the symbolic reliability analysis of multi-state k-out-of-n systems, *International Journal of Mathematical, Engineering and Management Sciences*, 4(2), 306–326.
- [30] Rushdi, A. M. 1983. How to hand-check a symbolic reliability expression, *IEEE Transactions on Reliability*, R-32(5), 402–408. DOI:10.1109/TR.1983.5221710.

- [31] Rushdi, A. M. & Ghaleb, F. A. 2020. Boolean-based symbolic analysis for the reliability of coherent multi-state systems of heterogeneous components, *Journal of King Abdulaziz University: Computing and Information Technology Sciences*, 9(2), 1–25. DOI:10.4197/comp.9-2.1.
- [32] Rushdi, A. M. & Ghaleb, F. A. 2021. Reliability characterization of binary-imaged multi-state coherent threshold systems, *International Journal of Mathematical, Engineering and Management Science*, 6(1), 309–321. DOI:10.33889/IJMEMS.2021.6.1.020.
- [33] Rushdi, A. M. & Rushdi, M. A. Switching-algebraic analysis of system reliability, In: Chapter 6 in Ram, M. & Davim, P., Editors *Advances in Reliability and System Engineering, Management and Industrial Engineering Series 2017*, 139–161, Springer International Publishing, Cham, Switzerland, DOI: 10.1007/978-3-319-48875-2.
- [34] Brown, F. M. *Boolean Reasoning: The Logic of Boolean Equations*, Kluwer Academic Publishers, Boston, USA, 1990, DOI: 10.1007/978-1-4757-2078-5.
- [35] Rushdi, A. M. & Ghaleb, F. A. 2016. A tutorial exposition of semi-tensor products of matrices with a stress on their representation of Boolean functions, *Journal of King Abdulaziz University: Computing and Information Technology Sciences*, 5(2), 3–30. DOI: 10.4197/comp5-1.
- [36] Rushdi, R. A. & Rushdi, A. M. Mathematics and Examples for Avoiding Common Probability Fallacies in Medical Disciplines, In: Chapter 11 *Current Trends in Medicine and Medical Research*, Vol. 1, 2019, 106–132, Book Publishers International, Hooghly, West Bengal, India, DOI:10.9734/BPI/ctmmr/v1.
- [37] Rushdi, A. M. Reliability of k-out-of-n systems, In: Chapter 5 Misra, K. B., Editor *New Trends in System Reliability Evaluation, Fundamental Studies in Engineering*, Vol. 16, 1993, 185–227, Elsevier Science Publishers, Amsterdam, The Netherlands, DOI: 10.1016/B978-0-444-81660-3.50014-9.
- [38] Rushdi, A. M. 2010. Partially-redundant systems: Examples, reliability, and life expectancy, *International Magazine on Advances in Computer Science and Telecommunications*, 1(1), 1–13.
- [39] Hammer, P. L. & Rudeanu, S. *Boolean Methods in Operations Research and Related Areas*, Springer-Verlag, New York, 1968, DOI: 10.1007/978-3-642-85823-9.
- [40] Rushdi, A. M. 1988. Performance indexes of a telecommunication network, *IEEE Transactions on Reliability*, 37(1), 57–64. DOI: 10.1109/24.3714.
- [41] Rushdi, A. M. & Hassan, A. K. 2015. Reliability of migration between habitat patches with heterogeneous ecological corridors, *Ecological Modelling*, 304, 1–10, DOI:10.1016/j.ecolmodel.2015.02.014.
- [42] Rushdi, A. M. & Hassan, A. K. 2016. An exposition of system reliability analysis with an ecological perspective, *Ecological Indicators*, 63, 282–295, DOI:10.1016/j.ecolind.2015.11.050.
- [43] Rushdi, A. M. & Hassan, A. K. On the Interplay Between Ecology and Reliability, Chapter 35 In: Misra, K. B., Editor. *Handbook of Advanced Performability Engineering*, 2020, 785–809, Springer, Cham, Switzerland, DOI:10.1007/978-3-030-55732-4_35.

Ying Chen

9 Complex system modeling method considering failure mechanism dependency

Abstract: The physics-of-failure (PoF) method has been more and more popular in engineering to understand the failure mechanism (FM) of products. However, due to lack of system modeling method and solving algorithm, the information of FM cannot be used to evaluate system reliability. This chapter presents a system reliability evaluation method with FMT (failure mechanism tree) considering physical dependency (PDEP) such as competition, trigger, acceleration, inhibition, damage accumulation, and parameter combination. The BDD (binary decision diagram) analytical algorithm is developed to solve system reliability model. The operation rules of *ite* operators for generating improved BDD are discussed. The flow chart of system reliability evaluation method based on FMT and BDD is proposed, and is applied in the case of a train speed control microelectronic system. Results show that the method is effective to evaluate system reliability from the perspective of failure mechanism.

Keywords: System reliability modeling, failure physical dependency, failure mechanism, failure mechanism tree, binary decision diagram

9.1 Introduction

Traditionally, reliability evaluation of complex system is usually based on system modeling method, in which the most important task is to model the dependency between failures and different parts of the system. These dependencies include functional dependency (FDEP) and physical dependency (PDEP). The former exists in the process of realizing system function, which includes common cause failure (CCF), load sharing effect, failure isolation effect, and so on, and can be modeled with reliability block diagram (RBD), fault trees (FT), Petri Net, Bayesian network (BN), and so on. PDEP describes the correlation between FMs, which includes failure mechanism (FM) trigger, acceleration and accumulation effect, and so on, which are caused by the interaction of failure physical factors.

Among traditional system reliability modeling methods, fault tree analysis (FTA) technique is the mostly popular one used in engineering. FT can be solved by the Markov method, Monte Carlo simulation, and binary decision diagram (BDD) method

Ying Chen, Laboratory on Reliability and Environmental Engineering Technology, School of Reliability and System Engineering, Beihang University, e-mail: chen@buaa.edu.cn

<https://doi.org/10.1515/9783110725599-009>

[1, 2]. The Markov method suffers from the well-known space explosion problem and requires exponential time-to-failure distribution for each component. The Monte Carlo simulation is a statistical method used to solve real problems in many engineering fields, in particular when analytical approaches are not feasible. Many studies concentrate on the Monte Carlo simulation method to solve FT and recently dynamic fault tree [3–6]; however, this approach can only offer approximate results and often involves long computational time if a higher degree of accuracy is required.

BDD method can be used for analyzing static FTs that represent the system failure in terms of logic AND/OR combinations of component failures [7]. As an extended version of traditional BDD, sequential BDD (SBDD) [8–11] can model a dependent behavior and the failure sequence of the components, such as the pAND behavior or sequence dependence.

For the PDEPs mentioned above, Chen et al. introduced a failure mechanism tree (FMT) analysis method [12], and the Monte Carlo simulation was used to solve FMT. In this chapter we propose an analytical BDD algorithm to solve FMT. The accuracy and efficiency of the proposed method are studied and compared with the Monte Carlo simulation results.

9.2 Preliminaries

Independent FMs are defined as mechanisms only triggered by environmental condition, loads, and inner parameters such as structure and material parameters. They will not be initiated, triggered, or affected by any other FMs. However, from a system aspect, they have competition correlation [13].

Definition 9.1 (Competition): Assume that there are n independent FMs in a system, that is, fm_i , $i = 1, \dots, n$, their failure time is t_i , $i = 1, \dots, n$, then system failure time is,

$$\zeta = \min\{t_1, \dots, t_i, \dots, t_n\} \quad (9.1)$$

The probability density function (PDF) of each FM in the system is $f_i(t)$, and the cumulative probability distribution function(CDF) of the system at time t can be expressed as

$$\begin{aligned} F(t) &= P(\zeta \leq t) = 1 - P(\zeta > t) \\ &= 1 - P(t_1 > t, t_2 > t, \dots, t_n > t) \\ &= 1 - \prod_{i=1}^n [1 - P(t_i \leq t)] \\ &= 1 - \prod_{i=1}^n \left[1 - \int_0^{t_i} f_i(t) dt \right] \end{aligned} \quad (9.2)$$

The FM dependencies in this chapter are physical dependencies. Most FMs in a system are not independent, and system failure is the result of the joint action of these FMs.

Definition 9.2 (Trigger): When an FM develops to a certain extent (trigger FM), it may change the surrounding environment, load, structure, and material characteristics, and trigger other FMs(dependent FMs), which is the trigger relationship between FMs.

Assume that FM fm_a develops independently, the failure time is t_{m_a} . After time T_{tr} , fm_a develops to some extent and trigger n new FMs fm_i , $i = 1, \dots, n$. Assume that the failure time of fm_i is t_i , $i = 1, \dots, n$, system failure time ζ is,

$$\zeta = \min\{t_{m_a}, T_{tr} + t_1, T_{tr} + t_2, \dots, T_{tr} + t_n\} \quad (9.3)$$

If $t < T_{tr}$, the system CDF, $F(t)$ is

$$F(t) = F_a(t) \quad (9.4)$$

where $F_a(t)$ is the CDF of fm_a .

If $t > T_{tr}$, $F(t)$ is

$$\begin{aligned} F(t) &= 1 - P(t_{m_a} > t, T_{tr} + t_1 > t, T_{tr} + t_2 > t, \dots, T_{tr} + t_n > t) \\ &= 1 - [1 - P(t_{m_a} \leq t)] \prod_{i=1}^n [1 - P_i(T_{tr} + t_i \leq t)] \\ &= 1 - [1 - F_a(t)] \prod_{i=1}^n [1 - F_i(t_i - T_{tr})] \\ &= 1 - \left[1 - \int_0^t f_a(t) dt\right] \prod_{i=1}^n \left[1 - \int_0^{t-T_{tr}} f_i(t) dt\right] \end{aligned} \quad (9.5)$$

where $f_a(t)$ is the PDF of fm_a , $F_i(t)$ and $f_i(t)$ are the CDF and PDF of fm_i , $i = 1, \dots, n$.

Definition 9.3 (Acceleration or inhibition): The acceleration or inhibition relationship is that one FM accelerates or slows down the development rate of other FMs.

Take the acceleration as an example; assume that when fm_b develops to some extent, and at time T_{ta} begins to accelerate fm_i , $i = 1, \dots, n$. Assume that if not being accelerated, their failure time is t_i , $i = 1, \dots, n$. After being accelerated, they turned into fm'_i , $i = 1, \dots, n$, and their development rate will be increased, the failure time at the accelerated rate is assumed to be t'_i . Their failure process can be divided into two phases, before T_{ta} and after T_{ta} , which have different development rates. $T_{t_{a_i}}$, $i = 1, \dots, n$ is the failure time after being accelerated.

For example, the failure time of fm_1 is

$$\zeta_1 = T_{ta} + T_{t_{a1}} \quad (9.6)$$

where

$$T_{t_{\alpha 1}} = \left(1 - \frac{T_{t_{\alpha}}}{t_1}\right) \times t_1' \quad (9.7)$$

then

$$\zeta_1 = T_{t_{\alpha}} + T_{t_{\alpha 1}} = T_{t_{\alpha}} + \left(1 - \frac{T_{t_{\alpha}}}{t_1}\right) \times t_1' \quad (9.8)$$

For the system, there are n accelerated FMs,

$$\begin{aligned} F(t) &= P(\zeta \leq t) = 1 - P(\zeta > t) \\ &= 1 - P(T_{t_{\alpha}} + T_{t_{\alpha 1}} > t, \dots, T_{t_{\alpha}} + T_{t_{\alpha n}} > t) \\ &= 1 - \prod_{i=1}^n [1 - F_{\alpha_i}(t - T_{t_{\alpha}})] \\ &= 1 - \prod_{i=1}^n \left[1 - \int_0^{t - T_{t_{\alpha}}} f_{\alpha_i}(t) dt\right] \end{aligned} \quad (9.9)$$

where $F_{\alpha_i}(t)$ and $f_{\alpha_i}(t)$ are the CDF and PDF of fm_i , $i = 1, \dots, n$.

Definition 9.4 (Damage accumulation or parameter combination): Dependent FMs cause the same type of damage or same parameter degradation, thus jointly impacting the system. This kind of relationship is damage accumulation or parameter combination.

Assume that n FMs, fm_i , $i = 1, \dots, n$ have damage accumulation relation (the damage threshold is normalized to be 1). Their failure time are t_i , $i = 1, \dots, n$. If they are independent, $\Delta D_i = 1/t_i$ is the unit damage of each FMs, then the total unit damage is,

$$\Delta D = \sum_{i=1}^n \lambda_i \cdot \Delta D_i \quad (9.10)$$

where λ_i is the damage factor. When the total damage exceeds 1, system will fail. Then the relation of system failure time ζ and the damage threshold is

$$\zeta \cdot \sum_{i=1}^n \lambda_i \cdot \Delta D_i = 1 \quad (9.11)$$

Then,

$$\zeta = \frac{1}{\sum_{i=1}^n \lambda_i \cdot \Delta D_i} = \frac{1}{\sum_{i=1}^n \lambda_i \cdot \frac{1}{t_i}} \quad (9.12)$$

The system CDF is

$$F(t) = P\{\zeta \leq t\} = P\left\{\frac{1}{\sum_{i=1}^n \lambda_i \cdot \frac{1}{t_i}} \leq t\right\}$$

(9.13)

9.3 Failure mechanism tree

9.3.1 Definitions

FMT can be used to represent the dependencies between FMs. First, some basic symbols of FMT are defined. Table 9.1 lists the graphical symbols of different types of events. Table 9.2 shows the symbols of typical FM dependencies.

Table 9.1: The graphical symbols of different types of events.

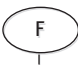

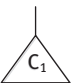
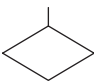

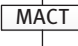
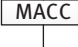


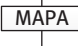
Items	Failure	Basic events	Trigger events	Undefined
Symbols				

Table 9.2: Symbols of typical FM dependency.

Dependency	Symbols	Description
Competition		Some FMs are independent of each other, system failure time is determined by the one which reaches the failure threshold firstly
Trigger		One FMs develops to a certain extent, some new FMs are triggered
Acceleration		One FM accelerates the development rate of other FMs
Inhibition		One FM slows down the development rate of other FMs
Damage accumulation		Different FMs lead to the same damage of the system, and the damage value is accumulated
Parameter union		Different FMs lead to the same parameter degradation, and the parameter change is accumulated

9.3.2 Dependencies of FMs in FMT

Figure 9.1 shows the dependency of FMs in FMT, which includes competition, trigger, acceleration, inhibition, damage accumulation, and parameter union.

The MACO gate has multiple FMs act as basic events and a single output event of component failure, which is shown in Figure 9.1(a). The FMs are independent of each other, they develop independently, and the one that evolves to reach its threshold would result in the failure of a component (i.e., output of this gate).

The MACT gate has a single trigger input event, one or multiple input basic events and one or multiple output basic event (illustrated in Figure 9.2(b)). The trigger event can be FMs or an intermediate event (i.e., output of another gate). The occurrence of the trigger event forces the input FM to initiate the output basic events (i.e., another FM) to occur.

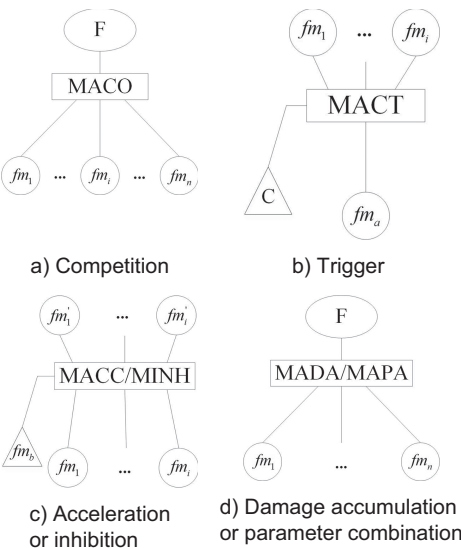


Figure 9.1: FMT of different physical dependencies.

The MACC or MINH gate has a trigger input event, one or multiple input basic events and one or multiple output basic event (illustrated in Figure 9.1(c)). Similar with MACT gate, the trigger event can be other FM or an intermediate event. The difference between MACC/MINH and MACT is that the former will not result in new FMs; they only accelerate or inhibit the developing speed of existing FMs.

The MADA or MADP gate has multiple FMs as basic events and a single output event, which is shown in Figure 9.1(d). The input FMs develop independently; however, the results of these FMs will accumulate. The difference of MADA and MADP

gate is that the former is used when the FMs can be characterized by damage, and the latter by performance parameters.

The output events of the gate in Figure 9.1 can be the failure mode of components or parts and can be directly connected to a basic event of an FT.

9.4 BDD analytical algorithms for FMT

The BDD method, which is based on Shannon decomposition rule [14], has been widely used in solving complex FT, and the basic expression is,

$$F = x \cdot F_{x=1} + \bar{x} \cdot F_{x=0} \quad (9.14)$$

Where F is a Boolean expression, x is a Boolean variable. $F_{x=1}$ and $F_{x=0}$ is the value of F when $x=1$ and $x=0$.

$$F = \text{ite}(x, F_{x=1}, F_{x=0}) = \text{ite}(x, F_1, F_0) \quad (9.15)$$

Ite represents the concise *if-then-else* format. The BDD is constituted by rooted, directed acyclic graph (DAG), which has two sink nodes, each labeled by a distinct logic value “0” and “1,” representing the system being in an operational or a failed state respectively. As illustrated in Figure 9.2, each non-sink node is associated with a Boolean variable x and has two outgoing edges called 1-edge (or *then*-edge) and 0-edge (or *else*-edge) respectively. The 1-edge represents the failure of the corresponding component and leads to the child node $F_{x=1}$. The 0-edge represents the operation of the component and leads to the child node $F_{x=0}$. Each non-sink node in the BDD encodes an *ite* expression.

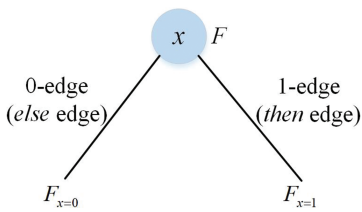


Figure 9.2: Graphic representation of *ite* expression of single Boolean variable.

The *ite* operator can describe the following three important relationships [15]:

- 1) Basic events

$$x = \text{ite}(x, 1, 0) \quad (9.16)$$

2) Logical “AND” relationship between events

$$\begin{aligned} x \bullet y &= ite(x, 1, 0) \bullet ite(y, 1, 0) \\ &= ite(x, ite(y, 1, 0), 0) \end{aligned} \quad (9.17)$$

3) Logical “OR” relationship between events

$$\begin{aligned} x + y &= ite(x, 1, 0) + ite(y, 1, 0) \\ &= ite(x, 1, ite(y, 1, 0)) \end{aligned} \quad (9.18)$$

With the *ite* operators, the FT logical relationship of the basic events can be easily described. Therefore, to use BDD method to solve FMT, it is necessary to study the *ite* of FMT logic relation, which is the foundation of constructing BDD.

9.4.1 Competition *ite* operation rules and BDD algorithm

The operation rules of *ite* for different PDEP logic are studied. In traditional BDD for competition dependency, the 0-edge represents the normally operating state and is connected to the sink nodes “0”. The 1-edge represents the failure of the corresponding component, which is not connected with each other and points to the sink nodes “1.” To integrate PDEP in BDD, all the 1-edges of non-sink nodes represent an integral value. Therefore, symbols $0 \rightarrow t$ are added to all 1-edges to represent the integral lower limit of zero and the upper limit is t . The value of sink nodes “1” is the probability of system state. In the *ite* expression, “ $1 - \int_0^t$ ” instead of “1” is used to represent 1-edge.

In particular, it is explained here that the 1 edge of the improved BDD in this chapter is different from that of the traditional BDD. In this chapter, all the 1-edges represent an integral value and different integral intervals are distinguished by dotted lines and solid lines. Solid lines mean that the integral interval is $0 \rightarrow t$, and dotted lines mean that the integral interval is changed. For clarity, some annotations are used next to the 1-edge.

Firstly, for MACO, if there are multiple competing FMs $fm_i (i = 1 \dots n)$, the operation rule of the *ite* is to replacing the “0” in $ite(fm_i, 1, 0)$ with $ite(fm_{i+1}, 1, 0)$ in turn and using “ $1 - \int_0^t$ ” to represent 1-edge. eq. (9.19) is the *ite* obtained from competition algorithm.

$$\begin{aligned}
& MACO\{fm_1, fm_2, \dots, fm_n\} \\
&= MACO\{ite(fm_1, 1, 0), ite(fm_2, 1, 0), \dots, ite(fm_n, 1, 0)\} \\
&= ite(fm_1, 1 - \int_0^t, ite(fm_2, 1 - \int_0^t \dots ite(fm_n, 1 - \int_0^t, 0)))
\end{aligned} \tag{9.19}$$

The BDD for competition can be constructed with eq. (9.19), which is shown in Figure 9.3.

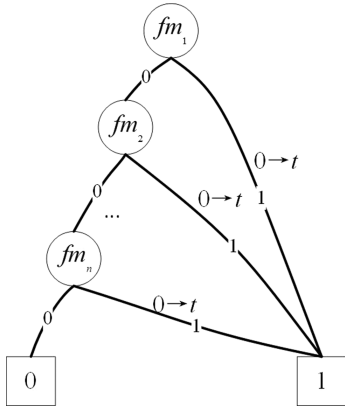


Figure 9.3: BDD model for competition dependency.

To solve the analytical algorithm of BDD model for competition, firstly, the number of FMs, the life distribution types and distribution parameters of each FM should be determined, then eq. (9.2) is used to calculate the CDF of the component or system.

9.4.2 Trigger *ite* operation rules and BDD algorithm

In the BDD for trigger, the FMs will be connected by 0-edge, and the 1-edge will not connected with each other. Symbol “ \succ ” is used to distinguish trigger FMs and dependent FMs. The FMs before the symbol are trigger FMs and the FMs after the symbol are dependent FMs, which will appear after the trigger time T_{tr} . Then the *ite* can be constructed according to the magnitude relationship between t and T_{tr} .

The operation rules of the *ite* operator are as follows:

- 1) Divide the 0-edge of fm_a into two paths, $t > T_{tr}$ and $t < T_{tr}$. “ $1 - \int_0^t$ ” is used in *ite* to represent 1-edge of fm_a .
- 2) When $t > T_{tr}$, “0” in $ite(fm_i, 1, 0)$ is replaced by $ite(fm_{i+1}, 1, 0)$, and “ $1 - \int_{t_r}^t$ ” is used to represent 1-edge of fm_i .
- 3) When $t < T_{tr}$, “0” in $ite(fm_a, 1, 0)$ is retained.

According to the operation rules, the *ite* expression for trigger is shown in eq. (9.20).

$$\begin{aligned}
& MACT\{fm_a \succ fm_1, \dots, fm_n\} \\
& = MACT\{ite(fm_a, 1, 0) \succ ite(fm_1, 1, 0), \dots, ite(fm_n, 1, 0)\} \\
& = ite(fm_a, 1 - \int_0^t, [ite(fm_1, 1' - \int_{T_{tr}}^t, \dots, ite(fm_n, 1' - \int_{T_{tr}}^t, 0)) | t > T_{tr} \diamond 0 | t < T_{tr}])
\end{aligned} \tag{9.20}$$

The BDD for trigger can be constructed according to eq. (9.20) but it needs to follow certain rules:

- 1) Paths: $t > T_{tr}$ and $t < T_{tr}$, they are connected with symbol \diamond in BDD, which indicates that there is only one path exists at any time.
- 2) When $t > T_{tr}$, 1-edge of fm_i is drawn by dotted line to indicate that the new FMs are triggered.
- 3) When $t < T_{tr}$, 1-edge of fm_a should be directly connected to sink nodes in BDD.

The BDD for trigger is shown in Figure 9.4.

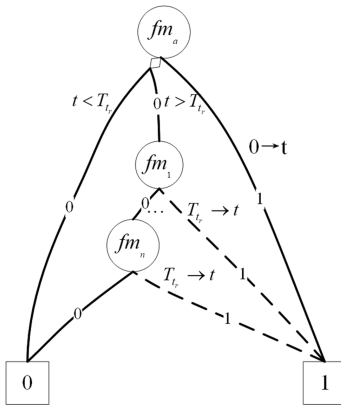


Figure 9.4: BDD model for trigger dependency.

In order to solve the analytical algorithm of BDD model for trigger, it is necessary to determine whether the dependent FMs are triggered or not by comparing t and T_{tr} . If they are triggered, the CDF are calculated by eq. (9.5) with the path of $t > T_{tr}$. If not, the CDF is calculated by eq. (9.4) with the path of $t < T_{tr}$.

9.4.3 Acceleration or inhibition *ite* operation rules and BDD algorithm

In the BDD for acceleration or inhibition, the FMs are connected by 0-edges, and 1-edges are not connected with each other. Assume fm_b keeps a constant development rate, $fm_i (i=1\dots n)$ will be accelerated or inhibited at T_{ta} , their development

speed will change. Construct the *ite* according to the magnitude relationship between t and $T_{t\alpha}$.

The *ite* operation rule for acceleration or inhibition dependency is,

- 1) Divide the 0-edge of m_b into two paths: $t > T_{t\alpha}$ and $t < T_{t\alpha}$, “ $1 - \int_0^t$ ” is used in *ite* to represent 1-edge of fm_b .
- 2) When $t > T_{t\alpha}$, firstly, “1” in $ite(fm_i, 1, 0)$ is replaced by $ite(fm'_i, 1, 0)$, “0” in $ite(fm_i, 1, 0)$ and $ite(fm'_i, 1, 0)$ is replaced by $ite(fm_{i+1}, 1, 0)$. Then “ $1 - \int_0^{t\alpha}$ ” is used to represent 1-edge of fm_i , “ $1' - \int_{t\alpha}^t$ ” is used to represent 1-edge of fm'_i .
- 3) When $t < T_{t\alpha}$, replace “0” in $ite(fm_i, 1, 0)$ with $ite(fm_{i+1}, 1, 0)$ and “ $1 - \int_0^{t\alpha}$ ” is used to represent 1-edge of fm_i .

According to the operation rules, the *ite* expression for acceleration or inhibition is shown in eq. (9.21):

$$\begin{aligned}
 & MACC/MINH\{fm_b \succ fm_1, \dots, fm_n\} \\
 &= MACC/MINH\{ite(fm_b, 1, 0) \succ ite(fm_1, 1, 0), \dots, ite(fm_n, 1, 0)\} \\
 &= ite(fm_b, 1 - \int_0^t, [ite(fm_1, ite(fm'_1, 1' - \int_{t\alpha}^t, \dots, ite(fm_n, ite(fm'_n, 1' - \int_{t\alpha}^t, 0), 0)) \mid t > T_{t\alpha} \diamond ite(fm_1, 1 - \int_0^t, \dots, ite(fm_n, 1 - \int_0^t, 0) \mid t < T_{t\alpha})]) \quad (9.21)
 \end{aligned}$$

The BDD for acceleration or inhibition is constructed according to eq. (9.21), which is shown in Figure 9.5. The rules in building BDD are as follows:

- 1) Paths: $t > T_{t\alpha}$ and $t < T_{t\alpha}$, they are connected with symbol \diamond in BDD, which indicates that there is only one path exists at any time.
- 2) When $t > T_{t\alpha}$, dashed lines are used to draw the 1-edge of fm'_i to show that the rate of development of FM has changed.
- 3) When $t < T_{t\alpha}$, solid lines are used to draw the 1-edge of fm'_i and they should be directly connected to sink nodes in BDD.

The analytical algorithm of BDD for acceleration or inhibition is as follows. Firstly, determine whether the FMs will be accelerated or inhibited or not by comparing t and $T_{t\alpha}$, if they are accelerated or inhibited, the CDF is calculated by eq. (9.9) with the path of $t > T_{t\alpha}$. If not, the CDF is calculated by eq. (9.2) with the path of $t < T_{t\alpha}$.

9.4.4 Damage accumulation or parameter combination *ite* operation rules and BDD algorithm

Take the damage accumulation effect as the example. λ_i -edge is used to represent the different rate of FMs, which should be connected by λ_i -edge with each other.

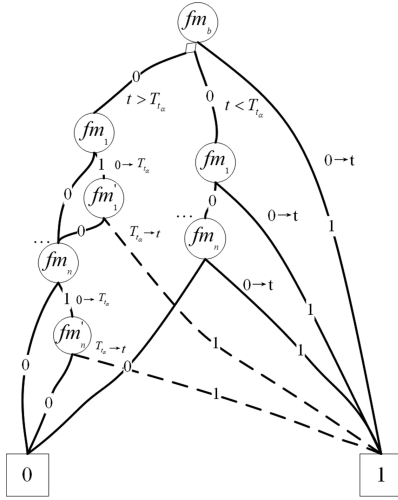


Figure 9.5: BDD model of acceleration or inhibition dependency.

The *ite* operation rule of accumulation is replacing the “ λ_i ” in $ite(fm_i, \lambda_i, 0)$ with $ite(fm_{i+1}, \lambda_{i+1}, 0)_{\lambda_i}$ in turn. The subscript λ_i outside the brackets is used to represent the scaling factor of m_i :

$$\begin{aligned} &MADA\{fm_1, fm_2, \dots, fm_n\} \\ &= MADA\{ite(fm_1, \lambda_1, 0), ite(fm_2, \lambda_2, 0), \dots, ite(fm_n, \lambda_n, 0)\} \\ &= ite(fm_1, ite(fm_2, \dots, ite(fm_n, \lambda_n, 0), 0)\lambda_2, 0)\lambda_1 \end{aligned} \quad (9.22)$$

According to eq. (9.22), the BDD for damage accumulation can be constructed, which is shown in Figure 9.6.

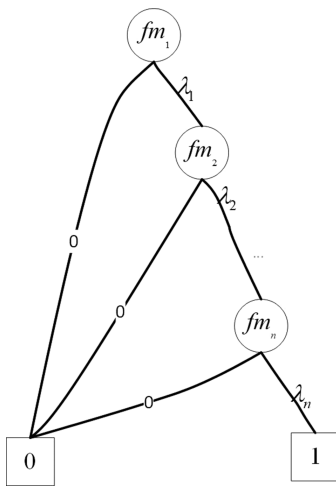


Figure 9.6: BDD model for damage accumulation dependency.

According to eq. (9.13), ΔD_i is the damage in unit time due to fm_i , then the PDF of unit damage due to fm_i is

$$\begin{aligned} D_i(t) &= \frac{d}{dt} P\{\Delta D_i < t\} = \frac{d}{dt} P\left\{\frac{1}{t_i} < t\right\} \\ &= \frac{1}{t^2} f_i\left(\frac{1}{t}\right) \end{aligned} \quad (9.23)$$

Then the PDF of damage value accumulated by two FMs can be expressed as,

$$\begin{aligned} D(t) &= \int_0^\infty D_i(t) \cdot D_{i+1}(t - \tau) d\tau \\ &= D_i(t) * D_{i+1}(t) \end{aligned} \quad (9.24)$$

The continuous function value will be discretized during simulation. Assume the convolution variables are sequence $p(n)$ and $q(n)$, the convolution calculation formula could be modified as eq. (9.25). When the degree of discretization is accurate enough, the resulting errors can be ignored.

$$c(n) = \sum_{i=0}^{N-1} p(i)q(n-i) = p(n) * q(n) \quad (9.25)$$

Where N and M are the length of the sequence $p(i)$ and $q(i)$, and $c(n)$ is the result of convolution sequence, with the total length of $N+M-1$. When the order $n=0$, the sequence $q(-i)$ is the reverse result of the time sequence $q(i)$, Timing inversion causes $q(i)$ to flip 180 degrees with the vertical axis, and n is the amount that makes $q(-i)$ to shift. Different n will correspond to different convolution results.

The convolution result of PDF of FMs is still a kind of PDF. Integrate the PDF on the time axis and with eqs. (9.26), (9.27), the CDF after convolution can be obtained. $d_i(S_i)$ is the area of a micro unit in the integral process,

$$d_i(S_i) = \frac{(f(x_i) + f(x_{i+1}))}{2} dx \quad (9.26)$$

$$F(x_i) = \sum_{j=1}^i d_j(S_i) \quad (9.27)$$

To solve the analytical algorithm of BDD for accumulation, first, the distribution function of FM should be modified to the distribution form which can be convoluted by eq. (9.23), and the system PDF is solved by eq. (9.24). Finally, the system CDF after convolution can be obtained by integrating PDF on time axis by eqs. (9.26, 9.27).

The complexity of BDD directly affects the difficulty of analysis. The following rules can sort the failure more reasonably to some extent.

Rule 1: Sort the priority of component failure mechanism relationship. The lower the complexity of failure is, the higher the priority is. The complexity of failure mechanism is: Competition > Damage accumulation or parameter combination > Trigger > Acceleration or inhibition.

Rule 2: Sort the priority of components in the system. According to the complexity of components, the lower the complexity of components, the higher the priority; the complexity of components is positively related to the number of failure mechanisms and the complexity of failure mechanisms.

According to the order of priority from high to low, *Ite* expressions of components are firstly established. Then, according to the logical relationship between components such as “AND” and “R,” the *ite* expression of the system is established according to eqs. (9.17), (9.18). On this basis, the complete BDD model can be constructed.

9.5 Practical application

DCFP (dependent competing failure process) describes two kinds of failure process: one is soft failure caused by continuous degradation; the other is hard failure caused by shock process. The mutually DCFP is the coupling effect between hard and soft failures. For example, hard failure may accelerate the development of soft failure; both soft and hard failure will cause the decrease of hard failure threshold value, and the system will eventually fail in the process of competition between soft and hard failures.

The train speed control system guarantees the safety of trains in the operation of high-speed railways. The control system module can compare the current speed of a train with the safe speed in real time to prevent the train from speeding and ensure its safety. As shown in Figure 9.7, the input voltage has many high-voltage pulses (electronic shock) caused by the segmented cables. Although many measures have been taken to reduce the electrical shocks, they still exist. Some of the wire-bonding ICs fail to operate due to the breaking of the bonding wires. There are two FMs acting on the wire. First, the electric shock introduced from outside will lead to instantaneous wire fracture and deteriorate the local material properties. Secondly, the degradation FM of thermal fatigue will result in micro-crack propagation and ultimately lead to wire fracture. The electric shock will accelerate the degradation process, and both of the degradation process and the shock process will decrease the shock failure threshold. The mutual DCFP effect in this practical case is analyzed in Figure 9.8.

The system is subject to the mutual dependencies between degradation and electric shock. As described in Figure 9.8, line ① indicates the degradation process

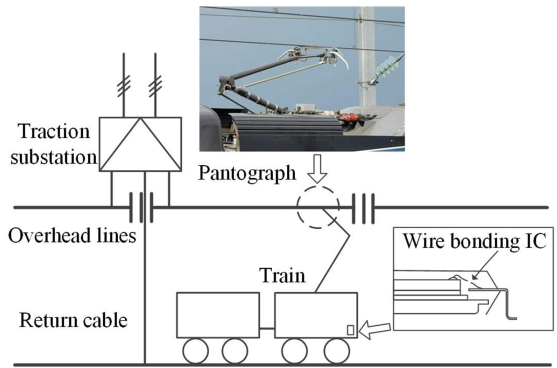


Figure 9.7: The electronic traction device for high-speed rail.

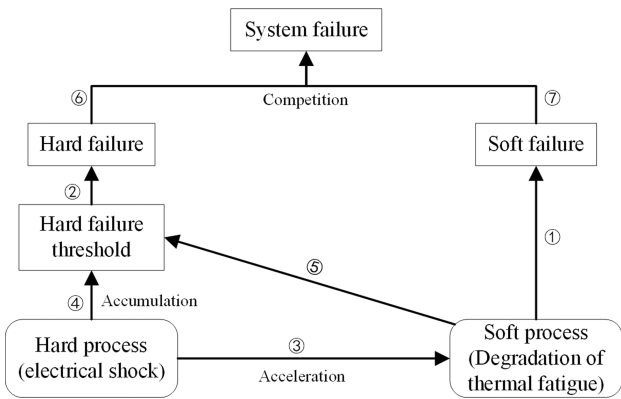


Figure 9.8: Dependencies between shock(hard failure) and degradation(soft failure).

due to thermal fatigue. Line ② refers to hard failure due to electric shock, and if electric shock exceeds the threshold, hard failure will occur. Line ③ is the shock-degradation dependence process, whereby the arriving electric shocks accelerate the degradation process by increasing degradation rate. In addition, considering the degradation-shock dependence, lines ④ and ⑤ indicate that the threshold of hard failure will decrease because of degradation and shock process, in other words, they have cumulative effect, which can be expressed by linear or non-linear cumulative rules. Finally, system failure is determined by the completion of lines ⑥ and ⑦.

According to Figure 9.8, the system FMT can be constructed in Figure 9.9.

Where M_D is the degradation process, M_S is the shock process. M'_D represents the degradation process after accelerated by M_S . S, H and F means soft failure, hard failure and system failure. M_{St} represents the impact of shock failure on the hard

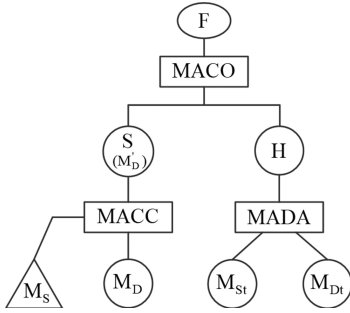


Figure 9.9: FMT for the case.

failure threshold, M_{Dt} represents the impact of degradation failure on the hard failure threshold.

The *ite* expression of M_{St} and M_{Dt} threshold accumulation effect is

$$\begin{aligned}
 & MADA\{M_{St}, M_{Dt}\} \\
 &= MADA(ite(M_{St}, 1, 0), ite(M_{Dt}, 1, 0)) \\
 &= ite(ite(M_{St}, ite(M_{Dt}, \lambda_2, 0)_{\lambda_1}, 0))
 \end{aligned} \quad (9.28)$$

Each time the shock comes, the hard failure accelerates the soft failure for one time, and $M_D^{(i)}$, $i = 0, 1, \dots, n$ indicates the degradation after i th shock, then the *ite* expression of the acceleration effect between M_S and $M_D^{(i)}$ is,

$$\begin{aligned}
 & MACC\{M_S \succ M_D\} \\
 &= MACC\{ite(M_S, 1, 0) \succ ite(M_D, 1, 0)\} \\
 &= ite(M_S, 1 - \int_0^t, ite(M_D^{(0)}, 1 - \int_0^{t_1}, 0)_{|0 \rightarrow t_1} \diamond ite(M_D^{(1)}, 1 - \int_{t_1}^{t_2}, 0)_{|t_1 \rightarrow t_2} \dots \diamond ite(M_D^{(n)}, 1 - \int_{t_n}^{t_{n+1}}, 0)_{|t_n \rightarrow t_{n+1}})
 \end{aligned} \quad (9.29)$$

The *ite* expression of the completion between hard failure and soft failure is

$$\begin{aligned}
 & MACO\{MADA\{M_{St}, M_{Dt}\}, MACC\{M_S \succ M_D\}\} \\
 &= ite(ite(M_{St}, ite(M_{Dt}, \lambda_2, ite(M_S, 1 - \int_0^t, ite(M_D^{(0)}, 1 - \int_0^{t_1}, 0)_{|0 \rightarrow t_1} \diamond ite(M_D^{(1)}, 1 - \int_{t_1}^{t_2}, 0)_{|t_1 \rightarrow t_2} \dots \diamond ite(M_D^{(n)}, 1 - \int_{t_n}^{t_{n+1}}, 0)_{|t_n \rightarrow t_{n+1}}))_{\lambda_1}, ite(M_S, 1 - \int_0^t, ite(M_D^{(0)}, 1 - \int_0^{t_1}, 0)_{|0 \rightarrow t_1} \diamond ite(M_D^{(1)}, 1 - \int_{t_1}^{t_2}, 0)_{|t_1 \rightarrow t_2} \dots \diamond ite(M_D^{(n)}, 1 - \int_{t_n}^{t_{n+1}}, 0)_{|t_n \rightarrow t_{n+1}}))
 \end{aligned} \quad (9.30)$$

According to the *ite*, the BDD model is established, as shown in Figure 9.10.

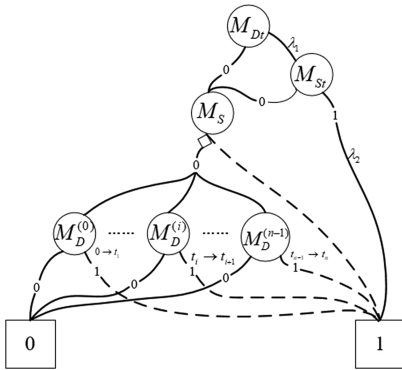


Figure 9.10: BDD model of the DCFP.

Table 9.3 shows the dependencies among FMs and the parameters used when solving the BDD. The distribution of each FM is calculated with PPoF method. The first four acceleration processes are considered in this case.

Table 9.3: FMs dependencies and parameters.

FMs	Descriptions	Dependency	Weibull distribution parameter	
			$\beta(\theta)$	$\eta(\sigma)$
M_{St}	Decrease of hard failure threshold due to soft failure	MADA	21,231	3
c	Decrease of hard failure threshold due to hard failure		18,231	2
$M_D^{(0)}$	Degradation process before the first shock	MACO	9,231	2.7
$M_D^{(1)}$	Degradation process after the first shock		8,831	2.1
$M_D^{(2)}$	Degradation process after the second shock	MACC	8,131	2.2
$M_D^{(3)}$	Degradation process after the third shock		7,832	2.3
$M_D^{(4)}$	Degradation process after the fourth shock		7,231	4.2
M_S	Shock process		2,332	1.8

The established BDD model is solved analytically and the reliability of the system is calculated. Figure 9.11 shows the system reliability results, where the solid line marked with black solid triangles represents that only M_{St} exists in the system, the dotted line represents that only M_{Dt} exists in the system, and the solid line represents that the accumulation effect of hard failure threshold decreases due to both M_{St} and M_{Dt} .

From Figure 9.11, when the accumulation effect is considered, the descent of system reliability is obvious than other the two conditions. This is due to the decrease of failure threshold caused by both soft and hard failure process.

Figure 9.12 shows the reliability results of the system with or without the acceleration effect. The solid line represents that the degradation process has no acceleration

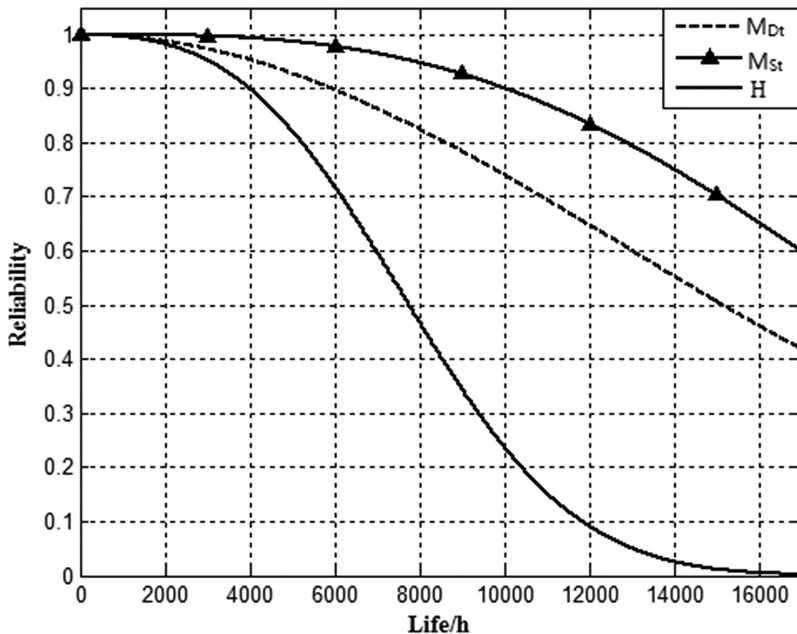


Figure 9.11: System reliability when consider accumulation effect or not.

effect. The dotted line, the line marked with hollow circle, the line marked with solid triangle, the line marked with hollow diamond represent that the i th shock happens and accelerate the degradation process. In practice, each shock may accelerate the degradation process, but the accelerated degradation effect caused by single shock cannot reflect in the change of the curve, so the damage threshold is set in the solution, and that is the reason why there are turning points at different times. With the increase of shock times the reliability decreases.

Figure 9.13 shows the system reliability considering the competition effect of soft failure and hard failure. The solid line represents that only accumulation between hard failure and soft failure are considered. The dotted line represents that only the acceleration effect of the electronic shock on the degradation process is considered. Hollow diamond solid line represents the reliability with DCFP effect. Results show that the FM physical dependent effect should be considered to make the prediction more close to the real condition.

Figure 9.14 is the reliability results calculated by analytical method and Monte Carlo method with 500 simulation times. When the sampling times are small, the error of Monte Carlo method is large and the reliability curve is discontinuous. The proposed analytic algorithm is theoretically derived from the PDF and CDF of the failure mechanism, and the failure mechanism is decoupled by repeatedly calling the embedded function to solve the coupling relationship of the failure mechanism.

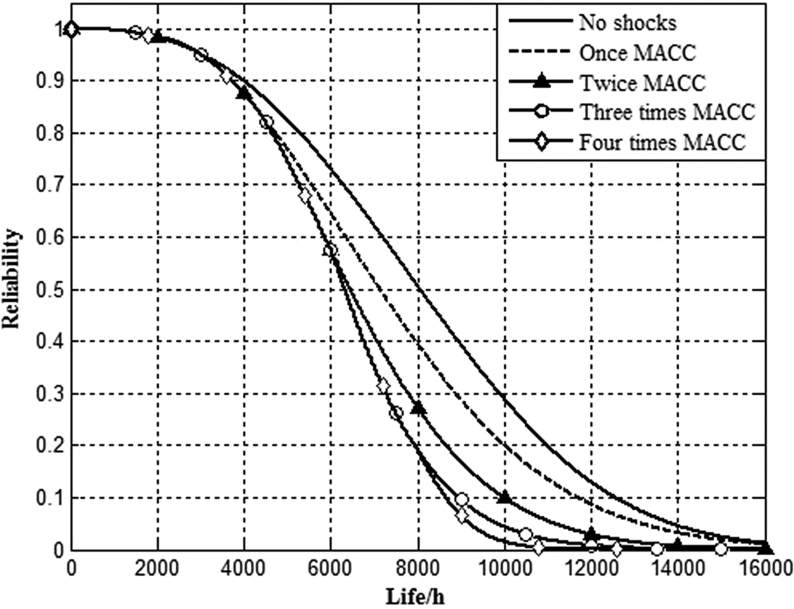


Figure 9.12: System reliability with or without acceleration effect.

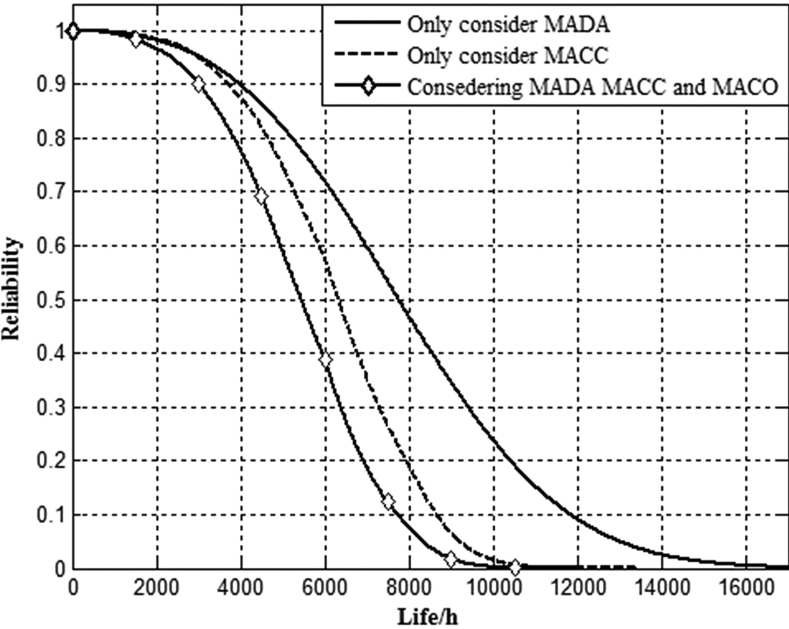


Figure 9.13: System reliability when consider competition effect or not.

Finally, the continuous and accurate reliability curve is obtained. Compared with the results obtained by Monte Carlo simulation, the system reliability curve obtained by analytical method is smoother. If Monte Carlo simulation times are higher than 1,000, the two results are nearly the same.

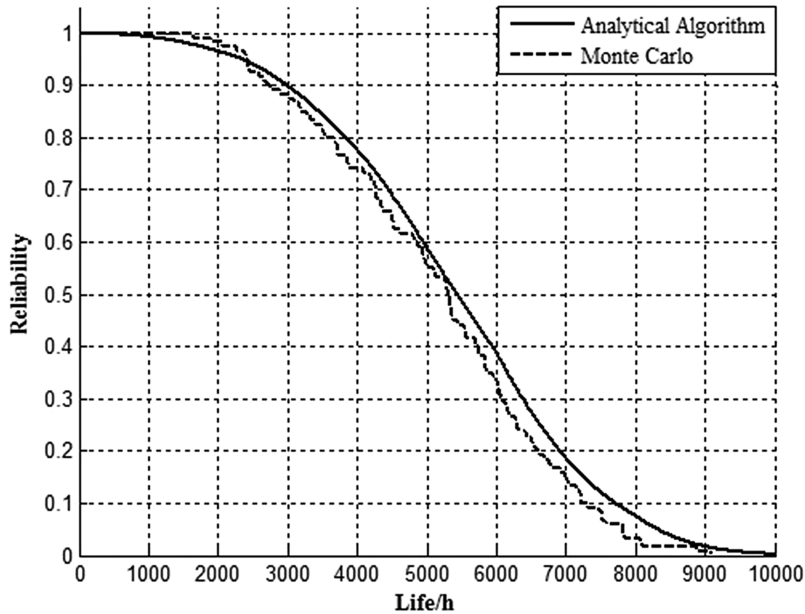


Figure 9.14: Comparison of analytical and Monte Carlo results.

9.6 Conclusions

This chapter introduces a BDD method to solve the problems when FM dependencies are considered in the system. BDD models can be established by FMT and *ite* rules, and the system reliability is obtained by solving the model. The research results can provide a way to predict the reliability in engineering practice when there are FM dependencies.

References

- [1] Rao, K. D., Gopika, V., Rao, V. S., Kushwaha, H. S., Verma, A. K. & Srividya, A. 2009. Dynamic fault tree analysis using Monte Carlo simulation in probabilistic safety assessment, *Reliability Engineering & System Safety*, 94(4), 872–883.
- [2] Zheng, W., Song, L. X. & Meian, L. 2007. Ad hoc distributed mutual exclusion algorithm based on token-asking, *Journal of Systems Engineering and Electronics*, 18(2), 398–406.
- [3] Sun, B. & Li, L. 2006. Reliable adaptive multicast protocol in wireless Ad hoc networks, *Journal of Systems Engineering and Electronics*, 17(1), 187–192.
- [4] Ke, J. C., Su, Z. L., Wang, K. H. & Hsu, Y. L. 2010. Simulation inferences for an availability system with general repair distribution and imperfect fault coverage, *Simulation Modelling Practice and Theory*, 18(3), 338–347.
- [5] Zhang, P. & Chan, K. W. 2012. Reliability evaluation of phasor measurement unit using Monte Carlo dynamic fault tree method, *IEEE Transactions on Smart Grid*, 3(3), 1235–1243.
- [6] Cai, Q., Wei, P. & Xiao, X. 2007. Single channel signal component separation using Bayesian estimation, *Journal of Systems Engineering and Electronics*, 18(1), 33–39.
- [7] Liudong, X., Akhilesh, S. & Yuanshun, D. 2011. Exact combinatorial reliability analysis of dynamic systems with sequence-dependent failure, *Reliability Engineering and System Safety*, 96, 1375–1385.
- [8] Liudong, X., Tannous, O. & Dugan, J. B. 2012. Reliability Analysis of Nonrepairable Cold-Standby Systems Using Sequential Binary Decision Diagrams, *IEEE Transactions on Systems*, 42, 715–726.
- [9] Xing, L. D. & Levitin, G. 2013. BDD-based reliability evaluation of phased-mission systems with internal/external common-cause failures, *Reliability Engineering & System Safety*, 112, 145–153.
- [10] Xing, L. D. 2007. Reliability evaluation of phased-mission systems with imperfect fault coverage and common-cause failures, *IEEE Transactions on Reliability*, 56(1), 58–68.
- [11] Mo, Y., Xing, L. D. & Dugan, J. B. 2014. MDD-Based Method for Efficient Analysis on Phased-Mission Systems with Multimode Failures, *IEEE Transactions on Systems Man & Cybernetics Systems*, 44(6), 757–769.
- [12] Chen, Y., Yang, L., Ye, C. & Kang, R. 2015. Failure mechanism dependence and reliability evaluation of non-repairable system, *Reliability Engineering & System Safety*, 138, 273–283.
- [13] Chen, Y., Yang, L., Ye, C. & Kang, R. 2015. Failure mechanism dependence and reliability evaluation of non-repairable system, *Reliability Engineering and System Safety*, 138, 273–283.
- [14] Bryant, R. E. 1986. Graph-Based Algorithms for Boolean Function Manipulation, *IEEE Trans. Computers*, 35(8), 677–691.
- [15] Rauzy, A. 1993. New algorithms for fault trees analysis, *Reliability Engineering & System Safety*, 40(3), 203–211.

Emmanuel A. Appiah, G. S. Ladde, Jay G. Ladde

10 Innovative interconnected nonlinear hybrid dynamic modeling for time-to-event processes

Abstract: In this work, we develop an innovative large-scale nonlinear hybrid dynamic model of survival species and its probabilistic binary states in a systematic and unified way. The presented approach is motivated by state and parameter estimation of time-to-event processes in biological, chemical, engineering, epidemiological, medical, military, multiple markets, and social dynamic processes under the influence of discrete-time intervention processes. Two conceptual computational dynamic procedures are initiated. Each procedure is composed of at least six sub-components. The developed algorithms are independent of any particular form of survival distribution functions or data sets. The introduction of intervention process generates and provides a measure of degree and influence of new updated options or tools in continuous-time states of time-to-event dynamic processes. The by-product of the procedures further leads to study the qualitative and quantitative properties of probabilistic binary state dynamic processes. In addition, the developed modified local lagged adapted generalized method of moments (LLGMM) measures the degree of confidence, prediction, and planning assessments. The usefulness, significance, and merits of the developed methods are illustrated by applying to three real data sets. Furthermore, the developed conceptual computational procedures are dynamic algorithms.

Keywords: Kaplan–Meier estimator, binary state of population, survival principle, interconnected discrete-time dynamic algorithm, modified LLGMM

Note: US Patent Application Pending

Acknowledgments: This research was supported by the Mathematical Sciences Division, U.S. Army Research Office, grant no. W911NF-15-1-0182.

Emmanuel A. Appiah, Department of Mathematics, Prairie View A&M University, Prairie View, TX 77446, USA

G. S. Ladde, Department of Mathematics and Statistics, University of South Florida, Tampa, FL 33620, USA

Jay G. Ladde, Department of Emergency Medicine, Orlando Regional Medical Center, 86 W Underwood Street, Orlando, FL 32806, USA

<https://doi.org/10.1515/9783110725599-010>

10.1 Introduction

In survival and reliability analysis, parametric methods are often applied to estimate the hazard/risk rate and survival functions [12]. A parametric approach is based on the assumption that the underlying survival distribution belongs to some specific family of distributions (e.g., Weibull, log-logistic, exponential). Mostly, classical likelihood-based models, methods, and their extensions/generalizations are developed and utilized [11, 12, 20, 23]. Moreover, the log-logistic distribution [20–23, 25] has played a significant role in the survival data analysis.

In this work, we present an alternative approach for modeling nonlinear time-to-event processes in biological, chemical, engineering, epidemiological, medical, military, multiple markets, and social dynamic processes. This approach does not require any knowledge of either a closed-form solution distribution or a class of distributions. The presented innovative approaches leads to development of a large-scale interconnected nonlinear hybrid dynamic model under the influence of time-to-event processes (INHDMTTEP).

The human mobility, electronic communications, technological changes, advancements in engineering, medical, and social sciences have diversified and extended the role and scope of time-to-event processes in biological, cultural, epidemiological, financial, military, and social sciences [1–5]. It is known that sudden changes in the hazard rate/risk at unspecified or specified times are frequently encountered in engineering and medical sciences [1]. These changes could occur multiple times. As a result of this, investigators [6–8] are often interested in (a) detecting the location of the changes, and (b) estimating the sizes of the detected changes. Based on INHDMTTEP and employing a nonlinear transformation, a theoretical interconnected discrete-time dynamic algorithm of time-to-event data statistic (IDATTEDS) is developed. Using IDATTEDS, several conceptual computational parameters and state estimation results are presented. In addition, theoretical modified LLGMM parameter and state estimation algorithm is also outlined. Furthermore, by introducing notions of data coordination, decomposition, and aggregation, conceptual computational dynamic algorithm and simulation are also developed for both IDATTEDS and modified LLGMM procedures. Finally, we apply IDATTEDS and modified LLGMM methods to three real-world data sets to illustrate the significance and merits of the developed procedures.

The presented approaches are motivated by parameter and state estimation problems of continuous-time time-to-event processes.

The organization of the chapter is as follows. A few basic existing concepts and its modifications coupled with definitions, terms, and observations are outlined in Section 10.2. Recognizing the rapid growth, increased efficiency and speed in communication, science and technology in the twenty-first century, we develop interconnected nonlinear hybrid probabilistic binary state dynamic model composed of both continuous- and discrete-time survival state of population under the influence of time-to-event processes in Section 10.3. In Section 10.4, a formulation of INHDMTTEP

is outlined. Employing INHDMTTEP, we present fundamental results regarding continuous- and discrete-time dynamic of survival species and its survival state in Section 10.5. Moreover, an interconnected discrete-time algorithm of data statistic (IDATTEDS) is established. Using the IDATTEDS, we develop several results concerning parameter and state estimation problems in time-to-event processes in Section 10.6. In addition, we develop conceptual computational modified LLGMM algorithm for parameter and state estimation in Section 10.7. Conceptual computational data organizational and simulation schemes in the framework of IDATTEDS and modified LLGMM methods are presented in Sections 10.8 and 10.9, respectively. We then apply IDATTEDS and modified LLGMM procedures to three real-world data sets in Sections 10.10 and 10.11, respectively. Moreover, the simulation results of both of these procedures are compared. Furthermore, the modified LLGMM method provides a measure for the degree of confidence, prediction, and planning assessments. In addition, we compare the IDATTEDS and modified LLGMM simulation results with existing methods, namely, maximum likelihood [11] and Kaplan–Meier [18] approach in Section 10.12. In Section 10.13, we present the conclusions regarding the role and scope of the presented deterministic process as well as further extensions and generalizations that are in progress. In fact, a large-scale interconnected nonlinear hybrid dynamic model under the influence of Ito–Doob stochastic time-to-event process is also developed, and will appear elsewhere.

10.2 Basic existing concepts and its modifications with definitions, terms, and observations

For better understanding of the development of nonlinear and non-stationary dynamic algorithm of time-to-event data analysis, we outline a few existing features and innovative ideas in the theory of survival analysis, as well as make some observations. Historically, it is known [11] that the study of time-to-event processes is centered around the medical and engineering sciences. Mostly, classical likelihood-based models, methods and its extensions/generalizations are developed and utilized [11]. The study is based on the concepts in the theory of probability and stochastic processes. In particular, probabilistic concepts of hazard rate function λ and survival/failure probability distributions of a random time variable T form a core of concepts. We note that for $t \in \mathbb{R}$, $F(t)$ stands for cumulative probability distribution of T at t , and $S(t)$ is a survival function of time-to-event process. Moreover, $S(t) + F(t) = 1$. In the existing literature, these probabilistic functions are treated to be evolving mutually exclusively corresponding to two mutually exclusive time-varying events. We refer S and F as cumulative distributions of two mutually disjoint output processes with respect to two mutually exclusive time-varying events of (deterministic or stochastic) dynamic process in any discipline. Moreover, S and F are referred

as probabilistic dynamic binary states describing binary status (options/features/condition) of population under the influence of time-to-event processes. This type of (deterministic or stochastic) dynamic process can be thought of as the Bernoulli-type of probabilistic (deterministic or stochastic) process. These two output processes of the Bernoulli-type of probabilistic (deterministic or stochastic) process, we associate with binary states dynamic under the influence of time-to-event process. In fact, a probabilistic (deterministic or stochastic) binary-state dynamic process is described by one of the following dynamic processes (binary status of population): {action, reaction}, {normal, abnormal}, {survival, failure}, {susceptible, infective}, {operational, non-operational}, {radical, non-radical}, and so on. This exhibits abstractions or generalizations of Newton's third law of dynamic motion process {action/reaction}.

A logistic-type survival distribution function has been introduced through a random time transformation. Moreover, the logistic distribution was introduced by recognizing the properties of the solution of logistic population dynamic model in the literature [11, 12]. We further note that the hazard rate function satisfies the conditions: $\lambda \geq 0$, and $\lim_{t \rightarrow \infty} [\int_0^t \lambda(s) ds] = \infty$. This is a very restrictive assumption.

In the following, using basic tools in mathematical sciences, we initiate a Newtonian-type dynamic approach for probabilistic binary state of population under the influence of time-to-event processes in the sciences, technologies, and engineering.

10.3 Formulation of probabilistic binary state dynamic model

We recognize the rapid growth and increased efficiency and speed [1, 3–5, 9, 10] in communication, science, engineering, and technology in the twenty-first century. Under continuous advancements in science and technology, the study of time-to-event processes in medical and engineering sciences have been significantly improved, and can be easily extended to other disciplines that are conceptually similar but apparently different. In fact, the scientific and technological changes are playing a role for extension to dynamic processes in business, economic, management, military and social sciences [2–5, 9, 10]. It is known that classical likelihood-based models and methods of time-to-event models are very restrictive. For example, most of the time-to-event processes studied in the literature [11, 12] are focused on exclusively either failure or survival state dynamic of time-to-event processes. In fact, in economic/financial/social sciences, the group of human beings is interacting with a fellow human consumer/associate or a user of similar goods/services/information/knowledge/background/entities easily and more frequently for making a decision/choice. Recently, by introducing the concept of network externality process and its dynamic principle [10], the consumer group network influence has led to the definition of network externality value. Moreover, network good value is determined by a

current market share/size. It has been further remarked that the collection of network externality functions includes sub-classes of survival/failure functions with finite domain of operation. We associate two mutually exclusive time-to-events in science and technology with respect to two mutually exclusive dynamic states operating/functioning in the sciences, engineering, and technologies to develop a dynamic model.

In this work, we initiate a nonlinear probabilistic binary state dynamic model under the influence of time-to-event processes in biological, medical, business, economic, management, military and social sciences as a binary-state probabilistic dynamic process interacting or influencing simultaneously instead of mutually exclusively (isolated manner). Let S (survival state), survival/operating/susceptible/action/normal, and F (failure state), failure/non-operating/infective/inaction/abnormal be probabilistic binary states of dynamic process (binary status of population) under the influence of time-to-event processes in the sciences, engineering, financial, medical, military, technological, and social disciplines. Let us assume that the probabilistic measures of these two dynamic states are represented by S and F , respectively. For this purpose, we introduce a dynamic principle for a probabilistic binary state of time-to-event process as follows:

Survival principle: A specific differential rate of survival state probability measure over an interval of time $[t, t + \Delta t]$ of binary state of population dynamic process is directly proportional to the product of failure state probability measure and the length of the interval Δt :

$$\frac{dS}{S} \propto Fdt,$$

that is,

$$\begin{aligned} dS &= -\lambda(t)SFdt \\ &= -\lambda(t)S(1-S)dt, \end{aligned} \tag{10.1}$$

where λ is a nonnegative function of proportionality; dS stands for a differential of survival state probability measure over an interval of length $\Delta t \equiv dt$; dS/S denotes a specific differential rate of survival state probability measure over the length of time interval Δt ; the negative sign in (10.1) signifies that survival state probability measure decreases as t increases; and $1 - S$ represents a potential of failure measure; in addition, $1 - S$ characterizes instantaneous effects of the failure state probability measure on the dynamic of survival state. Moreover, the differential of S in (10.1) is directly proportional to the product of the variance SF of binary states probability measure of population dynamic of time-to-event process and time Δt . The rate function λ may depend on time and or covariate states of Bernoulli-type dynamic process, and parameters of time-to-event process.

The development of nonlinear survival state dynamic model (10.1) motivates to study a very general survival state dynamic model of time-to-event process described by

$$dS = -\lambda(t, S, C) dt, \quad S(t_0) = S_0, \quad (10.2)$$

where λ is a continuous function defined on $\mathbb{R} \times \mathbb{R} \times B$ into \mathbb{R} , and it is smooth enough to assure the existence, uniqueness, and the non-negativity of solution process of (10.2) with $0 \leq S \leq 1$, whenever $0 \leq S_0 \leq 1$ and covariate $C \in B$. Moreover, the solution process $S(t, t_0, S_0)$ is increasing in S_0 for each $(t, t_0) \in \mathbb{R} \times \mathbb{R}$.

In the following, we present an example that exhibits the role and scope of the presented dynamic modeling approach.

Example 10.1: We consider the following very simple probabilistic binary state dynamic model under the influence of time-to-event dynamic process. We consider

$$\begin{cases} dS = (-\beta_S S + \alpha_S) dt, & S(t_0) = S_0, \quad 0 < S_0 < 1, \\ dF = (-\beta_F F + \alpha_F) dt, & F(t_0) = F_0, \quad 0 < F_0 < 1, \end{cases} \quad (10.3)$$

where $\beta_S, \alpha_S, \beta_F$ and α_F are positive real numbers; these positive parameters satisfy the following conditions: $0 < \alpha_S < \beta_S$ and $\alpha_F < \beta_F$. $S(t) = \exp[-\beta_S(t-t_0)]S_0 + \frac{\alpha_S}{\beta_S}(1 - \exp[-\beta_S(t-t_0)])$ and $F(t) = \exp[-\beta_F(t-t_0)]F_0 + \frac{\alpha_F}{\beta_F}(1 - \exp[-\beta_F(t-t_0)])$ are solution processes of (10.3). Moreover, $0 < F(t) \leq 1$ and $0 < S(t) \leq 1$. In addition, $F(t) + S(t) = 1$, provided $\beta \equiv \beta_S = \beta_F$ and $\alpha_S + \alpha_F = \beta$.

Remark 10.1: Currently, we do not have any real-world data to justify the validity of its usage. In fact, this opens a new avenue to undertake a study of time-to-event process. We note that this example provides a theoretical illustration for the measure of sustainability/unsustainability, stability/unstability, sustainable/unsustainable invariant sets, and attainable/unattainable sets.

Remark 10.2: Let (t_0, S_0) be a given initial condition. The initial data (t_0, S_0) together with (10.1) is referred to as the initial value problem (IVP)[3]. Employing an elementary technique, the initial value problem

$$dS = -\lambda(t)S(1-S) dt, \quad S(t_0) = S_0, \quad t \in [t_0, \infty), \quad (10.4)$$

has a unique non-negative solution.

Moreover, the closed-form solution process of (10.4) is represented by

$$S(t) = \frac{S(t_0) \exp\left[-\int_{t_0}^t \lambda(s) ds\right]}{1 - S(t_0) + S(t_0) \exp\left[-\int_{t_0}^t \lambda(s) ds\right]}. \quad (10.5)$$

The solution representation in (10.5) can be rewritten as

$$S(t) = \frac{1}{1 + \exp[H(t) - \alpha(t_0)]}, \quad S(t_0) = \frac{1}{1 + \exp[-\alpha(t_0)]}, \quad (10.6)$$

where $H(t) = H(t_0) + \int_{t_0}^t \lambda(s)ds$ and $\alpha(t_0) = H(t_0) - \ln \left[\frac{1-S(t_0)}{S(t_0)} \right]$.

From (10.6), we further note that

$$F(t) = \frac{1}{1 + \exp[\alpha(t_0) - H(t)]}. \quad (10.7)$$

F in (10.7) can be referred to as a generalized logistic distribution.

In the following, we exhibit a well-known log-logistic distribution as a special case of (10.4).

Example 10.2: Let us consider a transformation,

$$Y = \ln T = \alpha + \sigma X, \quad (10.8)$$

where $\alpha \in \mathbb{R}, \sigma > 0$, and a random variable X has the standard logistic cumulative distribution [11]. Under the transformation (10.8), (10.4) reduces to

$$dS = -\frac{1}{\sigma t} S(1-S)dt, \quad S(t_0) = S_0,$$

with $\lambda = \frac{1}{\sigma t}$, $H(t) = \frac{\ln t}{\sigma}$ and $\alpha(t_0) = -\ln \left[\frac{1-S_0}{S_0} \right] + \frac{\ln t_0}{\sigma}$.

The nonlinear survival state dynamic model described by (10.2) is too restrictive. It does not address the problems of external intervention processes generated by the usage of modern scientific, engineering, medical and technological tools/products/procedures/etc. In order to incorporate updated tools (intervention processes) for the betterment of services/results/benefits, dynamic model (10.2) needs to be modified. For this purpose, we introduce a definition and modify dynamic model (10.2).

Definition 10.1: Let $t_0 < t_1 < t_2 < \dots < t_k < t_{k+1}$ be a given partition (P) of a time interval $[t_0, T]$, and $t_{k+1} \leq \infty$. Let $\lambda_1, \lambda_2, \dots, \lambda_{k+1}$ be model parameters. We associate a finite increasing sequence $\{t_{j-1}\}_{j=1}^{k+1}$ of intervention process corresponding to the partition (P) of the overall time interval $[t_0, T]$ of study. Moreover, we decompose $[t_0, T]$ by the finite sequence of subintervals $\{[t_{j-1}, t_j]\}_{j=1}^{k+1}$ of $[t_0, T]$. A hazard/risk rate function for a nonnegative random variable T that characterizes time-to-event processes is of the following form:

$$\lambda(t) = \begin{cases} \lambda_1 & 0 \leq t < t_1 \\ \lambda_2 & t_1 \leq t < t_2 \\ \vdots & \\ \lambda_{k+1} & t \geq t_k, \end{cases} \quad (10.9)$$

where λ_j are positive real numbers for $j \in I(1, k+1)$, $(I(1, l) = \{1, 2, \dots, l\})$.

From Definition 10.1, we recognize that the sudden changes in $\lambda(t)$ are encountered due to various types of intervention processes (internal or external) [3] introduction. It is known [3] that many real-world time-to-event dynamic processes undergo

state adjustment processes, periodically. Due to constant changes in science, technology, medicine, cultural, environmental, educational, financial and socio-economic changes/behavior, continuous-time dynamic processes are frequently interrupted by discrete-time events. This results in a modification of (10.2) under the influence of intervention processes. Following the nonlinear hybrid dynamic model [3], a modified version of a probabilistic binary state dynamic model of population (10.2) under the influence of time-to-event process is described by

$$\begin{cases} dS = -\lambda(t, S)dt, & S(t_{j-1}) = S_{j-1}, \quad t \in [t_{j-1}, t_j), \\ S_j = \Lambda(t_j^-, S(t_j^-, t_{j-1}, S_{j-1})), & S(t_0) = S_0, \quad j \in I(1, k), \end{cases} \quad (10.10)$$

where λ is defined in (10.2), Λ is a Borel-measurable survival state discrete-time intervention rate function; $S(t_j^-) = S(t_j^-, t_{j-1}, S_{j-1})$ represents the left-hand limit of survival state function at time t_j . We note that system (10.10) is an interconnected nonlinear hybrid probabilistic binary state dynamic system composed of both continuous- and discrete-time survival state of population under the influence of time-to-event processes.

Remark 10.3: The hybrid dynamic model corresponding to (10.4) is as:

$$\begin{cases} dS = -\lambda(t)S(1-S)dt, & S(t_{j-1}) = S_{j-1}, \quad t \in [t_{j-1}, t_j), \\ S_j = S(t_j^-, t_{j-1}, S_{j-1}), & S(t_0) = S_0, \quad j \in I(1, k). \end{cases} \quad (10.11)$$

Imitating the procedure described in [3], the solution process of the initial value problem (IVP) (10.11) is as follows:

$$S(t, t_{j-1}, S_{j-1}) = \frac{1}{1 + \frac{1-S_{j-1}}{S_{j-1}} \exp \left[\int_{t_{j-1}}^t \lambda(s) ds \right]}, \quad t \in [t_{j-1}, t_j). \quad (10.12)$$

Furthermore, the solution process of the overall time-to-event dynamic process (10.11) on $[t_0, T]$ is

$$S(t, t_{j-1}, S_{j-1}) = \frac{1}{1 + \frac{1-S_{j-1}}{S_{j-1}} \exp \left[\int_{t_{j-1}}^t \lambda(s) ds \right]}, \quad t \in [t_0, T], \quad (10.13)$$

where

$$S_{j-1} = \frac{1}{1 + \frac{1-S_0}{S_0} \prod_{m=1}^{j-1} \exp \left[\int_{t_{m-1}}^{t_m} \lambda(s) ds \right]}, \quad \text{for } j \in I(1, k). \quad (10.14)$$

Moreover, from (10.13), we obtain

$$\ln \left[\frac{1-S(t, t_{j-1}, S_{j-1})}{S(t, t_{j-1}, S_{j-1})} \right] = \ln \left[\frac{1-S_{j-1}}{S_{j-1}} \right] + \int_{t_{j-1}}^t \lambda(s) ds, \quad t \in [t_0, T], \quad (10.15)$$

at time t .

In the following, we develop basic theoretical results that lay down a foundation for the development of an innovative approach for state and parameter estimation of time-to-event dynamic processes. Most of the parameter estimation methods in the survival analysis literature are centered around the closed-form representation of likelihood functions, whereby the entire data set has been utilized to estimate the parameters on the overall interval $[t_0, T]$ of study.

10.4 Formulation of large-scale nonlinear hybrid dynamic model

In this section, we develop a large-scale interconnected hybrid dynamic system composed of two subsystems. One of the systems is a hybrid dynamic population model for number of units/species/individuals/infectives, and the other is its nonlinear hybrid probabilistic binary state dynamic model of population under the influence of time-to-event process (10.10). In the light of this, the overall large-scale hybrid dynamic system is referred to as an INHDMTEP.

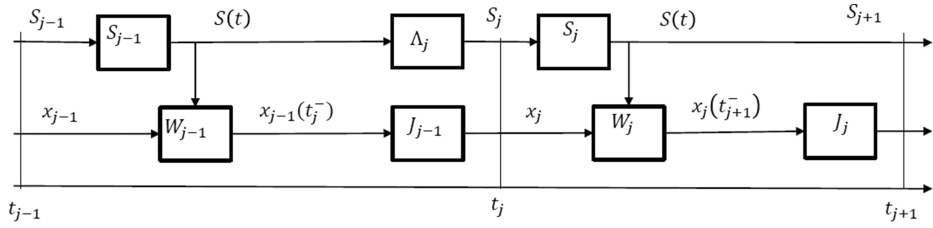
Let $x(t)$ be total number of units/individuals operating/alive (or survivals) at time t for $t \in [t_0, T]$ be described in (10.10). Let λ and S be the hazard rate and survival state functions of units/patients/infectives/species/individuals described in (10.2), respectively.

Following the argument outlined in developing dynamic models in [3, 13], we introduce the following systems of nonlinear and non-stationary differential equations:

$$\begin{cases} dx = W(t, Sx)d\eta(t), & x(t_0) = x_0, \quad t \in [t_{j-1}, t_j], \\ x_j = x_{j-1} + J(t_j^-, S(t_j^-, t_{j-1}, S_{j-1})x(t_j^-, t_{j-1}, x_{j-1}), x_{j-1}), \\ dS = -S\lambda(t, S)dt, \quad t \geq 0, \quad S(t_0) = S_0, \\ S_j = S_{j-1} + \Lambda(t_j^-, S(t_j^-, t_{j-1}, S_{j-1})), \quad S(t_0) = S_0, \end{cases} \quad (10.16)$$

where S is a survival state rate function; the finite sequence of subintervals $\{[t_{j-1}, t_j]\}_{j=1}^{k+1}$ is defined in Definition 10.1; λ is defined in (10.2); W is a continuous function defined on $[t_{j-1}, t_j] \times \mathbb{R}$ into \mathbb{R} for $j \in I(1, k)$; $J(t_j^-, S(t_j^-, t_{j-1}, S_{j-1})x(t_j^-, t_{j-1}, x_{j-1}), x_{j-1}) = \eta_j^- W(t_j^-, S(t_j^-, t_{j-1}, S_{j-1})x(t_j^-, t_{j-1}, S_{j-1})) - \eta_{j-1}^+ W(t_{j-1}, S_{j-1}x_{j-1})$; η_j^- and η_{j-1}^+ are positive constants; η is a function of bounded variation defined on $[t_{j-1}, t_j]$ into \mathbb{R} ; Λ is defined in (10.10).

In addition, it is assumed that (10.16) has a solution process [3]. It is denoted by (x, S) . The Flowchart 10.1 exhibits the structural and operational dynamic of INHDMTEP.



Flowchart 10.1: Structural and operational dynamic of INHDMTTEP.

Remark 10.4: In addition to the conditions on (10.16), if W and λ are non-negative functions (i.e. $W, \lambda \geq 0$), and if

$$\eta(t) = \begin{cases} 0, & t \in [t_{j-1}, t_j), \\ 1, & t = t_j, \end{cases}$$

then (10.16) reduces to a partially discrete-time interconnected nonlinear hybrid dynamic system:

$$\begin{cases} dx = 0 dt, & x(t_0) = x_0, & t \in [t_{j-1}, t_j), \\ x_j = x_{j-1} + J(t_j^-, S(t_j^-, t_{j-1}, S_{j-1})x(t_j^-, t_{j-1}, x_{j-1}), x_{j-1}), \\ dS = -S\lambda(t, S)dt, & t \in [t_{j-1}, t_j), \\ S_j = S_{j-1} + \Lambda(t_j^-, S(t_j^-, t_{j-1}, S_{j-1})), & S(t_0) = S_0. \end{cases} \quad (10.17)$$

Example 10.3: $S\lambda(t, S) = \lambda(t)S(1 - S)$ is an admissible function in (10.16) and (10.17).

In the following section, we derive a theoretical transformed interconnected discrete-time dynamic algorithm for time-to-event data statistic.

10.5 Derivation of theoretical interconnected discrete-time dynamic algorithm

Employing the interconnected hybrid dynamic model for time-to-event process described in (10.16), we present a fundamental result regarding continuous- and discrete-time dynamic of survival species and its survival state or operating objects or thoughts. Prior to this result, we introduce a few concepts that will be utilized, subsequently.

Definition 10.2: Let z be a function defined by $z(t) = x(t)S(t)$, where S and x are solution processes of (10.16) for $t \in [t_0, T)$. Moreover, for each $t \in [t_0, T)$, $z(t)$ stands for the number of survivals/operating units at t .

Definition 10.3: The sequence $\{t_{j-1}\}_{j=1}^k$ defined in Definition 10.1 is referred to as the conceptual data collection/observation/intervention sequence over the interval of time $[t_0, T)$, and the sequence of subinterval $\{[t_{j-1}, t_j]\}_{j=1}^k$ is called a continuous-time hybrid system operating subinterval sequence with its right-end-point as a conceptual data observation time.

Now, we are ready to present a fundamental theoretical result. The presented result provides a foundation for the development of survival data analysis of time-to-event processes in any field of interest that are conceptually similar but apparently different [3].

Theorem 10.1: Let (x, S) be a solution process of (10.16), and let t_{j-1} and t_j be consecutive conceptual data observation times in a given interval of time $[t_0, T)$. Then the transformed interconnected nonlinear hybrid dynamic model of survival species and state of time-to-event dynamic process described by (10.16) is reduced to

$$\begin{cases} dz = -z\lambda(t, S)dt + SW(t, z)d\eta(t), & z(t_{j-1}) = z_{j-1}, \quad \text{for } t \in [t_{j-1}, t_j), \text{ and } j \in I(1, k), \\ dS = -S\lambda(t, S)dt, & S(t_0) = S_0, \\ z_j = z_{j-1} + x_{j-1}\Lambda(t_j^-, S(t_j^-, t_{j-1}, S_{j-1})) + S_j J(t_j^-, z(t_j^-, t_{j-1}, x_{j-1}), x_{j-1}), & z(t_0) = z_0, \end{cases} \quad (10.18)$$

and corresponding transformed discrete-time conceptual computational interconnected dynamic algorithm

$$\begin{cases} z(t_j) = z(t_{j-1}) - \lambda(t_{j-1}, S(t_{j-1}))z(t_{j-1})\Delta t_j + \gamma_j, & z(t_0) = z_0, \\ S(t_j) = S(t_{j-1}) - \lambda(t_{j-1}, S(t_{j-1}))S(t_{j-1})\Delta t_j, & S(t_0) = S_0, \quad j \in I(1, k), \end{cases} \quad (10.19)$$

where z is defined in Definition 10.2; $\gamma_j = \eta_j^-(S(t_j^-)W(t_j^-, z_j^-) - \eta_{j-1}^+(S(t_{j-1})W(t_{j-1}, z_{j-1}))$, and it represents change in survivals due to either failure/censored/admitted or change-point process; and $\Delta t_j = t_j - t_{j-1}$ for $j \in I(1, k)$.

Proof. For $t \in [t_{j-1}, t_j)$, $j \geq 1$, from Definition 10.2 and the nature of S , we have

$$\begin{aligned} dz(t) &= x(t)dS + S(t)dx(t) \\ &= x(t)[-S(t)\lambda(t, S(t))dt] + S(t)W(t, S(t)x)d\eta(t) \\ &= -z(t)\lambda(t, S(t))dt + S(t)W(t, z(t))d\eta(t). \end{aligned} \quad (10.20)$$

This establishes the continuous-time dynamic subsystem in (10.18). The proofs of the discrete-time dynamic subsystem in (10.19) and iterative process (10.20) are outlined below.

From the discrete-time dynamic of population/species state x and survival state intervention process in (10.16), we have

$$z_j = z_{j-1} + x_{j-1}\Lambda(t_j^-, S(t_j^-, t_{j-1}, S_{j-1})) + S_j J(t_j^-, z(t_j^-, t_{j-1}, x_{j-1}), x_{j-1}) \quad (10.21)$$

This establishes the discrete-time dynamic subsystem in (10.18).

Now, applying the Euler-type numerical scheme [14] to (10.20) over an interval $[t_{j-1}, t_j]$, we obtain

$$z(t_j) - z(t_{j-1}) = -\lambda(t_{j-1}, S(t_{j-1}))z(t_{j-1})\Delta t_j + \int_{t_{j-1}}^{t_j} S(s)W(s, z(s))d\eta(s). \quad (10.22)$$

By applying the Riemann–Stieltjes integral property [24], we approximate (10.21) and (10.22) as

$$z(t_j) - z(t_{j-1}) = -\lambda(t_{j-1}, S(t_{j-1}))z(t_{j-1})\Delta t_j + \eta_j^- S(t_j^-)W(t_j^-, z(t_j^-)) - \eta_{j-1}^+ S(t_{j-1})W(t_{j-1}, z_{j-1}). \quad (10.23)$$

From (10.23), we have

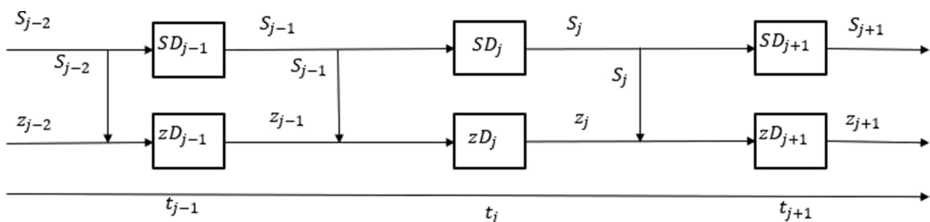
$$z(t_j) = [1 - \lambda(t_{j-1}, S(t_{j-1}))\Delta t_j]z(t_{j-1}) + \gamma_j \quad \text{for } j \in I(1, k), \quad (10.24)$$

where $\gamma_j = \eta_j^- S(t_j^-)W(t_j^-, z(t_j^-)) - \eta_{j-1}^+ S(t_{j-1})W(t_{j-1}, z_{j-1})$ is a jump at t_j , and it represents change in survivals due to an intervention process. Applying the Euler numerical scheme to the continuous-time dynamic in (10.16) over the interval $[t_{j-1}, t_j]$ yields

$$S(t_j) = S(t_{j-1}) - \lambda(t_{j-1}, S(t_{j-1}))S(t_{j-1})\Delta t_j. \quad (10.25)$$

Equations (10.24) and (10.25) establish the discrete-time conceptual theoretical dynamic for joint survival state process in the context of joint continuous-time interconnected nonlinear dynamic and the discrete-time intervention component processes (10.18). Moreover, (10.24) and (10.25) exhibit the derivation of (10.19). This establishes the proof of Theorem 10.1. Furthermore (10.19) is an approximation of the transformed intervention process in (10.18).

Remark 10.5: The transformed theoretical discrete-time computational dynamic process (10.19) provides a basis for the discrete-time conceptual computational and simulation dynamic processes. Flowchart 10.2 exhibits the structural and discrete-time operational dynamic of interconnected discrete-time algorithm of time-to-event data statistic (IDATTEDS). The theoretical procedure of IDATTEDS is considered to be a single shot approach.



Flowchart 10.2: Structural and operational dynamic of IDATTEDS.

Now, using (10.17), we present a result that is jointly totally discrete-time interconnected nonlinear hybrid system.

Corollary 10.1: *Let us consider a very special case of (10.17) as follows:*

$$\begin{cases} dx = 0 dt, & x(t_0) = x_0, & t \in [t_{j-1}, t_j], \\ x_j = x_{j-1} + J(t_j^-, S(t_j^-, t_{j-1}, S_{j-1}))x(t_j^-, t_{j-1}, x_{j-1}), \\ dS = 0, & t \in [t_{j-1}, t_j], \\ S_j = S_{j-1} + \Lambda(t_j^-, S(t_j^-, t_{j-1}, S_{j-1})), S(t_0) = S_0. \end{cases} \quad (10.26)$$

Then under the assumptions of Theorem 10.1, (10.26) reduces to

$$\begin{cases} dz = 0 dt, & z(t_{j-1}) = z_{j-1}, & t \in [t_{j-1}, t_j], \\ z_j = z_{j-1} + x_{j-1}\Lambda(t_j^-, S(t_j^-, t_{j-1}, S_{j-1})) + S_j J(t_j^-, z(t_j^-, t_{j-1}, x_{j-1}), x_{j-1}), & z(t_0) = z_0, \end{cases} \quad (10.27)$$

and

$$\begin{cases} z(t_j) = z(t_{j-1}) - \lambda(t_{j-1}, S(t_{j-1}))z(t_{j-1}) + \gamma_j, & z(t_0) = S_0 x_0, \\ S(t_j) = S(t_{j-1}) - \lambda(t_{j-1}, S(t_{j-1}))S(t_{j-1}), & S(t_0) = S_0, j \in I(1, k). \end{cases} \quad (10.28)$$

We remark that this corollary is transformed totally discrete-time version of nonlinear hybrid dynamic system operating under discrete-time intervention component processes.

In the next section, we establish theoretical discrete-time conceptual computational parameter and state estimation algorithms.

10.6 Conceptual computational parameter and state estimations

Using Definition 10.2 and the transformed theoretical discrete-time iterative process (10.19), we develop conceptual computational parameter dynamic estimation algorithms. This approach is referred to as IDATTEDS and is a single shot procedure. In addition, parameter and state estimations are determined, conceptually. For this purpose, we introduce a few definitions and notations.

Definition 10.4: Let t_{j-1} and t_j be consecutive conceptual data collection/observation times on $[t_0, T)$, and let $z(t)$ be as defined in Definition 10.2. $z(t_{j-1})$ stands for the number of survivals at the time t_{j-1} for each $j \in I(1, k)$. Moreover, the number of survivals $z(t_{j-1})$ are under observation/supervision over the sub-interval of time $[t_{j-1}, t_j)$ of length Δt_j . $z(t_{j-1})\Delta t_j$ is the amount of time spent by $z(t_{j-1})$ survivals under observation/testing/evaluation over the length Δt_j of time interval $[t_{j-1}, t_j)$.

Definition 10.5: For $j \in I(1, k)$, let t_{j-1} and t_j be consecutive data observation/supervision times of population/objects/entities and state survival dynamic process. The parameter estimate at t_j is defined by the quotient of change of entities/objects over the consecutive change time subinterval $[t_{j-1}, t_j)$ and the total time spent by the entities/objects under observation/supervision over the subinterval $[t_{j-1}, t_j)$ of length Δt_j .

Definition 10.6: Let $\{z_{j-1}\}_{j=1}^k$ be an overall sequence of transformed conceptual state data set with respect to the conceptual state data collection/observation time sequence $\{t_{j-1}\}_{j=1}^k$, and let $\{t_{j-1i-1}^f\}_{i=1}^{k_f}$, $\{t_{j-1l-1}^c\}_{l=1}^{k_c}$ and $\{t_{j-1m-1}^a\}_{m=1}^{k_a}$ be overall conceptual failure, censored and admitted increasing subsequences of the overall conceptual data collection time sequence $\{t_{j-1}\}_{j=1}^k$, respectively. Three subsequences of the overall conceptual state data sequence $\{z_{j-1}\}_{j=1}^k$ associated with the three overall conceptual subsequences of failure, censored and admitted time subsequences are represented by

$$\{z_{j-1i-1}^f\}_{i=1}^{k_f}, \quad \{z_{j-1l-1}^c\}_{l=1}^{k_c}, \quad \text{and} \quad \{z_{j-1m-1}^a\}_{m=1}^{k_a}, \quad (10.29)$$

respectively. These conceptual state data subsequences are called conceptual failure, censored and admitted state subsequences of $\{z_{j-1}\}_{j=1}^k$, respectively. We note that $k_f + k_c + k_a = k$.

Definition 10.7: The union of the boundary point set of the interval $[t_0, T)$ and the range of the overall failure subsequence $\{t_{j-1i-1}^f\}_{i=1}^{k_f+1}$ constitutes a partition of the interval $[t_0, T)$, $T \leq \infty$. This partition of $[t_0, T)$, $T \leq \infty$ is termed as overall conceptual failure-time partition of $[t_0, T)$, and it is denoted by $(P^f = \bigcup_{j=2}^k P_{j-1}^f)$. Moreover, $P^f \subseteq P$ in Definition 10.1. Furthermore, P^c and P^a can be defined similarly; in fact, $P^f \cup P^c \cup P^a = P$.

Definition 10.8: For $j \in I(1, k)$ and any consecutive pair $(t_{j-1i-1}^f, t_{j-1i}^f)$ of conceptual failure-times for $i \in I(1, k_f)$ under the notations $t_{j-100}^f = t_{j-1}^f$ for $i = 1$ and either $l = 1$ or $m = 1$; furthermore, $t_{j-100}^f = t_0$ if $i = j = 1$; either $t_{j-1i-1}^f + 1 = t_{j-1i-1}^f = t_{j-1i}^f$ or $t_{j-1i-1}^f = t_{j-1i-1m}^f = t_{j-1ika_i+1}^f = t_{j-1i}^f$ depending on whether $l = k_{c_i} + 1$ or $m = k_{a_i} + 1$; a $j - 1$ th consecutive conceptual failure-time subinterval is $[t_{j-1i-1}^f, t_{j-1i}^f)$ for $i \in I(1, k_f)$. In addition, the conceptual transformed state data associated with the consecutive conceptual initial failure times is denoted by $z_{j-100}^f = z_{j-1}^f$ and for $j = 1$, $z_{1-10}^f = z_{000}^f = z_0^f$.

Definition 10.9: Let $\{z_{j-1l-1}^c\}_{l=1}^{k_c}$ and $\{z_{j-1m-1}^a\}_{m=1}^{k_a}$ be overall censored and admitted conceptual transformed state data subsequences defined in Definition 10.6. Let $\{t_{j-1i-1p}^c\}_{p=1}^{k_{c_i}}$ and $\{t_{j-1i-1q}^a\}_{q=1}^{k_{a_i}}$ be conceptual subsequences restricted to the $j - 1$ th consecutive conceptual failure-time subinterval $[t_{j-1i-1}^f, t_{j-1i}^f)$ of overall conceptual censored and admitted subsequences $\{t_{j-1l-1}^c\}_{l=1}^{k_c}$ and $\{t_{j-1m-1}^a\}_{m=1}^{k_a}$ of times of the overall sequence $\{t_{j-1}\}_{j=1}^k$ of times, respectively. Moreover, the union of the boundary points of $[t_{j-1i-1}^f, t_{j-1i}^f)$ and the range of subsequences $\{t_{j-1i-1p}^c\}_{p=1}^{k_{c_i}}$ and $\{t_{j-1i-1q}^a\}_{q=1}^{k_{a_i}}$ form a subpartition P_{j-1}^f of P^f and the partition of $j - 1$ th subinterval $[t_{j-1i-1}^f, t_{j-1i}^f)$. Two

subsequences of the overall censored and/or admitted conceptual transformed state data subsequences $\{z_{j-1l-1}^c\}_{l=1}^{k_c}$ and/or $\{z_{j-1m-1}^a\}_{m=1}^{k_a}$ with respect to the two overall conceptual censored and admitted time subsequences of the overall sequence of times $\{[t_{j-1}, t_j]\}_{j=1}^k$ restricted to the $j-1$ th consecutive conceptual failure-time subinterval $[t_{j-1i-1}^f, t_{j-1i}^f]$ are represented by

$$\{z_{j-1i-1p-1}^c\}_{p=1}^{k_{c_i}} \quad \text{and} \quad \{z_{j-1i-1q-1}^a\}_{q=1}^{k_{a_i}}, \quad (10.30)$$

respectively. These conceptual transformed state data subsequences are called subsequences of the overall censored and admitted conceptual state data subsequences $\{z_{j-1l-1}^c\}_{l=1}^{k_c}$ and $\{z_{j-1m-1}^a\}_{m=1}^{k_a}$ of the overall conceptual sequence $\{z_{j-1}\}_{j=1}^k$ of data set, respectively. We note that $k_c = \sum_{l=1}^{k_c} k_{c_l}$ and $k_a = \sum_{m=1}^{k_a} k_{a_m}$. Moreover, for $p=1$ and $q=1$, (10.30) reduces to $z_{j-1i-10}^c = z_{j-1i-1}^c$ and $z_{j-1i-10}^a = z_{j-1i-1}^a$ respectively; for $p=k_{c_i}+2$, and $q=k_{a_i}+2$, we have $z_{j-1i-1k_{c_i}+1}^c = z_{ji}^c$ and $z_{j-1i-1k_{a_i}+1}^a = z_{ji}^a$ respectively.

Remark 10.6: The transformed discrete-time dynamic process (10.19) is referred to as conceptual computational interconnected dynamic algorithm for time-to-event data statistic (IDATTEDS). Moreover, from (10.19), we introduce three more special transformed theoretical numerical dynamic schemes for time-to-event dynamic processes, namely: (i) abnormal/failure/death/removal/infective/etc. species or objects, (ii) censored/quitting/withdrawn/etc. species or objects, and (iii) admitted/joining/re-lapsed/susceptible/etc. species or objects. We further note that the presented numerical dynamic schemes allow “ties” with deaths/failure or censored/quitting or admitted/susceptible process. In addition, the population/species under the presented observation/supervision process includes the abnormal/species/patient/objects/infectives population as a special case.

(i) (For each $j \in I(1, k)$, let t_{j-1}^{fca} be either failure, censored or admitting time at t_{j-1} . For $\gamma_j^f = 0$, the transformed discrete-time dynamic component (10.19) at t_j^f for failure/death/removal/infective/etc. process data set is described by

$$z(t_j^f) = \left[1 - \lambda(t_{j-1}^{fca}, S(t_{j-1}^{fca})) \Delta t_j^f \right] z(t_{j-1}^{fca}) \quad \text{for } j \in I(1, k). \quad (10.31)$$

This together with (10.19), one obtains

$$\begin{cases} z(t_j^f) - z(t_{j-1}^{fca}) = -\lambda(t_{j-1}, S(t_{j-1})) z(t_{j-1}^{fca}) \Delta t_j^f, & z(t_0) = z_0, \\ S(t_j) = S(t_{j-1}) - \lambda(t_{j-1}^f, S(t_{j-1}^f)) S(t_{j-1}^f) \Delta t_j^f, & S(t_0) = S_0, \end{cases} \quad (10.32)$$

where a pair (t_{j-1}^{fca}, t_j^f) stands for either (t_{j-1}^f, t_j^f) , or (t_{j-1}^c, t_j^f) or (t_{j-1}^a, t_j^f) ; t_j^f, t_{j-1}^c and t_{j-1}^a stand for failure, censored and admitting times, respectively; $\Delta t_j^f = t_j^f - t_{j-1}^{fca}$.

(ii) For each $j \in I(1, k)$, let t_{j-1}^{caf} be either censored, admitting or failure time at t_{j-1} . γ_j^c stands for the conceptual number of censored objects/infectives/quitting/withdrawn/etc. at a time t_j^c . The transformed discrete-time component (10.19) at t_j^c for censored/ listed/identified process data set is reduced to

$$z(t_j^c) = \left[1 - \lambda(t_{j-1}^{caf}, S(t_{j-1}^{caf})) \Delta t_j^c \right] z(t_{j-1}^{caf}) - \gamma_j^c \quad \text{for } j \in I(1, k), \quad (10.33)$$

where a pair (t_{j-1}^{caf}, t_j^c) stands for either (t_{j-1}^c, t_j^c) , (t_{j-1}^a, t_j^c) or (t_{j-1}^f, t_j^c) ; $\Delta t_j^c = t_j^c - t_{j-1}^{caf}$. Thus

$$\begin{cases} z(t_j^c) - z(t_{j-1}^{caf}) = -\lambda(t_{j-1}, S(t_{j-1})) z(t_{j-1}^{caf}) \Delta t_j^c - \gamma_j^c, z(t_0) = z_0, \\ S(t_j) = S(t_{j-1}) - \lambda(t_{j-1}^f, S(t_{j-1}^f)) S(t_{j-1}^f) \Delta t_j^f, S(t_0) = S_0. \end{cases} \quad (10.34)$$

(iii) For each $j \in I(1, k)$, let t_{j-1}^{acf} be either admitting, censored or failure time at t_{j-1} . γ_j^a stands for the conceptual number of objects/infectives/etc. arriving/joining at a time t_j^a . The transformed discrete-time dynamic component (10.19) at t_j^a for admitting/ joining/sustainable/recruiting/etc. process data set is represented by

$$z(t_j^a) = \left[1 - \lambda(t_{j-1}^{acf}, S(t_{j-1}^{acf})) \Delta t_j^a \right] z(t_{j-1}^{acf}) + \gamma_j^a \quad \text{for } j \in I(1, k), \quad (10.35)$$

where a pair (t_{j-1}^{acf}, t_j^a) belongs to a set: $(t_{j-1}^{acf}, t_j^a) \in \{(t_{j-1}^a, t_j^a), (t_{j-1}^c, t_j^a), (t_{j-1}^f, t_j^a)\}$; $\Delta t_j^a = t_j^a - t_{j-1}^{acf}$.

Hence

$$\begin{cases} z(t_j^a) - z(t_{j-1}^{acf}) = -\lambda(t_{j-1}, S(t_{j-1})) z(t_{j-1}^{acf}) \Delta t_j^a + \gamma_j^a, z(t_0) = z_0, \\ S(t_j) = S(t_{j-1}) - \lambda(t_{j-1}^f, S(t_{j-1}^f)) S(t_{j-1}^f) \Delta t_j^f, S(t_0) = S_0. \end{cases} \quad (10.36)$$

(iv) Remarks (i), (ii), and (iii) remain valid for the iterative process (10.28)

(I) For $\gamma_j^f = 0$, (10.28) reduces to

$$\begin{cases} z(t_j^f) - z(t_{j-1}^{fca}) = -\lambda(t_{j-1}, S(t_{j-1})) z(t_{j-1}^{fca}) \Delta t_j^f, z(t_0) = z_0, \\ S(t_j) = S(t_{j-1}) - \lambda(t_{j-1}^f, S(t_{j-1}^f)) S(t_{j-1}^f) \Delta t_j^f, S(t_0) = S_0. \end{cases} \quad (10.37)$$

(II) For $\gamma_j = \gamma_j^c$ in (10.28), (10.28) reduces to

$$\begin{cases} z(t_j^c) - z(t_{j-1}^{caf}) = -\lambda(t_{j-1}, S(t_{j-1})) z(t_{j-1}^{caf}) \Delta t_j^c - \gamma_j^c, z(t_0) = z_0, \\ S(t_j) = S(t_{j-1}) - \lambda(t_{j-1}^f, S(t_{j-1}^f)) S(t_{j-1}^f) \Delta t_j^f, S(t_0) = S_0. \end{cases} \quad (10.38)$$

(III) For $\gamma_j = \gamma_j^a$ in (10.28), (10.28) reduces to

$$\begin{cases} z(t_j^a) - z(t_{j-1}^{acf}) = -\lambda(t_{j-1}, S(t_{j-1})) z(t_{j-1}^{acf}) \Delta t_j^a + \gamma_j^a, z(t_0) = z_0, \\ S(t_j) = S(t_{j-1}) - \lambda(t_{j-1}^f, S(t_{j-1}^f)) S(t_{j-1}^f) \Delta t_j^f, S(t_0) = S_0. \end{cases} \quad (10.39)$$

In the following, we present very simple result that provides an insight for the understanding of the discrete-time dynamic of state and parameter estimation problems. Moreover, the result provides one of the assumptions of the principle of mathematical induction .

Theorem 10.2: Assume that the conditions of Theorem 10.1 in the context of Remarks 10.6 (i), (ii), and (iii) and Definitions 10.8 and 10.9 are satisfied.

(a) For $j \in I(1, k)$, let t_{j-1}^f and t_j^f be consecutive risk/failure/removal/death/non-operational times in $[t_0, T)$, $T \leq \infty$. Then the theoretical/computational estimation algorithm and parameter estimation for $\lambda(t, S(t))$ at t_j^f are described as

$$\begin{cases} z(t_j^f) = z(t_{j-1}^f) - \lambda(t_{j-1}^f, S(t_{j-1}^f))z(t_{j-1}^f)\Delta t_j^f, & z(t_0) = z_0, \\ S(t_j^f) = S(t_{j-1}^f) - \lambda(t_{j-1}^f, S(t_{j-1}^f))S(t_{j-1}^f)\Delta t_j^f, & S(t_0) = S_0, \end{cases} \quad (10.40)$$

and

$$\hat{\lambda}(t_{j-1}^f, S(t_{j-1}^f)) = \frac{z(t_{j-1}^f) - z(t_j^f)}{z(t_{j-1}^f)\Delta t_j^f}, \quad \Delta t_j^f = t_j^f - t_{j-1}^f. \quad (10.41)$$

Moreover an overall conceptual computational estimate for $\lambda(t, S(t))$, $S(t)$, and $z(t)$ on the time interval of study $[t_0, T)$, $T \leq \infty$ is

$$\begin{cases} \hat{\lambda}(t, \hat{S}(t_{j-1})) = \hat{\lambda}(t_{j-1}^f, \hat{S}(t_{j-1}^f)), & \text{for } t \in [t_{j-1}^f, t_j^f) \text{ and } j \in I(1, k), \\ \hat{S}(t, t_{j-1}, \hat{S}_{j-1}), \hat{S}(t_{j-1}) = \hat{S}_{j-1}, \\ \hat{z}(t, t_{j-1}, \hat{z}_{j-1}), \hat{z}(t_{j-1}) = \hat{z}_{j-1}. \end{cases} \quad (10.42)$$

(b) For $j \in I(1, k)$, if $t_{j-1}^f < t_j^c < t_j^f$, and t_j^c is censored time between a pair of consecutive failure times t_{j-1}^f and t_j^f in $[t_0, T)$, $T \leq \infty$, then the theoretical/computational estimation algorithm and parameter estimation for $\lambda(t, S(t))$ at t_j^f are respectively determined by

$$\begin{cases} z(t_j^f) = z(t_{j-1}^f) - \lambda(t_{j-1}^f, S(t_{j-1}^f)) \left[z(t_{j-1}^f)\Delta t_j^{cf} + z(t_j^c)\Delta t_j^{fc} \right] - \gamma_j^c, & z(t_0) = z_0, \\ S(t_j^f) = S(t_{j-1}^f) - \lambda(t_{j-1}^f, S(t_{j-1}^f))S(t_{j-1}^f)\Delta t_j^f, & S(t_0) = S_0, \end{cases} \quad (10.43)$$

and

$$\hat{\lambda}(t_{j-1}, \hat{S}(t_{j-1})) = \frac{z(t_{j-1}^f) - z(t_j^f) - \gamma_j^c}{\left[z(t_{j-1}^f)\Delta t_j^{fc} + z(t_j^c)\Delta t_j^{cf} \right]}, \quad (10.44)$$

where $\Delta t_j^{fc} = t_j^c - t_{j-1}^f$, $\Delta t_j^{cf} = t_j^f - t_j^c$. Moreover an overall conceptual computational estimate for $\lambda(t, S(t))$, $S(t)$, and $z(t)$ on the time interval of study $[t_0, T)$, $T \leq \infty$ is

$$\begin{cases} \hat{\lambda}(t, \hat{S}(t_{j-1})) = \hat{\lambda}(t_{j-1}^f, \hat{S}(t_{j-1}^f)), & \text{for } t \in [t_{j-1}^f, t_j^f) \text{ and } j \in I(1, k), \\ \hat{S}(t, t_{j-1}, \hat{S}_{j-1}), \hat{S}(t_{j-1}) = \hat{S}_{j-1}, \\ \hat{z}(t, t_{j-1}, \hat{z}_{j-1}), \hat{z}(t_{j-1}) = \hat{z}_{j-1}. \end{cases} \quad (10.45)$$

(c) For $j \in I(1, k)$, if $t_{j-1}^f < t_j^a < t_j^f$, and t_j^a is joining/admitting time between a pair of consecutive failure times t_{j-1}^f and t_j^f in $[t_0, T)$, $T \leq \infty$, then the theoretical/computational estimation algorithm and parameter estimation for $\lambda(t, S(t))$ at t_j^f are determined by

$$\begin{cases} z(t_j^f) = z(t_{j-1}^f) - \lambda(t_{j-1}^f, S(t_{j-1}^f)) [z(t_{j-1}^f) \Delta t_j^{af} + z(t_j^a) \Delta t_j^{af}] + \gamma_j^a, z(t_0) = z_0 \\ S(t_j^f) = S(t_{j-1}^f) - \lambda(t_{j-1}^f, S(t_{j-1}^f)) S(t_{j-1}^f) \Delta t_j^f, S(t_0) = S_0, \end{cases} \quad (10.46)$$

and

$$\hat{\lambda}(t_{j-1}^f, \hat{S}(t_{j-1}^f)) = \frac{z(t_{j-1}^f) - z(t_j^f) + \gamma_j^a}{[z(t_{j-1}^f) \Delta t_{j1}^{fa} + z(t_{j1}^a) \Delta t_{j1}^{af}]}, \quad (10.47)$$

where $\Delta t_j^{af} = t_j^a - t_{j-1}^f$, $\Delta t_j^{fa} = t_j^f - t_j^a$. Moreover an overall conceptual computational estimate for $\lambda(t, S(t))$, $S(t)$, and $z(t)$ and on the time interval of study $[t_0, T)$, $T \leq \infty$ is

$$\begin{cases} \hat{\lambda}(t, \hat{S}(t_{j-1})) = \hat{\lambda}(t_{j-1}^f, \hat{S}(t_{j-1}^f)), & \text{for } t \in [t_{j-1}^f, t_j^f) \text{ and } j \in I(1, k), \\ \hat{S}(t, t_{j-1}, \hat{S}_{j-1}), \hat{S}(t_{j-1}) = \hat{S}_{j-1}, \\ \hat{z}(t, t_{j-1}, \hat{z}_{j-1}), \hat{z}(t_{j-1}) = \hat{z}_{j-1}. \end{cases} \quad (10.48)$$

Proof. (a) Let t_{j-1}^f and t_j^f be two consecutive conceptual failure times. In this case, $k_{ci} = k_{ai} = 0$. From Definition 10.8, here $i = 1$, therefore, for the subinterval $[t_{j-1-i}^f, t_{j-i}^f)$, $i = 1$, and $t_{j1}^f = t_j^f$; $t_{j-1}^f = t_{j-100}^f$. Using the theoretical discrete-time iterative scheme (10.19) and Remark 6.1(i) to (6.4), we have

$$\begin{cases} z(t_j^f) = z(t_{j-1}^f) - \lambda(t_{j-1}^f, S(t_{j-1}^f)) z(t_{j-1}^f) \Delta t_j^f, z(t_0) = z_0, \\ S(t_j^f) = S(t_{j-1}^f) - \lambda(t_{j-1}^f, S(t_{j-1}^f)) S(t_{j-1}^f) \Delta t_j^f, S(t_0) = S_0. \end{cases}$$

This establishes a(i). For the validity of a(ii), from Definition 10.4, backward substitution, and using Definition 10.5, we obtain

$$\begin{cases} \hat{\lambda}(t, \hat{S}(t_{j-1})) = \hat{\lambda}(t_{j-1}^f, S(t_{j-1}^f)) = \frac{z(t_{j-1}^f) - z(t_j^f)}{z(t_{j-1}^f) \Delta t_j^f}, & \Delta t_j^f = t_j^f - t_{j-1}^f, \\ \hat{S}(t, t_{j-1}, \hat{S}_{j-1}), \hat{S}(t_{j-1}) = \hat{S}_{j-1}, \\ \hat{z}(t, t_{j-1}, \hat{z}_{j-1}), \hat{z}(t_{j-1}) = \hat{z}_{j-1}. \end{cases}$$

for $t \in [t_{j-1}^f, t_j^f)$ and $j \in I(1, k)$. This establishes (a)(ii). This completes the proof of (a).

(b) Let t_j^c be a censoring time between two consecutive conceptual risk/failure times, t_{j-1}^f and t_j^f . We consider a partition of subinterval $[t_{j-1}^f, t_j^f]$ to be $P_{ji}^f = [t_{j-1}^f, t_j^f]$: $t_{j-1} < t_{j-1}^c < t_j$. In addition, from Definitions 10.8 and 10.9, $k_{a_i} = 0, k_{c_i} = 1$, and $0 + k_{c_i} + 2 = 3$. Thus, the size of P_{ji}^f is 3. We note that $i = 1$, since $t_{j-1}^f = t_{j-10}^f$ and $t_j^f = t_{j-2}^f = t_{j-1k_{c_i}+1}^f$.

Employing Remark 10.6(ii) in the context of $[t_{j-1}^f, t_j^f]$ and $[t_j^c, t_j^f]$, respectively, and algebraic simplifications, we have

$$z(t_j^c) - z(t_{j-1}^f) = -\lambda(t_{j-1}^f, S(t_{j-1}^f))z(t_{j-1}^f)\Delta t_{j-1}^{cf} - \gamma_j^c$$

and

$$z(t_j^f) - z(t_j^c) = -\lambda(t_j^c, S(t_j^c))z(t_j^c)\Delta t_{j-1}^{fc} = -\lambda(t_{j-1}^f, S(t_{j-1}^f))z(t_{j-1}^f)\Delta t_{j-1}^{fc}.$$

Adding and simplifying, we obtain

$$z(t_j^f) - z(t_{j-1}^f) = -\lambda(t_{j-1}^f, S(t_{j-1}^f)) \left[z(t_{j-1}^f)\Delta t_{j-1}^{cf} + z(t_{j-1}^c)\Delta t_{j-1}^{fc} \right] - \gamma_j^c,$$

and hence

$$\begin{cases} z(t_j^f) = z(t_{j-1}^f) - \lambda(t_{j-1}^f, S(t_{j-1}^f)) \left[z(t_{j-1}^f)\Delta t_{j-1}^{cf} + z(t_{j-1}^c)\Delta t_{j-1}^{fc} \right] - \gamma_j^c, z(t_0) = z_0, \\ S(t_j^f) = S(t_{j-1}^f) - \lambda(t_{j-1}^f, S(t_{j-1}^f))S(t_{j-1}^f)\Delta t_j^f, S(t_0) = S_0. \end{cases} \quad (10.49)$$

This establishes (b)(i).

From (10.49) and the backward substitution, we conclude that $z(t_{j-1}^f) - z(t_j^f) - \gamma_j^c$ is the number of failure/non-operating objects and $z(t_{j-1}^f)\Delta t_{j-1}^{cf} + z(t_j^c)\Delta t_{j-1}^{fc}$ denotes the total amount of time spent by $z(t_{j-1}^f) - z(t_j^f) - \gamma_j^c$ over the interval $[t_{j-1}, t_j]$. Hence, solving for $\lambda(t_{j-1}^f, S(t_{j-1}^f))$ establishes (b)(ii).

(c) The proof of (c) can be constructed by slightly modifying the argument for the proof of (b). This establishes proof of the theorem.

In the following, we extend Theorem 10.2, for multiple censored and admitting times between two consecutive failure times.

Theorem 10.3: Let the hypotheses of Theorem 10.1 in the context of Remarks 10.6(i), 10.6(ii), and 10.6(iii) and Definitions 10.8 and 10.9 be satisfied. For each $j \in I(1, k)$, and each $i \in I(1, k_f)$, let t_{j-1i-1}^f and t_{j-1i}^f be consecutive failure times. Let $\{t_{j-1i-1p-1}^f\}_{p=1}^{k_{c_i}+1}$, $\{t_{j-1i-1q-1}^a\}_{q=1}^{k_{a_i}+1}$ be a finite subsequences of censored and admitted time observations, respectively, over a consecutive failure-time subinterval $[t_{j-1i-1}^f, t_{j-1i}^f]$, where k_{c_i} is the total number of censored objects/species/infective/quitting covered over the subinterval $[t_{j-1i-1}^f, t_{j-1i}^f]$; k_{a_i} is the total number of admitting/entering/joining/susceptible/etc. covered over the subinterval $[t_{j-1i-1}^f, t_{j-1i}^f]$. Then the theoretical transformed/computational estimation algorithm and parameter estimation for $\lambda(t, S(t))$ at t_{j-1i}^f are respectively determined by

$$\begin{cases} z(t_{j-1i}^f) = z(t_{j-1i-1}^f) - \lambda(t_{j-1i-1}^f, S(t_{j-1i-1}^f)) \left[\sum_{l=1}^{k_{b_i}+1} z(t_{j-1i-1-l}^{c/a}) \Delta(t_{j-1i-1-l}^{c/a}) \right] - k_{c_i} + k_{a_i}, z(t_0) = z_0, \\ S(t_{j-1i}^f) = S(t_{j-1i-1}^f) - \lambda(t_{j-1i-1}^f, S(t_{j-1i-1}^f)) S(t_{j-1i-1}^f) \Delta t_{j-1i}^f, S(t_0) = S_0, \end{cases} \quad (10.50)$$

for $i \in I(1, k_f), j \in I(1, k)$ and

$$\hat{\lambda}(t_{j-1i-1}^f, \hat{S}(t_{j-1i-1}^f)) = \frac{z(t_{j-1i-1}^f) - z(t_{j-1i}^f) - k_{c_i} + k_{a_i}}{\sum_{l=1}^{k_{b_i}+1} z(t_{j-1i-1-l}^{c/a}) \Delta(t_{j-1i-1-l}^{c/a})}, t \in [t_{j-1i-1}^f, t_{j-1i}^f], \quad (10.51)$$

where $k_{b_i} = k_{c_i} + k_{a_i}$.

Moreover an overall conceptual parameter estimate for $z(t), S(t)$ and $\lambda(t, S(t))$ on the time interval of study $[t_0, T)$ are determined by

$$\begin{cases} \hat{\lambda}(t, \hat{S}(t_{j-1i-1}^f)) = \hat{\lambda}(t_{j-1i-1}^f, \hat{S}(t_{j-1i-1}^f)) \quad \text{for } t \in [t_{j-1i-1}^f, t_{j-1i}^f], j \in I(1, k) \text{ and } i \in I(1, k_f), \\ \hat{S}(t) = \hat{S}(t, t_{j-1i-1}^f, \hat{S}(t_{j-1i-1}^f)), \hat{S}(t_{j-1i-1}^f) = S_{j-1i-1}, \\ \hat{z}(t) = \hat{z}(t, t_{j-1i-1}^f, \hat{z}(t_{j-1i-1}^f)). \end{cases} \quad (10.52)$$

Proof. From Definitions 10.8 and 10.9, $l=p=j=i=1, t_{000}^f = t_0$ and $t_{0i-1k_{b_i}+1}^f = t_{01}^f$ and the application of Theorem 6.1, we note that one of the fundamental assumptions of the principle of mathematical induction (PMI) [3] is satisfied. For the validity of the application of PMI, we assume that (10.50) is valid for $j-1 \in I(1, k)$, and then need to show that (10.50) is satisfied for $j \in I(1, k)$. For this purpose, we note that for $j \in I(1, k)$, each $i \in I(1, k_f)$, and $t_{j-1i-1}^f, t_{j-1i}^f \in [t_0, T]$, k_{c_i} and k_{a_i} objects/species/subjects are censored and admitted over the subinterval $[t_{j-1i-1}^f, t_{j-1i}^f]$ of consecutive failure times, respectively. Let P_{j-1i}^f be a partition corresponding to the union of the range of two finite subsequences of censored and admitted times over the consecutive failure-time subinterval $[t_{j-1i-1}^f, t_{j-1i}^f]$, and let it be represented by

$$\begin{aligned} P_{j-1i}^f: t_{j-1i-11}^f = t_{j-1i-10}^f = t_{j-1i-1}^f < t_{j-1i-11}^{c/a} < \dots < t_{j-1i-1l-1}^{c/a} < t_{j-1i-1l}^{c/a} < \dots \\ < t_{j-1i-1k_{b_i}}^{c/a} < t_{j-1i-1k_{b_i}+1}^{c/a} = t_{j-1i}^f. \end{aligned} \quad (10.53)$$

In short, P_{j-1i}^f is a partition of $[t_{j-1i-1}^f, t_{j-1i}^f]$ with the size of the partition $k_{b_i} + 2$, and $k_{b_i} = k_{c_i} + k_{a_i}$.

For $j \in I(1, k)$ and $i \in I(1, k_f)$, using the iterative schemes (10.32), (10.34), and (10.36) and noting the nature of the process $\lambda(t_{j-1i-1-l}^{c/a}, S(t_{j-1i-1-l}^{c/a})) = \lambda(t_{j-1i-1}^f, S(t_{j-1i-1}^f))$ in the context of Definitions 10.8 and 10.9 for $l \in I(1, k_{b_i})$, we have

$$\begin{aligned}
z(t_{j-1i}^f) - z(t_{j-1i-1}^f) &= -\lambda(t_{j-1i-1}^f, S(t_{j-1i-1}^f))z(t_{j-1i-1}^{c/a})\Delta t_{j-1i-1}^{c/a} + \gamma_{j-1i-1}^{c/a} \\
&\quad - \sum_{m=2}^{k_{b_i}} \left[\lambda(t_{j-1i-1m-1}^{c/a}, S(t_{j-1i-1m-1}^{c/a}))z(t_{j-1i-1m-1}^{c/a})\Delta t_{j-1i-1m}^{c/a} + \gamma_{j-1i-1m-1}^{c/a} \right] \\
&\quad + \lambda(t_{j-1i-1k_{b_i}}^{c/a}, S(t_{j-1i-1k_{b_i}}^{c/a}))z(t_{j-1i-1k_{b_i}}^{c/a})\Delta t_{j-1i-1k_{b_i}+1}^f \\
&= -\lambda(t_{j-1i-1}^f, S(t_{j-1i-1}^f)) \left[\sum_{l=1}^{k_{b_i}+1} z(t_{j-1i-1l-1}^{c/a})\Delta t_{j-1i-1l}^{c/a} \right] - k_{b_i}.
\end{aligned}$$

Hence,

$$\begin{cases} z(t_{j-1i}^f) = z(t_{j-1i-1}^f) - \lambda(t_{j-1i-1}^f, S(t_{j-1i-1}^f)) \left[\sum_{l=1}^{k_{b_i}+1} z(t_{j-1i-1l-1}^{c/a})\Delta t_{j-1i-1l}^{c/a} \right] - k_{c_j} + k_{a_j}, z(t_0) = z_0 \\ S(t_{j-1i}^f) = S(t_{j-1i-1}^f) - \lambda(t_{j-1i-1}^f, S(t_{j-1i-1}^f))S(t_{j-1i-1}^f)\Delta t_{j-1i}^f, S(t_0) = S_0. \end{cases} \quad (10.54)$$

This establishes (i).

From (10.54), we note that $z(t_{j-1i-1}^f) - z(t_{j-1i}^f) - k_{c_i} + k_{a_i}$ is a change in the number of items/subjects that are under observation over the subinterval $[t_{j-1i-1}^f, t_{j-1i}^f]$, and $\sum_{l=1}^{k_{b_i}+1} z(t_{j-1i-1l-1}^{c/a})\Delta t_{j-1i-1l}^{c/a}$ is a total amount of time spent under the observation/testing/evaluation/monitoring of $z(t_{j-1i-1l}^{c/a})$ items/patients/infectives/subjects on the interval $[t_{j-1i-1l-1}^{c/a}, t_{j-1i-1l}^{c/a}]$ for $l \in I(1, k_{b_i})$, $j \in I(1, n)$ and $i \in I(1, k_f)$. From this and Definition 10.5, and the backward substitution, we obtain

$$\begin{aligned}
\hat{\lambda}(t_{j-1i-1}^f, \hat{S}(t_{j-1i-1}^f)) &= \frac{z(t_{j-1i-1}^f) - z(t_{j-1i}^f) - k_{c_j} + k_{a_j}}{\sum_{l=1}^{k_{b_i}+1} z(t_{j-1i-1l-1}^{c/a})\Delta t_{j-1i-1l}^{c/a}}, \quad t \in [t_{j-1i-1}^f, t_{j-1i}^f] \\
&\text{for } i \in I(1, k_f) \text{ and } j \in I(1, k).
\end{aligned}$$

This establishes (10.51). Moreover,

$$\begin{cases} \hat{\lambda}(t, \hat{S}(t_{j-1i-1}^f)) = \hat{\lambda}(t_{j-1i-1}^f, \hat{S}(t_{j-1i-1}^f)), \text{ for } t \in [t_{j-1i-1}^f, t_{j-1i}^f], j \in I(1, k) \text{ and } i \in I(1, k_f), \\ \hat{S}(t) = \hat{S}(t, t_{j-1i-1}^f, \hat{S}(t_{j-1i-1}^f)), \quad \hat{S}(t_{j-1i-1}^f) = S_{j-1i-1}, \\ \hat{z}(t) = \hat{z}(t, t_{j-1i-1}^f, \hat{z}(t_{j-1i-1}^f)). \end{cases}$$

This completes the proof of the theorem.

In the following, we present a special case, when $\lambda(t, S)$ takes a specific form.

Example 10.4: For $\lambda(t, S) = \lambda(t)(1 - S)$, (10.51) reduces to

$$\hat{\lambda}(t_{j-1i-1}^f) = \frac{z(t_{j-1i-1}^f) - z(t_{j-1i}^f) - k_{c_i} + k_{a_i}}{(1 - S(t_{j-1i-1}^f)) \left[\sum_{l=1}^{k_{b_i}+1} z(t_{j-1i-1-l}^{c/a}) \Delta(t_{j-1i-1}^{c/a}) \right]}, \quad t \in [t_{j-1i-1}^f, t_{ji}^f], \quad (10.55)$$

for $i \in I(1, k_f)$ and $j \in I(1, k)$.

Example 10.5: Let $\lambda(t) = (1/\sigma t)$, where σ is a parameter to be estimated from empirical data. Then applying Theorem 6.2, we obtain

$$\frac{1}{\hat{\sigma}(t_{j-1i-1}^f)} = \frac{z(t_{j-1i-1}^f) - z(t_{j-1i}^f) - k_{c_i} + k_{a_i}}{(1 - S(t_{j-1i-1}^f)) \left[\sum_{l=1}^{k_{b_i}+1} z(t_{j-1i-1-l}^{c/a}) \frac{\Delta(t_{j-1i-1}^{c/a})}{t_{j-1i-1-l}^{c/a}} \right]}, \quad t \in [t_{j-1i-1}^f, t_{ji}^f], \quad (10.56)$$

for $i \in I(1, k_f)$ and $j \in I(1, k)$.

In the following, we present a few results that are very special cases of Theorem 10.3.

Corollary 10.2: Let the hypotheses of Theorem 10.3 be satisfied except $k_a = 0$. Then the theoretical/conceptual estimation algorithm and parameter estimation for $\lambda(t, S(t))$ at t_{ji}^f are respectively determined by

$$\begin{cases} z(t_{ji}^f) = z(t_{j-1i-1}^f) - \lambda(t_{j-1i-1}^f, S(t_{j-1i-1}^f)) \left[\sum_{p=1}^{k_{c_i}+1} z(t_{j-1i-1-p}^{c/a}) \Delta(t_{j-1i-1-p}^{c/a}) \right] - k_{c_i}, & z(t_0) = z_0, \\ S(t_{j-1i}^f) = S(t_{j-1i-1}^f) - \lambda(t_{j-1i-1}^f, S(t_{j-1i-1}^f)) S(t_{j-1i-1}^f) \Delta t_{j-1i}^f, & S(t_0) = S_0, \end{cases} \quad (10.57)$$

and

$$\hat{\lambda}(t_{j-1i-1}^f, \hat{S}(t_{j-1i-1}^f)) = \frac{z(t_{j-1i-1}^f) - z(t_{j-1i}^f) - k_{c_i}}{\sum_{p=1}^{k_{c_i}+1} z(t_{j-1i-1-p}^{c/a}) \Delta(t_{j-1i-1-p}^{c/a})}, \quad t \in [t_{j-1i-1}^f, t_{j-1i}^f], \quad (10.58)$$

for $i \in I(1, k_f)$ and $j \in I(1, k)$. Moreover an overall conceptual computational estimate for $\lambda(t, S(t))$, $S(t)$ and $z(t)$ on the time interval of study $[t_0, T)$ is

$$\begin{cases} \hat{\lambda}(t, \hat{S}(t_{j-1i-1}^f)) = \hat{\lambda}(t_{j-1i-1}^f, \hat{S}(t_{j-1i-1}^f)), & \text{for } t \in [t_{j-1i-1}^f, t_{j-1i}^f], \quad j \in I(1, k) \text{ and } i \in I(1, k_f), \\ \hat{S}(t) = \hat{S}(t, t_{j-1i-1}^f, \hat{S}(t_{j-1i-1}^f)), & \hat{S}(t_{j-1i-1}^f) = S_{j-1i-1}, \\ \hat{z}(t) = \hat{z}(t, t_{j-1i-1}^f, \hat{z}(t_{j-1i-1}^f)). \end{cases}$$

Corollary 10.3: Let the hypotheses of Theorem 10.3 be satisfied except $k_c = 0$. Then the theoretical/conceptual estimation algorithm and parameter estimation for $\lambda(t, S(t))$ at t_{j-1i}^f are respectively determined by

$$\begin{cases} z(t_{ji}^f) = z(t_{j-1i-1}^f) - \lambda(t_{j-1i-1}^f, S(t_{j-1i-1}^f)) \left[\sum_{p=1}^{k_{a_i}+1} z(t_{j-1i-1q-1}^a) \Delta(t_{j-1i-1q}^a) \right] + k_{a_i}, z(t_0) = z_0, \\ S(t_{j-1i}^f) = S(t_{j-1i-1}^f) - \lambda(t_{j-1i-1}^f, S(t_{j-1i-1}^f)) S(t_{j-1i-1}^f) \Delta t_{j-1i}^f, S(t_0) = S_0, \end{cases} \quad (10.59)$$

and

$$\hat{\lambda}(t_{j-1i-1}^f, \hat{S}(t_{j-1i-1}^f)) = \frac{z(t_{j-1i-1}^f) - z(t_{j-1i}^f) + k_{a_i}}{\sum_{q=1}^{k_{a_i}+1} z(t_{j-1i-1q-1}^a) \Delta(t_{j-1i-1q}^a)}, t \in [t_{j-1i-1}^f, t_{ji}^f], \quad (10.60)$$

for $i \in I(1, k_f)$ and $j \in I(1, k)$. Moreover an overall conceptual computational estimate for $\lambda(t, S(t))$, $S(t)$, and $z(t)$ on the time interval of study $[t_0, T]$ is

$$\begin{cases} \hat{\lambda}(t, \hat{S}(t_{j-1i-1}^f)) = \hat{\lambda}(t_{j-1i-1}^f, \hat{S}(t_{j-1i-1}^f)), \text{ for } t \in [t_{j-1i-1}^f, t_{ji}^f], j \in I(1, k) \text{ and } i \in I(1, k_f), \\ \hat{S}(t) = \hat{S}(t, t_{j-1i-1}^f, \hat{S}(t_{j-1i-1}^f)), \hat{S}(t_{j-1i-1}^f) = S_{j-1i-1}, \\ \hat{z}(t) = \hat{z}(t, t_{j-1i-1}^f, \hat{z}(t_{j-1i-1}^f)). \end{cases}$$

The following special case of Theorem 10.3 is with respect to the totally discrete-time hybrid dynamic model for time-to-event dynamic process .

Corollary 10.4: Let us assume that the conditions of Corollary 10.1 in the context of Definitions 10.8 and 10.9 and Remarks 10.6(iv) (I), (II), and (III) are satisfied. For each $j \in I(1, k)$, and each $i \in I(1, k_f)$, let t_{j-1i-1}^f and t_{j-1i}^f be consecutive failure times. Let $\{t_{j-1i-1p}^c\}_{p=1}^{k_{c_j}}$, $\{t_{j-1i-1q}^a\}_{q=1}^{k_{a_i}}$ be a finite subsequences of censored and admitted time observations, respectively, over a consecutive failure-time subinterval $[t_{j-1i-1}^f, t_{j-1i}^f)$, where k_{c_i} is the total number of censored objects/species/infective/quitting covered over the subinterval $[t_{j-1i-1}^f, t_{j-1i}^f)$; k_{a_i} is the total number of admitting/entering/joining/susceptible/etc. covered over the subinterval $[t_{j-1i-1}^f, t_{j-1i}^f)$. Then the theoretical/conceptual estimation algorithm and parameter estimation for $\lambda(t, S(t))$ at t_{j-1i}^f are determined by

$$\begin{cases} z(t_{j-1i}^f) = z(t_{j-1i-1}^f) - \lambda(t_{j-1i-1}^f, S(t_{j-1i-1}^f)) \left[\sum_{l=1}^{k_{b_l}+1} z(t_{j-1i-1l-1}^{c/a}) \right] - k_{c_i} + k_{a_i}, z(t_0) = z_0, \\ S(t_{j-1i}^f) = S(t_{j-1i-1}^f) - \lambda(t_{j-1i-1}^f, S(t_{j-1i-1}^f)) S(t_{j-1i-1}^f) \Delta t_{j-1i}^f, S(t_0) = S_0, \end{cases} \quad (10.61)$$

and

$$\hat{\lambda}(t_{j-1i-1}^f, \hat{S}(t_{j-1i-1}^f)) = \frac{z(t_{j-1i-1}^f) - z(t_{j-1i}^f) - k_{c_i} + k_{a_i}}{\sum_{l=1}^{k_{b_i}+1} z(t_{j-1i-1l-1}^{f/c/a})}, \quad t \in [t_{j-1i-1}^f, t_{j-1i}^f], \quad (10.62)$$

respectively for $i \in I(1, k_f)$ and $j \in I(1, k)$.

Moreover an overall conceptual computational estimate for $\lambda(t, S(t))$, $S(t)$, and $z(t)$ on the time interval of study $[t_0, T]$ is

$$\begin{cases} \hat{\lambda}(t, \hat{S}(t_{j-1i-1}^f)) = \hat{\lambda}(t_{j-1i-1}^f, \hat{S}(t_{j-1i-1}^f)), \text{ for } t \in [t_{j-1i-1}^f, t_{j-1i}^f], j \in I(1, k) \text{ and } i \in I(1, k_f), \\ \hat{S}(t) = \hat{S}(t, t_{j-1i-1}^f, \hat{S}(t_{j-1i-1}^f)), \quad \hat{S}(t_{j-1i-1}^f) = S_{j-1i-1}, \\ \hat{z}(t) = \hat{z}(t, t_{j-1i-1}^f, \hat{z}(t_{j-1i-1}^f)). \end{cases} \quad (10.63)$$

Now, we state a very general theorem that provides a theoretical estimate for $\lambda(t, S)$ between two consecutive change point times, t_{j-1r-1}^{cp} and t_{j-1r}^{cp} .

Theorem 10.4: Let the hypotheses of Theorem 10.1 in the context of Definitions 10.8 and 10.9 and Remarks 10.4, 10.6(i), 10.6(ii), and 10.6(iii) be satisfied. For each $j \in I(1, k)$ and each $r \in I(1, n)$, let t_{j-1r-1}^{cp} and t_{j-1r}^{cp} be consecutive change point times. Let $\{t_{j-1r-1i-1}^f\}_{i=1}^{k_{f_r}}$, $\{t_{j-1r-1p-1}^c\}_{p=1}^{k_{c_r}}$, and $\{t_{j-1r-1q-1}^a\}_{q=1}^{k_{a_r}}$ be the a sequence of failure, censored and admission times respectively in the interval $[t_{j-1r-1}^{cp}, t_{j-1r}^{cp}]$. k_{f_r} , k_{c_r} , and k_{a_r} are respectively, the total number of failures, censored and admitting items/objects/species/etc. in the consecutive change-point subinterval $[t_{j-1r-1}^{cp}, t_{j-1r}^{cp}]$. Then the theoretical/conceptual estimation algorithm and parameter estimation for $\lambda(t, S(t))$ at t_{j-1r}^{cp} are determined by

$$\begin{cases} z(t_{j-1r}^{cp}) = z(t_{j-1r-1}^{cp}) - \lambda(t_{j-1r-1}^{cp}, S(t_{j-1r-1}^{cp})) \left[\sum_{l=1}^{k_{b_r}+1} z(t_{j-1r-1l-1}^{f/c/a}) \Delta(t_{j-1r-1l}^{f/c/a}) \right] \\ - k_{f_r} - k_{c_r} + k_{a_r}, \quad z(t_0) = z_0, \\ S(t_{j-1r}^{cp}) = S(t_{j-1r-1}^{cp}) - \lambda(t_{j-1r-1}^{cp}, S(t_{j-1r-1}^{cp})) S(t_{j-1r-1}^{cp}) \Delta(t_{j-1r}^{cp}), \quad S(t_0) = S_0, \end{cases} \quad (10.64)$$

and

$$\hat{\lambda}(t_{j-1r-1}^{cp}, \hat{S}(t_{j-1r-1}^{cp})) = \frac{z(t_{j-1r-1}^{cp}) - z(t_{j-1r}^{cp}) - k_{f_r} - k_{c_r} + k_{a_r}}{\sum_{l=1}^{k_{b_r}+1} z(t_{j-1r-1l-1}^{f/c/a}) \Delta(t_{j-1r-1l}^{f/c/a})}, \quad t \in [t_{j-1r-1}^{cp}, t_{j-1r}^{cp}], \quad (10.65)$$

respectively for $r \in I(1, n)$ and $j \in I(1, k)$. $k_{b_r} = k_{f_r} + k_{c_r} + k_{a_r}$. Moreover an overall conceptual estimate for $\lambda(t, S(t))$, $S(t)$, and $z(t)$ on the time interval of study $[t_0, T]$ is

$$\begin{cases} \hat{\lambda}(t, \hat{S}(t_{j-1r-1}^{cp})) = \hat{\lambda}(t_{j-1r-1}^{cp}, \hat{S}(t_{j-1r-1}^{cp})), & \text{for } t \in [t_{j-1r-1}^{cp}, t_{j-1r}^{cp}), \quad r \in I(1, n) \text{ and } j \in I(1, k), \\ \hat{S}(t) = \hat{S}(t, t_{j-1r-1}^{cp}, \hat{S}(t_{j-1r-1}^{cp})), \quad \hat{S}(t_{j-1i-1}^{cp}) = S_{j-1i-1}, \\ \hat{z}(t) = \hat{z}(t, t_{j-1r-1}^{cp}, \hat{z}(t_{j-1r-1}^{cp})). \end{cases} \quad (10.66)$$

Proof. Imitating the proof of Theorem 10.3, one can establish the proof of the Theorem 10.4.

Remark 10.7: Corollaries parallel to Corollaries 10.2 and 10.3 can be formulated. The following special case of Theorem 10.4 is with respect to the totally discrete-time hybrid dynamic model for time-to-event dynamic process.

Corollary 10.5 *Let us assume that all conditions of Corollary 10.1 in the context of Definitions 10.8 and 10.9 and Remarks 10.6(iv) (I), (II), and (III) are satisfied. For each $j \in I(1, k)$ and each $r \in I(1, n)$, let t_{j-1r-1}^{cp} and t_{j-1r}^{cp} be consecutive change point times. Let $\{t_{j-1r-1i-1}^f\}_{i=1}^{k_{f_r}}$, $\{t_{j-1r-1p-1}^c\}_{p=1}^{k_{c_r}}$, and $\{t_{j-1r-1q-1}^a\}_{q=1}^{k_{a_r}}$ be a sequence of failure, censored and admission times respectively in the interval $[t_{j-1r-1}^{cp}, t_{j-1r}^{cp})$. k_{f_r} , k_{c_r} , and k_{a_r} are respectively, the total number of failures, censored and admitting items/objects/species/etc. in the consecutive change-point subinterval $[t_{j-1r-1}^{cp}, t_{j-1r}^{cp})$. Then the theoretical/conceptual estimation algorithm and parameter estimation for $\lambda(t, S(t))$ at t_{j-1r}^{cp} are determined by*

$$\begin{cases} z(t_{j-1r}^{cp}) = z(t_{j-1r-1}^{cp}) - \lambda(t_{j-1r-1}^{cp}, S(t_{j-1r-1}^{cp})) \left[\sum_{l=1}^{k_{b_r}+1} z(t_{j-1r-1l-1}^f/c/a) \right] - k_{f_r} - k_{c_r} + k_{a_r}, \quad z(t_0) = z_0, \\ S(t_{j-1r}^{cp}) = S(t_{j-1r-1}^{cp}) - \lambda(t_{j-1r-1}^{cp}, S(t_{j-1r-1}^{cp})) S(t_{j-1r-1}^{cp}), \quad S(t_0) = S_0, \end{cases} \quad (10.67)$$

and

$$\hat{\lambda}(t_{j-1r-1}^{cp}, \hat{S}(t_{j-1r-1}^{cp})) = \frac{z(t_{j-1r-1}^{cp}) - z(t_{j-1r}^{cp}) - k_{f_r} - k_{c_r} + k_{a_r}}{\sum_{l=1}^{k_{b_r}+1} z(t_{j-1r-1l-1}^f/c/a)}, \quad t \in [t_{j-1r-1}^{cp}, t_{j-1r}^{cp}), \quad (10.68)$$

respectively. Moreover an overall conceptual estimate for $\lambda(t, S(t))$, $S(t)$, and $z(t)$ and on the time interval of study $[t_0, T)$ is

$$\begin{cases} \hat{\lambda}(t, \hat{S}(t_{j-1r-1}^{cp})) = \hat{\lambda}(t_{j-1r-1}^{cp}, \hat{S}(t_{j-1r-1}^{cp})), & \text{for } t \in [t_{j-1r-1}^{cp}, t_{j-1r}^{cp}), \quad r \in I(1, n) \text{ and } j \in I(1, k), \\ \hat{S}(t) = \hat{S}(t, t_{j-1r-1}^{cp}, \hat{S}(t_{j-1r-1}^{cp})), \quad \hat{S}(t_{j-1i-1}^{cp}) = S_{j-1i-1}, \\ \hat{z}(t) = \hat{z}(t, t_{j-1r-1}^{cp}, \hat{z}(t_{j-1r-1}^{cp})). \end{cases} \quad (10.69)$$

In the following section, we develop conceptual computational modified LLGMM parameter and state estimation procedure.

10.7 Conceptual computational modified LLGMM parameter and state estimation

In this section, employing the results of Sections 10.3–10.5, we develop a modified version of the local lagged adapted generalized method of moments (LLGMM) [15]. This is achieved by utilizing the developed alternative procedure in Section 10.6 and the LLGMM method. We also make an attempt to coordinate and compare the developed innovative approach for parameter and state estimation of time-to-event process with recently developed LLGMM approach. We note that the transformed conceptual computational interconnected dynamic algorithm for time-to-event data statistic (IDATTEDS) is local. It is centered around each consecutive pair of failure or change time ordered subinterval $[t_{j-1i-1}^f, t_{j-1i}^f)$ or $[t_{j-1i-1}^{cp}, t_{j-1i}^{cp})$ with its right-end-point data observation/collection process for $i \in I(1, k_f)$ or $i \in I(1, k_{cp})$. Moreover, parameter and state estimation of the time-to-event process is relative to each consecutive pair of failure or change time subinterval operation of the time-to-event dynamic process. This type of parameter and state estimation problem in time-to-event processes can be characterized by the local single-shot procedure identified by the right-end point of the $j-1$ th consecutive failure or change point subinterval for each $i \in I(1, k_f)$ or $i \in (1, k_{cp})$.

These above observations motivate to extend this single-shot parameter and state estimation problem to a finite multi-choice local lagged consecutive failure or change time subintervals with right-end-point data observation/collection process. For this, we introduce a couple of definitions that form a bridge to connect the IDATTEDS approach with the LLGMM approach. From Definitions 10.4–10.9, we recall that $\{t_{j-1i-1}^f\}_{i=1}^{k_f}$, $\{[t_{j-1i-1}^f, t_{j-1i}^f)\}_{i=1}^{k_f}$, P_{j-1}^f , $\{z_{j-1i-1}\}_{i=1}^{k_f}$, $\{P_{j-1i}^f\}_{i=1}^{k_f}$, are increasing sequences of overall consecutive failure-times, consecutive failure-time subintervals, failure-time partition of $[t_0, T)$, conceptual data sequence at failure-time, sequence of sub-partition of consecutive time subinterval $[t_{j-1i-1}^f, t_{j-1i}^f)$, respectively for $i \in I(1, k_f)$.

Definition 10.10: For each $i \in I(1, k_f)$ and each $m_i \in I(1, i-1)$, a partition of closed interval $[t_{j-1i-m_i}^f, t_{j-1i}^f]$ is called local at a failure-time t_{j-1i}^f , and it is defined by

$$P_{j-1i-m_i}^f := t_{j-1i-m_i}^f < t_{j-1i-m_i+1}^f < \cdots < t_{j-1i-1}^f < t_{j-1i}^f. \quad (10.70)$$

A m_i -size consecutive failure time subinterval subsequence $\{[t_{j-1i+l}^f, t_{j-1i+l+1}^f)\}_{l=-m_i}^{-1}$ of the overall consecutive failure time subinterval sequence $\{[t_{j-1i-1}^f, t_{j-1i}^f)\}_{i=1}^{k_f}$ is called local lagged moving failure-time subsequence at t_{j-1i}^f that is a cover of $[t_{j-1i-m_i}^f, t_{j-1i}^f)$:

$$\bigcup_{l=-m_i}^{-1} [t_{j-1i+l}^f, t_{j-1i+l+1}^f) = [t_{j-1i-m_i}^f, t_{j-1i}^f). \quad (10.71)$$

$P_{j-1i-m_i}^f$ is a sub-partition of the partition $P_{j-1}^f \subset P^f$.

Definition 10.11: For each $i \in I(1, k_f)$ and each $m_i \in I(1, i-1)$, a local lagged moving consecutive failure time subsequence of subintervals, $\{[t_{j-1i+l}^f, t_{j-1i+l+1}^f]\}_{l=-m_i}^{-1}$ at failure time t_{j-1i}^f of the size m_i is identified by the restriction of overall failure time state data subsequence $\{z_{j-1i-1}\}_{i=1}^{k_f}$ to $P_{j-1i-m_i}^f$ in (10.70), and it is defined by

$$s_{m_i, j-1i} = \{F^l z_{j-1i}\}_{l=-m_i}^0. \quad (10.72)$$

Here, F is a forward-shift operator, and $F^{-1} = B$, B is the backward shift operator. m_i varies from 1 to i ; the corresponding local sequence $s_{m_i, i}$ at t_{j-1i}^f varies from $\{F^l z_{j-1i}\}_{l=-1}^0$ to $\{F^l z_{j-1i}\}_{l=-i+1}^0$. As a result of this, the sequence defined in (10.72) is also called a m_i -local moving sequence of failure-time state data associated with m_i -local lagged finite sequence of subintervals at a failure-time t_{j-1i}^f for each $i \in I(1, k_f)$.

In the following, we outline a computational scheme for the survival state data analysis problem. Using the concept of m_i -moving sequence of failure-time state data at a failure time t_{j-1i}^f , computational schemes for the change point problem can be developed analogously.

Hereafter, we utilize Definitions 10.10 and 10.11, and recast the LLGMM algorithm [9, 15]. For each $m_i \in I(1, i-1)$, using (10.51) and $l \in I(-m_i, -1)$, we determine estimates of λ at each failure time t_{j-1i}^f for the special case of $S\lambda(t, S) = S\lambda(t)(1-S)$ (without loss of generality), as follows:

$$\hat{\lambda}_{m_i, i} = \frac{\sum_{l=-m_i}^{-1} [z(t_{j-1i+l}) - z(t_{j-1i+l+1}) - k_{c_{i+l}} + k_{a_{i+l}}]}{\sum_{l=-m_i}^{-1} (1 - F^l S(t_{j-1i}^f)) \sum_{n=1}^{k_{b_{i+l}}+1} z(t_{j-1i+ln-1}^{c/a}) \Delta t_{j-1i+ln}^{c/a}}, \quad (10.73)$$

where $\lambda(t, S) = \lambda(t)(1-S)$; $m_i \in I(1, i-1)$; $k_{c_{i+l}}$ is the total number of censored objects/species/infective/quitting covered over the subinterval $[t_{j-1i+l}^f, t_{j-1i+l+1}^f]$; $k_{a_{i+l}}$ is the total number of admitting/entering/joining/susceptible/etc. covered over the subinterval $[t_{j-1i+l}^f, t_{j-1i+l+1}^f]$; $k_{b_{i+l}} = k_{c_{i+l}} + k_{a_{i+l}}$.

Remark 10.8: For the special case of $\lambda(t) = \frac{1}{\sigma t}$, (10.73) reduces to

$$\hat{\sigma}_{m_i, i} = \frac{\sum_{l=-m_i}^{-1} (1 - F^l S(t_{j-1i})) \sum_{n=1}^{k_{b_{i+l}}+1} z(t_{j-1i+ln-1}^{c/a}) \frac{\Delta t_{j-1i+ln}^{c/a}}{t_{j-1i+ln-1}^{c/a}}}{\sum_{l=-m_i}^{-1} [z(t_{j-1i+l}) - z(t_{j-1i+l+1}) - k_{c_{i+l}} + k_{a_{i+l}}]}. \quad (10.74)$$

In short, the usage of the transformed continuous-time deterministic dynamic hybrid model for time-to-event process, and discrete-time interconnected hybrid dynamic algorithm of local sample mean lead to an innovative alternative method for parameter and state estimation problems for continuous-time dynamic models described by both linear and nonlinear deterministic differential equations.

In the next section, we outline computational, data organizational, and IDAT-TEDS simulation schemes.

10.8 Conceptual computational and organizational dynamic algorithm

In this section, we outline a conceptual computational dynamic algorithm that includes both (a) survival state and (b) change point survival state and parameter estimation problems in a systematic and unified way. For the undertaking of this task, we need to know conceptually coordinated data collection, numerical scheme, and simulation times with theoretical discrete-time dynamic algorithm. In addition, it is essential to decompose, reorganize, and re-aggregate a given overall data set in a suitable manner to meet the overall goal(s). Prior to the development of the scheme, we define, introduce notations and reorganize the observed data set for the usage of a conceptual computational dynamic algorithm. We formulate the outline of the conceptual computational dynamic algorithm for survival state data analysis problem.

10.8.1 Data collection coordination with iterative processes

Without loss of generality, we assume that the real data observation/collection schedule is indeed a finite sequence $\{t_{j-1}\}_{j=1}^k$ corresponding to the partition P of $[t_0, T)$ defined in Section 10.3. Moreover, the real-world data set and its data observation/collection times are coordinated with conceptual data set sequence and data collection sequence of times.

10.8.2 Data decomposition, reorganization, and aggregation

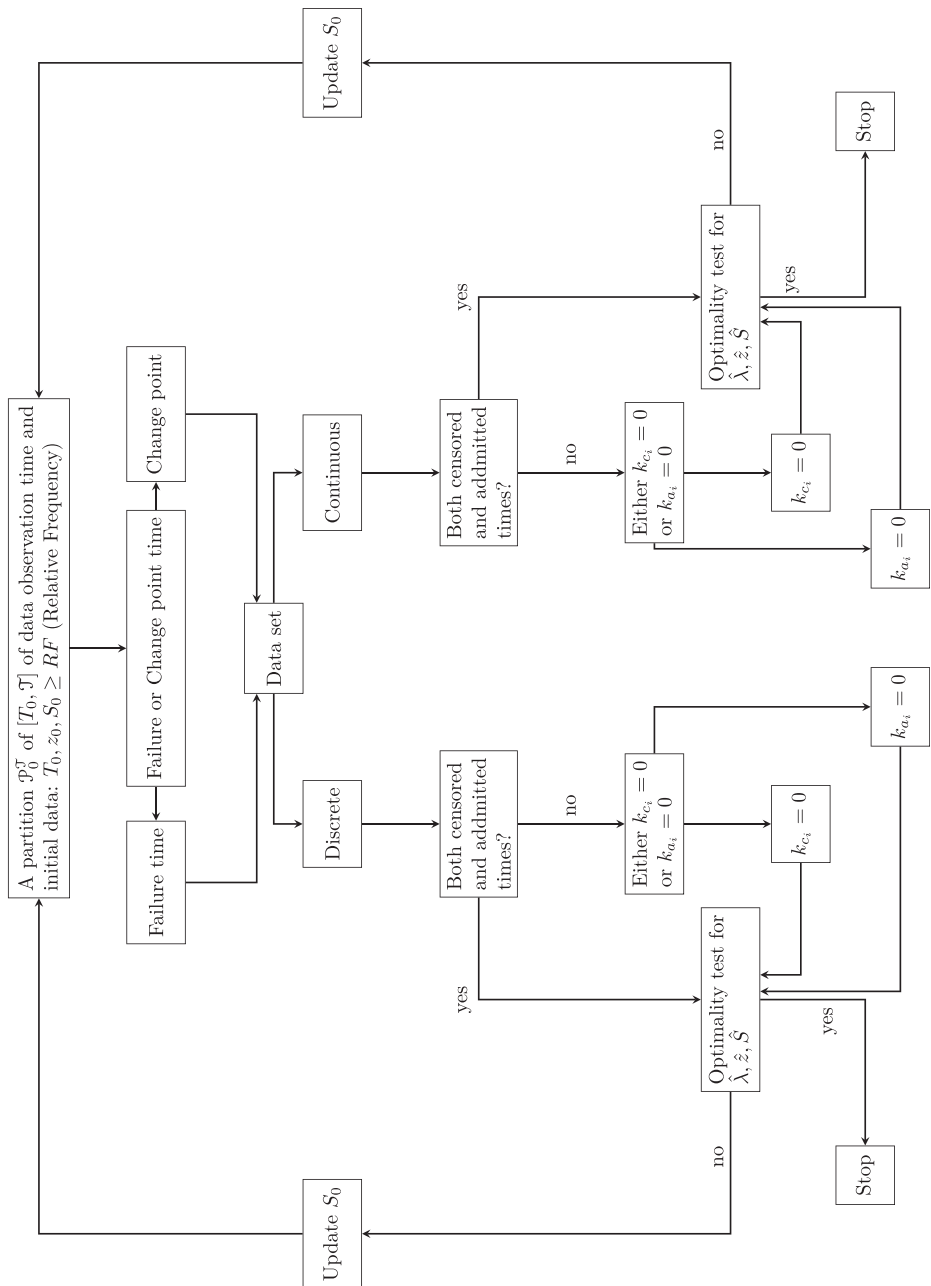
Based on our research, we recognize that there are two major problems of interests in a time-to-event dynamic process, namely: (1) Survival state and (2) change point state estimation analysis problems. For the study of these problems, we decompose, reorganize and re-aggregate the original real-world data set in a respective framework of (1) Survival state and (2) change point study in a time-to-event process. The original data is coordinated, decomposed, reorganized, and aggregated with reference to the conceptual data coordination, decomposition, reorganization, and aggregation in a manner analogous to Definitions 10.6–10.9.

10.8.3 Conceptual computational parameter and state estimations scheme

For the conceptual computational parameter estimation, we use nonlinear discrete-time conceptual computational interconnected dynamic algorithm (10.19) for time-to-event data statistic (Flowchart 10.2-IDATTEDS)). The original state data subsequences are associated with conceptual data set. The decomposition of the original real-world data set into three types of subsequences of data are as defined in the context of Definition 10.6. We consider the original data set as the real data set. For $i \in (1, k_f)$, conceptual computational dynamic estimation algorithms in (10.50) and (10.51) are used for continuous-time and totally discrete-time real-world data sets, respectively. The parameter and state estimates at t_{j-1}^f are determined using (10.51) and (10.62) for continuous-time and totally discrete-time real-world data sets, respectively. Finally, employing the principle of mathematical induction [3], an overall parameter and state estimations for $z(t), S(t)$ and $\lambda(t, S(t))$ over the time interval $[t_0, T]$ of study are determined from (10.52) and (10.63).

10.8.4 Conceptual computational state simulation scheme

We utilize the common sense ideas, namely, range of finite sequence of data collection time, the initial relative frequency of the survival and the range of relative frequency. In addition, we employ the fundamental properties of solution process of initial value problems in the theory of differential equations [3], in particular the continuous dependence of solutions with respect to initial data and other properties. We identify the initial data (t_0, S_0, z_0) for various choices of S_0 . The best estimates are obtained when near optimal convergence is achieved for a particular choice of initial survival state, S_0 . In short, the conceptual computational algorithm consists of three-step nested processes. In summary, the conceptual simulation algorithm is outlined in Flowchart 10.2-IDATTEDS is outlined in Flowchart 10.3. We present an algorithm and a flowchart for the simulation schemes described above.



Flowchart 10.3: Simulation algorithm for survival and change point data analysis problems-IDATTEDS.

Given t_0, S_0 and z_0

```

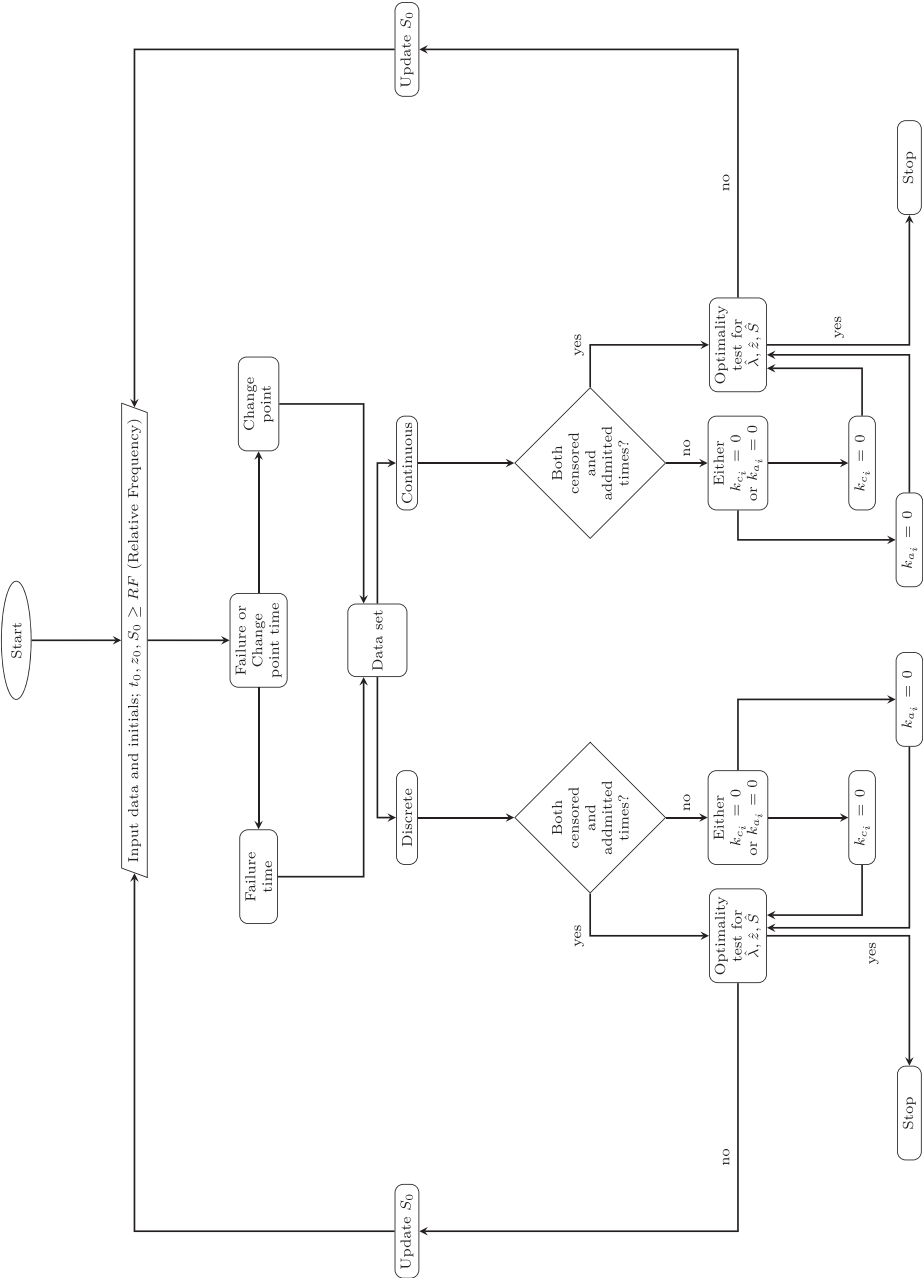
for  $j = 1$  to  $k$  do
  if Failure time then
    for  $i = 1$  to  $k_f$  do
      Compute  $k_{c_i}, k_{a_i}, z(t_{j-1i-1}^f), z(t_{ji}^f)$ 
    if Continuous then
      Compute  $\sum_{l=1}^{k_{b_i}+1} z(t_{j-1i-1l-1}^{c/a}) \Delta(t_{j-1i-1l}^{c/a})$ 
    else
      Compute  $\sum_{l=1}^{k_{b_i}+1} z(t_{j-1i-1l-1}^{c/a})$ 
    end if
  Compute  $\hat{\lambda}, \hat{z}$  and  $\hat{S}$ 
  end for
  else
    Change point analysis
    .
    .
    .
  end if
end for

```

Algorithm 10.1: IDATTEDS Simulation Scheme.

10.8.5 Change point data analysis problem

In this subsection, we address the usage of the study of time-to-event process. A change-point process in the time-to-event process measures the effects of intervention process. Here, again the overall pair of sequence of discrete-time interconnected state dynamic data set is characterized by single right-end point data set with two consecutive change point dynamic processes. A sequence of two consecutive change point times is assumed to be a single subsequence of overall sequence $\{t_{j-1}\}_{j=1}^k$ of conceptual state data observation times. The sequence of two consecutive change point times is denoted by $\{t_{j-1r-1}^{cp}\}_{r=1}^n$ for $r \in I(1, n)$ with $n \leq k$. Generally, using the time-to-event state dynamic data set, the change point sequence of times is estimated. The rest of the data collection coordination with conceptual iterative process is parallel to the survival state problem, except notational changes. For example, replacing $[t_{j-1i-1}^f, t_{j-1i}^f)$ by $[t_{j-1r-1}^{cp}, t_{j-1r}^{cp})$, the entire conceptual computational procedure regarding the survival state data analysis problem is imitated for the change-point problem analogously. For $i \in I(1, n)$ the conceptual computational dynamic algorithms in (10.64) and (10.67) are used for continuous-time and totally discrete-time real-world data sets, respectively. The parameter and state estimates at



Flowchart 10.4: Simulation algorithm for survival and change point data analysis problems.

t_{j-1r}^{cp} are determined using (10.65) and (10.68) for continuous-time and totally discrete-time real-world data sets, respectively. Finally, employing the principle of mathematical induction, an overall parameter and state estimation for $\lambda(t, S(t))$, $S(t)$ and $z(t)$ over the time interval $[t_0, T)$ of study are determined from (10.66) and (10.69).

In the next section, we outline computational, data organizational, and modified LLGMM simulation schemes.

10.9 Conceptual computational and organizational dynamic modified LLGMM algorithm

The numerical approximation and simulation processes need to be synchronized with the existing data collection process in the context of the partition of $[t_0, T]$. For each $i \in I(1, k_f)$, we assume that t_{j-1i}^f is the scheduled time clock for the $j-1$ th collected data of the state of the system under investigation. The iterative and simulation time processes are both t_{j-1i}^f . For each $m_i \in OS_{j-1i} = I(1, i-1)$ at t_{j-1i}^f , from Definition 10.11, we pick a m_i local admissible sequence $\{F^l z_{j-1i}\}_{l=-m_i}^0$. Using the terms of this sequence and (10.73), we compute the state and parameter estimates of the continuous-time dynamic equation. These estimates form a local finite sequence of parameter estimates at t_{j-1i}^f corresponding to $AS_{j-1i} = \{s_{m_i, j-1i} : m_i \in I(1, i-1)\}$ for each $i \in I(1, k_f)$. The principle of mathematical induction is employed for the development of a conceptual computational scheme.

For each admissible sequence in AS_{j-1i} , let $z_{m_i, j-1i}^s$ be a simulated value of $s_{m_i, j-1i}$ at t_{j-1i}^f . This engenders an m_i local sequence of simulated data $\{z_{m_i, j-1i}^s\}_{m_i \in OS_{j-1i}}$. The simulated $z_{m_i, j-1i}^s$ satisfies the following scheme:

$$z_{j-1i}^s = z_{j-1i-1}^s - \hat{\lambda}_{j-1i-1} z_{j-1i-1}^s (1 - S_{j-1i-1}^s) \Delta t_{j-1i} - k_{c_i} + k_{a_i}. \quad (10.75)$$

To find the best estimate of $z(t_{j-1i})$, let us define

$$\Xi_{m_i, j-1i, z_{j-1i}} = \left| z(t_{j-1i}) - z_{m_i, j-1i}^s \right| \quad (10.76)$$

to be the absolute error of $z(t_{j-1i}^f)$ relative to each member of the term of local admissible sequences $\{z_{m_i, j-1i}^s\}_{m_i \in OS_{j-1i}}$ of simulated values. For any preassigned arbitrary small positive number ε and for each time t_{j-1i}^f , to find the best estimate from admissible simulated values, we determine the following sub-optimal admissible set of data at t_{j-1i}^f as:

$$M_{j-1i} = \{m_i : \Xi_{m_i, j-1i, z_{j-1i}} < \varepsilon \text{ for } m_i \in OS_{j-1i}\}. \quad (10.77)$$

Among these collected sub-optimal set of values, the value that gives the minimum $\Xi_{m_i, j-1i, z_{j-1i}}$ is recorded as \hat{m}_i . The parameters corresponding to \hat{m}_i is referred to as the ε -level sub-optimal estimates of the true parameters. These sub-optimal estimates

are estimated at time t_{j-1i}^f with \hat{m}_i . The simulated value $z_{\hat{m}_i, j-1i}^s$ at t_{j-1i}^f corresponding to \hat{m}_i is recorded as the best estimate for $z(t_{j-1i})$ at t_{j-1i}^f . Having obtained the best estimate for λ , we then proceed to find the optimal/best estimate for the survival function at t_{j-1i}^f via the following:

$$\hat{S}(t_{j-1i}) = \hat{S}(t_{j-1i-1}) - \hat{\lambda}(t_{j-1i}, \hat{m}_i) \hat{S}(t_{j-1i-1})(1 - \hat{S}(t_{j-1i-1})) \Delta t_{j-1i}. \quad (10.78)$$

Finally, an estimate of $S_{\hat{m}_i, j-1i}$ at t_{j-1i}^f corresponding to \hat{m}_i is also recorded as the best estimate for $S(t_{j-1i})$ at t_{j-1i}^f .

10.9.1 Modified LLGMM conceptual computational parameter and state estimation schemes

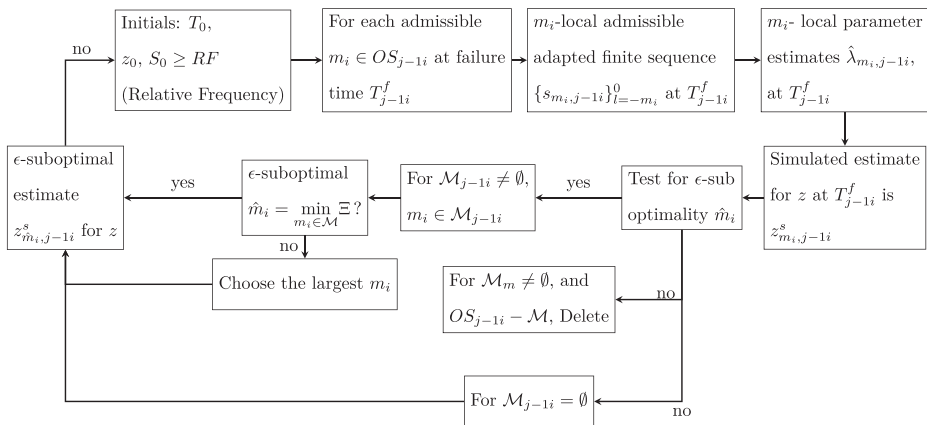
To summarize the computation, a modified LLGMM conceptual computational algorithm is outlined in Flowchart 10.5.

Remark 10.9: Equation (10.75) specializes to

$$z_{m_i j-1i}^s = z_{m_i-1j-1i-1}^s - \frac{1}{\hat{\sigma}_{m_i-1j-1i-1}} z_{m_i-1j-1i-1}^s (1 - S_{m_i-1j-1i-1}^s) \frac{\Delta t_{j-1i}}{t_{j-1i-1}} - k_{c_i} + k_{a_i}, \quad (10.79)$$

and (10.78) reduces to

$$\hat{S}(t_{j-1i}) = \hat{S}(t_{j-1i-1}) - \frac{1}{\hat{\sigma}(t_{j-1i}, \hat{m}_i)} \hat{S}(t_{j-1i-1})(1 - \hat{S}(t_{j-1i-1})) \frac{\Delta t_{j-1i}}{t_{j-1i-1}}. \quad (10.80)$$



Flowchart 10.5: Modified LLGMM conceptual computational algorithm.

10.9.2 Modified LLGMM conceptual computational simulation schemes and algorithms

We present an algorithm and flowchart for the simulation scheme described above.

```

Given initials  $t_0, S_0, z_0, \varepsilon$ ,
  for  $i = 1$  to  $k_f$  do
    Compute  $m_i = 1$  to  $i$ 
    for  $m_i = 0$  to  $i$  do
      Compute  $\hat{\lambda}_{m_i, j-1i}$   $m_i = 0$  to  $i$ 
      Compute  $z_{m_i, j-1i}^S, \Xi_{m_i, j-1i, z_{j-1i}} \Xi_{m_i, i, z_{j-1i}} < \varepsilon$ 
      end for
    end for
  end for
  if  $\Xi_{m_i, i, z_{j-1i}} < \varepsilon$  then
    Save  $\hat{m}_i$ 
  else
    Find  $\hat{m}_i$  that minimizes  $\Xi_{m_i, j-1i, z_{j-1i}}$ 
  end if
  Compute  $\lambda_{\hat{m}_i, j-1i}, z_{\hat{m}_i, j-1i}^S, S_{\hat{m}_i, j-1i}$ .

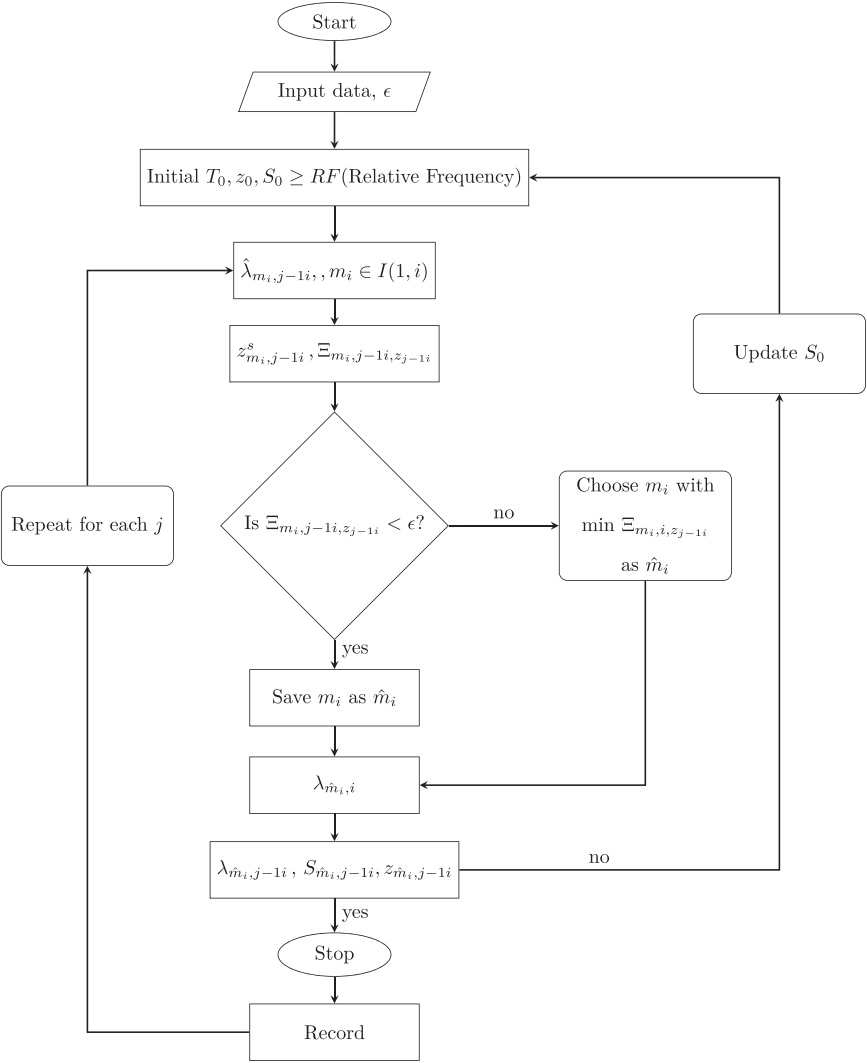
```

Algorithm 10.2: Modified LLGMM simulation scheme.

We note that the above presented innovative algorithm is valid for state and parameter estimation problems for continuous-time dynamic models described by linear hybrid deterministic differential equations for time-to-event processes. We further note that the algorithm also allows for the admission/joining of individuals/items.

Remark 10.10: We remark that intervention processes provide a measure of influence of new tools/procedures/approaches in continuous-time states of time-to-event dynamic process. In particular, it generates a measure of the degree of sustainability, survivability, reliability of the system. This further leads to sustainable/unsustainable, survivable/failure, reliable/unreliable binary state invariant sets. In addition, intervention processes provides the comparison between the past and currently used tools/procedures/approaches/attitudes/etc.

In the following section, we apply the IDATTEDS procedure to three real data sets. This exhibits the usefulness of the theoretical algorithms and procedures.



Flowchart 10.6: Modified LLGMM simulation algorithm.

10.10 Applications of IDATTEDS to time-to-event data sets

In this section, using the conceptual computational dynamic algorithm, we exemplify our theoretical algorithms and procedures for estimating parameters and survival state for three data sets: (i) 96 locomotive control failure data set in number of thousand miles [12, 16], (ii) a follow-up time and vital status of 100 subjects in the

Worcester heart attack study [17], and (iii) data set describing time (in months) of death and losses of a sample of 8 items found in [18] that was analyzed in [19].

Illustration 10.1: The data in Table 10.1 was discussed in [12, 16] regarding the number of thousand miles at which different locomotive controls failed in a life test involving 96 controls. The test was terminated after 135,000 miles, by which time 37 failures had occurred. Fifty-nine locomotive controls were censored at 135,000 miles.

We apply the developed conceptual computational algorithm. Employing (10.56) with $k_a = 0$, we demonstrate our innovative alternative approach for finding parameter and survival function estimates on consecutive failure time intervals.

Table 10.1: Locomotive control life-test data set [12, 16].

Data observation per 1,000 miles	Failure/censor time	Frequency of failure or censors at t_i	Survival or operating units at t_i ; $z(t_i)$	Data observation per 1,000 miles	Failure or censor time	Frequency of failure or censors at t_i	Survival or operating units at t_i ; $z(t_i)$
$t_0 = 1.0$	Initial		96	$t_{20} = 91.5$	Failure	1	76
$t_1 = 22.5$	Failure	1	95	$t_{21} = 93.5$	Failure	1	75
$t_2 = 37.5$	Failure	1	94	$t_{22} = 102.5$	Failure	1	74
$t_3 = 46.5$	Failure	1	93	$t_{23} = 107.0$	Failure	1	73
$t_4 = 48.5$	Failure	1	92	$t_{24} = 108.5$	Failure	1	72
$t_5 = 51.5$	Failure	1	91	$t_{25} = 112.5$	Failure	1	71
$t_6 = 53.5$	Failure	1	90	$t_{26} = 113.5$	Failure	1	70
$t_7 = 54.5$	Failure	1	89	$t_{27} = 116.0$	Failure	1	69
$t_8 = 57.5$	Failure	1	88	$t_{28} = 117.0$	Failure	1	68
$t_9 = 66.5$	Failure	1	87	$t_{29} = 118.5$	Failure	1	67
$t_{10} = 68.0$	Failure	1	86	$t_{30} = 119.0$	Failure	1	66
$t_{11} = 69.5$	Failure	1	85	$t_{31} = 120.0$	Failure	1	65
$t_{12} = 76.5$	Failure	1	84	$t_{32} = 122.5$	Failure	1	64
$t_{13} = 77.0$	Failure	1	83	$t_{33} = 123.0$	Failure	1	63
$t_{14} = 78.5$	Failure	1	82	$t_{34} = 127.5$	Failure	1	62
$t_{15} = 80.0$	Failure	1	81	$t_{35} = 131.0$	Failure	1	61
$t_{16} = 81.5$	Failure	1	80	$t_{36} = 132.5$	Failure	1	60
$t_{17} = 82.5$	Failure	1	79	$t_{37} = 134.0$	Failure	1	59
$t_{18} = 83.0$	Failure	1	78	$t_{38} = 135.0$	Censored	59	0
$t_{19} = 84.0$	Failure	1	77				

Table 10.2: Estimates $\sigma\hat{\alpha}(t_{j-i}) \equiv \hat{\sigma}_{j-i}$ and $\hat{S}(t_{j-i-1}) \equiv \hat{S}_{j-i-1}$ using (10.56) with $ka = 0$ and the procedure outlined in Section 10.8 with $S_0 = 0.985$, 0.98900 , 0.99000 , 0.99900 , 0.99990 , 0.99999 , 0.999999 .

Consecutive failure time interval, $[t_{j-1-i}, t_{j-i})$	$S_0 = 0.985$		$S_0 = 0.98900$		$S_0 = 0.99000$		$S_0 = 0.99900$		$S_0 = 0.9999$		$S_0 = 0.99999$		$S_0 = 0.999999$	
	$\hat{\sigma}_{j-i}$	\hat{S}_{j-i-1}	$\hat{\sigma}_{j-i}$	\hat{S}_{j-i-1}	$\hat{\sigma}_{j-i}$	\hat{S}_{j-i-1}	$\hat{\sigma}_{j-i}$	\hat{S}_{j-i-1}	$\hat{\sigma}_{j-i}$	\hat{S}_{j-i-1}	$\hat{\sigma}_{j-i}$	\hat{S}_{j-i-1}	$\hat{\sigma}_{j-i}$	\hat{S}_{j-i-1}
[1, 22.5)	30.9600	0.9850	22.7040	0.9890	20.6400	0.9900	2.0640	0.9990	0.2064	0.9999	0.0206	0.99999	0.0021	0.999999
[22.5, 37.5)	1.5998	0.9747	1.3491	0.9787	1.2865	0.9797	0.7224	0.9886	0.6660	0.9895	0.6603	0.9896	0.6598	0.9896
[37.5, 46.5)	0.8014	0.9645	0.7130	0.9684	0.6909	0.9694	0.4921	0.9782	0.4722	0.9791	0.4702	0.9792	0.4700	0.9792
[46.5, 48.5)	0.1831	0.9542	0.1676	0.9581	0.1637	0.9591	0.1289	0.9678	0.1254	0.9687	0.1250	0.9687	0.1250	0.9687
[48.5, 51.5)	0.3189	0.9440	0.2971	0.9478	0.2916	0.9488	0.2426	0.9574	0.2377	0.9582	0.2372	0.9583	0.2371	0.9583
[51.5, 53.5)	0.2343	0.9337	0.2209	0.9375	0.2176	0.9384	0.1874	0.9470	0.1844	0.9478	0.1841	0.9479	0.1841	0.9479
[53.5, 54.5)	0.1288	0.9234	0.1225	0.9272	0.1209	0.9281	0.1067	0.9366	0.1053	0.9374	0.1052	0.9375	0.1051	0.9375
[54.5, 57.5)	0.4254	0.9132	0.4072	0.9169	0.4026	0.9178	0.3618	0.9262	0.3577	0.9270	0.3573	0.9271	0.3572	0.9271
[57.5, 66.5)	1.3372	0.9029	1.2867	0.9066	1.2741	0.9075	1.1605	0.9158	1.1491	0.9166	1.1480	0.9167	1.1478	0.9167
[66.5, 68.0)	0.2107	0.8927	0.2035	0.8963	0.2018	0.8972	0.1858	0.9053	0.1842	0.9062	0.1840	0.9062	0.1840	0.9062
[68.0, 69.5)	0.2231	0.8824	0.2163	0.8860	0.2146	0.8869	0.1993	0.8949	0.1978	0.8957	0.1976	0.8958	0.1976	0.8958
[69.5, 76.5)	1.0947	0.8721	1.0643	0.8757	1.0568	0.8766	0.9885	0.8845	0.9817	0.8853	0.9810	0.8854	0.9810	0.8854
[76.5, 77.0)	0.0758	0.8619	0.0739	0.8654	0.0734	0.8663	0.0691	0.8741	0.0687	0.8749	0.0686	0.8750	0.0686	0.8750
[77.0, 78.5)	0.2399	0.8516	0.2343	0.8551	0.2329	0.8559	0.2204	0.8637	0.2191	0.8645	0.2190	0.8646	0.2190	0.8646
[78.5, 80.0)	0.2486	0.8414	0.2432	0.8448	0.2419	0.8456	0.2298	0.8533	0.2286	0.8541	0.2285	0.8542	0.2285	0.8542

[80.0, 81.5)	0.2565	0.8311	0.2514	0.8345	0.2501	0.8353	0.2386	0.8429	0.2374	0.8437	0.2373	0.8437	0.2373	0.8437
[81.5, 82.5)	0.1759	0.8208	0.1726	0.8242	0.1718	0.8250	0.1644	0.8325	0.1637	0.8332	0.1636	0.8333	0.1636	0.8333
[82.5, 83.0)	0.0907	0.8106	0.0891	0.8139	0.0887	0.8147	0.0852	0.8221	0.0848	0.8228	0.0848	0.8229	0.0848	0.8229
[83.0, 84.0)	0.1877	0.8003	0.1846	0.8036	0.1838	0.8044	0.1770	0.8117	0.1763	0.8124	0.1762	0.8125	0.1762	0.8125
[84.0, 91.5)	1.4434	0.7901	1.4213	0.7933	1.4158	0.7941	1.3662	0.8013	1.3612	0.8020	1.3607	0.8021	1.3607	0.8021
[91.5, 93.5)	0.3658	0.7798	0.3606	0.7830	0.3592	0.7838	0.3474	0.7909	0.3462	0.7916	0.3461	0.7917	0.3461	0.7917
[93.5, 102.5)	1.6638	0.7695	1.6413	0.7727	1.6356	0.7734	1.5849	0.7805	1.5798	0.7812	1.5793	0.7812	1.5792	0.7812
[102.5, 107.0)	0.7821	0.7593	0.7721	0.7624	0.7696	0.7631	0.7470	0.7701	0.7448	0.7708	0.7445	0.7708	0.7445	0.7708
[107.0, 108.5)	0.2569	0.7490	0.2537	0.7521	0.2530	0.7528	0.2460	0.7597	0.2453	0.7603	0.2452	0.7604	0.2452	0.7604
[108.5, 112.5)	0.6935	0.7388	0.6855	0.7417	0.6835	0.7425	0.6656	0.7493	0.6638	0.7499	0.6636	0.7500	0.6636	0.7500
[112.5, 113.5)	0.1714	0.7285	0.1695	0.7314	0.1690	0.7322	0.1648	0.7388	0.1644	0.7395	0.1644	0.7396	0.1644	0.7396
[113.5, 116.0)	0.4344	0.7182	0.4300	0.7211	0.4288	0.7219	0.4187	0.7284	0.4177	0.7291	0.4176	0.7292	0.4176	0.7292
[116.0, 117.0)	0.1737	0.7080	0.1720	0.7108	0.1716	0.7116	0.1677	0.7180	0.1673	0.7187	0.1673	0.7187	0.1673	0.7187
[117.0, 118.5)	0.2635	0.6977	0.2611	0.7005	0.2604	0.7013	0.2549	0.7076	0.2543	0.7083	0.2543	0.7083	0.2543	0.7083
[118.5, 119.0)	0.0884	0.6874	0.0876	0.6902	0.0874	0.6909	0.0856	0.6972	0.0854	0.6978	0.0854	0.6979	0.0854	0.6979
[119.0, 120.0)	0.1790	0.6772	0.1775	0.6799	0.1771	0.6806	0.1737	0.6868	0.1734	0.6874	0.1733	0.6875	0.1733	0.6875
[120.0, 122.5)	0.4510	0.6669	0.4474	0.6696	0.4465	0.6703	0.4382	0.6764	0.4374	0.6770	0.4373	0.6771	0.4373	0.6771
[122.5, 123.0)	0.0897	0.6567	0.0890	0.6593	0.0888	0.6600	0.0872	0.6660	0.0871	0.6666	0.0871	0.6667	0.0871	0.6667
[123.0, 127.5)	0.8150	0.6464	0.8089	0.6490	0.8074	0.6497	0.7938	0.6556	0.7925	0.6562	0.7923	0.6562	0.7923	0.6562
[127.5, 131.0)	0.6193	0.6361	0.6149	0.6387	0.6138	0.6394	0.6039	0.6452	0.6029	0.6458	0.6028	0.6458	0.6028	0.6458

(continued)

Table 10.2 (continued)

Consecutive failure time interval, $[t_{j-1}, t_j)$	$S_0 = 0.985$		$S_0 = 0.98900$		$S_0 = 0.99000$		$S_0 = 0.99000$		$S_0 = 0.99999$		$S_0 = 0.99999$		$S_0 = 0.999999$	
	$\hat{\sigma}_{j-1}$	\hat{S}_{j-1}	$\hat{\sigma}_{j-1}$	\hat{S}_{j-1}	$\hat{\sigma}_{j-1}$	\hat{S}_{j-1}	$\hat{\sigma}_{j-1}$	\hat{S}_{j-1}	$\hat{\sigma}_{j-1}$	\hat{S}_{j-1}	$\hat{\sigma}_{j-1}$	\hat{S}_{j-1}	$\hat{\sigma}_{j-1}$	\hat{S}_{j-1}
[131.0, 132.5)	0.2613	0.6259	0.2595	0.6284	0.2591	0.6291	0.2551	0.6348	0.2547	0.6354	0.2547	0.6354	0.2547	0.6354
[132.5, 134.0)	0.2611	0.6156	0.2594	0.6181	0.2590	0.6188	0.2551	0.6244	0.2548	0.6249	0.2547	0.6250	0.2547	0.6250
(134)		0.6054		0.6078		0.6084		0.6140		0.6145		0.6146		0.6146

We utilize the range of finite sequence of data collection time. We note the initial relative frequency of the survival locomotive control to be $\frac{95}{96}$. In fact the range of relative frequency is $[0.6146, 0.9896]$. We chose the initial survival probabilities to be $S_0 = 0.985, 0.989, 0.99, 0.999, 0.9999, 0.99999$ and 0.999999 and applied the conceptual computational simulation algorithm for consecutive failure-time subintervals. The results are recorded in Table 10.2. The simulation results exhibit the almost optimal convergence of survival state probability estimates for $S_0 = 0.99999$. We then conclude that the best survival state estimate is obtained by choosing $S_0 = 0.99999$ for the locomotive control data set. This was further reaffirmed by the application of the modified version of LLGMM method that assures a certain degree of confidence in the survival state estimates. In addition, the modified version of LLGMM method provides a test for the best optimality of state and parameter estimates. Moreover, it provides a confidence interval for the survival state estimates. Furthermore, it also provides a measure of significance for the usage of new procedures/tools/etc.

In the following illustration, we apply the developed algorithm to a follow-up time and vital status of 100 patients in the Worcester heart attack study [17].

Illustration 10.2: The data in Table 10.3 shows follow-up time and vital status (failure or censored) for 100 subjects in the Worcester heart attack study [17]. We note that there are multiple censored times occurring between any two consecutive failure times unlike the data set in Table 10.1, where all censored times occurred after the last failure time. We note that the initial relative frequency of the survival of patient data is 0.98. In fact the range of the relative frequency is $[0.51, 0.98]$. Here also, we choose initial survival probabilities to be $S_0 = 0.985, 0.989, 0.99, 0.999, 0.9999, 0.99999, 0.999999$ and apply the conceptual computational simulation algorithm (10.56) with $k_a = 0$ for consecutive failure-time subintervals. The results are recorded in Table 10.4. The simulation results exhibit the optimal convergence of survival state probability estimates for $S_0 = 0.99999$. We conclude that the almost best survival state estimate is for $S_0 = 0.99999$ for the Worcester heart attack study data set. This was also confirmed by the application of the modified version of LLGMM method that assures a certain degree of confidence in the survival state estimates.

In the following illustration, we apply the developed alternative innovative algorithm to a data set used by [19].

Illustration 10.3: The data set in Table 10.5 is originally from [18]. Malla et al. used the data set to exemplify their approach.

Malla et al. assumed that the largest observation 12.1 is uncensored. They also assumed that $0 = a_0 \leq a_1 \leq a_2 < \dots \leq a_m$ are jumps of the Kaplan–Meier [18] survival estimator in magnitude, and thus obtained $a_1 = 0.125, a_2 = 0.175, a_3 = 0.175, a_4 = 0.2625, a_5 = 0.2625$. They then proceeded to calculate the hazard rate function using the following equation:

Table 10.3: A follow-up time of 100 Worcester heart attack study data set [17].

Data Observation	Failure or Censor Time	Frequency of Failure/ Censors at t_i	Survival or Operating units at t_i : $z(t_i)$	Data Observation	Failure or Censor Time	Frequency of Failure/ Censors at t_i	Survival or Operating units at t_i : $z(t_i)$
$t_0 = 1.0$	Initial		100	$t_{28} = 1011$	Failure	1	70
$t_1 = 6$	Failure	2	98	$t_{29} = 1048$	Failure	1	69
$t_2 = 14$	Failure	1	97	$t_{30} = 1054$	Failure	1	68
$t_3 = 44$	Failure	1	96	$t_{31} = 1172$	Failure	1	67
$t_4 = 62$	Failure	1	95	$t_{32} = 1205$	Failure	1	66
$t_5 = 89$	Failure	1	94	$t_{33} = 1278$	Failure	1	65
$t_6 = 98$	Failure	1	93	$t_{34} = 1401$	Failure	1	64
$t_7 = 104$	Failure	1	92	$t_{35} = 1497$	Failure	1	63
$t_8 = 107$	Failure	1	91	$t_{36} = 1557$	Failure	1	62
$t_9 = 114$	Failure	1	90	$t_{37} = 1577$	Failure	1	61
$t_{10} = 123$	Failure	1	89	$t_{38} = 1624$	Failure	1	60
$t_{11} = 128$	Failure	1	88	$t_{39} = 1669$	Failure	1	59
$t_{12} = 148$	Failure	1	87	$t_{40} = 1806$	Failure	1	58
$t_{13} = 182$	Failure	1	86	$t_{41} = 1836$	Censored/alive	2	56
$t_{14} = 187$	Failure	1	85	$t_{42} = 1846$	Censored/alive	1	55
$t_{15} = 189$	Failure	1	84	$t_{43} = 1859$	Censored/alive	1	54
$t_{16} = 274$	Failure	2	82	$t_{44} = 1860$	Censored/alive	1	53
$t_{17} = 302$	Failure	1	81	$t_{45} = 1870$	Censored/alive	1	52
$t_{18} = 363$	Failure	1	80	$t_{46} = 1874$	Failure	1	51
$t_{19} = 374$	Failure	1	79	$t_{47} = 1876$	Censored/alive	1	50
$t_{20} = 451$	Failure	1	78	$t_{48} = 1879$	Censored	1	49
$t_{21} = 461$	Failure	1	77	$t_{49} = 1883$	Censored	1	48
$t_{22} = 492$	Failure	1	76	$t_{50} = 1889$	Censored	1	47
$t_{23} = 538$	Failure	1	75	$t_{51} = 1907$	Failure	1	46
$t_{24} = 774$	Failure	1	74	$t_{52} = 1912$	Censored	1	45
$t_{25} = 841$	Failure	1	73	$t_{53} = 1916$	Censored	1	44
$t_{26} = 936$	Failure	1	72	$t_{54} = 1922$	Censored	1	43
$t_{27} = 1002$	Failure	1	71	$t_{55} = 1923$	Censored	1	42

Table 10.3 (continued)

Data Observation	Failure or Censor Time	Frequency of Failure/Censors at t_i	Survival or Operating units at t_i : $z(t_i)$	Data Observation	Failure or Censor Time	Frequency of Failure/Censors at t_i	Survival or Operating units at t_i : $z(t_i)$
$t_{56} = 1929$	Censored	1	41	$t_{76} = 2145$	Censored	1	19
$t_{57} = 1934$	Censored	1	40	$t_{77} = 2157$	Censored	1	18
$t_{58} = 1939$	Censored	2	38	$t_{78} = 2173$	Censored	1	17
$t_{59} = 1969$	Censored	1	37	$t_{79} = 2174$	Censored	1	16
$t_{60} = 1984$	Censored	1	36	$t_{80} = 2183$	Censored	1	15
$t_{61} = 1993$	Censored	1	35	$t_{81} = 2190$	Censored	1	14
$t_{62} = 2003$	Censored	1	34	$t_{82} = 2201$	Failure	1	13
$t_{63} = 2012$	Failure	1	33	$t_{83} = 2421$	Failure	1	12
$t_{64} = 2013$	Censored	1	32	$t_{84} = 2573$	Censored	1	11
$t_{65} = 2031$	Failure	1	31	$t_{85} = 2574$	Censored	1	10
$t_{66} = 2052$	Censored	1	30	$t_{86} = 2578$	Censored	1	9
$t_{67} = 2054$	Censored	1	29	$t_{87} = 2595$	Censored	1	8
$t_{68} = 2061$	Censored	1	28	$t_{88} = 2610$	Censored	1	7
$t_{69} = 2065$	Failure	1	27	$t_{89} = 2613$	Censored	1	6
$t_{70} = 2072$	Censored	1	26	$t_{90} = 2624$	Failure	1	5
$t_{71} = 2074$	Censored	1	25	$t_{91} = 2631$	Censored	1	4
$t_{72} = 2084$	Censored	1	24	$t_{92} = 2638$	Censored	1	3
$t_{73} = 2114$	Censored	1	23	$t_{93} = 2641$	Censored	1	2
$t_{74} = 2124$	Censored	1	22	$t_{94} = 2710$	Failure	1	1
$t_{75} = 2137$	Censored	2	20	$t_{95} = 2719$			

$$\hat{\lambda}(t) = \frac{a_k}{1 - A_{k-1} \cdot \Delta d_k}, \quad (10.81)$$

where d_k is distinct failure time and $A_0 = 0$, $A_k = \sum_{i=1}^k a_i$ for $d_{k-1} \leq t < d_k$, $1 \leq k \leq m$. The survival estimate on $[0, d_m]$ was defined as follows:

Table 10.4: Estimates $\hat{\sigma}(t_{j-i}) \equiv \hat{\sigma}_{j-i}$ and $\hat{S}(t_{j-i-1}) \equiv \hat{S}_{j-i-1}$ using (10.56) with $k_d = 0$ and the procedure outlined in Section 10.8 with $S_0 = 0.985, 0.98900, 0.99000, 0.99900, 0.99999, 0.99999, 0.999999$.

Consecutive failure time interval, $[t_{j-i-1}, t_{j-i})$	$S_0 = 0.985$		$S_0 = 0.98900$		$S_0 = 0.99000$		$S_0 = 0.99900$		$S_0 = 0.99999$		$S_0 = 0.999999$	
	$\hat{\sigma}_{j-i}$	\hat{S}_{j-i-1}	$\hat{\sigma}_{j-i}$	\hat{S}_{j-i-1}	$\hat{\sigma}_{j-i}$	\hat{S}_{j-i-1}	$\hat{\sigma}_{j-i}$	\hat{S}_{j-i-1}	$\hat{\sigma}_{j-i}$	\hat{S}_{j-i-1}	$\hat{\sigma}_{j-i}$	\hat{S}_{j-i-1}
[1.0, 6.0]	3.7500	0.9850	2.7500	0.9890	2.5000	0.9900	0.2500	0.9990	0.0250	0.9999	0.0025	0.999999
[6.0, 14.0]	4.5341	0.9653	4.0219	0.9692	3.8939	0.9702	2.7414	0.9790	2.6261	0.9799	2.6146	0.9800
[14.0, 44.0]	9.2600	0.9554	8.4535	0.9593	8.2519	0.9603	6.4373	0.9690	6.2559	0.9699	6.2377	0.9700
[44.0, 62.0]	2.1364	0.9456	1.9856	0.9494	1.9479	0.9504	1.6086	0.9590	1.5747	0.9599	1.5713	0.9600
[62.0, 89.0]	2.6581	0.9357	2.5009	0.9396	2.4616	0.9405	2.1079	0.9490	2.0725	0.9499	2.0689	0.9500
[89.0, 98.0]	0.7044	0.9259	0.6686	0.9297	0.6597	0.9306	0.5793	0.9391	0.5712	0.9399	0.5704	0.9400
[98.0, 104.0]	0.4780	0.9160	0.4568	0.9198	0.4515	0.9207	0.4039	0.9291	0.3991	0.9299	0.3986	0.9300
[104.0, 107.0]	0.2489	0.9062	0.2392	0.9099	0.2367	0.9108	0.2147	0.9191	0.2126	0.9199	0.2123	0.9200
[107.0, 114.0]	0.6171	0.8963	0.5954	0.9000	0.5900	0.9009	0.5412	0.9091	0.5363	0.9099	0.5358	0.9100
[114.0, 123.0]	0.8064	0.8865	0.7809	0.8901	0.7745	0.8910	0.7169	0.8991	0.7112	0.8999	0.7106	0.9000
[123.0, 128.0]	0.4463	0.8766	0.4334	0.8802	0.4302	0.8811	0.4012	0.8891	0.3983	0.8899	0.3980	0.8900
[128.0, 148.0]	1.8315	0.8668	1.7831	0.8703	1.7710	0.8712	1.6621	0.8791	1.6512	0.8799	1.6501	0.8800
[148.0, 182.0]	2.8591	0.8569	2.7895	0.8604	2.7721	0.8613	2.6156	0.8691	2.6000	0.8699	2.5984	0.8700
[182.0, 187.0]	0.3612	0.8471	0.3531	0.8505	0.3511	0.8514	0.3328	0.8591	0.3310	0.8599	0.3308	0.8600
[187.0, 189.0]	0.1480	0.8372	0.1449	0.8407	0.1441	0.8415	0.1371	0.8491	0.1364	0.8499	0.1364	0.8500

[189.0, 274.0)	3.2602	0.8274	3.1968	0.8308	3.1809	0.8316	3.0381	0.8392	3.0238	0.8399	3.0224	0.8400	3.0222	0.8400
[274.0, 302.0)	1.6114	0.8077	1.5839	0.8110	1.5770	0.8118	1.5152	0.8192	1.5090	0.8199	1.5084	0.8200	1.5083	0.8200
[302.0, 363.0)	3.3074	0.7978	3.2544	0.8011	3.2411	0.8019	3.1218	0.8092	3.1099	0.8099	3.1087	0.8100	3.1086	0.8100
[363.0, 374.0)	0.5139	0.7880	0.5062	0.7912	0.5042	0.7920	0.4868	0.7992	0.4850	0.7999	0.4849	0.8000	0.4849	0.8000
[374.0, 451.0)	3.6083	0.7781	3.5569	0.7813	3.5441	0.7821	3.4284	0.7892	3.4169	0.7899	3.4157	0.7900	3.4156	0.7900
[451.0, 461.0)	0.4007	0.7683	0.3953	0.7714	0.3940	0.7722	0.3818	0.7792	0.3806	0.7799	0.3805	0.7800	0.3805	0.7800
[461.0, 492.0)	1.2507	0.7584	1.2348	0.7615	1.2308	0.7623	1.1949	0.7692	1.1913	0.7699	1.1910	0.7700	1.1909	0.7700
[492.0, 538.0)	1.7864	0.7486	1.7648	0.7516	1.7594	0.7524	1.7108	0.7592	1.7059	0.7599	1.7054	0.7600	1.7054	0.7600
[538.0, 774.0)	8.5950	0.7387	8.4963	0.7418	8.4717	0.7425	8.2496	0.7492	8.2274	0.7499	8.2252	0.7500	8.2249	0.7500
[774.0, 841.0)	1.7366	0.7289	1.7176	0.7319	1.7129	0.7326	1.6702	0.7393	1.6660	0.7399	1.6655	0.7400	1.6655	0.7400
[841.0, 936.0)	2.3168	0.7190	2.2927	0.7220	2.2867	0.7227	2.2325	0.7293	2.2271	0.7299	2.2265	0.7300	2.2265	0.7300
[936.0, 1002.0)	1.4764	0.7092	1.4617	0.7121	1.4581	0.7128	1.4252	0.7193	1.4219	0.7199	1.4216	0.7200	1.4215	0.7200
[1002.0, 1011.0)	0.1917	0.6993	0.1899	0.7022	0.1895	0.7029	0.1854	0.7093	0.1850	0.7099	0.1849	0.7100	0.1849	0.7100
[1011.0, 1048.0)	0.7954	0.6895	0.7883	0.6923	0.7865	0.6930	0.7703	0.6993	0.7687	0.6999	0.7686	0.7000	0.7685	0.7000
[1048.0, 1054.0)	0.1266	0.6796	0.1255	0.6824	0.1252	0.6831	0.1227	0.6893	0.1225	0.6899	0.1225	0.6900	0.1225	0.6900
[1054.0, 1172.0)	2.5138	0.6698	2.4931	0.6725	2.4879	0.6732	2.4413	0.6793	2.4366	0.6799	2.4362	0.6800	2.4361	0.6800
[1172.0, 1205.0)	0.6415	0.6599	0.6365	0.6626	0.6352	0.6633	0.6238	0.6693	0.6227	0.6699	0.6226	0.6700	0.6226	0.6700
[1205.0, 1278.0)	1.3990	0.6501	1.3885	0.6527	1.3858	0.6534	1.3621	0.6593	1.3597	0.6599	1.3595	0.6600	1.3594	0.6600
[1278.0, 1401.0)	2.2505	0.6402	2.2343	0.6429	2.2302	0.6435	2.1936	0.6493	2.1900	0.6499	2.1896	0.6500	2.1896	0.6500

(continued)

Table 10.4 (continued)

Consecutive failure time interval, $[t_{j-1}, t_j)$	$S_0 = 0.985$		$S_0 = 0.98900$		$S_0 = 0.99000$		$S_0 = 0.99900$		$S_0 = 0.9999$		$S_0 = 0.99999$		$S_0 = 0.999999$	
	$\hat{\sigma}_{j-1}$	\hat{S}_{j-1}	$\hat{\sigma}_{j-1}$	\hat{S}_{j-1}	$\hat{\sigma}_{j-1}$	\hat{S}_{j-1}	$\hat{\sigma}_{j-1}$	\hat{S}_{j-1}	$\hat{\sigma}_{j-1}$	\hat{S}_{j-1}	$\hat{\sigma}_{j-1}$	\hat{S}_{j-1}	$\hat{\sigma}_{j-1}$	\hat{S}_{j-1}
[1401.0, 1497.0)	1.6209	0.6304	1.6096	0.6330	1.6068	0.6336	1.5816	0.6394	1.5790	0.6399	1.5788	0.6400	1.5788	0.6400
[1497.0, 1557.0)	0.9581	0.6205	0.9518	0.6231	0.9502	0.6237	0.9359	0.6294	0.9344	0.6299	0.9343	0.6300	0.9343	0.6300
[1557.0, 1577.0)	0.3100	0.6107	0.3081	0.6132	0.3076	0.6138	0.3031	0.6194	0.3027	0.6199	0.3026	0.6200	0.3026	0.6200
[1577.0, 1624.0)	0.7257	0.6008	0.7212	0.6033	0.7201	0.6039	0.7101	0.6094	0.7091	0.6099	0.7090	0.6100	0.7090	0.6100
[1624.0, 1669.0)	0.6800	0.5910	0.6760	0.5934	0.6750	0.5940	0.6660	0.5994	0.6651	0.5999	0.6650	0.6000	0.6650	0.6000
[1669.0, 1806.0)	2.0285	0.5811	2.0171	0.5835	2.0142	0.5841	1.9885	0.5894	1.9859	0.5899	1.9857	0.5900	1.9856	0.5900
[1806.0, 1874.0)	0.8921	0.5713	0.8873	0.5736	0.8861	0.5742	0.8752	0.5794	0.8741	0.5799	0.8740	0.5800	0.8740	0.5800
[1874.0, 1907.0)	0.3686	0.5610	0.3667	0.5632	0.3662	0.5638	0.3619	0.5689	0.3614	0.5694	0.3614	0.5695	0.3614	0.5695
[1907.0, 2012.0)	0.9364	0.5492	0.9317	0.5514	0.9306	0.5520	0.9202	0.5570	0.9191	0.5575	0.9190	0.5576	0.9190	0.5576
[2012.0, 2031.0)	0.1408	0.5346	0.1401	0.5368	0.1400	0.5374	0.1385	0.5422	0.1383	0.5427	0.1383	0.5428	0.1383	0.5428
[2031.0, 2065.0)	0.2424	0.5180	0.2414	0.5201	0.2411	0.5206	0.2387	0.5253	0.2385	0.5258	0.2385	0.5258	0.2385	0.5258
[2065.0, 2201.0)	0.6657	0.5007	0.6630	0.5027	0.6623	0.5033	0.6562	0.5078	0.6556	0.5083	0.6555	0.5083	0.6555	0.5083
[2201.0, 2421.0)	0.6809	0.4760	0.6784	0.4779	0.6778	0.4784	0.6721	0.4827	0.6716	0.4832	0.6715	0.4832	0.6715	0.4832
[2421.0, 2624.0)	0.5114	0.4394	0.5097	0.4411	0.5093	0.4416	0.5057	0.4456	0.5053	0.4460	0.5053	0.4461	0.5053	0.4461
[2624.0, 2710.0)	0.0479	0.3990	0.0477	0.4006	0.0477	0.4010	0.0474	0.4046	0.0474	0.4050	0.0474	0.4050	0.0474	0.4050
(2710.0)		0.2348		0.2357		0.2360		0.2381		0.2383		0.2384		0.2384

Table 10.5: Data set describing time (in months) to death (failure) and losses (censored) [19].

Data observation	Failure or censor time	Frequency of failure/censors at t_i	Survival or operating units at t_i : $z(t_i)$
$t_0 = 0$	Initial		8
$t_1 = 0.8$	Failure	1	7
$t_2 = 1.0$	Censored	1	6
$t_3 = 2.7$	Censored	1	5
$t_4 = 3.1$	Failure	1	4
$t_5 = 5.4$	Failure	1	3
$t_6 = 7.0$	Censored	1	2
$t_7 = 9.2$	Failure	1	1
$t_8 = 12.1$	Censored	1	0

$$\hat{S}(t) = \hat{S}(d_{k-1}) \exp \left[- \int_{d_{k-1}}^t \frac{a_k}{(1 - A_{k-1}) \Delta d_k} du \right], \quad d_{k-1} \leq t < d_k, \quad 1 \leq k \leq m. \quad (10.82)$$

Utilizing (10.1) and (10.2), the following estimates summarized in Table 10.6 were obtained.

Table 10.6: Estimates $\hat{\lambda}(t_j)$ and $\hat{S}(t_{j-1})$ using sing the procedure outlined in [19].

Consecutive failure time interval		
$[t_{j-1}, t_j)$	$\hat{\lambda}(t_{j-1})$	$\hat{S}(t_{j-1})$
$[0, 0.8)$	0.1563	1.0000
$[0.8, 3.1)$	0.0870	0.8824
$[3.1, 5.4)$	0.1087	0.7224
$[5.4, 9.2)$	0.1316	0.5626
$[9.2, 12.1)$	0.3448	0.3412

In the following, we apply our innovative alternative algorithm to the data set in Table 10.5. Specifically, we used (10.55) in Example 10.4 with $k_{a_i} = 0$ for all i for

parameter estimation. Additionally, survival state estimates at the failure times were estimated using the Euler scheme:

$$S(t_{ji}^f) = S(t_{j-i-1}^f) - \hat{\lambda}(t_{j-i-1}^f)S(t_{j-i-1}^f)(1 - S(t_{j-i-1}^f))\Delta t_{ji}^f. \quad (10.83)$$

We used initial survival probability to be $S_0 = 0.999, 0.9999, 0.99999, 0.999999$ and applied the conceptual computational simulation algorithm (10.55) for consecutive failure-time subintervals. Optimal convergence of survival state probability estimates were obtained for $S_0 = 0.9999$. Thus, we conclude that the best survival state estimate is for $S_0 = 0.9999$ for the data set in Table 10.5. The results are summarized in Table 10.7. Again, these results were confirmed by the application of the modified version of LLGMM method that assures a certain degree of confidence in the survival state estimates as compared to the estimates obtained in Table 10.3.

Table 10.7: Estimates $\hat{\lambda}(t_{j-i})$ and $\hat{S}(t_{j-i-1})$ using $S_0 = 0.99900, 0.99990, 0.99999, 0.999999$.

Consecutive failure time interval								
$[t_{j-i-1}, t_{j-i-1})$	$S_0 = 0.99900$		$S_0 = 0.9999$		$S_0 = 0.99999$		$S_0 = 0.999999$	
	$\hat{\lambda}(t_{j-i})$	$\hat{S}(t_{j-i-1})$	$\hat{\lambda}(t_{j-i})$	$\hat{S}(t_{j-i-1})$	$\hat{\lambda}(t_{j-i})$	$\hat{S}(t_{j-i-1})$	$\hat{\lambda}(t_{j-i})$	$\hat{S}(t_{j-i-1})$
$[0, 0.8)$	156.25	0.9990	1562.5	0.9999	15,625.0	0.99999	156,250.0	0.99,9999
$[0.8, 3.1)$	0.5841	0.8741	0.5878	0.8749	0.5882	0.8750	0.5882	0.8750
$[3.1, 5.4)$	0.3971	0.7263	0.3981	0.7269	0.3982	0.7270	0.3982	0.7270
$[5.4, 9.2)$	0.2387	0.5447	0.2390	0.5452	0.2390	0.5453	0.2390	0.5453
$[9.2, 12.1)$	0.5069	0.3197	0.5071	0.3200	0.5071	0.3200	0.5071	0.3200

In the following section, we illustrate the usefulness of the modified LLGMM algorithm by applying to the data sets described in Tables 10.1, 10.3, and 10.5. Moreover, the results of the IDATTEDS and modified LLGMM are compared.

10.11 Applications of modified LLGMM to time-to-event data sets

Illustration 11.1: (Application of LLGMM-type conceptual computational algorithm to the data sets in Tables 10.1, 10.3, 10.5: kmwhasdata1 and malladataset): We apply the modified LLGMM procedure to the three data sets in Tables 10.1, 10.3, and 10.5 by utilizing (10.74), (10.79), and (10.80) with $\varepsilon = 0.001$. The results are summarized in Tables 10.8–10.10, respectively.

Table 10.8: LLGMM-based estimates using $S_0 = 0.985, 0.98900, 0.99000, 0.99900, 0.99990, 0.99999$ using procedure outlined in Section 10.9.

t_{j-y}^f	\hat{m}_I	$S_0 = 0.985$		$S_0 = 0.98900$		$S_0 = 0.99000$		$S_0 = 0.99900$		$S_0 = 0.9999$		$S_0 = 0.99999$	
		σ_{I-y}, \hat{m}_I	S_{I-y}, \hat{m}_I	σ_{I-y}, \hat{m}_I	S_{I-y}, \hat{m}_I	σ_{I-y}, \hat{m}_I	S_{I-y}, \hat{m}_I	σ_{I-y}, \hat{m}_I	S_{I-y}, \hat{m}_I	σ_{I-y}, \hat{m}_I	S_{I-y}, \hat{m}_I	σ_{I-y}, \hat{m}_I	S_{I-y}, \hat{m}_I
22.5	1	30.9600	0.9747	30.9600	0.9787	20.6400	0.9797	2.0640	0.9886	0.2064	0.9895	0.0206	0.9896
37.5	1	1.5998	0.9645	1.5998	0.9684	1.2865	0.9694	0.7224	0.9782	0.6660	0.9791	0.6603	0.9792
46.5	1	0.8013	0.9542	0.8013	0.9581	0.6909	0.9591	0.4921	0.9678	0.4722	0.9687	0.4702	0.9687
48.5	1	0.1831	0.9440	0.1831	0.9478	0.1637	0.9488	0.1289	0.9574	0.1254	0.9582	0.1250	0.9583
51.5	1	0.3189	0.9337	0.3189	0.9375	0.2916	0.9384	0.2426	0.9470	0.2377	0.9478	0.2372	0.9479
53.5	1	0.2343	0.9234	0.2343	0.9272	0.2176	0.9281	0.1874	0.9366	0.1844	0.9374	0.1841	0.9375
54.5	1	0.1288	0.9132	0.1288	0.9169	0.1209	0.9178	0.1067	0.9262	0.1053	0.9270	0.1052	0.9271
57.5	1	0.4254	0.9029	0.4254	0.9066	0.4026	0.9075	0.3618	0.9158	0.3577	0.9166	0.3573	0.9167
66.5	1	1.3372	0.8927	1.3372	0.8963	1.2741	0.8972	1.1605	0.9053	1.1491	0.9062	1.1480	0.9062
68.0	1	0.2107	0.8824	0.2107	0.8860	0.2018	0.8869	0.1858	0.8949	0.1842	0.8957	0.1840	0.8958
69.5	1	0.2231	0.8721	0.2231	0.8757	0.2146	0.8766	0.1993	0.8845	0.1978	0.8853	0.1976	0.8854
76.5	1	1.0947	0.8619	1.0947	0.8654	1.0568	0.8663	0.9885	0.8741	0.9817	0.8749	0.9810	0.8750
77.0	1	0.0758	0.8516	0.0758	0.8551	0.0734	0.8559	0.0691	0.8637	0.0687	0.8645	0.0686	0.8646
78.5	1	0.2399	0.8414	0.2399	0.8448	0.2329	0.8456	0.2204	0.8533	0.2191	0.8541	0.2190	0.8542
80.0	1	0.2486	0.8311	0.2486	0.8345	0.2419	0.8353	0.2298	0.8429	0.2286	0.8437	0.2285	0.8437
81.5	1	0.2565	0.8208	0.2565	0.8242	0.2501	0.8250	0.2386	0.8325	0.2374	0.8332	0.2373	0.8333

(continued)

Table 10.8 (continued)

t_{j-y}^f	\hat{m}_j	$S_0 = 0.985$		$S_0 = 0.98900$		$S_0 = 0.99000$		$S_0 = 0.99900$		$S_0 = 0.9999$		$S_0 = 0.99999$		$S_0 = 0.999999$	
		σ_{j-y}, \hat{m}_j	S_{j-y}, \hat{m}_j	σ_{j-y}, \hat{m}_j	S_{j-y}, \hat{m}_j	σ_{j-y}, \hat{m}_j	S_{j-y}, \hat{m}_j	σ_{j-y}, \hat{m}_j	S_{j-y}, \hat{m}_j	σ_{j-y}, \hat{m}_j	S_{j-y}, \hat{m}_j	σ_{j-y}, \hat{m}_j	S_{j-y}, \hat{m}_j	σ_{j-y}, \hat{m}_j	S_{j-y}, \hat{m}_j
82.5	1	0.1759	0.8106	0.1759	0.8139	0.1718	0.8147	0.1644	0.8221	0.1637	0.8228	0.1636	0.8229	0.1636	0.8229
83.0	1	0.0907	0.8003	0.0907	0.8036	0.0887	0.8044	0.0852	0.8117	0.0848	0.8124	0.0848	0.8125	0.0848	0.8125
84.0	1	0.1877	0.7901	0.1877	0.7933	0.1838	0.7941	0.1770	0.8013	0.1763	0.8020	0.1762	0.8021	0.1762	0.8021
91.5	1	1.4434	0.7798	1.4434	0.7830	1.4158	0.7838	1.3662	0.7909	1.3612	0.7916	1.3607	0.7917	1.3607	0.7917
93.5	1	0.3658	0.7695	0.3658	0.7727	0.3592	0.7734	0.3474	0.7805	0.3462	0.7812	0.3461	0.7812	0.3461	0.7812
102.5	1	1.6638	0.7593	1.6638	0.7624	1.6356	0.7631	1.5849	0.7701	1.5798	0.7708	1.5793	0.7708	1.5792	0.7708
107.0	1	0.7821	0.7490	0.7821	0.7521	0.7696	0.7528	0.7470	0.7597	0.7448	0.7603	0.7445	0.7604	0.7445	0.7604
108.5	1	0.2569	0.7388	0.2569	0.7417	0.2530	0.7425	0.2460	0.7493	0.2453	0.7499	0.2452	0.7500	0.2452	0.7500
112.5	1	0.6935	0.7285	0.6935	0.7314	0.6835	0.7322	0.6656	0.7388	0.6638	0.7395	0.6636	0.7396	0.6636	0.7396
113.5	1	0.1714	0.7182	0.1714	0.7211	0.1690	0.7219	0.1648	0.7284	0.1644	0.7291	0.1644	0.7292	0.1644	0.7292
116.0	1	0.4344	0.7080	0.4344	0.7108	0.4288	0.7116	0.4187	0.7180	0.4177	0.7187	0.4176	0.7187	0.4176	0.7187
117.0	1	0.1737	0.6977	0.1737	0.7005	0.1716	0.7013	0.1677	0.7076	0.1673	0.7083	0.1673	0.7083	0.1673	0.7083
118.5	1	0.2635	0.6874	0.2635	0.6902	0.2604	0.6909	0.2549	0.6972	0.2543	0.6978	0.2543	0.6979	0.2543	0.6979
119.0	1	0.0884	0.6772	0.0884	0.6799	0.0874	0.6806	0.0856	0.6868	0.0854	0.6874	0.0854	0.6875	0.0854	0.6875
120.0	1	0.1790	0.6669	0.1790	0.6696	0.1771	0.6703	0.1737	0.6764	0.1734	0.6770	0.1733	0.6771	0.1733	0.6771

122.5	1	0.4510	0.6567	0.4510	0.6593	0.4465	0.6600	0.4382	0.6660	0.4374	0.6666	0.4373	0.6667	0.4373	0.6667	0.6667
123.0	1	0.0897	0.6464	0.0897	0.6490	0.0888	0.6497	0.0872	0.6556	0.0871	0.6562	0.0871	0.6562	0.0871	0.6562	0.6562
127.5	1	0.8150	0.6361	0.8150	0.6387	0.8074	0.6394	0.7938	0.6452	0.7925	0.6458	0.7923	0.6458	0.7923	0.6458	0.6458
131.0	1	0.6193	0.6259	0.6193	0.6284	0.6138	0.6291	0.6039	0.6348	0.6029	0.6354	0.6028	0.6354	0.6028	0.6354	0.6354
132.5	1	0.2613	0.6156	0.2613	0.6181	0.2591	0.6188	0.2551	0.6244	0.2547	0.6249	0.2547	0.6250	0.2547	0.6250	0.6250
134.0	1	0.2611	0.6054	0.2611	0.6078	0.2590	0.6084	0.2551	0.6140	0.2548	0.6145	0.2547	0.6146	0.2547	0.6146	0.6146

Table 10.9: LLGMM-based estimates using $S_0 = 0.985, 0.98900, 0.99000, 0.99900, 0.99999, 0.999999$ using procedure outlined in Section 10.9.

t_{j-u}^f	\hat{m}_i	$S_0 = 0.985$		$S_0 = 0.98900$		$S_0 = 0.99000$		$S_0 = 0.99900$		$S_0 = 0.99999$		$S_0 = 0.999999$	
		σ_{j-4i}, \hat{m}_i	S_{j-4i}, \hat{m}_i	σ_{j-4i}, \hat{m}_i	S_{j-4i}, \hat{m}_i	σ_{j-4i}, \hat{m}_i	S_{j-4i}, \hat{m}_i	σ_{j-4i}, \hat{m}_i	S_{j-4i}, \hat{m}_i	σ_{j-4i}, \hat{m}_i	S_{j-4i}, \hat{m}_i	σ_{j-4i}, \hat{m}_i	S_{j-4i}, \hat{m}_i
6.0	1	3.7500	0.9653	2.7500	0.9692	2.5000	0.9702	0.2500	0.9790	0.0250	0.9799	0.0025	0.9800
14.0	1	4.5341	0.9554	4.0219	0.9593	3.8939	0.9603	2.7414	0.9690	2.6261	0.9699	2.6146	0.9700
44.0	1	9.2600	0.9456	8.4535	0.9494	8.2519	0.9504	6.4373	0.9590	6.2559	0.9599	6.2377	0.9600
62.0	1	2.1364	0.9357	1.9856	0.9396	1.9479	0.9405	1.6086	0.9490	1.5747	0.9499	1.5713	0.9500
89.0	1	2.6581	0.9259	2.5009	0.9297	2.4616	0.9306	2.1079	0.9391	2.0725	0.9399	2.0689	0.9400
98.0	1	0.7044	0.9160	0.6686	0.9198	0.6597	0.9207	0.5793	0.9291	0.5712	0.9299	0.5704	0.9300
104.0	1	0.4780	0.9062	0.4568	0.9099	0.4515	0.9108	0.4039	0.9191	0.3991	0.9199	0.3986	0.9200
107.0	1	0.2489	0.8963	0.2392	0.9000	0.2367	0.9009	0.2147	0.9091	0.2126	0.9099	0.2123	0.9100
114.0	1	0.6171	0.8865	0.5954	0.8901	0.5900	0.8910	0.5412	0.8991	0.5363	0.8999	0.5358	0.9000
123.0	1	0.8064	0.8766	0.7809	0.8802	0.7745	0.8811	0.7169	0.8891	0.7112	0.8899	0.7106	0.8900
128.0	1	0.4463	0.8668	0.4334	0.8703	0.4302	0.8712	0.4012	0.8791	0.3983	0.8799	0.3980	0.8800
148.0	1	1.8315	0.8569	1.7831	0.8604	1.7710	0.8613	1.6621	0.8691	1.6512	0.8699	1.6501	0.8700
182.0	1	2.8591	0.8471	2.7895	0.8505	2.7721	0.8514	2.6156	0.8591	2.6000	0.8599	2.5984	0.8600
187.0	1	0.3612	0.8372	0.3531	0.8407	0.3511	0.8415	0.3328	0.8491	0.3310	0.8499	0.3308	0.8500
189.0	1	0.1480	0.8274	0.1449	0.8308	0.1441	0.8316	0.1371	0.8392	0.1364	0.8399	0.1364	0.8400
274.0	1	3.2602	0.8077	3.1968	0.8110	3.1809	0.8118	3.0381	0.8192	3.0238	0.8199	3.0224	0.8200
302.0	1	1.6114	0.7978	1.5839	0.8011	1.5770	0.8019	1.5152	0.8092	1.5090	0.8099	1.5084	0.8100

363.0	1	3.3074	0.7880	3.2544	0.7912	3.2411	0.7920	3.1218	0.7992	3.1099	0.7999	3.1087	0.8000	3.1086	0.8000
374.0	1	0.5139	0.7781	0.5062	0.7813	0.5042	0.7821	0.4868	0.7892	0.4850	0.7899	0.4849	0.7900	0.4849	0.7900
451.0	1	3.6083	0.7683	3.5569	0.7714	3.5441	0.7722	3.4284	0.7792	3.4169	0.7799	3.4157	0.7800	3.4156	0.7800
461.0	1	0.4007	0.7584	0.3953	0.7615	0.3940	0.7623	0.3818	0.7692	0.3806	0.7699	0.3805	0.7700	0.3805	0.7700
492.0	1	1.2507	0.7486	1.2348	0.7516	1.2308	0.7524	1.1949	0.7592	1.1913	0.7599	1.1910	0.7600	1.1909	0.7600
538.0	1	1.7864	0.7387	1.7648	0.7418	1.7594	0.7425	1.7108	0.7492	1.7059	0.7499	1.7054	0.7500	1.7054	0.7500
774.0	1	8.5950	0.7289	8.4963	0.7319	8.4717	0.7326	8.2496	0.7393	8.2274	0.7399	8.2252	0.7400	8.2249	0.7400
841.0	1	1.7366	0.7190	1.7176	0.7220	1.7129	0.7227	1.6702	0.7293	1.6660	0.7299	1.6655	0.7300	1.6655	0.7300
936.0	1	2.3168	0.7092	2.2927	0.7121	2.2867	0.7128	2.2325	0.7193	2.2271	0.7199	2.2265	0.7200	2.2265	0.7200
1002.0	1	1.4764	0.6993	1.4617	0.7022	1.4581	0.7029	1.4252	0.7093	1.4219	0.7099	1.4216	0.7100	1.4215	0.7100
1011.0	1	0.1917	0.6895	0.1899	0.6923	0.1895	0.6930	0.1854	0.6993	0.1850	0.6999	0.1849	0.7000	0.1849	0.7000
1048.0	1	0.7954	0.6796	0.7883	0.6824	0.7865	0.6831	0.7703	0.6893	0.7687	0.6899	0.7686	0.6900	0.7685	0.6900
1054.0	1	0.1266	0.6698	0.1255	0.6725	0.1252	0.6732	0.1227	0.6793	0.1225	0.6799	0.1225	0.6800	0.1225	0.6800
1172.0	1	2.5138	0.6599	2.4931	0.6626	2.4879	0.6633	2.4413	0.6693	2.4366	0.6699	2.4362	0.6700	2.4361	0.6700
1205.0	1	0.6415	0.6501	0.6365	0.6527	0.6352	0.6534	0.6238	0.6593	0.6227	0.6599	0.6226	0.6600	0.6226	0.6600
1278.0	1	1.3990	0.6402	1.3885	0.6429	1.3858	0.6435	1.3621	0.6493	1.3597	0.6499	1.3595	0.6500	1.3594	0.6500
1401.0	1	2.2505	0.6304	2.2343	0.6330	2.2302	0.6336	2.1936	0.6394	2.1900	0.6399	2.1896	0.6400	2.1896	0.6400
1497.0	1	1.6209	0.6205	1.6096	0.6231	1.6068	0.6237	1.5816	0.6294	1.5790	0.6299	1.5788	0.6300	1.5788	0.6300
1557.0	1	0.9581	0.6107	0.9518	0.6132	0.9502	0.6138	0.9359	0.6194	0.9344	0.6199	0.9343	0.6200	0.9343	0.6200
1577.0	1	0.3100	0.6008	0.3081	0.6033	0.3076	0.6039	0.3031	0.6094	0.3027	0.6099	0.3026	0.6100	0.3026	0.6100

(continued)

Table 10.9 (continued)

t_{j-y}^f	\hat{m}_j	$S_0 = 0.985$		$S_0 = 0.98900$		$S_0 = 0.99000$		$S_0 = 0.99900$		$S_0 = 0.9999$		$S_0 = 0.99999$		$S_0 = 0.999999$	
		σ_{j-y}, \hat{m}_j	S_{j-y}, \hat{m}_j	σ_{j-y}, \hat{m}_j	S_{j-y}, \hat{m}_j	σ_{j-y}, \hat{m}_j	S_{j-y}, \hat{m}_j	σ_{j-y}, \hat{m}_j	S_{j-y}, \hat{m}_j	σ_{j-y}, \hat{m}_j	S_{j-y}, \hat{m}_j	σ_{j-y}, \hat{m}_j	S_{j-y}, \hat{m}_j	σ_{j-y}, \hat{m}_j	S_{j-y}, \hat{m}_j
1624.0	1	0.7257	0.5910	0.7212	0.5934	0.7201	0.5940	0.7101	0.5994	0.7091	0.5999	0.7090	0.6000	0.7090	0.6000
1669.0	1	0.6800	0.5811	0.6760	0.5835	0.6750	0.5841	0.6660	0.5894	0.6651	0.5899	0.6650	0.5900	0.6650	0.5900
1806.0	1	2.0285	0.5713	2.0171	0.5736	2.0142	0.5742	1.9885	0.5794	1.9859	0.5799	1.9857	0.5800	1.9856	0.5800
1874.0	6	0.9324	0.5614	0.9269	0.5637	0.9255	0.5643	0.9131	0.5694	0.9119	0.5699	0.9118	0.5699	0.9118	0.5699
1907.0	1	0.3682	0.5496	0.3663	0.5519	0.3658	0.5524	0.3615	0.5574	0.3611	0.5579	0.3610	0.5576	0.3610	0.5580
2012.0	19	1.1562	0.5378	1.1472	0.5400	1.1449	0.5405	1.1247	0.5454	1.1226	0.5458	1.1342	0.5580	1.1224	0.5459
2031.0	1	0.1398	0.5211	0.1392	0.5231	0.1390	0.5237	0.1376	0.5283	0.1374	0.5288	1.1224	0.5459	0.1374	0.5288
2065.0	1	0.2409	0.5037	0.2398	0.5057	0.2396	0.5062	0.2372	0.5107	0.2370	0.5112	0.2370	0.5112	0.2370	0.5112
2201.0	13	0.9086	0.4856	0.9031	0.4875	0.9017	0.4880	0.8894	0.4922	0.8881	0.4927	0.8880	0.4927	0.8880	0.4927
2421.0	1	0.6684	0.4482	0.6660	0.4500	0.6653	0.4504	0.6598	0.4544	0.6592	0.4548	0.6592	0.4548	0.6592	0.4548
2624.0	8	0.5512	0.4106	0.5488	0.4122	0.5481	0.4126	0.5426	0.4161	0.5420	0.3961	0.5420	0.4164	0.5420	0.4164
2710.0	2	0.2751	0.3818	0.2742	0.3832	0.2740	0.3836	0.2721	0.3868	0.2719	0.3871	0.2719	0.3871	0.2719	0.3872

Table 10.10: LLGMM-based estimates using $S_0 = 0.99900, 0.99990, 0.99999, 0.999999$ using procedure outlined in Section 10.9.

t_{j-1i}^f	\hat{m}_i	$S_0 = 0.99900$		$S_0 = 0.9999$		$S_0 = 0.99999$		$S_0 = 0.999999$	
		$\lambda_{j-1i, \hat{m}_i}$	S_{j-1, \hat{m}_i}	$\lambda_{j-1i, \hat{m}_i}$	S_{j-1, \hat{m}_i}	$\lambda_{j-1i, \hat{m}_i}$	S_{j-1, \hat{m}_i}	$\lambda_{j-1i, \hat{m}_i}$	S_{j-1, \hat{m}_i}
0.8	1	156.25	0.8741	1562.5	0.8749	15,625.0	0.8750	156,250.0	0.8750
3.1	1	0.5841	0.7263	0.5878	0.7269	0.5882	0.7270	0.5882	0.7270
5.4	1	0.3971	0.5447	0.3981	0.5452	0.3982	0.5453	0.3982	0.5453
9.2	1	0.2387	0.3197	0.2390	0.3200	0.2390	0.3200	0.2390	0.3200
12.1	1	0.5069	0.0000	0.5071	0.0000	0.5071	0.0000	0.5071	0.0000

Remark 10.11: We remark that using the LLGMM-type estimation approach yields the almost close simulation results as the estimation procedure outlined in Illustrations 10.1, 10.2, and 10.3 with the added bonus of survival estimates at the last failure time for both data sets in Tables 10.1, 10.3, and 10.5.

In the following, we compare the IDATTEDS and modified LLGMM results with the existing methods, namely, maximum likelihood and Kaplan–Meier approach.

10.12 Comparison of IDATTEDS and modified LLGMM with existing methods

In this section, the presented simulation results are compared with the existing methods, namely, maximum likelihood and Kaplan–Meier [18] estimates. The simulation results are recorded in Tables 10.11 and 10.12. In Table 10.13, we compare our results with Kaplan–Meier and Malla et al. estimates.

In the following section, we present the conclusions regarding the role and scope of the presented deterministic process as well as further extensions and generalizations that are in progress. In fact, a large-scale interconnected nonlinear hybrid dynamic model under the influence of Ito–Doob stochastic time-to-event process is developed and will appear elsewhere.

Table 10.11: Comparison of survival function estimates for data set in Table 10.1.

Failure Time:	I D A T T E D S	L L G M M Based	Maximum Likelihood Method:	Kaplan– Meier– Type Estimate	Failure Time:	I D A T T E D S	L L G M M Based	Maximum Likelihood Method:	Kaplan– Meier– Type Estimate
t_{j-1i}	$\hat{S}(t_{j-1i})$	S_{j-1i}, \hat{m}_i	$\hat{S}_{ML}(t_{j-1i})$	$\hat{S}_{KM}(t_{j-1i})$	t_{j-1i}	$\hat{S}(t_{j-1i})$	S_{j-1i}, \hat{m}_i	$\hat{S}_{ML}(t_{j-1i})$	$\hat{S}_{KM}(t_{j-1i})$
22.5	0.9896	0.9896	0.9941	0.9896	91.5	0.7917	0.7917	0.8139	0.7917
37.5	0.9792	0.9792	0.9781	0.9792	93.5	0.7812	0.7812	0.8052	0.7813
46.5	0.9687	0.9687	0.9623	0.9686	102.5	0.7708	0.7708	0.7650	0.7708
48.5	0.9583	0.9583	0.9581	0.9583	107.0	0.7604	0.7604	0.7442	0.7604
51.5	0.9479	0.9479	0.9513	0.9473	108.5	0.7500	0.7500	0.7373	0.7500
53.5	0.9375	0.9375	0.9465	0.9375	112.5	0.7396	0.7396	0.7186	0.7396
54.5	0.9271	0.9271	0.9440	0.9271	113.5	0.7292	0.7292	0.7139	0.7292
57.5	0.9167	0.9167	0.9362	0.9167	116.0	0.7187	0.7187	0.7022	0.7188
66.5	0.9062	0.9062	0.9094	0.9063	117.0	0.7083	0.7083	0.6975	0.7083
68.0	0.8958	0.8958	0.9045	0.8958	118.5	0.6979	0.6979	0.6905	0.6979
69.5	0.8854	0.8854	0.8995	0.8854	119.0	0.6875	0.6875	0.6881	0.6875
76.5	0.8750	0.8750	0.8746	0.8750	120.0	0.6771	0.6771	0.6834	0.6771
77.0	0.8646	0.8646	0.8727	0.8646	122.5	0.6667	0.6667	0.6717	0.6667
78.5	0.8542	0.8542	0.8670	0.8542	123.0	0.6562	0.6562	0.6694	0.6563
80.0	0.8437	0.8437	0.8612	0.8438	127.5	0.6458	0.6458	0.6483	0.6458
81.5	0.8333	0.8333	0.8553	0.8333	131.0	0.6354	0.6354	0.6321	0.6354
82.5	0.8229	0.8229	0.8514	0.8229	132.5	0.6250	0.6250	0.6252	0.6250
83.0	0.8125	0.8125	0.8494	0.8125	134.0	0.6146	0.6146	0.6183	0.6146
84.0	0.8021	0.8021	0.8453	0.8021					

Table 10.12: Comparison of survival function estimates for data set in Table 10.2.

Failure Time:	I D A T T E D S	L L G M M Based	Maximum Likelihood Method:	Kaplan– Meier– Type Estimate	Failure Time:	I D A T T E D S	L L G M M Based	Maximum Likelihood Method:	Kaplan– Meier– Type Estimate
t_{j-1i}	$\hat{S}(t_{j-1i})$	S_{j-1i}, \hat{m}_i	$\hat{S}_{ML}(t_{j-1i})$	$\hat{S}_{KM}(t_{j-1i})$	t_{j-1i}	$\hat{S}(t_{j-1i})$	S_{j-1i}, \hat{m}_i	$\hat{S}_{ML}(t_{j-1i})$	$\hat{S}_{KM}(t_{j-1i})$
6.0	0.9800	0.9800	0.9928	0.98	936.0	0.7200	0.7200	0.6753	0.72
14.0	0.9700	0.9700	0.9856	0.97	1002.0	0.7100	0.7100	0.6627	0.71
44.0	0.9600	0.9600	0.9636	0.96	1011.0	0.7000	0.7000	0.6611	0.70
62.0	0.9500	0.9500	0.9521	0.95	1048.0	0.6900	0.6900	0.6543	0.69
89.0	0.9400	0.9400	0.9364	0.94	1054.0	0.6800	0.6800	0.6533	0.68
98.0	0.9300	0.9300	0.9314	0.93	1172.0	0.6700	0.6700	0.6330	0.67
104.0	0.9200	0.9200	0.9282	0.92	1205.0	0.6600	0.6600	0.6276	0.66
107.0	0.9100	0.9100	0.9266	0.91	1278.0	0.6500	0.6500	0.6161	0.65
114.0	0.9000	0.9000	0.9230	0.90	1401.0	0.6400	0.6400	0.5979	0.64
123.0	0.8900	0.8900	0.9183	0.89	1497.0	0.6300	0.6300	0.5846	0.63
128.0	0.8800	0.8800	0.9158	0.88	1557.0	0.6200	0.6200	0.5766	0.62
148.0	0.8700	0.8700	0.9060	0.87	1577.0	0.6100	0.6100	0.5740	0.61
182.0	0.8600	0.8600	0.8903	0.86	1624.0	0.6000	0.6000	0.5681	0.60
187.0	0.8500	0.8500	0.8881	0.85	1669.0	0.5900	0.5900	0.5625	0.59
189.0	0.8400	0.8400	0.8872	0.84	1806.0	0.5800	0.5800	0.5463	0.58
274.0	0.8200	0.8200	0.8524	0.82	1874.0	0.5696	0.5699	0.5386	0.5688
302.0	0.8100	0.8100	0.8420	0.81	1907.0	0.5576	0.5580	0.5350	0.5566
363.0	0.8000	0.8000	0.8205	0.80	2012.0	0.5428	0.5459	0.5239	0.5402
374.0	0.7900	0.7900	0.8169	0.79	2031.0	0.5258	0.5288	0.5220	0.5233
451.0	0.7800	0.7800	0.7924	0.78	2065.0	0.5083	0.5112	0.5185	0.5046
461.0	0.7700	0.7700	0.7894	0.77	2201.0	0.4832	0.4927	0.5053	0.4685
492.0	0.7600	0.7600	0.7802	0.76	2421.0	0.4461	0.4548	0.4855	0.4325

Table 10.12 (continued)

Failure Time:	I	L	Maximum Likelihood Method:	Kaplan–Meier–Type Estimate	Failure Time:	I	L	Maximum Likelihood Method:	Kaplan–Meier–Type Estimate
	D	L				D	L		
	A	G				A	G		
	T	M				T	M		
	T	M				T	M		
	E	Based				E	Based		
	D					D			
	S					S			
t_{j-1i}	$\hat{S}(t_{j-1i})$	S_{j-1i}, \hat{m}_i	$\hat{S}_{ML}(t_{j-1i})$	$\hat{S}_{KM}(t_{j-1i})$	t_{j-1i}	$\hat{S}(t_{j-1i})$	S_{j-1i}, \hat{m}_i	$\hat{S}_{ML}(t_{j-1i})$	$\hat{S}_{KM}(t_{j-1i})$
538.0	0.7500	0.7500	0.7672	0.75	2624.0	0.4050	0.4164	0.4688	0.3604
774.0	0.7400	0.7400	0.7089	0.74	2710.0	0.2384	0.3871	0.46208	0.1802
841.0	0.7300	0.7300	0.6945	0.73					

Table 10.13: Comparison of survival function estimates for data set in Table 10.2.

Failure time:	I	L	Maximum likelihood method:	Kaplan–Meier–type estimate
	D	L		
	A	G		
	T	M		
	E	M		
	D	based		
	S			
t_{j-1i}	$\hat{S}(t_{j-1i})$	S_{j-1i}, \hat{m}_i	$\hat{S}_{ML}(t_{j-1i})$	$\hat{S}_{KM}(t_{j-1i})$
0.8	0.8741	0.8741	0.8824	0.8750
3.1	0.7263	0.7623	0.7224	0.7000
5.4	0.5447	0.5447	0.5626	0.525
9.2	0.3197	0.3197	0.3412	0.2625
12.1	0.0000	0.0000	0.126	0.2625

10.13 Conclusions

In the area of survival/reliability analysis, most of the research work is centered around the probabilistic analysis approach. In general, a closed-form probability distribution is not feasible. The presented linear/nonlinear deterministic dynamic modeling is more appropriate for complex and more diversified time-to-event processes. Furthermore, the results are also extended to stochastic linear and nonlinear dynamic time-to-event processes. This alternative approach does not require knowledge of either a closed-form probability distribution or a class of distributions. It does not require restrictive conditions on hazard rate functions. The time domain of a survival function need not be positively infinite. The influence of human mobility, rapid electronic communication devices, frequent technological changes, the rapidly growing knowledge, tools, and procedures, advancements in biological, engineering, medical, military, physical, and social sciences have generated a greater influence for the expansion of time-to-event processes beyond engineering and medical sciences. Naturally, these ideas motivated to initiate, formulate, and develop an innovative interconnected dynamic modeling approach for generalized version of time-to-event processes in biological, chemical, engineering, epidemiological, medical, multiple markets, and social dynamic processes through discrete-time intervention processes under deterministic and stochastic perturbations. The presented innovative modeling approach enhances our motivation to develop parameter and state estimation procedures. Moreover, the parameter and state estimation approach is dynamic. The dynamic nature is more natural rather than the existing static and single-shot approach. The dynamic approach adapts with current changes and updates the statistic process. This plays a very significant role in parameter and state estimation problems in a systematic and unifying way. Recently, developed LLGMM approach is extended to the problems in the time-to-event dynamic processes in all disciplines. On the other hand, the MLE is centered on the parameter and state estimates using the entire data. In addition, the LLGMM stabilizes the parameter and state estimation procedure with a finite data set. On the contrary, the MLE does not have this flexibility. The extended version of the LLGMM method is used to study time-to-event processes. Intervention processes provide a measure of influence of new tools/procedures/approaches in continuous-time states of time-to-event dynamic process. In particular, it generates a measure of the degree of sustainability, survivability, and reliability of the system. This further leads to sustainable/unsustainable, survivable/failure, reliable/unreliable binary state invariant sets. In addition, intervention processes provide the comparison between the past and currently used tools/procedures/approaches/attitudes/etc. The procedures developed in this work provide insight, tips, and tools for undertaking similar tasks in the context of stochastic framework. In fact, it allows having a time-varying covariate state influence on the dynamic of a complex survival/reliability of systems. This is the basis for future work in modeling time-to-event processes. These results will appear elsewhere.

References

- [1] Anis, M. Z. 2009. Inference on a sharp jump in hazard rate: A review, *Economic Quality Control*, 24(2), 213–229.
- [2] Chandra, J. & Ladde, G. S. 2014. Multi-cultural dynamics on social networks under external random perturbations, *International Journal of Communications, Network and System Sciences*, 7(06), 181–195.
- [3] Ladde, A. G., & Ladde G. S. An introduction to differential equations. *Deterministic Modeling, Methods and Analysis*, 1, World Scientific, Singapore, 2012.
- [4] Ladde, G. S. Network dynamic processes under stochastic perturbations. Technical report, U.S. Army Research Office, Mathematical Sciences Division, Research Triangle Park, NC, 2015.
- [5] Wanduku, D. & Ladde, G.S. 2011. A two-scale network dynamic model for human mobility process, *Mathematical Biosciences*, 229(1), 1–15.
- [6] Fang, L. & Zheng, S. 2011. A hybrid approach to predicting events in clinical trials with time-to-event outcomes, *Contemporary Clinical Trials*, 32(5), 755–759.
- [7] Goodman, M. S., Li, Y. Tiwari, R. C. 2011. Detecting multiple change points in piecewise constant hazard functions, *Journal of Applied Statistics*, 38(11), 2523–2532.
- [8] He, P., Kong, G. & Su, Z. 2013. Estimating the survival functions for right-censored and interval-censored data with piecewise constant hazard functions, *Contemporary Clinical Trials*, 35(2), 122–127.
- [9] Otunuga, O. M., Ladde, G. S. & Ladde, N. G. 2017. Local lagged adapted generalized method of moments and applications. *Stochastic analysis and applications*, 35(1), 110–143.
- [10] Paothong, A. & Ladde, G. S. 2012. Generalized network externality function, *Economic Analysis and Policy*, 42(3), 363–387.
- [11] Kalbfleisch, J. D. & Prentice, R. L. The statistical analysis of failure time data, 360, John Wiley & Sons, New Jersey, 2011.
- [12] Lawless, J. F. Statistical models and methods for lifetime data, Vol. 362, John Wiley & Sons, New Jersey, 2011.
- [13] Appiah, E. A. & Ladde, G. S. 2016. Linear hybrid deterministic dynamic modeling for time-to-event processes: State and parameter estimations, *International Journal of Statistics and Probability*, 5(6), 32.
- [14] Atkinson, K. E. An introduction to numerical analysis, John Wiley & Sons, New York, 2008.
- [15] Otunuga, O. M. Stochastic modeling and analysis of energy commodity spot price processes. Technical report, DTIC Document, 2014.
- [16] Schme, J. & Nelson, W. Estimates and approximate confidence limits for (log) normal life distributions from singly censored samples by maximum likelihood. Technical report, DTIC Document, 1977.
- [17] Hosmer, D. W., Lemeshow, S. & May, S. Applied survival analysis. 2011.
- [18] Kaplan, E. L. & Meier, P. 1958. Nonparametric estimation from incomplete observations, *Journal of the American statistical association*, 53(282), 457–481.
- [19] Malla, G. & Mukerjee, H. 2010. A new piecewise exponential estimator of a survival function, *Statistics & probability letters*, 80(23), 1911–1917.
- [20] Bennett, S. 1983. Log-logistic regression models for survival data. *Journal of the Royal Statistical Society: Series C (Applied Statistics)*, 32(2) 165–171.
- [21] Cox, D. R. & Oakes, D. Analysis of survival data. CRC Press, Boca Raton, FL, 1984.
- [22] Howlader, H. A. & Weiss, G. 1992. log-logistic survival estimation based on failure-censored data, *Journal of Applied Statistics*, 19(2), 231–240.

- [23] Langlands, A. O. & Pocock, S. J. & Kerr, G. R. & Gore, S. M. 1979. Long-term survival of patients with breast cancer: a study of the curability of the disease, *BMJ*, 2(6200), 1247–1251.
- [24] Apostol, T. M., *Mathematical analysis*, Addison Wesley Publishing Company, Reading, MA, 1974.
- [25] O'Quigley, J. & Struthers, L. 1982. Survival models based upon the logistic and log-logistic distributions, *Computer programs in Biomedicine*, 15(1), 3–11.

Tao Yuan, Manish Kothawade, Yuan Chen

11 A Bayesian design of zero-failure reliability demonstration tests for multicomponent systems

Abstract: This chapter proposes a Bayesian methodology for planning system-level zero-failure reliability demonstration tests (RDTs) for multicomponent systems by integrating available prior information at the component level. The proposed methodology consists of three essential steps. The first step specifies a parametric failure-time distribution for each component in a system and derives the system reliability function according to the system structure function. The second step formulates and integrates component-level prior distributions. The third step determines the minimum sample size for the RDT using the integrated component-level prior information and a posterior assurance criterion considering the consumer's risk. A Markov chain Monte Carlo simulation-based algorithm is presented for the posterior computation. Two examples are used to illustrate the proposed methodology. Numerical results demonstrate the applicability of the proposed methodology to a broad range of failure-time distributions and system structures.

Keywords: Reliability demonstration tests, Bayesian approach, multicomponent systems, prior distribution, Gibbs sampling

11.1 Introduction

The reliability demonstration test (RDT) is often used to demonstrate that the reliability of a system or component meets a given standard or requirement, with a certain level of confidence [1]. A non-sequential, time-censoring RDT usually tests n sample units until time t_c at the normal or accelerated operating conditions, and the demonstration is successful if no more than r failures by the end of the test [2]. A RDT with $r = 0$ is referred to as the zero-failure RDT (also known as the minimum sample size RDT). It is often necessary to specify the sample size n and/or the test duration t_c for the zero-failure RDT plan. The RDT plan depends on the reliability requirement, confidence level, and underlying failure-time distribution. This study proposes a Bayesian method for planning the zero-failure RDTs for multicomponent systems by integrating prior knowledge regarding failure-time distributions of components.

Tao Yuan, Yuan Chen, Department of Industrial and Systems Engineering, Ohio University, Athens, Ohio, USA

Manish Kothawade, Wolverine Corporation, Saint Joseph, Michigan, USA

<https://doi.org/10.1515/9783110725599-011>

Both classical likelihood-based and Bayesian methods have been used to plan RDTs. Chen [3] recently provided a comprehensive review on planning RDTs. The classical methods to plan RDTs are usually based on the construction of a one-sided lower confidence bound of a reliability index if the index is the larger the better, for example, the p -quantile life or reliability at a given mission time. Meeker and Escobar [1] and Wang [4] discussed the classical method for planning the zero-failure RDT for the Weibull distribution with a given shape parameter. For a Weibull random variable T with a given shape parameter β , T^β follows the exponential distribution and one can construct one-sided lower confidence bounds for the Weibull scale parameter, p -quantile life, and mission reliability even when there is zero failure in a reliability test. Those lower confidence bounds can then be used to plan the zero-failure RDT. One can decide the minimum sample size required for a pre-specified test duration or the minimum test duration for a given sample size. McKane et al. [5] considered the sample size selection problem for demonstration tests with failure-censoring from location-scale and log-location-scale distributions. A test with failure censoring (or called Type-II censoring) terminates after a specified number of failures r , $1 \leq r \leq n$. One-sided lower confidence bounds for the p -quantile life and mission reliability can be obtained using the maximum likelihood (ML) method and pivotal quantity approach for failure-censoring tests. However, their method cannot be applied to plan zero-failure RDTs because ML estimates for general location-scale and log-location-scale distributions cannot be computed for test data without failures [1].

Martz and Waller [6] developed a Bayesian zero-failure fixed time (i.e., time-censoring) demonstration testing procedure for the exponential distribution considering the consumer's risk criterion. Assuming a conjugate Gamma prior distribution for the exponential rate parameter, they derived the posterior distribution for the rate parameter when no failures are observed in the RDT and obtained the required unit-hours nt_c . Their results demonstrated that the Bayesian test plan may require less unit-hours of testing than the classical test plans and there is no need to conduct RDTs when the prior information is sufficient to meet the assurance requirement. Fan and Chang [7] later considered a Bayesian zero-failure demonstration test for an accelerated life test with the exponential distribution. The exponential rate parameter was assumed to have a log-linear life-stress relationship with the temperature and prior distributions were assumed for the coefficients in the life-stress relationship. Bayesian methods for planning RDTs involving some other distributions have also been considered. For example, Chen et al. [8] investigated the optimal binomial RDTs under acceptance decision uncertainty. Kleyner et al. [9] considered the sample size determination of binomial RDTs after product design changes, using RDT results collected on previous version(s) of the product to derive a prior distribution for the reliability of the revised product. Jeon and Ahn [10] designed the Bayesian RDT for finite populations assuming the hypergeometric distribution.

The RDT for a system with multiple components can be conducted at either the system or component (or subsystem) level. Some studies proposed various system-based component test plans for demonstrating the system reliability by testing the components or subsystems [11–16]. Those studies emphasized that the component test plans should be based on the system configurations, that is, system-based. The early work of Gal [11] derived zero-failure subsystem test plans to demonstrate the system reliability considering the consumer's risk. Mazumdar [15] later extended this study to allow non-zero numbers of component failures and considered both the consumer's and producer's risks for series systems composed of components with exponential failure-time distributions. Easterling et al. [14] derived optimum system-based component test plans for binomial data and illustrated them for series and series-parallel systems. Rajgopal and Mazumdar [12] provided a comprehensive study on component test plans to demonstrate system reliability of series systems. Assuming that the components have exponential failure-time distributions, and the component failure rates have known upper bounds, they derived minimum cost component test plans that satisfy both the producer's and consumer's risks. In a later study, Rajgopal and Mazumdar [13] proposed minimum cost component test plans for demonstrating the reliability of highly reliable parallel systems, assuming exponential failure-time distributions for components and considering both the producer's and consumer's risks.

Some studies have considered system-level RDTs by incorporating prior knowledge and/or test data at the component level. Guo et al. [17] developed a hybrid approach for finding the sample size n of the zero-failure RDT for one-shot systems utilizing component-level test data and prior information. For a given sample size n , the number of successes in the system RDT follows the binomial distribution with n trials, of which the probability of success in each trial equals the system reliability. They obtained a Beta prior distribution for the system reliability from component tests information. The component tests are assumed to result in zero component failures. A hybrid approach that combines the Bayesian approach and variance propagation technique was proposed to derive the prior distribution for the system reliability. With that system reliability prior distribution, the minimum sample size required for the system-level zero-failure RDT can be obtained. Their results indicated that a much smaller sample size is required if the prior reliability information obtained from the component-level tests are incorporated into the system RDT design. Ten and Xie [18] also considered the Bayesian RDT plan for series systems with binomial subsystem data. They used the Mann's approximately optimum lower confidence bound model to derive the system-level prior distribution based on binomial subsystem data. Li et al. [19] considered the design of system zero-failure RDTs with binomial elements (e.g., system, subsystems, and components). A Beta prior distribution for the system reliability is derived by integrating prior knowledge and test data available at lower level elements.

This study focuses on the planning of zero-failure system-level RDTs using the Bayesian approach to incorporate prior information at the component level. We aim to develop a flexible framework that is applicable to a broad range of failure-time distributions and system structures. The proposed framework is based on the Bayesian integration of multilevel reliability information. Three approaches have been proposed to integrate multilevel reliability information to model and predict the system reliability: top-down approach, bottom-up approach, and Bayesian hierarchical approach.

Mastran [20] and Mastran and Singpurwalla [21] proposed a top-down approach to estimate system reliability assuming that a prior distribution is available for system reliability. The top-down approach consists of the following steps: (1) combine the system-level prior distribution with the system-level reliability data, if available, using Bayes' theorem to obtain a revised prior distribution of system reliability; (2) derive the prior distributions of component reliability that are consistent with the revised prior distribution of system reliability, given the configuration of components in the system; (3) combine the derived component-level prior distributions with component-level data using Bayes' theorem to obtain the posterior distributions of component reliability; (4) derive the posterior distribution of system reliability consistent with the posterior distributions of component reliability.

Martz et al. [22] and Martz and Waller [23] proposed an approximate bottom-up approach for integrating multilevel binary data. In this approach, lower level posterior distributions were obtained by integrating data and prior information at that level. At the next higher level, an "induced" higher-level prior distribution is obtained by propagating the lower level posterior distributions up through the system reliability block diagram and combining this induced prior distribution with data and "native" prior distribution at the higher level to obtain a posterior distribution at this level. Both the induced prior distributions and their integration with data and prior information at the higher-level are achieved through approximations. This bottom-up process continues until the top level, or system level, is reached. This was later extended to consider failure time and repair data [24]. Some recent studies on multilevel systems with interdependent subsystems and components [25] and proportional hazard modeling for hierarchical systems [26] adopted this bottom-up approach.

Both the top-down and bottom-up approaches use approximations in the computation, and approximation errors may occur especially when sample sizes are small. Moreover, these approaches are subject to aggregation errors [27]; that is, different posterior results are obtained when the data integration is accomplished in different ways. Several recent papers considered a fully Bayesian hierarchical approach, which can naturally eliminate the approximation and aggregation errors [28–35]. In this approach, system and subsystem failure-time distributions are re-expressed in terms of component failure-time distributions using deterministic relations derived from the reliability block diagrams, fault trees, or Bayesian networks. Multilevel data are integrated into a joint likelihood function, and therefore are

combined and analyzed simultaneously. This approach has been applied to analyze binomial pass/fail, failure time, and degradation data. This chapter adopts this approach and proposes a method for planning the system RDTs using prior information available at the component level.

The remainder of this chapter is organized as follows. Section 11.2 outlines the proposed Bayesian method for planning the system-level zero-failure RDTs. Section 11.3 uses two examples to illustrate the potential applicability of the proposed Bayesian RDT planning method. Finally, Section 11.4 concludes this chapter and states possible future research directions.

11.2 Methodology

This section outlines the proposed Bayesian method for planning the system-level zero-failure RDTs using component-level prior distributions. We make the following assumptions:

- Components in a system are independent.
- Failure-time distributions of components are known.
- Prior information regarding the failure-time distribution of each component is available and is expressed as the prior distribution(s) for the component's failure-time distribution parameter(s).
- The system-level RDT is non-sequential and time-censoring.
- The consumer's risk is considered.

Assume an m -component coherent system represented by a reliability block diagram. The components are labeled C_i , $i = 1, 2, \dots, m$. Let T_i be the random variable denoting the failure time of the component C_i , with the probability density function (pdf) $f_i(t|\theta_i)$, cumulative distribution function (Cdf) $F_i(t|\theta_i)$, and reliability function $R_i(t|\theta_i)$, where θ_i denotes the parameter vector of the i th component's failure-time distribution. Commonly used failure-time distributions include those location-scale-based probability distributions, for example, the exponential, Weibull, and lognormal distributions. Please see Meeker and Escobar [1] for a comprehensive list of failure-time distributions.

The system reliability function is then derived according to the deterministic system structure function as $R_0(t|\theta_1, \theta_2, \dots, \theta_m) = \varphi(R_1(t|\theta_1), R_2(t|\theta_2), \dots, R_m(t|\theta_m))$, where the structure function $\varphi(\cdot)$ depends on the system configuration. For the example combined series-parallel system shown in Figure 11.1, the reliability function of the system is expressed as

$$R_0(t|\theta_1, \theta_2, \theta_3) = \varphi(R_1(t|\theta_1), R_2(t|\theta_2), R_3(t|\theta_3)) = [1 - (1 - R_1(t|\theta_1))(1 - R_2(t|\theta_2))]R_3(t|\theta_3) \quad (11.1)$$

assuming independent components. No parametric reliability function is directly assumed for the system. Instead, the system reliability function is re-expressed in terms of the component reliability functions and based on the component reliability functions' parameters.

Let $f(\theta_1, \theta_2, \dots, \theta_m)$ denote the joint prior distribution for all model parameters. If the component parameter vectors are independent, then

$$f(\theta_1, \theta_2, \dots, \theta_m) = f(\theta_1)f(\theta_2) \cdots f(\theta_m) \quad (11.2)$$

where $f(\theta_i)$ represents the prior distribution for θ_i , for $i = 1, 2, \dots, m$. Prior distributions play a critical role in the Bayesian modeling and inference. One may obtain the component-level prior distributions from historical data and/or experts' opinions. For example, components may be supplied from various external vendors who have conducted reliability tests to demonstrate the component reliability. The existing reliability testing data and results may be used to formulate the component-level prior distribution for each component. Here, we assume that the component-level prior distribution is specified for the component's failure-time distribution parameter(s). In practice, it may be more convenient to formulate prior distributions for quantities other than the distribution parameters. For example, when performing Bayesian inference using the Weibull distribution, Meeker and Escobar [1] chose to specify prior distributions for the Weibull shape parameter and 0.01-quantile life because they are approximately independent, and one can conveniently formulate independent prior distributions for them. Then the joint prior distribution for the Weibull shape and scale parameters can be obtained via transformation of random variables.

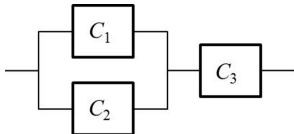


Figure 11.1: A combined series–parallel system with three components.

This study assumes that the reliability requirement is specified as the p -quantile life of the system, denoted by t_{0p}^* . Other reliability index, for example, the mission reliability, can be used as well. The RDT plans need to satisfy the posterior assurance criterion given by

$$\Pr(t_{0p} \geq t_{0p}^* | \text{Test is passed}, n, t_c) \geq 1 - \gamma \quad (3)$$

where $1 - \gamma$ is called the posterior assurance and γ is the posterior risk. $\Pr(t_{0p} \geq t_{0p}^* | \text{Test is passed}, n, t_c)$ is the posterior probability that, given the demonstration test is passed, the system p -quantile life t_{0p} meets the pre-specified requirement t_{0p}^* . The systems pass the zero-failure RDT with the sample size n and test duration t_c if no failures occur within the test duration. The criterion given

by (3) considers the consumer's risk. Assuming that the consumer accepts the systems if the demonstration test is passed, the probability that the consumer wrongly accepts systems that do not meet the reliability requirement is γ .

Given that the demonstration test is passed, the joint posterior distribution of the model parameters $\theta_0 \equiv (\theta_1, \theta_2, \dots, \theta_m)$ is derived according to the Bayes theorem by

$$\begin{aligned} f(\theta_1, \theta_2, \dots, \theta_m | \text{Test is passed}, n, t_c) &\propto \Pr(\text{Zero failure} | \theta_1, \theta_2, \dots, \theta_m, n, t_c) \\ f(\theta_1, \theta_2, \dots, \theta_m) &\propto R_0(t_c | \theta_1, \theta_2, \dots, \theta_m)^n f(\theta_1, \theta_2, \dots, \theta_m) \end{aligned} \quad (11.4)$$

where $\Pr(\text{Zero failure} | \theta_1, \theta_2, \dots, \theta_m, n, t_c) = R_0(t_c | \theta_1, \theta_2, \dots, \theta_m)^n$ is the likelihood function. Let $f(t_{0p})$ and $f(t_{0p} | \text{Test is passed}, n, t_c)$ denote, respectively, the prior and posterior distributions of the system p -quantile life t_{0p} . Because t_{0p} is a function of the model parameters given by

$$t_{0p} = R_0^{-1}(1 - p | \theta_1, \theta_2, \dots, \theta_m) \quad (11.5)$$

$f(t_{0p})$ and $f(t_{0p} | \text{Test is passed}, n, t_c)$ can be obtained from $f(\theta_1, \theta_2, \dots, \theta_m)$ and $f(\theta_1, \theta_2, \dots, \theta_m | \text{Test is passed}, n, t_c)$, respectively, through transformation of random variables. Then the posterior probability $\Pr(t_{0p} \geq t_{0p}^* | \text{Test is passed}, n, t_c)$ can be evaluated by

$$\Pr(t_{0p} \geq t_{0p}^* | \text{Test is passed}, n, t_c) = \int_{t_{0p}^*}^{\infty} f(t_{0p} | \text{Test is passed}, n, t_c) dt_{0p} \quad (11.6)$$

This integral generally has no closed-form solutions. Markov chain Monte Carlo (MCMC)-based methods, for example, Gibbs sampling [36], can be used to evaluate $\Pr(t_{0p} \geq t_{0p}^* | \text{Test is passed}, n, t_c)$. In each iteration, Gibbs sampling can conveniently draw a sample from the joint posterior distribution $f(\theta_1, \theta_2, \dots, \theta_m | \text{Test is passed}, n, t_c)$, namely $(\theta_1^{(k)}, \theta_2^{(k)}, \dots, \theta_m^{(k)})$, for $k = 1, 2, \dots, K$, where K is the total number of Gibbs sampling iterations. Then for the parameter vectors $(\theta_1^{(k)}, \theta_2^{(k)}, \dots, \theta_m^{(k)})$ drawn in the k th Gibbs sampling iteration, the system p -quantile life, denoted by $t_{0p}^{(k)}$, can be obtained according to eq. (11.5). Finally, $\Pr(t_{0p} \geq t_{0p}^* | \text{Test is passed}, n, t_c)$ can be estimated by the fraction of $t_{0p}^{(k)}$ values that are greater than or equal to t_{0p}^* , that is,

$$\begin{aligned} \Pr(t_{0p} \geq t_{0p}^* | \text{Test is passed}, n, t_c) &\approx \frac{1}{K} \sum_{k=1}^K I(t_{0p}^{(k)} \geq t_{0p}^*) \\ &= \frac{1}{K} \sum_{k=1}^K I(R_0^{-1}(1 - p | \theta_1^{(k)}, \theta_2^{(k)}, \dots, \theta_m^{(k)}) \geq t_{0p}^*) \end{aligned} \quad (11.7)$$

Our objective is to find the minimum sample size n^* that satisfies the assurance criterion given by eq. (11.3) for a pre-specified test duration t_c . Because there is no closed-form solution to n^* , we choose to enumerate the sample size n within a certain range

and evaluate the posterior probability $\Pr(t_{0p} \geq t_{0p}^* | \text{Test is passed}, n, t_c)$ using the MCMC method shown in eq. (11.7) for each n .

Similarly, if $(\theta_1^{(k)}, \theta_2^{(k)}, \dots, \theta_m^{(k)})$ are randomly drawn from the prior distribution $f(\theta_1, \theta_2, \dots, \theta_m)$, we can estimate the prior probability $\Pr(t_{0p} \geq t_{0p}^*)$ defined by

$$\Pr(t_{0p} \geq t_{0p}^*) = \int_{t_{0p}^*}^{\infty} f(t_{0p}) dt_{0p} \quad (11.8)$$

This is the probability that the system reliability requirement is satisfied based on the prior distributions.

In summary, this section outlines the Bayesian method for planning the system-level zero-failure RDTs using prior information available at the component level. It is flexible as it can be applied to any failure-time distributions and system structures if the system's reliability function can be derived from the reliability functions of its components via some deterministic structure function.

11.3 Numerical examples

This section uses two examples to illustrate the proposed methodology. The first example is a two-component series system of which the two components have the Weibull failure-time distributions. We assume the two components have a known identical Weibull shape parameter so that the classical method is applicable. The second example considers the three-component combined series-parallel system shown in Figure 11.1, of which the three components have three different failure-time distributions to demonstrate that the proposal methodology is applicable to a wide range of failure-time distributions.

11.3.1 Example 1

Example 1 assumes that the two components in a simple series system have the Weibull failure-time distributions with the following reliability functions

$$R_i(t | \alpha_i, \beta) = \exp\left(-\left(\frac{t}{\alpha_i}\right)^\beta\right) \quad (11.9)$$

for $i = 1, 2$, where β is the identical shape parameter and α_i is the scale parameter of the i th component. The system reliability is then given by

$$\begin{aligned}
 R_0(t|\beta, \alpha_1, \alpha_2) &= R_1(t|\alpha_1, \beta) \times R_1(t|\alpha_2, \beta) = \exp\left(-\left(\frac{t}{\alpha_1}\right)^\beta - \left(\frac{t}{\alpha_2}\right)^\beta\right) \\
 &= \exp\left(-\left(\frac{t}{\alpha_0}\right)^\beta\right) \sim W(\alpha_0, \beta)
 \end{aligned}
 \quad (11.10)$$

where $W(\alpha_0, \beta)$ denotes the Weibull distribution with the shape parameter β and scale parameter α_0 . When the two components have an identical Weibull shape parameter β , the system's failure time also follows the Weibull distribution with the shape parameter β and scale parameter α_0 given by

$$\alpha_0 = \left[\sum_{i=1}^2 \left(\frac{1}{\alpha_i} \right)^\beta \right]^{-\frac{1}{\beta}} \quad (11.11)$$

Assuming the Weibull shape parameter is known to be $\beta = 2$, we can apply the classical method to plan the zero-failure RDT for this system. We assume that the test duration $t_c = 1,500$ h, the system reliability requirement is specified as the p -quantile life of the system with $p = 0.10$ as $t_{0p}^* = 750$ h, and the assurance criterion is $(1 - \gamma) = 0.95$, that is, $\gamma = 0.05$. Note that the failure-time distributions $R_i(t|\theta_i)$, for $i = 1, 2$, test duration t_c , and reliability requirement t_{0p}^* are specified at the normal operating conditions of the system. In practice, the RDT can be conducted at accelerated operating conditions and the test duration at the accelerated test conditions can be obtained using some acceleration factors [1].

Using the classical method for planning the zero-failure RDT for the Weibull distribution with a given shape parameter, the minimum sample size n^* that satisfies the assurance criterion (11.3) is the smallest integer satisfying [1]

$$n \geq \frac{1}{\kappa^\beta} \times \frac{\ln \gamma}{\ln(1-p)} \quad (11.12)$$

where $\kappa = t_c/t_{0p}^*$. It can be shown that $n^* = 8$ for this example using the classical planning method.

Next we assume prior distributions are available for the two component-level Weibull scale parameters α_1 and α_2 . Independent Gamma prior distributions are assumed for the two positive Weibull scale parameters. The pdf of the Gamma distribution for a positive random variable X is given by

$$f(x|a, b) = \frac{b}{\Gamma(a)} x^{a-1} e^{-bx}, \quad x > 0 \quad (11.13)$$

where $a > 0$ and $b > 0$ are the shape and scale parameters, respectively, and $\Gamma(\cdot)$ is the Gamma function. The mean and variance of the Gamma distribution are $E(X) = ab$ and $\text{VAR}(X) = ab^2$, respectively. Herein and hereafter, we use $G(a, b)$ to denote the Gamma prior distribution for a parameter. One can choose the a and b values for

each parameter based on historical data and/or experts' opinions to reflect one's prior knowledge and uncertainty on each parameter.

Table 11.1 lists the minimum sample size n^* needed to satisfy the assurance criterion (3) under seven sets of prior distributions for α_1 and α_2 . For each set of prior, the prior mean and standard deviation for t_{op} and the prior probability that the system reliability satisfies the requirement, $\Pr(t_{op} \geq t_{op}^*)$, are computed. As seen from Table 11.1, the minimum sample size determined by the Bayesian planning method may be more than or less than the minimum sample size derived from the classical method given by (11.12). In brief, if the prior knowledge provides evidence that the system reliability requirement may be satisfied, the Bayesian approach has the potential to reduce the sample size over the classical method. On the other hand, if the prior knowledge indicates that the system reliability requirement may be unsatisfied, the Bayesian planning method may need more sample than the classical method to demonstrate the system reliability.

Table 11.1: Minimum sample size needed n^* assuming various prior distributions in Example 1.

	Prior					n^*	$\text{Pr}(\text{Zero failure} n^*, t_c)$
	α_1	α_2	$E(t_{op})$	$STD(t_{op})$	$\text{Pr}(t_{op} \geq t_{op}^*)$		
1	$G(10.5, 0.002)$	$G(15.5, 0.003)$	1130.0	239.0	0.9554	0	–
2	$G(10.0, 0.002)$	$G(15.0, 0.003)$	1082.0	235.2	0.9327	1	0.8046
3	$G(39.0, 0.01)$	$G(78.0, 0.02)$	882.3	88.2	0.9382	2	0.5465
4	$G(176.0, 0.05)$	$G(352.0, 0.1)$	805.3	37.2	0.9335	4	0.2360
5	$G(344.0, 0.1)$	$G(688.0, 0.2)$	788.2	26.1	0.9304	6	0.1041
6	$G(1011.0, 0.3)$	$G(1685.0, 0.5)$	773.0	15.4	0.9330	9	0.0289
7	$G(1014.0, 0.3)$	$G(1690.0, 0.5)$	775.3	15.4	0.9506	0	–

There are two factors affecting the minimum sample size n^* obtained from the Bayesian approach. The first factor is the prior probability that the system reliability satisfies the requirement, $\Pr(t_{op} \geq t_{op}^*)$. Assuming Priors 1 and 7, $\Pr(t_{op} \geq t_{op}^*) \geq 1 - \gamma$, that is, the assurance criterion is satisfied using the prior knowledge, hence there is no need to conduct system tests, that is, $n^* = 0$. Under Priors 2–6, $\Pr(t_{op} \geq t_{op}^*) < 1 - \gamma$, hence additional system tests are needed. Although the prior probabilities $\Pr(t_{op} \geq t_{op}^*)$ are very close under Priors 2–6, the minimum sample size n^* increases from Priors 2–6. From Priors 2–6, the prior uncertainty on t_{op} , measured by $STD(t_{op})$, decreases; that is, we become more certain that the reliability assurance criterion is not satisfied according to the prior knowledge. Hence, the minimum sample size needed to demonstrate the system reliability increases from Priors 2 to 6. Figure 11.2 depicts the prior density functions of the system p -quantile life, $f(t_{op})$, under Priors

2–6 to show the decrease of prior uncertainty on t_{0p} from Priors 2 to 6. The Bayesian approach inferses the system reliability by combining information from the prior knowledge and test data. If our prior knowledge is relatively certain that the system reliability requirement is not satisfied, a large sample size would be needed so that the posterior inference is largely influenced by the information from test data in order to successfully demonstrate the system reliability.

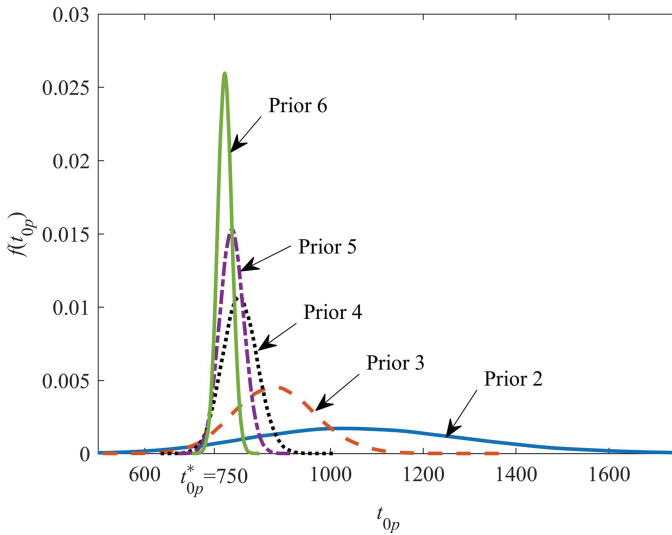


Figure 11.2: Prior density of t_{0p} under different priors in Example 1.

A quantity of interest to the producer is the unconditional probability that the demonstration test will be successful for a given sample size,

$$\Pr(\text{Zero failure}|n, t_c) = \int_0^\infty \int_0^\infty R_0(t_c|\beta, \alpha_1, \alpha_2)^n f(\alpha_1) f(\alpha_2) d\alpha_1 d\alpha_2 \quad (11.14)$$

From Priors 2–6, the minimum sample size n^* increases and the probability of a successful demonstration using the sample size n^* decreases. For example, Under Prior 6, we are relatively certain that the assurance criterion is not satisfied and a minimum sample size of 9 would be needed. However, the probability that the demonstration test will be successful is only 0.0289. Figure 11.3 shows the posterior assurance $\Pr(t_{0p} \geq t_{0p}^* | \text{Test is passed}, n, t_c)$ and the unconditional probability of a successful demonstration $\Pr(\text{Zero failure}|n, t_c)$ as functions of the sample size n under Prior 5. As the sample size n increases, the posterior assurance after a successful demonstration (i.e., zero failure in the RDT) increases, but the probability for a successful demonstration decreases rapidly. Martz and Waller [6] regarded

the unconditional probability of not passing the test as a modified producer's risk because the probability of not passing the test should be sufficiently small for the producer to be willing to perform the RDT.

An alternative method for planning the RDT in this example is to derive a prior distribution for the system-level Weibull scale parameter α_0 . Because α_0 is a function of the two component-level Weibull scale parameters given by eq. (11.11), the prior distribution of α_0 may be obtained from the prior distributions of α_1 and α_2 via the transformation of random variables. A computationally convenient method is to approximate the prior distribution of α_0 by a Gamma $G(a_0, b_0)$ distribution, of which the two parameters a_0 and b_0 are obtained by matching the prior mean and variance of α_0 . That is, a_0 and b_0 are obtained from solving the two equations $a_0 b_0 = E(\alpha_0)$ and $a_0 b_0^2 = \text{VAR}(\alpha_0)$. The system failure time is then described by the Weibull $W(\alpha_0, \beta)$ distribution with the known shape parameter β and the $G(a_0, b_0)$ prior distribution for α_0 . Given that the demonstration is successful, the posterior distribution of α_0 is given by

$$f(\alpha_0 | \text{Test is passed}, n, t_c, \beta) \propto R_W(t_c | \alpha_0, \beta)^n f(\alpha_0) \propto \exp\left(-n\left(\frac{t_c}{\alpha_0}\right)^\beta\right) \times \alpha_0^{a_0-1} e^{-b_0 \alpha_0} \quad (11.15)$$

where $R_W(t)$ denotes the Weibull reliability function. Because $t_{0p} = \alpha_0 (-\ln(1-p))^{1/\beta}$, the posterior distribution of t_{0p} , denoted by $f(t_{0p} | \text{Test is passed}, n, t_c, \beta)$, can be obtained from $f(\alpha_0 | \text{Test is passed}, n, t_c, \beta)$ via the transformation of random variables. The posterior probability that the system reliability requirement is satisfied given a successful demonstration, $\Pr(t_{0p} \geq t_{0p}^* | \text{Test is passed}, n, t_c)$, defined by eq. (11.6) and can be evaluated again using the Gibbs sampling method. Figure 11.4 uses Prior 5 as an example to compare the prior density function of α_0 to its Gamma approximation. The Gamma distribution overall approximates the prior distribution of α_0 well with some noticeable discrepancy around the peak of the density function. Table 11.2 lists the approximated $G(a_0, b_0)$ prior for α_0 corresponding to the seven sets of prior distributions used in Table 11.1 and the minimum sample size required using the alternative method. Except for Priors 5 and 6, the two methods produce the same minimum sample sizes required.

11.3.2 Example 2

The second example uses the three-component combined series-parallel system shown in Figure 11.1 to illustrate the proposed Bayesian RDT planning method. The failure-time distributions of the three components are assumed to be Weibull, exponential, and lognormal, respectively, that is,

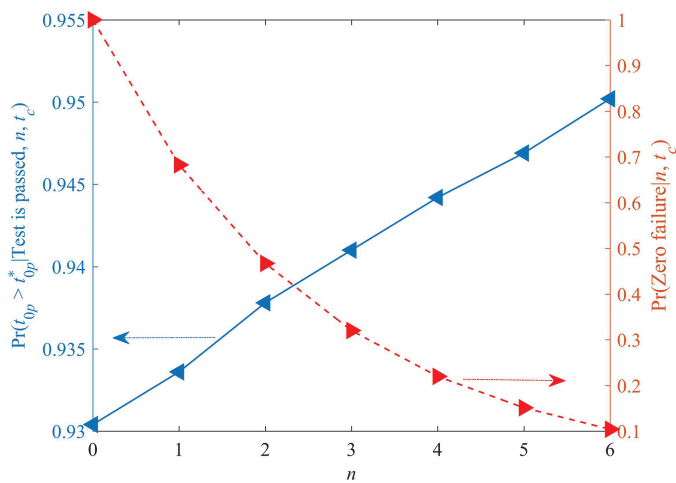


Figure 11.3: $\Pr(t_{0p} \geq t_{0p}^* | \text{Test is passed}, n, t_c)$ and $\Pr(\text{Zero failure} | n, t_c)$ versus the sample size n under the Prior 5 in Example 1.

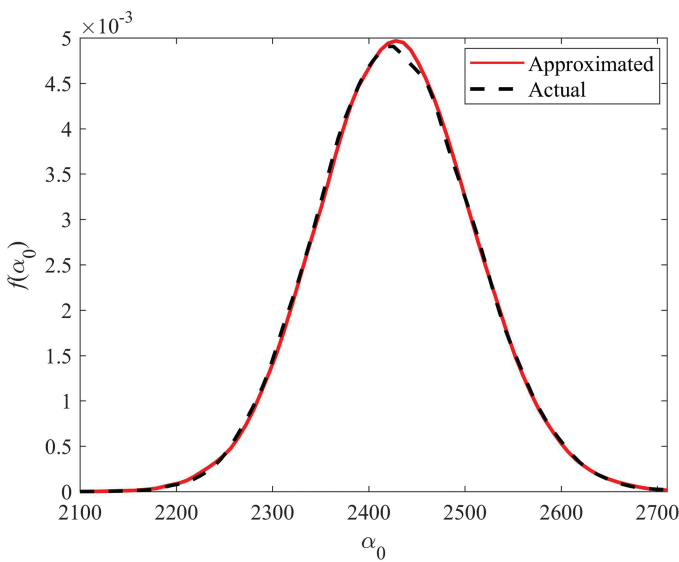


Figure 11.4: Prior density of α_0 under Prior 5 in Example 1.

Table 11.2: Minimum sample size needed n^* with an approximated system-level prior in Example 1.

Prior	$E(\alpha_0)$	$VAR(\alpha_0)$	a_0	b_0	n^*
1	3481.0	736.4	22.35	0.0064	0
2	3335.0	724.5	21.19	0.0064	1
3	2718.0	271.6	100.15	0.037	2
4	2481.0	114.5	469.51	0.19	4
5	2428.0	80.4	911.30	0.38	7
6	2381.0	47.4	2519.01	1.06	10
7	2388.0	47.5	2525.32	1.06	0

$$R_1(t|\boldsymbol{\theta}_1) = R_1(t|\alpha_1, \beta_1) = \exp\left(-\left(\frac{t}{\alpha_1}\right)^{\beta_1}\right) \quad (11.16)$$

$$R_2(t|\boldsymbol{\theta}_2) = R_2(t|\mu_2) = \exp\left(-\frac{t}{\mu_2}\right) \quad (11.17)$$

$$R_3(t|\boldsymbol{\theta}_3) = R_3(t|\eta_3, \sigma_3) = 1 - \Phi\left(\frac{\ln t - \eta_3}{\sigma_3}\right) \quad (11.18)$$

where Φ is the Cdf of standardized normal distribution, μ is the mean parameter of the exponential distribution, and η and σ are, respectively, the location and shape parameters of the lognormal distribution. If the components are assumed to be independent, the system reliability function is given by

$$R_0(t|\boldsymbol{\theta}_0) = \left[1 - \left(1 - \exp\left(-\left(\frac{t}{\alpha_1}\right)^{\beta_1}\right)\right)\left(1 - \exp\left(-\frac{t}{\mu_2}\right)\right)\right] \left[1 - \Phi\left(\frac{\ln t - \eta_3}{\sigma_3}\right)\right] \quad (11.19)$$

where $\boldsymbol{\theta}_0 \equiv (\alpha_1, \beta_1, \mu_2, \eta_3, \sigma_3)$. Since all five parameters are positive, independent Gamma prior distributions are assumed for those parameters. Table 11.3 lists three sets of prior distributions assumed for the five parameters. The three prior distributions for each parameter have the same prior mean, but from Priors I to III, the prior uncertainty for the parameter increases. Assume that the system reliability requirement is again specified as the p -quantile life of the system with $p = 0.1$. That is, t_{0p} is the time by which 10% of systems in the population will have failed. Figure 11.5 compares the prior density functions of t_{0p} under the three sets of prior distributions. From Priors I to III, the uncertainty in t_{0p} increases.

In this numerical example, we assume that the test duration t_c is pre-specified. Then our objective is to determine the minimum sample size n^* satisfying the posterior

assurance criterion given by eq. (11.3). Herein the posterior risk is assumed to be $\gamma = 0.05$. Table 11.4 summarizes the results for various t_c and t_{op}^* values under the three sets of prior distributions. $\Pr(t_{op} \geq t_{op}^*)$ is the prior probability that the reliability requirement is satisfied. When $\Pr(t_{op} \geq t_{op}^*) \geq 1 - \gamma$, that is, the assurance criterion is satisfied according to the prior knowledge and/or historical data, there is no need to conduct the demonstration test, for example, $n^* = 0$ when $t_{op}^* = 130$ under Prior I.

Table 11.3: Three sets of prior distributions assumed in Example 2.

Prior I		Prior II		Prior III		
β_1	$G\left(100, \frac{200}{3}\right)$	$\frac{E(\beta_1) = 1.5}{STD(\beta_1) = 0.15}$	$G\left(25, \frac{50}{3}\right)$	$\frac{E(\beta_1) = 1.5}{STD(\beta_1) = 0.30}$	$G\left(4, \frac{8}{3}\right)$	$\frac{E(\beta_1) = 1.5}{STD(\beta_1) = 0.75}$
α_1	$G(100, 0.2)$	$\frac{E(\alpha_1) = 500}{STD(\alpha_1) = 50}$	$G(25, 0.05)$	$\frac{E(\alpha_1) = 500}{STD(\alpha_1) = 100}$	$G\left(4, \frac{1}{125}\right)$	$\frac{E(\alpha_1) = 500}{STD(\alpha_1) = 250}$
μ_2	$G(100, 0.2)$	$\frac{E(\mu_2) = 500}{STD(\mu_2) = 50}$	$G(25, 0.05)$	$\frac{E(\mu_2) = 500}{STD(\mu_2) = 100}$	$G\left(4, \frac{1}{125}\right)$	$\frac{E(\mu_2) = 500}{STD(\mu_2) = 250}$
η_3	$G(100, 0.1)$	$\frac{E(\eta_3) = 1,000}{STD(\eta_3) = 100}$	$G(25, 0.025)$	$\frac{E(\eta_3) = 1,000}{STD(\eta_3) = 200}$	$G\left(4, \frac{1}{250}\right)$	$\frac{E(\eta_3) = 1,000}{STD(\eta_3) = 500}$
σ_3	$G(100, 100)$	$\frac{E(\sigma_3) = 1}{STD(\sigma_3) = 0.1}$	$G(25, 25)$	$\frac{E(\sigma_3) = 1}{STD(\sigma_3) = 0.2}$	$G(4, 4)$	$\frac{E(\sigma_3) = 1}{STD(\sigma_3) = 0.5}$

If $\Pr(t_{op} \geq t_{op}^*) \geq 1 - \gamma$ is not satisfied, demonstration tests are needed. In terms of the effect of the prior distribution on the test plan, there are again two factors affecting the minimum sample size required. The first factor is the prior probability that the reliability requirement is satisfied, that is, $\Pr(t_{op} \geq t_{op}^*)$. When $\Pr(t_{op} \geq t_{op}^*)$ decreases, the minimum sample size n^* tends to increase. For example, when $t_c = 200$ and $t_{op}^* = 130$, the prior probability $\Pr(t_{op} \geq t_{op}^*)$ decreases and the minimum sample size n^* increases from Priors I to III. The second factor is the prior uncertainty of t_{op} . When the prior knowledge indicates that the assurance criterion is not satisfied and the prior uncertainty is low; that is, when the prior knowledge is relatively certain that the reliability requirement is not satisfied, one may need to use a large sample size to demonstrate the system reliability. Because the Bayesian approach combines the prior knowledge and the data collected from the demonstrate test to make inference on the system reliability. When the prior knowledge indicates that the system reliability requirement is not satisfied, one would need to rely on sufficient information obtained from the demonstration test to reach the decision that the system reliability satisfies the requirement. The lower the prior uncertainty, the more information would be needed from the test and hence more

sample systems are needed to be tested. For example, when $t_c = 200$ and $t_{0p}^* = 155$, although the prior probability $\Pr(t_{0p} \geq t_{0p}^*)$ assuming Prior II is 0.6994, which is higher than the prior probability of 0.4042 assuming Prior III, the Prior III requires less minimum sample size than Prior II due to the higher prior uncertainty under Prior III. In addition, for a given prior distribution, a higher test duration t_c requires a less minimum sample size; and a higher reliability requirement t_{0p}^* requires a larger minimum sample size.

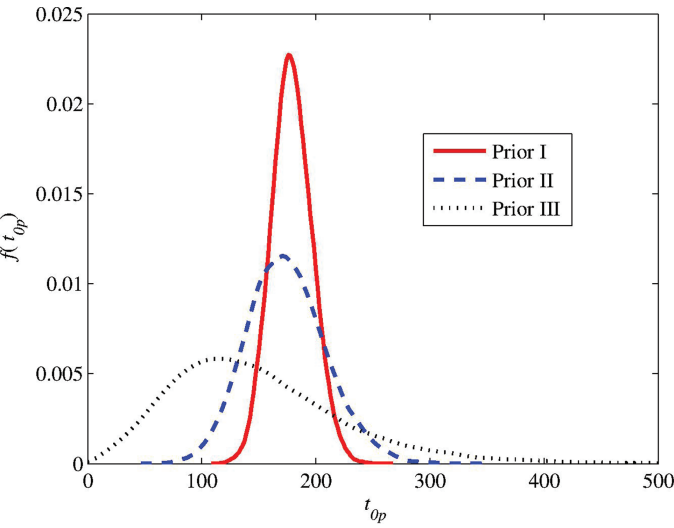


Figure 11.5: Prior density functions for t_{0p} under three sets of priors in Example 2.

Table 11.4: Minimum sample size needed n^* , when $p = 0.1$ and $\gamma = 0.05$, for various t_c and t_{0p}^* values in Example 2.

t_c	t_{0p}^*	Prior	n^*	$\Pr(t_{0p} \geq t_{0p}^* \text{Test is passed, } n^*, t_c)$	$\Pr(t_{0p} \geq t_{0p}^*)$
200	130	I	0	—	0.9977
		II	6	0.9551	0.9062
		III	13	0.9524	0.5416
	155	I	10	0.9513	0.9118
		II	22	0.9523	0.6994
		III	19	0.9502	0.4042

Table 11.4 (continued)

t_c	t_{0p}^*	Prior	n^*	$\Pr(t_{0p} \geq t_{0p}^* \text{Test is passed, } n^*, t_c)$	$\Pr(t_{0p} \geq t_{0p}^*)$
180	130	I	0	—	0.9977
		II	6	0.9523	0.9062
		III	15	0.9532	0.5416
	155	I	11	0.9505	0.9118
		II	26	0.9561	0.6994
		III	22	0.9510	0.4042

11.4 Conclusions and future work

This study proposed a fully Bayesian approach to planning the system-level zero-failure RDTs using available component-level prior distributions. The proposed approach may have the potential to be applied to arbitrary component failure-time distributions and system structures if the system reliability function can be derived from the component-level reliability functions according to the system structures. If the component-level prior knowledge provides evidence that the system reliability requirement is satisfied, the Bayesian method has the potential to reduce the minimum sample size needed over the classical likelihood-based methods. On the other hand, if the component-level prior knowledge provides evidence that the system reliability requirement is not satisfied, the Bayesian method may need more samples than the classical methods to demonstrate the system reliability.

This study only used prior information at the component level. A possible future extension is to integrate prior distributions at multiple levels, for example, the system, subsystem, and component levels. This study only considered failure-time tests under the binary-state assumption. In the future, one may consider multistate or continuous-state assumptions, and multiple test types, for example, the pass/fail test, failure-time test, and degradation test. In addition, one limitation of the proposed method may be the high computational requirement when the system is very complex with many components, and therefore, a possible future research direction is to develop computationally efficient methods to derive an approximated system-level prior distribution from the component-level prior distributions.

References

- [1] Meeker, W. Q. & Escobar, L. A. 1998. Statistical methods for reliability data, New York, Wiley.
- [2] Elsayed, E. A. 2012. Overview of reliability testing, *IEEE Transactions on Reliability*, 61(2), 282–291.
- [3] Chen, S. (2020) Some recent advances in design of Bayesian binomial reliability demonstration test, PhD Dissertation, University of South Florida, Tampa, Florida.
- [4] Wang, C. J. 1990. Sample size determination of bogey tests without failures, *Journal of Quality Technology*, 7, 35–38.
- [5] McKane, S. W., Escobar, L. A. & Meeker, W. Q. 2005. Sample size and number of failure requirement for demonstration tests with log-location-scale distributions and failure censoring, *Technometrics*, 47(2), 182–190.
- [6] Martz, H. F. & Waller, R. A. 1979. A Bayesian zero-failure (BAZE) reliability demonstration testing procedure, *Journal of Quality Technology*, 11(3), 128–138.
- [7] Fan, T.-H. & Chang, -C.-C. 2009. A Bayesian zero-failure reliability demonstration test of high quality electro-explosive devices, *Quality and Reliability Engineering International*, 25, 913–920.
- [8] Chen, S., Lu, L., Zhang, Q. & Li, M. 2020. Optimal binomial reliability demonstration tests design under acceptance decision uncertainty, *Quality Engineering*, 32(3), 492–508.
- [9] Kleyner, A., Elmore, D. & Boukai, B. 2015. A Bayesian approach to determine test sample size requirements for reliability demonstration retesting after product design change, *Quality Engineering*, 27, 289–295.
- [10] Joen, J. & Ahn, S. 2018. Bayesian methods for reliability demonstration test for finite population using lot and sequential sampling, *Sustainability*, 10, 3671.
- [11] Gal, S. 1974. Optimal test design for reliability demonstration, *Operations Research*, 22, 1235–1242.
- [12] Rajgopal, J. & Mazumdar, M. 1995. Designing component test plans for series system reliability via mathematical programming, *Technometrics*, 37(2), 195–212.
- [13] Rajpogal, J. & Mazumdar, M. 1997. Minimum cost component test plans for evaluating reliability of a highly reliable parallel system, *Naval Research Logistics*, 44(5), 401–418.
- [14] Easterling, R. G., Mazumdar, M., Spencer, F. W. & Diegert, K. V. 1991. System-based component-test plans and operating characteristics: binomial data, *Technometrics*, 33(3), 287–298.
- [15] Mazumdar, M. 1977. An optimum procedure for component testing in the demonstration of series system reliability, *IEEE Transactions on Reliability*, 26(5), 342–345.
- [16] Altinel, K. I. 1992. The design of optimum component test plans in the demonstration of a series system reliability, *Computational Statistics & Data Analysis*, 14, 281–292.
- [17] Guo, H., Jin, T. & Mettas, A. 2011. Designing reliability demonstration tests for one-shot systems under zero component failures, *IEEE Transactions on Reliability*, 60(1), 286–294.
- [18] Ten, L. M. & Xie, M. (1998) Bayes reliability demonstration test plan for series-system with binomial subsystem data, In *Proceedings of Annual Reliability and Maintainability Symposium*, 241–246.
- [19] Li, M., Zhang, W., Hu, Q., Guo, H. & Liu, J. 2017. Design and risk evaluation of reliability demonstration test for hierarchical systems with multilevel information aggregation, *IEEE Transactions on Reliability*, 66(1), 135–147.
- [20] Mastran, D. V. 1976. Incorporating component and system test data into the same assessment: a Bayesian approach, *Operations Research*, 24, 491–499.
- [21] Mastran, D. V. & Singpurwalla, N. D. 1978. A Bayesian estimation of the reliability of coherent structures, *Operations Research*, 26, 663–672.

- [22] Martz, H. F., Waller, R. A. & Fickas, E. T. 1988. Bayesian reliability analysis of series systems of binomial subsystems and components, *Technometrics*, 30(2), 143–154.
- [23] Martz, H. F. & Waller, R. A. 1990. Bayesian reliability analysis of complex series/parallel systems of binomial subsystems and components, *Technometrics*, 32(4), 407–416.
- [24] Hulting, F. L. & Robinson, J. A. 1994. The reliability of a series system of repairable subsystems: a Bayesian approach, *Naval Research Logistics*, 41, 483–506.
- [25] Liu, J., Li, J. & Kim, B. U. (2011) Bayesian reliability modeling of multi-level system with interdependent subsystems and components, In *Proceedings of IEEE International Conference on Intelligence and Security*, 252–257.
- [26] Li, M., Hu, Q. & Liu, J. 2013. Proportional hazard modeling for hierarchical systems with multilevel information aggregation, *IIE Transactions*, 46(2), 149–163.
- [27] Bier, V. M. 1994. On the concept of perfect aggregation in Bayesian estimation, *Reliability Engineering and System Safety*, 46, 271–281.
- [28] Johnson, V. E., Moosman, A. & Cotter, P. 2005. A hierarchical model for estimating the early reliability of complex systems, *IEEE Transactions on Reliability*, 54(2), 224–231.
- [29] Johnson, V. E., Graves, T. L., Hamada, M. & Reese, C. S. 2001. A hierarchical model for estimating the reliability of complex systems, In: *Bayesian Statistics*, 7, Bernardo, J. M., Bayarri, M. J., Berger, J. O., Dawid, A. P., Heckerman, D., Smith, A. F. M. & West, M. Eds, Oxford, UK, Oxford University Press, 199–213.
- [30] Reese, C. S., Wilson, A. G., Gao, J., Hamada, M. S. & Johnson, V. E. 2011. A Bayesian model for integrating multiple sources of lifetime information in system-reliability assessments, *Journal of Quality Technology*, 43(2), 127–141.
- [31] Graves, T. L., Hamada, M. S., Klamann, R. M., Koehler, A. C. & Martz, H. F. 2008. Using simultaneous higher-level and partial lower-level data in reliability assessments, *Reliability Engineering and System Safety*, 93, 1273–1279.
- [32] Graves, T. L., Hamada, M. S., Klamann, R. M., Koehler, A. C. & Martz, H. F. 2007. A fully Bayesian approach for combining multi-level information in multi-state fault tree qualification, *Reliability Engineering and System Safety*, 92, 1476–1483.
- [33] Hamada, M. S., Martz, H. F., Reese, C. S., Graves, T. L., Johnson, V. E. & Wilson, A. G. 2004. A fully Bayesian approach for combining multilevel information in fault tree quantification and optimal follow-on resource allocation, *Reliability Engineering and System Safety*, 86, 297–305.
- [34] Guo, J. & Wilson, A. G. 2013. Bayesian methods for estimating the reliability of complex systems using heterogeneous multilevel information, *Technometrics*, 55(4), 461–472.
- [35] Peng, W., Huang, H.-Z., Xie, M., Yang, Y. & Liu, Y. 2013. A Bayesian approach for system reliability analysis with multilevel pass-fail, lifetime and degradation data sets, *IEEE Transactions on Reliability*, 62(3), 689–699.
- [36] Gelman, A., Carlin, J. B., Stern, H. S. & Rubin, D. B. 2004. *Bayesian data analysis*, London, Chapman and Hall.

Index

- 0-edge 159–163
- 1-edge 159–163
- $[n, f, k]$ 66

- acceleration 153, 158, 162–164, 168–171
- acyclic paths tree 120
- all-highest vector 136
- all-lowest vector 137
- analytical method 170
- attack mitigation service 88
- average degree of network nodes 28

- backward shift operator 201
- backward substitution 192–193, 195
- basic event 158–160
- Bayes theorem 243
- Bayesian method 241
- BDD 153–154, 159–166, 168–169, 172
- Bernoulli-type dynamic process 179
- Bernoulli-type of probabilistic (deterministic or stochastic) process 178
- binary elements 68
- binary sequences 69
- binary state of population dynamic process 179
- binary states dynamic 178
- binary-imaged 132, 149
- binary-state probabilistic dynamic process 178
- Birnbbaum importance measure 2, 6, 9, 14–16
- Boolean expression 121
- Boolean product 121
- Boolean quotients 138, 140
- Boolean sum 121
- Boolean variable 121
- Boole–Shannon expansion 140
- Borel-measurable survival state discrete-time intervention rate function 182

- cascading failures 21
- causality 133
- CDF 154–157, 161–163, 165, 170
- change point 66
- change point times 198–199, 205
- classical likelihood based models 178
- classical likelihood-based models 176–177
- cloud storage 85–86
- cloud-RAID-5 87, 91–93, 101
- coherent 133, 149
- coherent system 122
- combinatorics 93
- competition 154, 158, 160–161, 166, 170–171
- complement 133
- completely specified 149
- component 133
- conceptual computational parameter dynamic estimation algorithms 187
- consecutive- k -out-of- n : F system 66
- consumer's risk 243
- continuous-time dynamic subsystem 185
- Copeland method 3, 7–10, 15–16
- Copeland score 7–8, 9, 10, 11, 13, 16, 18
- cumulative distribution functions (CDF) 88
- cut-set 119
- cyberattacks 85–86, 88

- damage accumulation 156, 158, 163–164
- damage threshold 156, 170
- DCFP 166, 169–170
- DDoS attacks 88, 94
- De Morgan's rules 142
- degradation 156, 166–170
- demand nodes 4–5, 9, 14
- denial-of-service (DoS) 85
- dependence 22
- dependence cluster collapsing threshold 32
- dependence clusters 23
- design parameters 67, 73
- differential of survival state probability measure 179
- discrete-time dynamic algorithm of time-to-event data statistic 176, 184
- disjointness 139
- distribution parameter 161
- distribution type 161
- dominant 133

- efficiency of the shortest path 33
- embedded Markov chain (EMC) 89
- ER random network 26
- expected value 137, 145
- expected values 142, 144
- exponential baseline distribution 77
- exponential distribution 88
- external intervention processes 181
- failure state 179

<https://doi.org/10.1515/9783110725599-012>

- failure threshold 157, 166, 168–169
- failure time 154–157
- failure-time partition 188, 200
- fault tolerance 87
- first-order phase transition 28
- FM 153–163, 165–170, 172
- FMT 154, 157–160, 167–168, 172
- forward-shift operator 201
- Fussell–Vesely importance measure 7

- generalized logistic distribution 181
- Gibbs sampling 243

- hard failure 166–170
- hardware failure 88
- hazard rate 77
- hazard rate function 177–178, 215, 233
- hazard rate/risk 176
- hazard/risk rate function 181
- heterogeneous disks 91
- homogeneous disks 91
- hybrid probabilistic binary state dynamic model 176, 183

- importance measure 1–3, 5–10, 14–16, 19
- inclusion–exclusion (IE) principle 141
- infrastructure network performance 4–5
- inhibition 155, 158, 162–164, 166
- initial value problem 180, 182, 203
- input event 158
- instant 133–134
- integer solutions 70–71
- integral value 160
- interconnected discrete-time algorithm of data statistic 177
- interconnected hybrid dynamic model 184
- interconnected nonlinear hybrid probabilistic binary state dynamic system 176, 182
- invariant sets 180, 209, 233
- invulnerability 85, 91, 93, 96
- ite* operator 159–161
- ite* rule 172
- Ito–Doob stochastic time-to-event process 177, 229

- Kaplan–Meier 177, 229
- Karnaugh maps 132
- kernel matrix 89

- large-scale interconnected hybrid dynamic system 183
- likelihood function 243
- linear equations 71
- linear system 69
- load 22
- local admissible sequences 207
- local lagged moving failure-time subsequence 200
- logistic population dynamic model 178
- logistic-type survival distribution function 178
- log-logistic distribution 176, 181
- lower value 134–135

- maintenance engineering predictions 49
- market share/size 179
- maximal lower vector (MLV) 136
- maximal lower vector 132
- maximal lower vectors (MLVs) 141, 149
- maximum likelihood 177, 229
- m*-consecutive-*k*-out-of-*n*: *F* system 66
- mean size of dependence clusters 28
- mean time to failure 72
- media error 88
- minimal cutset 132
- minimal path 132
- minimal upper vector (MUV) 132
- minimal upper vectors (MUVs) 141, 148
- MIRCE Functionability Equation 49, 51, 55–58, 62–64
- mixed cascading failures model 25
- monotonicity 133
- Monte Carlo 153–154, 170, 172
- MSS 105–110, 113, 116–117
- MSU 105, 107, 109, 112, 117
- MTTF 68, 77
- multiple-valued logic 131
- multistate 91
- multistate systems 131
- multivalued 133
- multivalued decision diagrams (MDDs) 140
- multivalued decision diagrams 86
- multivalued Karnaugh map (MVKM) 134
- multi-valued Karnaugh map (MVKM) 140, 149
- mutually exclusive time-varying events 177

- network connectivity 26
- Network efficiency 33

- network externality functions 179
- network externality value 178
- Newtonian-type dynamic 178
- Newton's third law of dynamic motion
 - process 178
- Node capacity 24
- nonlinear and non-stationary differential equations 183
- nonlinear hybrid dynamic model 176–177, 182–183, 185, 229
- nonlinear survival state dynamic model 180–181
- non-overlapping 144
- non-overlapping loops 142
- non-redundant 121
- non-sink node 159–160
- normalization of system engineering design 51
- number of survivals 184, 187
- numbers of initially failed nodes 35

- OPT importance measure 5, 9–10, 14–16
- optimal residual resilience 6–7
- optimal state 5
- orthogonality 139
- orthonormal set 133
- output event 158–159
- overloaded 22

- parallel 139, 147
- parameter combination 156, 166
- parity 87
- partially discrete-time interconnected nonlinear hybrid dynamic system 184
- PDEP 153–154, 160
- PDF 154–156, 165, 170
- perfect induction 140
- physical dependencies 155
- physical failures 85–86
- pmf 107–108, 112, 114–115
- PoF 169
- posterior assurance 242
- posterior distribution 243
- posterior risk 242
- predictions of the expected work 63
- prime implicant 132, 148
- Principle of Mathematical Induction 191, 194, 203, 207
- prior distribution 242

- probabilistic binary state dynamic model 176, 178–180, 182–183
- probabilistic binary states 176, 178–180, 182–183
- probability mass function 73
- probability transform 137
- probability-ready expression 132, 138
- producer's risk 248
- pseudo-Boolean expression 145

- quantitative reliability 86
- quantitative security 86

- random number of units 73
- RAW importance measure 6, 9–10, 14, 16
- Rayleigh distribution 88
- recovery capability 94
- recovery time 32
- redundancy 139
- redundant 121
- redundant array of independent disks 85
- relevancy 133
- relevant element 120
- reliability 66, 72, 76, 80
- reliability achievement worth 6
- reliability analysis 131
- reliability demonstration test 237
- reliability function 68, 73, 79
- reliability reduction worth 6
- repair proportion 34
- repair sequence 3–5, 15, 19
- residual resilience 1, 3–5, 6, 7, 8, 15–16, 19
- resilience 1–2, 3, 5–7, 11, 15, 17, 19, 22
- resilience metric 33
- restoration strategies 34
- Riemann–Stieltjes integral property 186
- RRW 6–7, 9, 14–16

- scale parameter 94
- second-order transition 29
- security threats 88
- sequence-dependent 86
- sequential attack 101
- series 139, 147
- shape parameter 98
- shock process 166–167
- single change point 67, 69–70, 72–73, 76–77, 81

- SMP 86–91, 101
- soft failure 166–170
- statistical independence 139
- steady-state probability 90, 101
- stopping rule 65
- structure function 121, 241
- structure or success function 133
- subfunctions 140
- sum-of-products 144, 150
- supply nodes 4, 9, 14
- survivability 85, 91, 93, 96, 150
- survival data analysis 176, 185
- survival function 176–177, 208, 211, 230–233
- survival principle 179
- survival state 176, 178–186, 201–203, 205, 210, 215, 222
- survival state dynamic model of time-to-event process 180
- survival state function 182–183
- survival state intervention process 185
- survival/failure functions 179
- survival/failure probability distributions 177
- switching algebra 132
- system failure 142
- system failure time 155
- system failures 148
- system successes 147

- the largest connected component of the network 26
- theoretical/computational estimation algorithm and parameter estimation 191
- theoretical/computational estimation algorithm and parameter estimation* 191–192
- time-dependent 101
- time-to-event data statistic 176, 184, 186, 189, 200, 203
- time-to-event dynamic processes 181, 183, 189, 233
- time-to-event processes 176–179, 181–182, 185, 200, 209, 233
- total amount of time spent 193, 195
- total probability theorem 140
- totally discrete-time hybrid dynamic model for time-to-event dynamic process* 197
- totally discrete-time hybrid dynamic model for time-to-event dynamic process 199
- transformed interconnected nonlinear hybrid dynamic model 185
- transformed intervention process 186
- trigger 153–155, 157–158, 161–162

- UGF 107–108, 111–113, 115–117
- upper value 134
- upper vector 135
- upper vectors 135

- verbal description 147
- vulnerability 95

- Weibull distribution 88, 94

De Gruyter Series on the Applications of Mathematics in Engineering and Information Sciences

Already published in the series

Volume 7: Mathematical Fluid Mechanics. Advances on Convection Instabilities and Incompressible Fluid Flow

B. Mahanthesh (Ed.)

ISBN 978-3-11-069603-5, e-ISBN (PDF) 978-3-11-069608-0

e-ISBN (EPUB) 978-3-11-069612-7

Volume 6: Distributed Denial of Service Attacks. Concepts, Mathematical and Cryptographic Solutions

Rajeev Singh, Mangey Ram (Eds.)

ISBN 978-3-11-061675-0, e-ISBN (PDF) 978-3-11-061975-1

e-ISBN (EPUB) 978-3-11-061985-0

Volume 5: Systems Reliability Engineering. Modeling and Performance Improvement

Amit Kumar, Mangey Ram (Eds.)

ISBN 978-3-11-060454-2, e-ISBN (PDF) 978-3-11-061737-5

e-ISBN (EPUB) 978-3-11-061754-2

Volume 4: Systems Performance Modeling

Adarsh Anand, Mangey Ram (Eds.)

ISBN 978-3-11-060450-4, e-ISBN (PDF) 978-3-11-061905-8

e-ISBN (EPUB) 978-3-11-060763-5

Volume 3: Computational Intelligence. Theoretical Advances and Advanced Applications

Dinesh C. S. Bisht, Mangey Ram (Eds.)

ISBN 978-3-11-065524-7, e-ISBN (PDF) 978-3-11-067135-3

e-ISBN (EPUB) 978-3-11-066833-9

Volume 2: Supply Chain Sustainability. Modeling and Innovative Research Frameworks

Sachin Kumar Mangla, Mangey Ram (Eds.)

ISBN 978-3-11-062556-1, e-ISBN (PDF) 978-3-11-062859-3,

e-ISBN (EPUB) 978-3-11-062568-4

Volume 1: Soft Computing. Techniques in Engineering Sciences

Mangey Ram, Suraj B. Singh (Eds.)

ISBN 978-3-11-062560-8, e-ISBN (PDF) 978-3-11-062861-6,

e-ISBN (EPUB) 978-3-11-062571-4

www.degruyter.com